Contents

A STUDY OF THE ADSORPTION OF SOME POLYMERS AND LANGMUIR BLODGETT FILM SYSTEMS BY INELASTIC ELECTRON TUNNELLING SPECTROSCOPY

MICHAEL JOHN LINE

A thesis submitted in part fulfilment of the requirements of De Montfort University for the degree of Doctor of Philosophy

June
1994

School of Applied Sciences De Montfort University
The Gateway Leicester
LEI 9BH United kingdom

Abstract

The work in this thesis can be split into three areas.

In the first, inelastic electron tunnelling spectroscopy (IETS) is used to investigate resistive and bias polarity dependent effects on vibrational mode energy in metal - aluminium oxide - metal tunnel junctions. It is shown that even when four point-probe techniques are used the ratio of width to thickness of the electrodes used in IET junctions has an effect on both the breadth and position of spectral lines. A simple treatment based upon work done by Giaever allows for such effects to be corrected. Work done on top metal and polarity effects in undoped IET junctions investigated the effect on the position of the 450 meV mode on reversing the applied bias. The investigation revealed that any dependence on the nature of the top-metal electrode was outside the accuracy of the work. Calculation of q/e for the hydroxyl group on alumina within the tunnel junction has been extended to include other electrode materials.

A new and exciting facility within the university provided the impetus for the second area of work. A class 100 clean room housing a Langmuir Blodgett (LB) trough offered the opportunity to produce metal - insulator - Langmuir Blodgett film
- metal tunnel junctions. It was realised at the outset that IETS using LB films would be difficult, previous workers had tried using a home-made tank with only limited success. However, the added sophistication of the new tank did not improve matters as was hoped. Although the results were disappointing, only a few junctions had resistances low enough to be usable in the spectrometer, the investigation produced some of the very few IET specra using junctions doped with LB films. The results also revealed the important role that imperfections and pin-holes play in the tunnelling process.

The last area used IETS to investigate two commercially important and interesting polymers, hydrogels and polymeric electrolytes. Hydrogel have many applications in the field of implants, prosthetic, and cosmetics and have been studied and developed for many years. Polymeric electrolytes have many commercial applications especially in the field of solid-state batteries and conducting polymers. The way in which hydrogels swell as they absorb water is important, as is the way they adsorb onto a surface and much work has been done to investigate these characteristics using bulk samples. The study done by this group is the first to investigate the swelling and adsorption behaviour of a monolayer of the hydrogel poly 2-hydroxylethyl methacrylate. The results from both investigations indicate that ester cleavage occurs in p-HEMA and that water incorporated within a hydrogel has a limited structure with the first layer being thinner than the second and subsequent layers.

Acknowledgements

I would like to thank the following:

My supervisors Dr. R G Pritchard and Professor D P Oxley for their encouragement and guidance throughout the course of this work. I also offer my thanks to Dr. A Evans and Dr. J Comyn for their advice regarding matters of spectroscopic interpretation and polymer chemistry and the members of the polymeric electrolyte team for their advice regarding conducting polymers.

A special appreciation is offered to the technical staff in the School of Applied Sciences and in particular to Mr. Norman Bevan, Les Gregson, and Dave Bazely for their help and assistance.

My thanks also to the National Academic Board for their funding of the Langmuir Blodgett trough and clean room facilities.

My grateful thanks go to the Directors and Governors of De Montfort University for providing the laboratory resources.

Finally I want to thank my wife Sheila, who has always supported and encouraged me throughout the time of this study - without her it would not have been possible.

INDEX

Contents

CHAPTER 1

INTRODUCTION

1.1. An Outline of the Present Work

The initial experimental work done by the present group investigated three parameters that have an effect on peak positions in inelastic electron tunnelling (IET). These were the resistance of the bottom junction electrode, the polarity of the applied bias, and the type of metal used in the manufacture of junction electrodes [1]. This was followed by a study of Langmuir films of mixed stearic acid / stearic acid salts to decide the optimum manufacturing parameters. Langmuir films are monolayers of amphiphillic molecules such as fatty acids formed into monolayers on the surface of an uncontaminated subphase. Once a Langmuir film has been fabricated and transferred to a substrate it is conventionally called a Langmuir Blodgett or LB film. Once formed the LB films were subsequently incorporated in tunnel junctions before their study by inelastic electron tunnelling spectroscopy (IETS). An IETS spectroscopic study of several commercially important materials, including the etch-resist co-tricosenoic acid, were also planned. These materials were to be polymerised in situ after being formed into a Langmuir film and before their incorporation in an IET junction.

A previous group had shown that it was very difficult to use Langmuir Blodgett films to produce junctions that were suitable for use with IETS [2]. It was therefore realised at the outset that the present program of work would be difficult. The earlier team had been disadvantaged by having to use a homemade Langmuir trough to produce the films and transfer them to the substrate. Whereas the present group had access to a new commercially produced state-of-the-art instrument, housed

within a class 100 clean room. However, the advantages proved to be of no consequence because the present group were also unable to consistently produce usable IET junctions.

Although originally frustrating, the difficulties experienced with the LB films did prove to have interesting and important consequences regarding tunnelling through ultra thin layers. These consequences having been explored, it was decided to abandon the study of polymerised Langmuir Blodgett monolayers and turn attention to the study of two commercially important polymers using a conventional liquid phase doping technique.

One of the polymers studied was a hydrogel which has extensive and important uses in the biomedical field, and the other was a polymeric `electrolyte having applications in storage batteries. A very great interest has already been focused on these two materials using various analytical techniques and this IETS study adds to the store of this knowledge.

1.2. Inelastic Electron Tunnelling Spectroscopy

Inelastic electron tunnelling spectroscopy (IETS) was discovered by Jaklevic and Lamb [3,4] whilst investigating the band structure of metal electrodes in metal - insulator - metal (MUM) junctions. The junctions were called tunnel junctions because electrons may be transferred from one metal electrode to the other through a classically forbidden barrier by a quantum mechanical phenomena known as tunnelling.

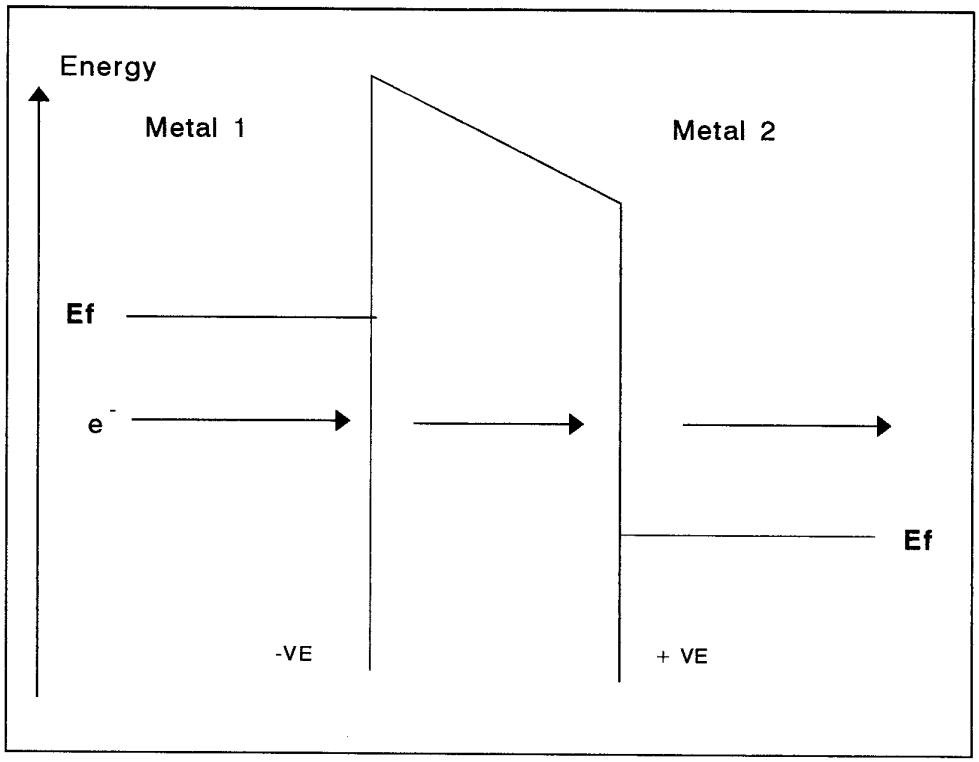

Figure 1.1a

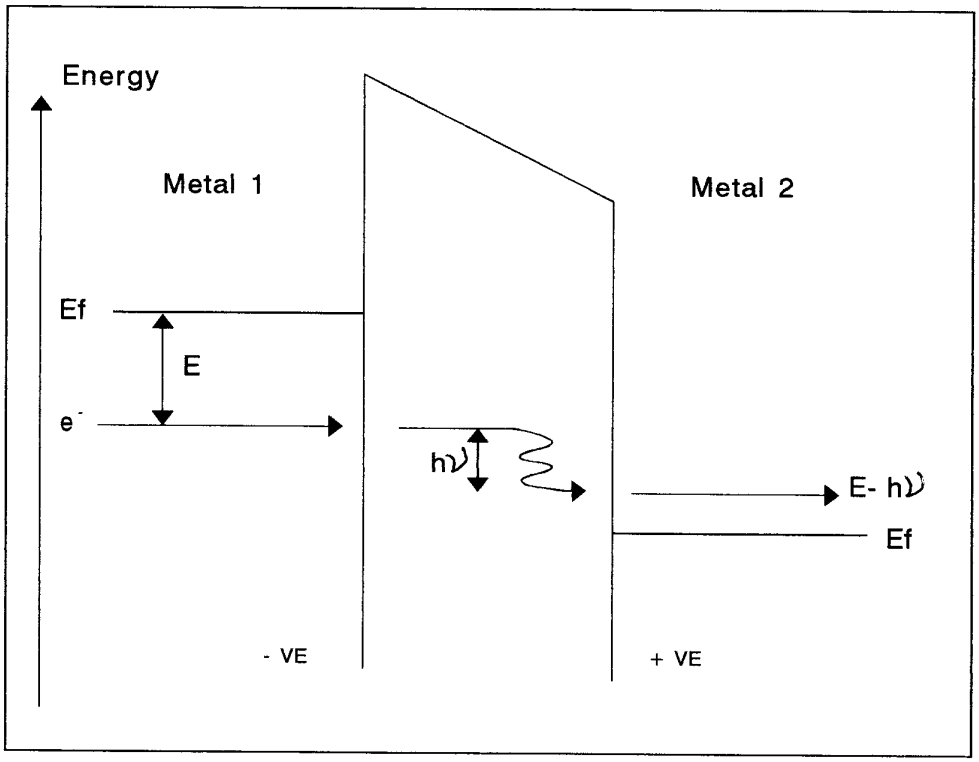

Figure 1.1b

Figure 1.La

Shows here is a representation of an elastic tunnelling, where the electrons progress which is represented the arrows tunnels isoenergetically across the potential barrier

Figure 1.1b

Represented in this diagram is an inelastic tunnelling process. The electron loses energy within the barrier by exciting vibrational mode/s of molecules which have been incorporated within the IETS junction.

This followed on from the earlier work of Giaever [5], Fisher and Giaever [6], and Simmons [7].

IETS uses tunnelling electrons to excite vibrational modes of the molecules incorporated within an IETS junction. There are two ways in which electrons can tunnel through the sample molecule. The first way involves electrons tunnelling elastically and is by far the most predominant method accounting for more than 99% of the total tunnelling current. Elastic tunnelling occurs in all situations where a bias voltage is applied across two metals which are separated by a very thin layer of an insulating material; this is illustrated in Figure l.la & b. In elastic electron tunnelling, under the influence of the applied bias electrons tunnel isoenergetically through the insulator transferring from filled states in one metal to empty states in the other metal. The second way in which the electrons traverse the potential barrier presented by the insulating layer is inelastically. In the inelastic process, electrons from filled states in one metal tunnel through to empty states in the other but in doing so they lose energy within the barrier by exciting a vibrational mode within the insulating layer. The amount of energy lost in the process is hp, which is the energy of the vibrational mode.

The manufacture of the junctions for use in the IET spectrometer is carried out in four stages. A metal which forms the base of the junction and the bottom electrode is deposited through a masking device onto a glass substrate by vacuum deposition. The freshly prepared electrode, which is usually aluminium, is allowed to grow an oxide film a few nanometres thick on its top surface. The oxide layer is then covered with a monolayer of the molecule to be investigated and then a top electrode (which is usually made from lead) is evaporated under vacuum through a mask to complete the junction. When in use the junctions are connected to the spectrometer and immersed

in liquid helium at 4.2K. The cooling of the junction has a twofold purpose, it reduces thermal broadening of the lines in the spectra and the lead electrode becomes superconducting which further increases the resolution of the spectral lines.

A d.c. bias together with a small a.c. current superimposed upon it is applied across the junction area and then slowly ramped between 0 and 500 mV. A plot of the second derivative of the Junctions IN characteristic versus the applied bias produces the IET spectrum. The spectrum reveals details of the vibrational excitations of the adsorbed molecules and/or their host adsorbent - the layer of oxide. The spectra obtained from IETS do differ slightly from the equivalent spectra taken by IR and Raman due to the way in which the compound is adsorbed onto the oxide layer. Many books and papers have been written on the tunnelling process involved in IETS and the author refers to some which are a representative collection of general reviews [8-13].

Shown for reference are IET spectra of an undoped or clean junction and a junction which has been doped with stearic acid - see Figure 1.2a and 1.2b.

1.3 Methodology of This Group's Work

The first work undertaken during the research period was an investigation into the effect of the resistance of the bottom electrode. This work was done to elucidate the changes in the positions of peaks in IET spectra brought about by the potential drop resulting from the finite resistance of the bottom electrode in the area of the junction. The work with LB films of stearic acid produced one of the

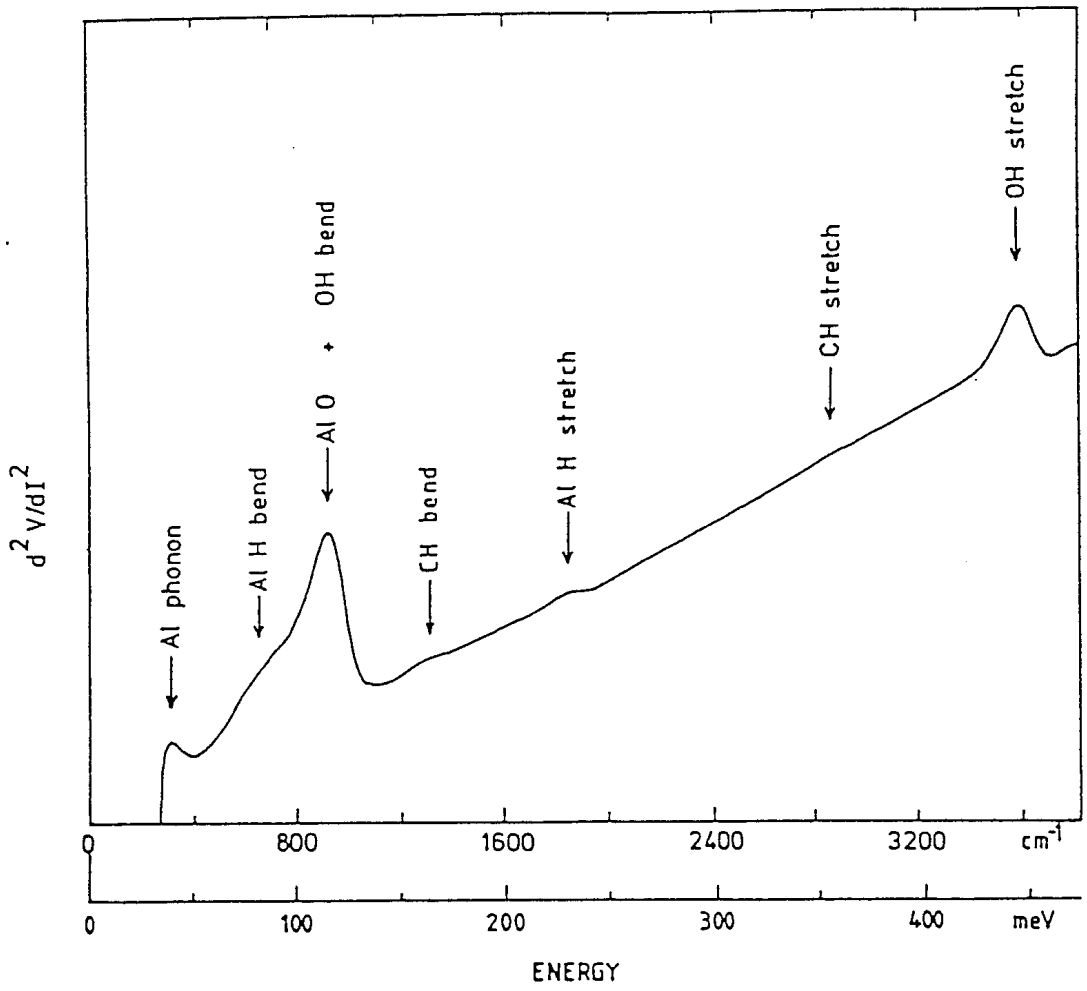

Figure 1.2

A reproduction of inelastic electron tunnelling spectra of a clean or undoped junction. To conform to the convention used by infrared spectroscopist a conversion factor of 1meV = 8.065 cm"' [14] is employed. The main features in the spectrum are as indicated in the figure.

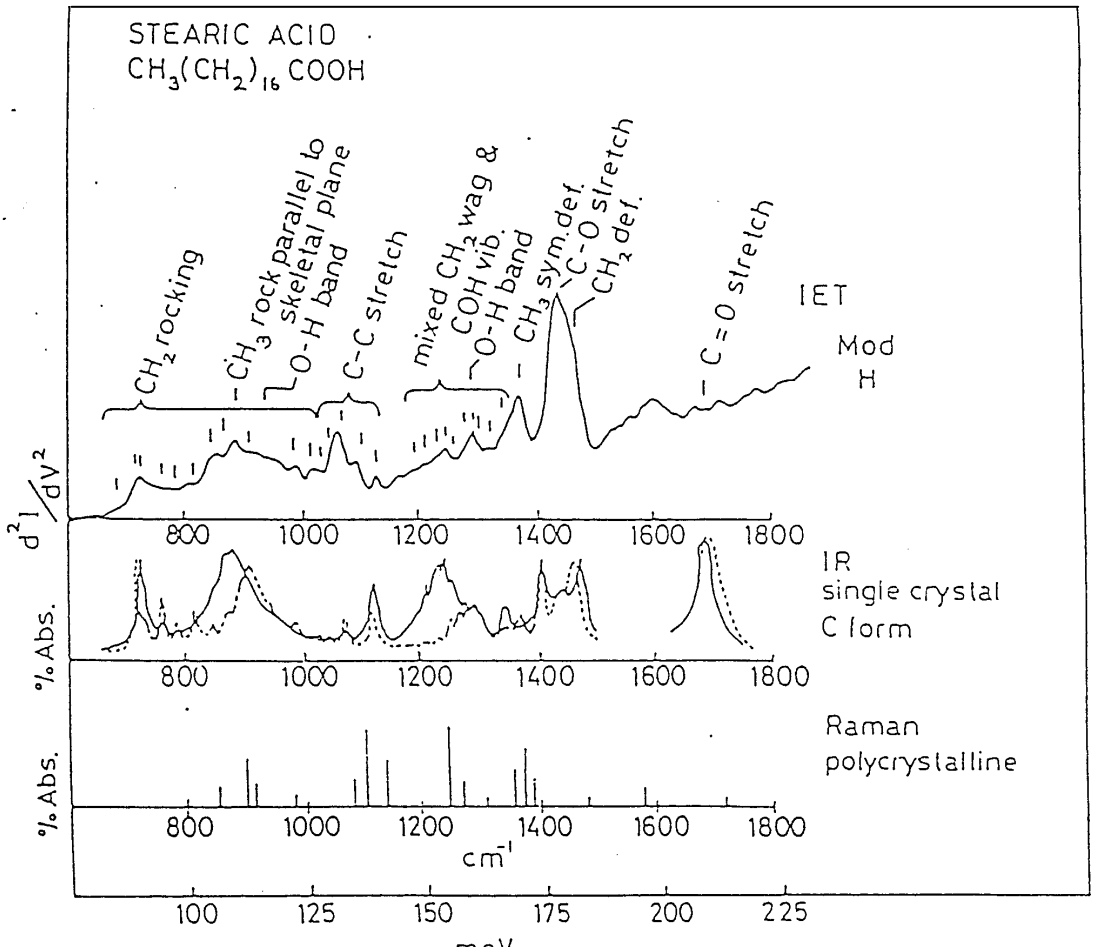

Figure 1.3

Illustrated here are comparisons between IET and a spectrum taken from a junction which had been liquid phase doped with stearic acid and the spectra obtained using single crystal infra-red and Raman. The range covered is the fingerprint region of the spectra ranges to 225 meV, after Keil et al [10]. The assignment of the peaks is discussed in Chapter 8.

very few spectra obtained from an IET tunnel junction which incorporated a Langmuir Blodgett film. The study highlights the very important role played by structural defects within the monolayer when electrons tunnel through adsorbed monolayers. The conclusions modify the way in which the adsorbed monolayer, within a tunnel junction, are viewed and point the way for further research using surface imaging techniques such as scanning tunnelling microscopy (STM) and atomic force microscopy (AFM).

The data from previous polymer studies demonstrates that it is possible to use inelastic electron tunnelling spectra to study the way in which polymers are adsorbed onto aluminium oxide [15] and so two unique IETS studies were undertaken. In the first the adsorption of a polymeric electrolyte onto aluminium oxide was investigated, and in the second the adsorption of the hydrogel p-HEMA onto aluminium oxide.

A further investigation which used an infusion doping technique [16] to study the processes by which water is incorporated into the hydrogel was also undertaken. The technique of infusion doping depends upon the migration of the dopant molecules through the grain boundaries in the top lead electrode. Proof that the dopant penetrates the top electrode material (lead in our case) and did not ingress via the edges has been previously established by various workers [17-19].

When the infusing water reaches the hydrogel it is incorporated into polymer, which swells to accommodate it. As the hydrogel is sandwiched between the top and bottom electrodes of a tunnel junction the resultant swelling caused the separation of the electrodes to increase which in turn results in a decrease of the tunnel conductance; the changes in conductance therefore mimic the dimensional changes of the hydrogel. Monitoring conductance changes during the time water infuses through the top electrode of an aluminium - aluminium oxide - hydrogel - lead IETS junction

allows inferences about the way in which the water is adsorbed into the hydrogel to be made. The present group has shown that there is some evidence that once water is adsorbed into the hydrogel it exhibits two differing structural forms.

References

[1] Line M J, Pritchard R G and Oxley D P 1989 *J.Phys. Condens. Matter* **1** 6835.
[2] Ginnai T 1982 *PhD Thesis* Leicester Polytechnic.
[3] Jaklevic R C and Lamb J 1966 *Phys. Rev. Lett.* **17** 1139.
[4] Lamb J and Jaklevic 1968 *Phys. Rev.* **165** 821.
[5] Giaever 1 1960 *Phys. Rev. Lett*. 5 **(4)** 147.
[6] Fisher J C and Giaever 1 1961 *J. Appl. Phys.* **32 (2)** 172.
[7] Simmons J G 1963 *J. Appl. Phys*. 34 (6) 1793.
[8] Hansma PK 1977 *Phys. Rep. C*. 30 2 146.
[9] Kirtley R J 1980 *J. Am. Chem. Soc. 80* 217.
[10] Keil R G, Graham T P 1976 and Roenker K P 1976 *Appl. Spectrosc.* 30 1 1.
[11] Weinberg W H 1978 *Ann. Rev. Phys. Chem. 29* 115.
[12] Wolfram T (Ed.) 1978 *Inelastic Electron Tunnelling Spectroscopy* (Springer-Verlag : Heidelberg).
[13] Hansma P K (Ed) 1982 *Tunnelling Spectroscopy - Capabilities, Applications, and NewTechniques* (Peenum : New York).
[14] White H W and Wolfram T 1980 *Methods Ex. Phys*. 16 A 149.
[15] Mallik R R, Pritchard R G, Horley C C, and Comyn J 1985 *Polymer* 26 551.
[16] Mallik R R, Pritchard R G, Oxley D P, Horley C C, and Comyn J 1984 *Thin Solid Films* 112 193.
[17] Jacklevic R C and Gaerttner M R 1977 *Appl. Phys. Lett*. 30 (12) 646.
[18] Mallik R R 1985 *PhD Thesis* Leicester Polytechnic.
[19] Reynolds S 1983 *PhD Thesis* Leicester Polytechnic.

Contents

CHAPTER 2

THE THEORY OF INELASTIC ELECTRON TUNNELLING SPECTROSCOPY

2.0 *Introduction*

In this chapter we will consider the methods by which electrons can traverse a barrier which in classical terms is seemingly impassable . Classically any electron with total energy E can only cross a potential barrier if the height of the barrier (V_o) is less than the total energy of the impinging electron. Figure 2.1. is an illustration of a one dimensional potential barrier of height V_o , shown incident upon the diagram is an electron of energy E < V0.

However, electrons with energy E < V_o can traverse the barrier with a non-zero probability, provided the barrier is thin - of the order of a few nanometres. This quantum mechanical phenomenon is named tunnelling and as will be shown in later sections the magnitude of the current formed by tunnelling electrons is very dependent upon the magnitude and width of the potential energy barrier formed by the insulating layer.

The chapter will provide a theoretical basis for the present work, and will be presented in the following way. First it will be shown how electrons tunnel across a simple hypothetical rectangular barrier see Figure 2.1. The theory will then be extended to cover tunnelling in metal-oxide-metal layers - MIM junctions - which closely model the blank or undoped junctions used in IETS. These two models deal only with the current formed by electrons which traverse the barrier elastically, losing none of their energy in the process.

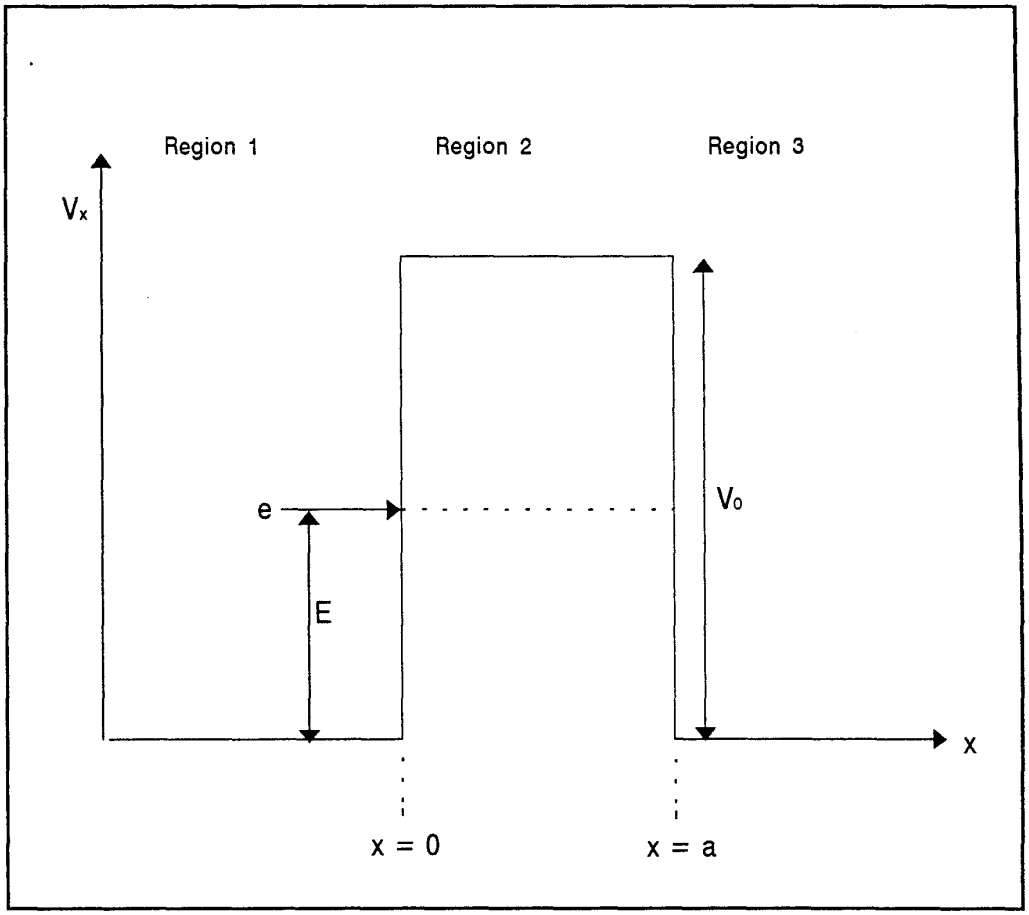

Figure 2.1

An electron of total energy E is shown incident on a rectangular barrier of height Vo and width a,

The dominant tunnelling mechanism occurring in metal-insulator-metal junctions is elastic tunnelling.

Under certain conditions, a tunnelling electron may lose some energy to an excitation within the barrier region but still have enough energy to finish up in an empty state of lower energy on the other side of the barrier. This process is termed inelastic tunnelling and it is this phenomenon which forms the basis of inelastic electron tunnelling spectroscopy (IETS).

The problem will only be treated as one-dimensional, assuming that if the barrier extends from x = 0 to x = a in the x direction then the momenta in the y and z directions can be taken as constants of the motion.

2.1 Barrier Penetration

Classically if an electron with total energy less than the barrier height ($E< V_o$) is incident on the barrier its motion will be limited to the region to the left of x = 0 and it will be reflected back without loss of energy. However quantum mechanics predicts that the electron will not necessarily be reflected back from the barrier.

Consider an electron of rest mass m and total energy E incident upon a simple one dimension rectangular potential barrier of height V_o such that $E < V_0$; as shown in figure 2.1. There are three distinct regions to be considered when approaching the problem in the first region at the metal 1 - insulator interface there will be incoming plane waves and plane waves which have been reflected back from the interface, in the second region, the barrier region, there will be an exponentially decaying wave which describes the tunnelling process, and in the third region at the metal 2 – insulator interface there will be only transmitted plane waves.

The three regions shown in the diagram are as follows:

Region 1 **where V(x) = 0** **for x < 0**

Region 2 **where V(x) = V_o** **for 0 < x < a**

Region 3 **where V(x) = 0** **for x > a**

Since V, the barrier height is not a function of time, the motion of the electron can be described by the time-independent Schrödinger equation.

$$E\psi(x) = -\frac{\hbar^2}{2m}\frac{d^2\psi(x)}{dx^2} + V(x)\psi(x) \qquad (2.1.)$$

Where m is the mass of the electron, h = h / 2π , and ψ(x) is the wave function associated with the electron, which is given by the general solutions of the equations in the regions l, 2, and 3 as shown in figure 2.1.

In the following discussion only cases where the energy of the electron, E, is less than the height of the barrier will be considered. For regions 1 and 3 where V(x) = 0 the time-independent Schrödinger wave equation is:

$$-\frac{\hbar^2}{2mE}\frac{d^2\psi(x)}{dx^2} + 0 = \psi(x)$$

giving

$$\frac{d^2\psi(x)}{dx^2} + \frac{2mE\psi}{\hbar^2} = 0 \qquad (2.2.)$$

The solution to this equation for region 1 is:

$$\psi_1(x) = Ie^{ikx} + Re^{-ikx} \qquad \textbf{(2.3a.)}$$

Where I, R, and T are the incident, reflected, and transmitted amplitudes respectively and the positive exponent refers to the incident wave and the negative to the reflected wave and

$$k = \frac{\sqrt{2mE}}{\hbar} .$$

and for region 3:

$$\psi_3(x) = Te^{ikx} \qquad \textbf{(2.3b.)}$$

For region 2, the time-independent Schrödinger equation is:

$$\frac{d^2\psi}{dx^2} - \frac{2m}{\hbar^2}(V_0 - E)\psi(x) = 0 \qquad \textbf{(2.4.)}$$

The solution of the equation for region 2 is:

$$\psi_2(x) = Ae^{k'x} + Be^{-k'x} \qquad \textbf{(2.5.)}$$

Where A and B are constants and

$$k' = \frac{\sqrt{2m(V_0 - E)}}{\hbar^2}$$

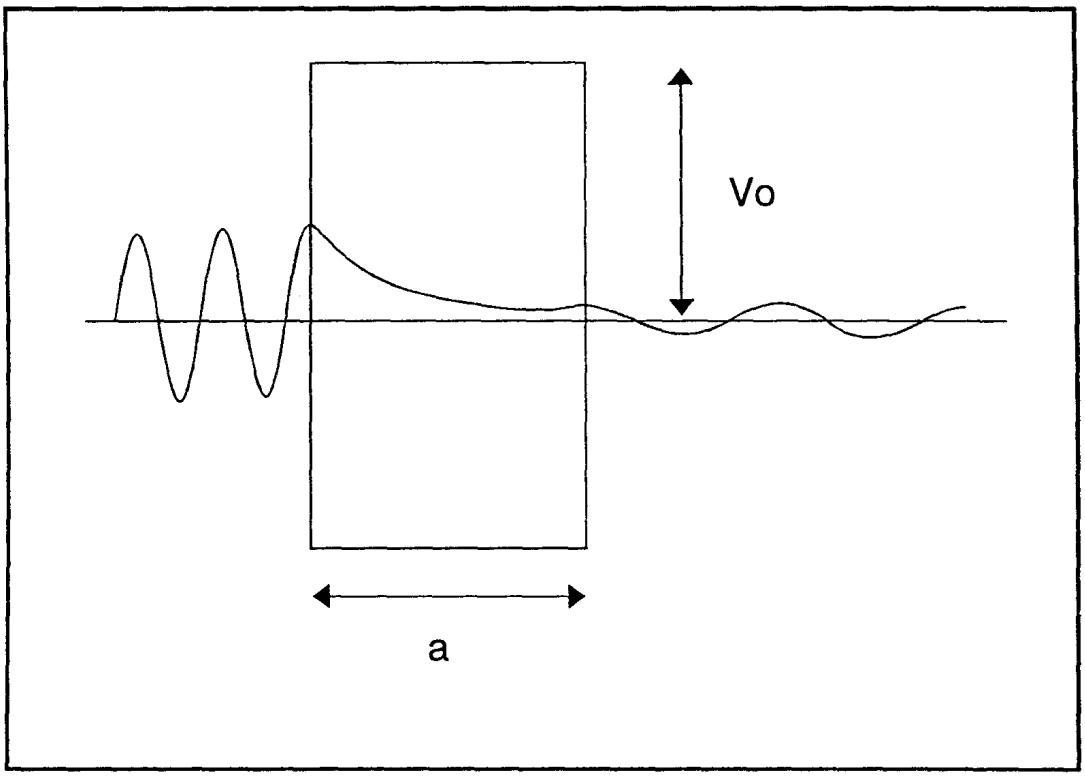

Figure 2.2

An illustration, after Giaever, of an idealised rectangular barrier of width 'a' and height Vo. The incident and reflected waves on the left would be matched to the transmitted wave on the right by using the continuity conditions referred to in the text. Within the barrier region the wave has an exponential decaying form.

The functions are sinusoidal before and after the barrier. If the functions and their derivatives are matched at the boundaries the wave function will have the form illustrated in Figure 2.2 and there will be a probability that the particle/electron will penetrate the barrier. Only the form of the eigenfunction obtained is shown in figure 2.2, $\psi(x)$ is a complex function and the figure plots only the real part of $\psi(x)$. Its exact form in region 2 as well as the ratio of its amplitudes in regions 1 and 3 will depend upon the values of Eo, Vo , a, and m.

The probability of an electron penetrating the potential barrier is defined in terms of the intensity of the probability of the transmitted flux in region 3 and the intensity of the incident probability flux. The probability flux is the probability per second of finding an electron a particular reference point and it is proportional to both the intensity of the wave and the velocity of the electron at the point.

From the equations 2.3 to 2.5 the following set of equation are obtained:

$$\mathbf{I + R = A + B} \qquad \textbf{(2.6.)}$$

$$\mathbf{ik\,(I - R) = k'\,(A - B)} \qquad \textbf{(2.7.)}$$

$$\mathbf{Ae^{k'a} + Be^{-k'a} = Te^{ika}} \qquad \textbf{(2.8.)}$$

$$\mathbf{k'\,(Ae^{k'a} - Be^{-k'a}) = ikTe^{ika}} \qquad \textbf{(2.9)}$$

Eliminating the reflected component - we require only the transmitted part - from equations 2.6 and 2.7 and then solving equations 2.8 and 2.9 to evaluate the constants A and B we obtain:

$$\frac{A}{B} = e^{-2k'a}\,\frac{(ik + k')}{(ik - k')} \qquad \textbf{(2.10.)}$$

Since for the simple rectangular barrier proposed in this analysis k'a is large

compared with unity A << B and equation 2.5 reduces to:

$$\Psi_2(a) = Be^{-k'a}$$

The form of which highlights the exponentially decaying form of the wavefunction within the barrier.

Relating this to a quantity which a physically measurable quantity the transmission probability given by:

$$\mathbf{P} = |\mathbf{T}^2| / |\mathbf{I}^2|$$

is introduced. Equation 2.10 can be simplified if it is assumed:

$$\frac{p}{q} = \frac{\sqrt{2me}}{\sqrt{2m(V_0 - E)}} = \sqrt{\frac{E}{V_0 - E}} \approx 1$$

and also if qa / ħ >> 1 equation 2.13 further reduces to:

$$I \approx Te^{ika}e^{\frac{qa}{\hbar}}$$

and the probability of transmission is:

$$P = \frac{|T|^2}{|I|^2} \approx e^{-\frac{2qa}{\hbar}} \qquad \textbf{(2.11.)}$$

e.g.

$$P = \exp\left(-2\sqrt{\frac{2m(V_0 - E)}{\hbar^2 a}}\right) \qquad \textbf{(2.12.)}$$

The analysis presented here predicts that an electron of energy E, incident on a potential barrier of height $V_o >$ E and of finite thickness - a - does have a probability of penetrating a potential barrier and being transmitted through it to

the other side. The probability is small as indicated by the large exponential term in equation 2.14 - but it is not zero as predicted by classical theory. In classical terms the limit for the transmission is as a $\rightarrow \infty$ and here the probability of transmission tends to be vanishingly small.

Assuming a mean barrier height of 5eV and an electron energy of 2eV and inserting some values for the barrier thickness (a) into 2.12, will serve to illustrate critical nature of barrier thickness.

Using equation 2.12 gives the following values for P:

a/nm	P
0.5	10-4
1.0	10^{-1}
5.0	10^{-39}
10.0	10^{-78}

Table 2.1.

Model data to illustrate the dramatic way in which the probability of tunnelling decreases as the barrier width is increased.

2.2 *Elastic Tunnelling in the presence of a Slowly Varying Potential Barrier*

The previous paragraphs of this chapter have attempted to provide some insight into quantum mechanical tunnelling via the simple model of an electron incident upon a finite barrier potential. Extending this simple model to

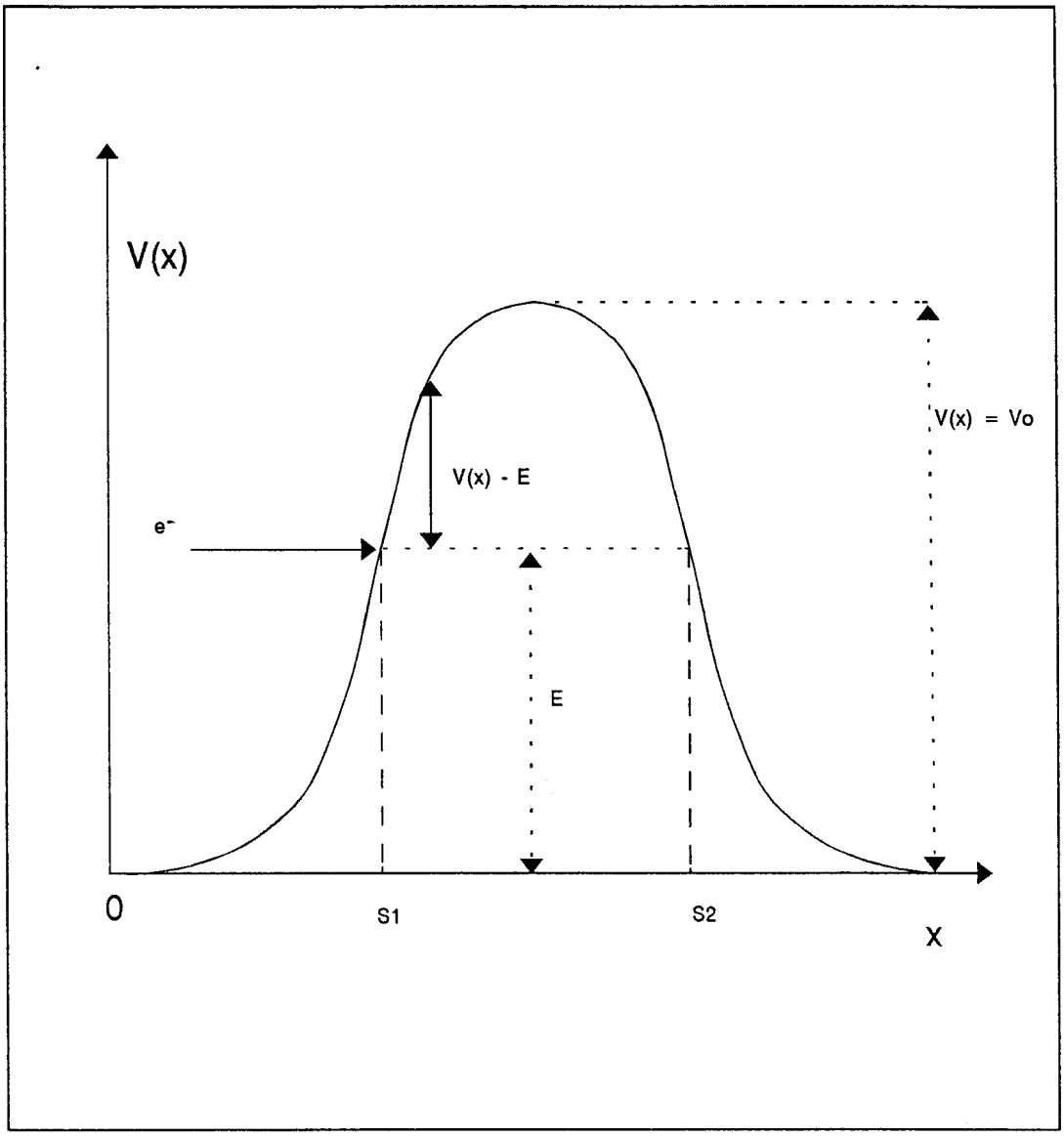

Figure 2.3

An electron incident upon a slowly varying potential barrier of an arbitrary shape.

The classical turning points are shown as S1 and S2 on the diagram.

the real case of a metal-insulator-metal junction is the subject of the next section.

Solving the Schrödinger equation exactly for more complex model to account for a varying potential in region 2 is an extremely difficult assignment [1,2]. The problem can be overcome by using an approximation known as the Wentzel-Kramers Brillouin (WKB) approximation [3]. The WKB approximation is best applied when the transmission probability through the potential barrier is small i.e. for low fields and electrons with energies close to the Fermi energy - an almost classical situation when transmission through the barrier is very small.

Consider a barrier where V(x) is now a slowly varying potential as illustrated in Figure 2.3. This is compared with the constant picture presented by the rectangular barrier. The classical turning points are shown by the positions marked s, and s, on the diagram.

A solution to the Schrödinger equation:

$$\frac{d^2\phi(x)}{dx^2} = \beta^2(x)\ \psi(x) \qquad \textbf{(2.13.)}$$

is needed, where

$$\beta(x) = \left(\frac{2m(V_0(x) - E)}{\hbar^2}\right)^{1/2}$$

Initially it is assumed that in this region the solution is of the form:

$$\psi(x) = \exp\ (\ -g(x)) \qquad \textbf{(2.14.)}$$

From which the WKB approximation for the transmission probability in region 2 may be obtained and is given by:

$$P_{WKB} = \exp\left(-2 \int_{s_1}^{s_2} \beta(x)\,dx \right) \qquad \textbf{(2.15.)}$$

Where s_1 and s_2 are the classical turning points. Substitution for β gives:

$$P_{WKB} = \exp\left(-2 \left(\frac{2m}{\hbar^2}\right)^{1/2} \int_{s_1}^{s2} [V_0(x) - E)]^{1/2}\,dx \right) \qquad \textbf{(2.16.)}$$

If V(x) is assumed to be constant at Vo within the barrier region then the expression given by Equation 2.16 reduces to the transmission coefficient for a rectangular barrier - Equation 2.12.

Amongst the many workers in the field of IETS who discussed the applicability of the WKB approximation to trapezoidal barriers and compared the results with exact transmission coefficients Gundlach and Simmon's [2] results show a correlation in which the functional form is preserved; the only difference between the absolute and WKB values is in a small pre-exponential factor.

The previous paragraphs have assumed that the motion of the electrons is one-dimensional. A three dimensional approach to the problem does not invalidate the above analysis. Most cases will involve resolving the motion of the electrons which are incident on the barrier into components which are normal and parallel to the plane of the junction. The one dimensional approach relies on the fact that since it is only the normal component of motion which instigates electron transfer it is valid to insert these values into the one dimension transmission probability. The analysis assumes implicitly that electron momentum normal to the plane of the junction is conserved during tunnelling.

2.2.1 The Elastic Current Density

Consider a theoretical MIM junction at OK shown in Figures 2.4a and 2.4b. Figure 2.4a is a simplified diagram of a plane parallel junction at zero Kelvin with no applied bias and neither metal superconducting. Figure 2.4b is of a plane parallel junction as before but now a bias V has been applied between the electrodes. Elastic tunnelling of electrons which is the predominant form of conduction in such a junction involves the isoenergetic transfer of electrons from occupied states in metal electrode (metal 1) to empty states in the opposite metal electrode (metal 2). A number of authors have discussed rigorous solutions of the equations for tunnelling electrons in metal-insulator-metal structures [1,2,4,5]. The analysis presented here will utilise a simplified treatment of the problem to estimate the elastic tunnel current density.

Taking the situation illustrated in Figure 2.4 the number of electrons available for tunnelling from metal 1 to metal 2 in unit time is proportional to the number of filled states - Z, (E) in metal 1 in an incremental energy range dE. The number of tunnelling electrons is also proportional to the number of empty states in metal 2. The total current density incident on the barrier in the x direction (J_i) is given by the product of the number of electrons (n), their charge (e), and their velocity (v_x).

$$\mathbf{J_i = nev_x}$$

Using the Sommerfield free-electron model [6] where the electrodes are considered to be free-electron metals in which the electrons are non-interacting fermions with zero potential energy within the metal and infinite potential energy everywhere else.

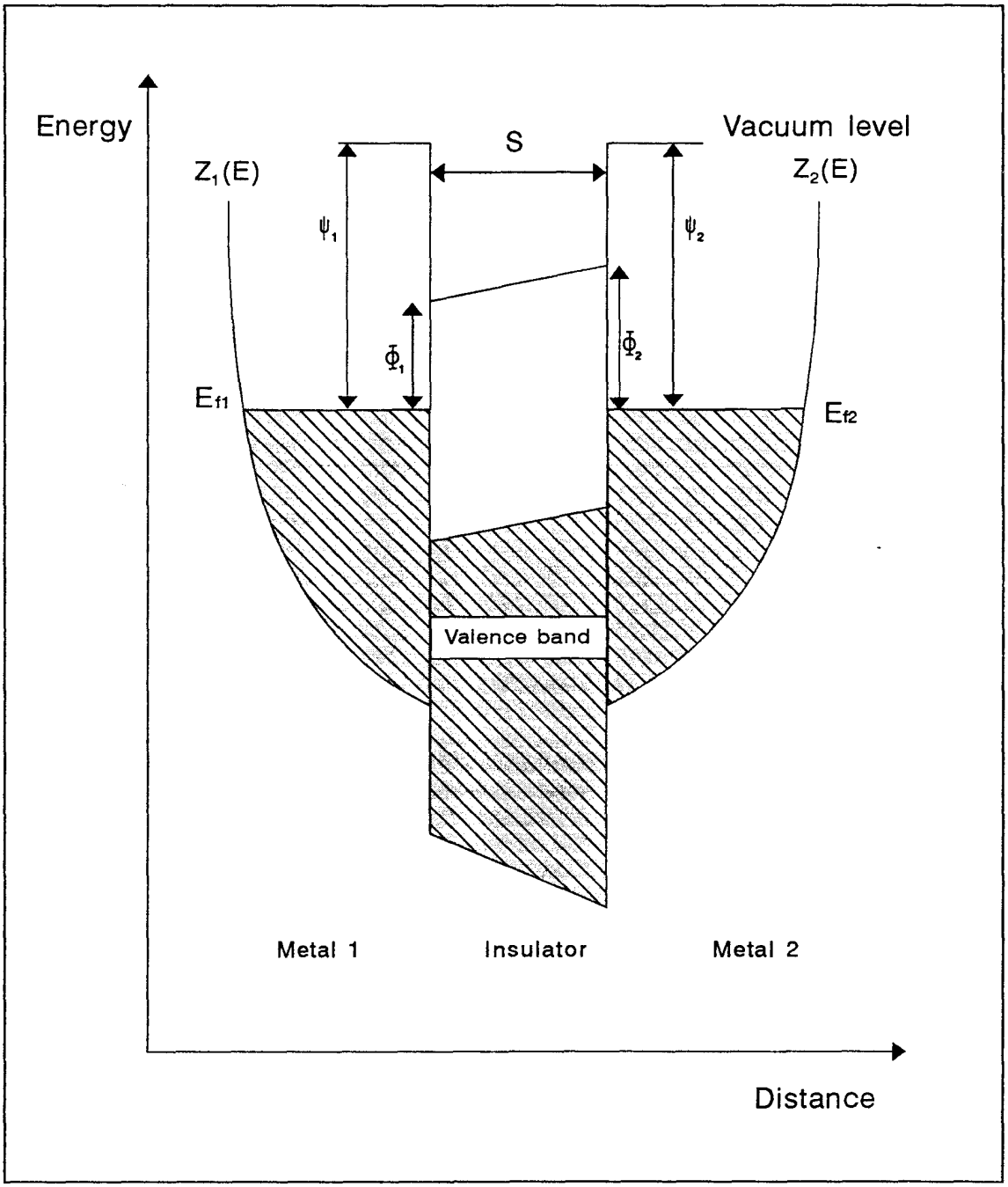
Energy
Vacuum level
S
$Z_1(E)$
$Z_2(E)$
ψ_1
ψ_2
Φ_1
Φ_2
E_{f1}
E_{f2}
Valence band
Metal 1
Insulator
Metal 2
Distance

Figure 2.4a

Figure 2.4a

This illustration is a simplified energy diagram form a metal-insulator--metal IET junction at zero Kelvin with no applied bias and where neither metal is superconducting. the Fermi energies E_{f1} and E_{f2} are at the same level. Z_1 (E) and Z_2 (E) are the density of states functions for the electrons in the two metals; Φ_1 and Φ_2^- are the interfacial barrier heights. The hatched regions in the illustrations represent the filled states within the system

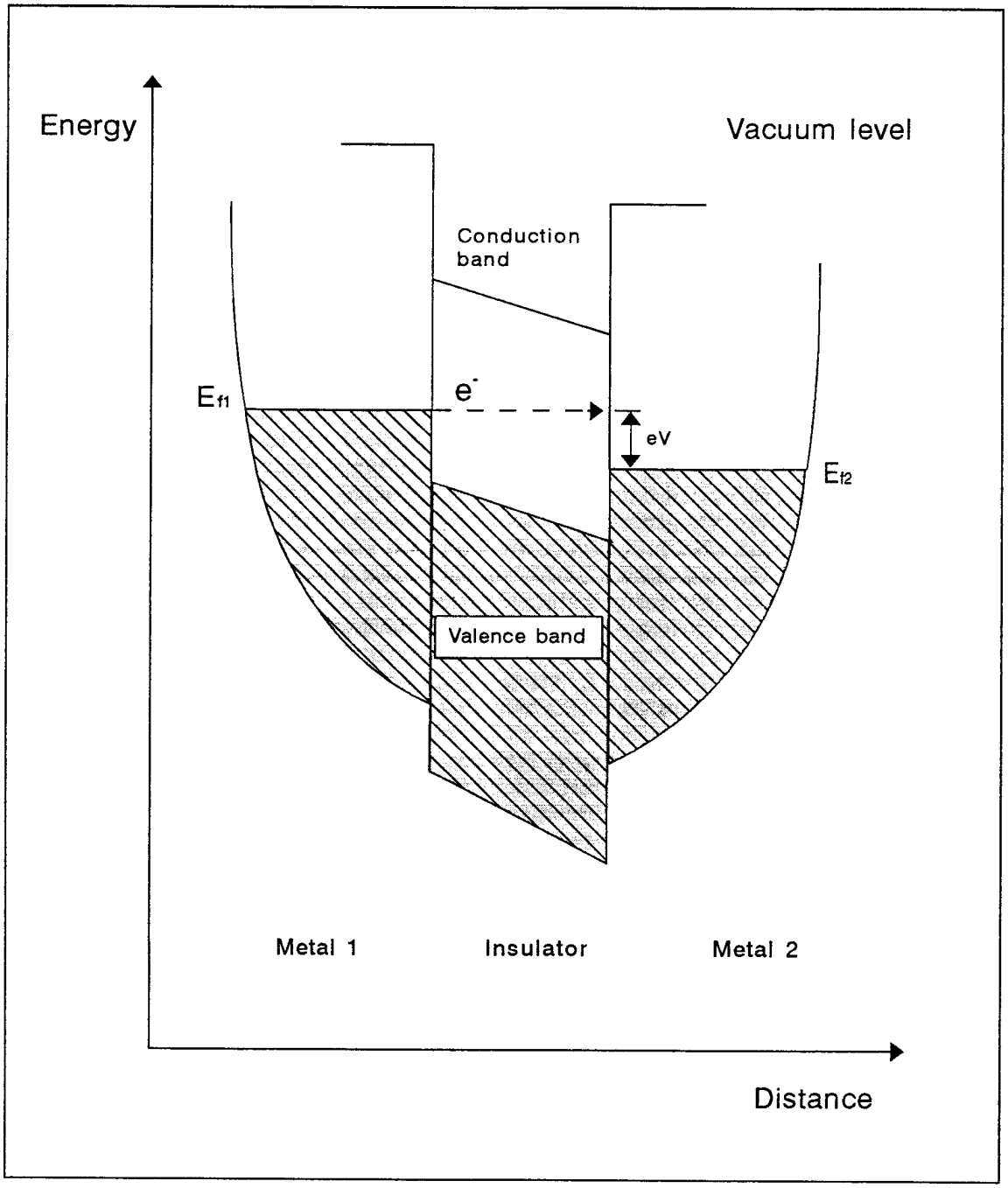
Energy
Vacuum level
Conduction band
E_{f1}
e^-
eV
E_{f2}
Valence band
Metal 1
Insulator
Metal 2
Distance

Figure 2.4b.

Figure 2.4b

This figure represents the energy diagram for a metal-insulator-metal IETS junction at zero Kelvin, neither of the metals is superconducting but in this case a d.c. bias (V) has been applied across the junction. Applying the bias has the effect of separating the Fermi energy by an amount eV as shown. Also shown in the diagram is an arrow to represent the path of an electron tunnelling elastically across the junction.

Floyd and Walmsley [5] showed that the current density incident in the x direction on the barrier is given by:

$$J_i = \frac{2e}{h}\int_{k_x}\int_{k_t} f(E)\frac{d^2k_t}{(2\pi)^2}\,dE_x \qquad (2.17.)$$

Equation 2.17 represents the number of electrons which are incident upon the potential barrier. Some of them will tunnel through the barrier and so the probability of this happening must be taken into account , also before they can tunnel through the barrier there must be empty states in the opposite electrode. If the transmission probability and the number of empty states in the second metal are taken into account the current density transmitted from metal one to metal two is given by:

$$J_{1\to 2} = \frac{2e}{h}\int_{E_x}\int_{k_t} f(E)(1-f(E+eV))\,P(E_x)\frac{d^2k_t}{(2\pi)^2}\,dE_x \qquad (2.18.)$$

where V is the potential difference applied between the two metal electrodes. It is assumed also that during tunnelling the momentum in the plane of the barrier is conserved. A similar expression - equation 2.19 below - can be obtained for the total current density flowing in the opposite direction

$$J_{2\to 1} = \frac{2e}{h}\int_{E_x}\int_{k_t} f(E+eV)(1-fE)\,P(E_x)\frac{d^2k_t}{(2\pi)^2}\,dE_x \qquad (2.19.)$$

Hence if the transmission probability for a given $E_{,,}$ is the same in either direction; the net current density is just the difference of the two equations 2.18 and

2.19 above.

$$J_T = J_{2\to1} - J_{1\to2}$$

Giving :

$$J_T = \frac{2e}{h}\int_{E_x}\int_{k_t} P(E_x)f(E) - (f(E+eV))\frac{d^2k_t}{(2\pi)^2}dE_x \qquad \textbf{(2.20.)}$$

Equation 2.20 predicts the net current density at any temperature but a more useful form of the equation can be obtained by taking a low temperature limit of T = 0 and noting that in this situation the net current density from metal 2 to metal is zero for $V \geq 0$. Using these assumptions the following expression for the tunnelling current is obtained (6]:

$$J_T = \frac{4\pi me}{h^3}\left[eV\int_0^{e_f-eV} P(E_x)dE_x + \int_{E_F-eV}^{E_F} P(E_x)(E_F-E_x)dE_x\right] \qquad \textbf{(2.21.)}$$

This equation is an expression which is representative of the relationship between the final current density and the applied voltage. If we assume that, with an applied bias V which is very much smaller than the barrier height D, P (E_X) remains constant. Equation 2.21 can be re-written as:

$$J_T = \frac{4\pi me}{h^3} P\, eV \frac{2E_F - eV}{2} \qquad \textbf{(2.22.)}$$

Equation 2.22 is of the form y = mx demonstrating that for a small applied bias, with the junction at a temperature of zero Kelvin, the elastic tunnel current should vary in a linear manner with applied bias - the current versus voltage characteristic is Ohmic in form.

2.2.3 Electron Tunnelling as a Time Dependent Perturbation

The approach outlined above has been used to calculate the elastic tunnel current density in situations where relatively simple barrier potentials exist [7]. But once the barrier potential become more complicated the calculations become very unwieldy. A more flexible method of calculating the elastic tunnel current density to a good approximation was introduced by Bardeen in 1982 [8]. Initially it was used to explain the energy gap in the current versus voltage characteristics of metal-insulator - metal with superconducting electrodes, which had been observed by Giaever [9]. The approach used by Bardeen is usually referred to the as the Transfer Hamiltonian theory of tunnelling.

It has been shown in the previous section that the probability of an electron tunnelling through a potential barrier, if its energy is less than that of the barrier, is extremely small. Therefore electron tunnelling can be treated as a small perturbating interaction between the electron states which are on opposite sides of the barrier. Small terms representing the perturbations are be added to the Hamiltonian used to describe the wave functions of the electrons [8]. Therefore the perturbation theory may be used to calculate the probability density of electrons tunnelling across the barrier and subsequently the tunnel current through the barrier [10,11].

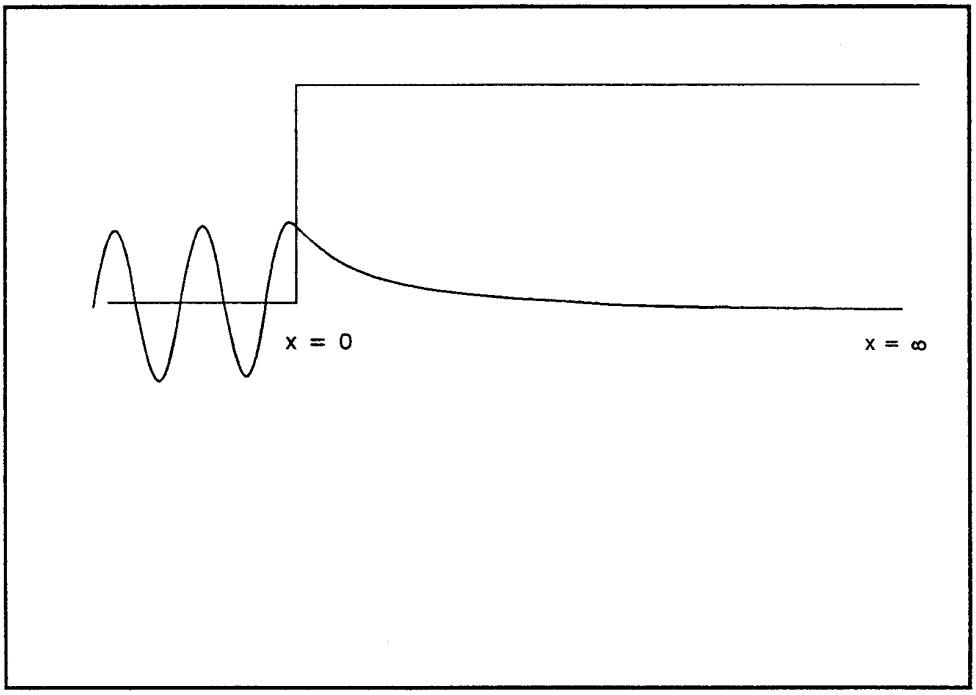

Figure 2.5a.

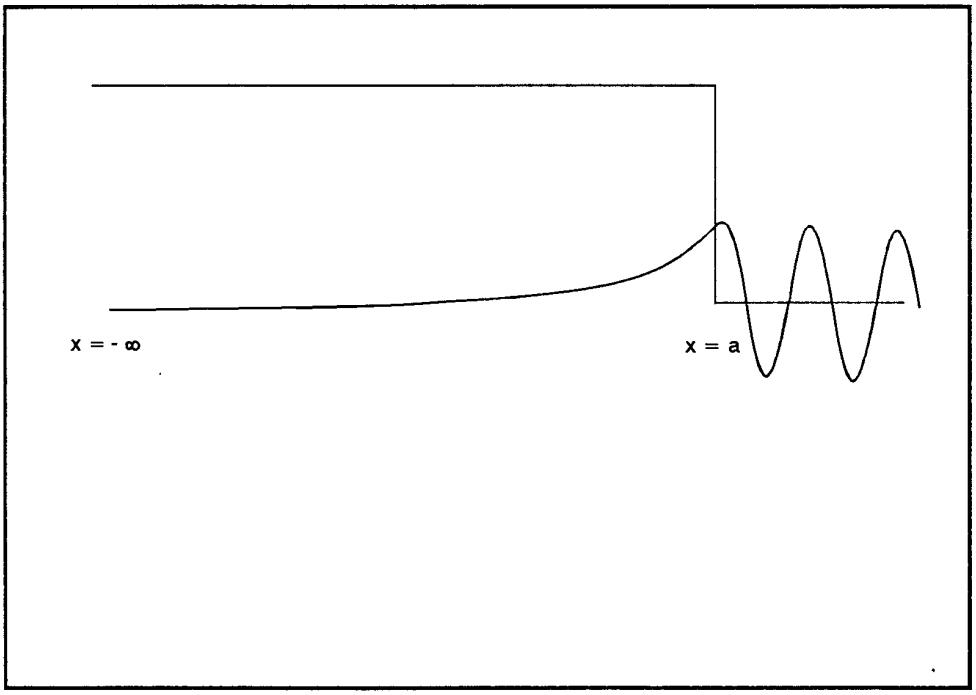

Figure 2.5b.

Figure 2.5a

In calculating the initial state wave function the transfer Hamiltonian formalism taken by Bardeen places the interface between the second metal and the insulator at infinity - compare this with the second interface situated at x = a in Figure 2.2 in the approach taken by Giaever [9].

Figure 2.5b

Continuing on the theme taken above, calculation of the final state wave function involves placing between the first metal and the insulator at minus infinity. An interaction potential is used to transfer the electron from its initial state to its final state.

Both diagrams after Kirtley [7]

The core feature of the approach taken by Bardeen was the assumption that the a MIM junction can be described by a Hamiltonian which is the sum of three terms. Two of the terms describe the wave functions in the metal electrodes, and the third is a Hamiltonian which describes the tunnelling of the electrons between the barriers:

$$\mathbf{H_S = H_A + H_B + H_T}$$

Where H_A is the function for the initial electronic state, H_B is the function for the final electronic state, and H_T is the transfer Hamiltonian which describes the tunnelling of the electrons between the two states.

Bardeen's concept of the tunnel barrier was that the potential barrier could be divided into two distinct parts. By extending x = a to x = ∞ the initial electronic state is localised on the left hand side of the barrier and the final electronic state can be treated in a similar manner by extending x = 0 to x = - ∞ to localize it on the right hand side of the tunnelling barrier - see Figures 2.5a and 2.5 b..

Then, using the WKB approximation Bardeen showed that normal to the interface the two wave functions - solutions to H_A and H_B - are sinusoidal outside the barrier and exponentially decaying within the barrier region. Then the total elastic transition rate was calculated by isolating the tunnelling matrix element and applying the 'Golden Rule' which states that the transfer rate is proportional to the matrix element squared. From the transition rate the total elastic current density was calculated.

To summarise Bardeen's approach to the problem was to turn it around and instead of introducing states which are exact solutions of the approximate Hamiltonian he chose approximate solutions of the exact Hamiltonian; this method is now usually called transfer Hamiltonian formalism.

2.2.2 Temperature Dependence of Tunnel Conductance

The above analysis of electron tunnelling does not take into account any effects on the elastic tunnel current which might be due a finite temperature. The effect of smearing the Fermi surface when T ;4 OK has been investigated by Simmons [12] and presented by Duke [1] and Stratton [13]. This section will present an overview of their findings.

At first sight it might seem that if the temperature was to be increased - at a constant bias voltage - the current flowing would also increase. But, when the height of a typical barrier of approximately 2 eV, is compared with the value of only 1/40 of an eV for kT at 300K, only small changes in conductance might be anticipated. Of course varying the other parameters to give smaller barrier heights or larger applied bias voltages will lead to larger temperature-dependant fractional increases in the conductance of the barrier. Calculations by Stratton, Duke, and Simmons [13,1,12] substantiate these assumptions. The method they used reveals a percentage conductance (OG) change relative to 0K of approximately:

$$\Delta G\ \% \ = \ 3 \times 10^{-5} \ (sT)^2 \ / \ \Phi_0 \qquad (2.23.)$$

Where s = the barrier width in nm and Φ is the mean height of the barrier in electron volts.

Taking $eV < \Phi_0 /2$ gives the results listed in Table 2.2 on the following page.

Φ_0 / V	T / K	s/nm	ΔG%
1.5	300	1.5	4.1
1.5	300	3.0	16
3.0	300	1.5	3.4
3.0	300	3.0	13.5

Table 2.2

Percentage conductance change for two value of barrier thickness and two values of barrier height.

The calculation shown in Table 2.2 show the variation in conductance for two values of barrier thickness. Equation 2.34 also shows that there is a slight quadratic dependence of the conductance on temperature. The feature outlined in the equation was used by Ginnai [14] to determine whether tunnelling was the dominant conduction process, within a given range of temperature/ voltage.

2.3 Superconductivity

Conclusive proof of electron tunnelling between metal electrodes requires that at least one of the metals is in a superconducting state [15]. Although superconductivity was discovered around 1911 by Kamerlingh Onnes [16], it was not until 1957 when Bardeen, Cooper, and Shrieffer [17] published a theory which utilised the concept of paired electrons proposed by Cooper in 1956. The theory which earned Bardeen, Cooper, and Shrieffer a Nobel prize in 1972, is now called

the BCS theory. The theory postulates the existence of a forbidden energy gap centred on the fermi level of superconductors. Which results in deviations from the ohmic tunnelling characteristics obtained when tunnelling in normal metals. The theory proposes that below a temperature electrons within a metal can form into pairs, each pair being held together by an attractive force whiah is transmitted via a virtual phonon.

2.3.1. The BCS Theory of Superconductivity

A theory was put forward by Frohlich which proposed that an electron - phonon interaction was able to couple two electrons together in such a way as if there was a direct interaction between them. Because of the conservation of energy and momentum when an electron is scattered by the lattice one of the vibrational modes of the lattice must be excited. The vibrational motion is quantized and considered to be the emission or adsorption of a phonon. Frohlich was able to show that in certain circumstances if an electron caused the emission of a phonon which was then immediately absorbed by another electron a weak interaction could exist between the two electrons. The interaction between the two electrons can be thought of as being transmitted by the phonon.

It was demonstrated by Cooper that if a net attractive force existed between pairs of electrons , at zero Kelvin the lowest energy state of the system, would be one in which the electrons would be associated in pairs, now termed Cooper pairs. Bardeen, Cooper, and Schrieffer used Cooper pairs to provide a more complete explanation of superconductivity.

The following explanation follows that given in " Introduction to Superconductivity" [18]. Consider an electron being scattered by the lattice, energy and momentum

must be conserved during the process and one of the vibrational modes of the lattice is excited – emitting or absorbing a phonon in the process. Fröhlich proposed that if the emitted phonon was immediately absorbed by another electron there would be a weak attractive interaction between the two electrons. Let the phonon have energy $q = h\upsilon / s$ where υ is the vibrational frequency of the phonon, s is the velocity of sound, and h is Plank's constant. During the emission of the phonon momentum is conserved and for the first electron we may put - $p_1 = p`_1 + q$. where $p_1$ and $p`_1$ are the momenta of the electron before and after scattering respectively. Consider that the phonon is now immediately absorbed by a second electron whose momentum changes from p_2 to p'_2 and so we can write $p_2 + q = p´_2$. Where p_2 and $p´_2$ are respectively the momenta of the electron before and after absorbing the phonon. Therefore from the two equations it con be shown that $p_1 + p_2 = p´_1 + p´_2$. this shows that the momentum before and after the interaction is conserved as we would expect it to be.

During the scattering process there is a mutual interaction between the electrons and if this is an attractive one, the resulting potential energy is negative. Over a period of time there are any scattering events and the energy of any two electrons is decreased by the time average of this negative potential energy – the amount of the decrease being proportional to the number of scattering events. The largest number of events yields the maximum lowering of the energy and this occurs when the momenta of the two electrons is equal and opposite.

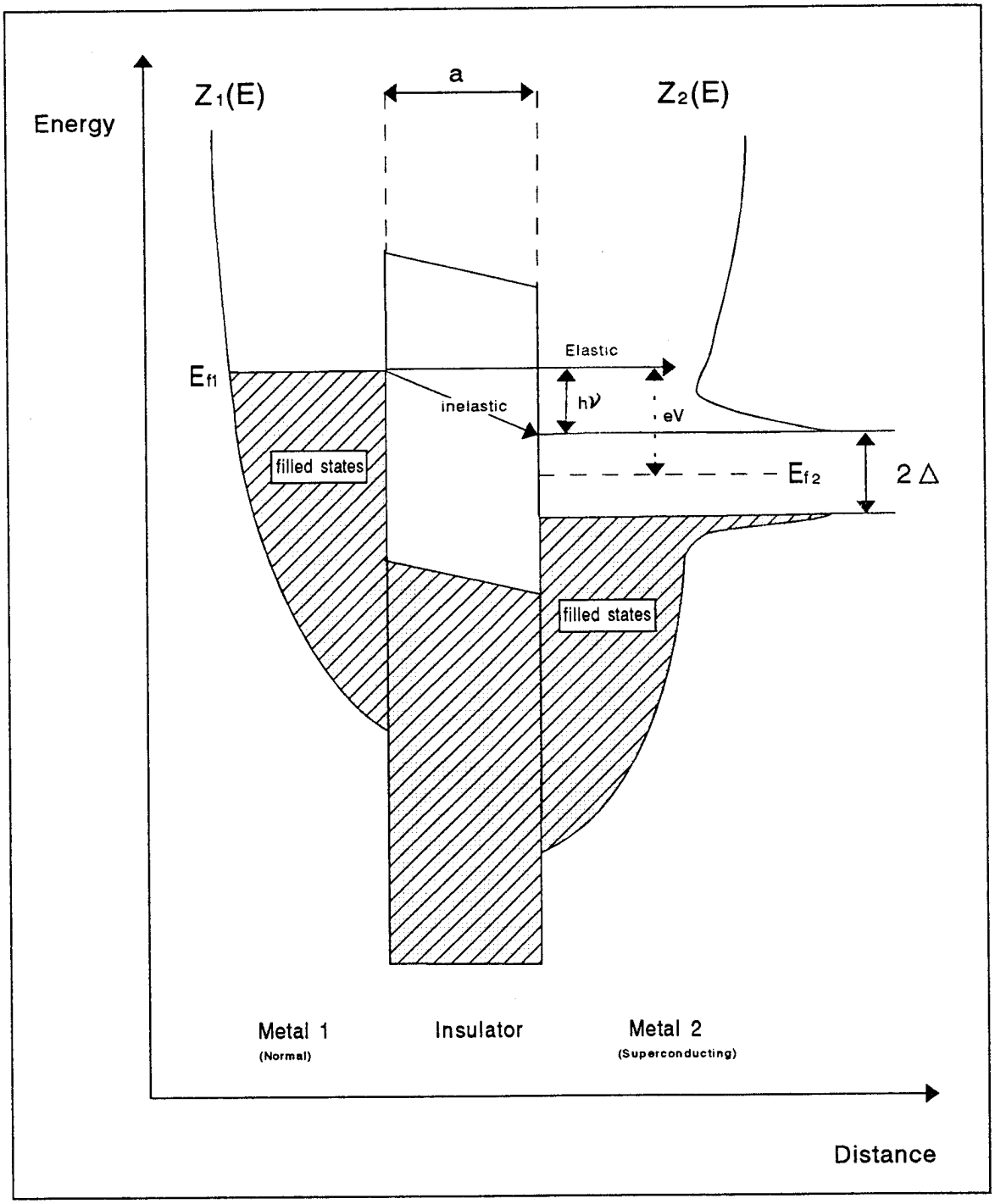
Energy
Z1(E)
a
Z2(E)
Elastic
Ef1
inelastic
hν
eV
filled states
Ef2
2 Δ
filled states
Metal 1
(Normal)
Insulator
Metal 2
(Superconducting)
Distance

Figure 2.6.

Figure 2.6

A simplified diagram showing the electron energy for a normal metal - insulator - superconducting metal IETS junction a zero Kelvin. Illustrated on the diagram are the transitions for both elastic and inelastic tunnelling of electrons.

After Keil et. al. [20).

A situation can also exist where an interaction has taken place and a phonon has been emitted but not yet absorbed. Provided that the time taken for the event is very short the uncertainty principle dictates that energy need not be conserved between the initial and intermediate state – where the first electron has emitted a phonon but the second has not yet absorbed it, or between the intermediate state and the final state. This is because there exists an uncertainty relationship between the energy (E) and time (t) whish has the form:

$$\Delta(E)\ (\Delta t) \approx \hbar$$

If the lifetime of the intermediate state is very short, there will be a large uncertainty in its energy, so that the energy does not have to be conserved in the emission and absorption process. These processes in which energy is not conserved are termed *virtual processes* and a virtual emission of a phonon is only possible if there is a second electron ready to absorb the phonon almost immediately after its emission.

It can also be shown that if the energy of the emitted phonon is greater than the energy reduction of the emitting electron then there will be an attraction between the two electrons. Opposing this attraction will be a Coulomb repulsion due to the like charge of the two particles, but if this is less than the attractive force the two will co-exist as a Cooper pair. The interactive phonon process will continue to scatter paired electrons between states whilst conserving their momentum. The probability of scattering can only be appreciable if there is only a small difference in energy between the initial and intermediate states; the initial and final energies of the emitting electron cannot be much more than the average lattice phonon energy = $h\nu_p$.

When paired, the electrons have a propensity to collect in a single state energy called the BCS ground state. This has the effect of redistributing the electron

energy of the system into a state where its total energy is less than that found in a normal metal at the same temperature. The new energy distribution is characterised by a forbidden energy gap 2ΔE, centred on the Fermi level of the superconductor - see Figure 2.6. The width of this gap is equivalent to the energy which is needed to break a Cooper pair at the temperature of the experiment. The BCS ground state described above produces a new electron energy distribution in which the total energy of the system is less than that found in normal metals at the same temperature. This new density of states function has the following forms [19]:

1. for $|E| \geq \Delta$

$$N_s(E) = N_n(E)\left[\frac{|E|}{(E^2-\Delta_0^2)^{1/2}}\right] \qquad (2.24.)$$

and

$$N_s(E) = 0 \qquad (2.25.)$$

2. for $|E| < \Delta$

Where N_n is the density of states for 'normal' electrons, 2Δ is the energy gap, and the two subscripts s and n stand for superconducting and normal states of the metal respectively. Therefore from 2.26 and 2.27 it can be seen that the density of states is zero in the range $\pm \Delta_O$ at the Fermi energy - there is a gap - whereas above and below this gap the density of states is large and decreases/increases asymptotically towards the gap from above and below.

As stated before the tunnel current is proportional to the density of isoenergetic filled and unfilled states of the two metals forming the electrodes of the tunnel junction. Giaever and Megerle [15] built upon the work done by Bardeen [8]

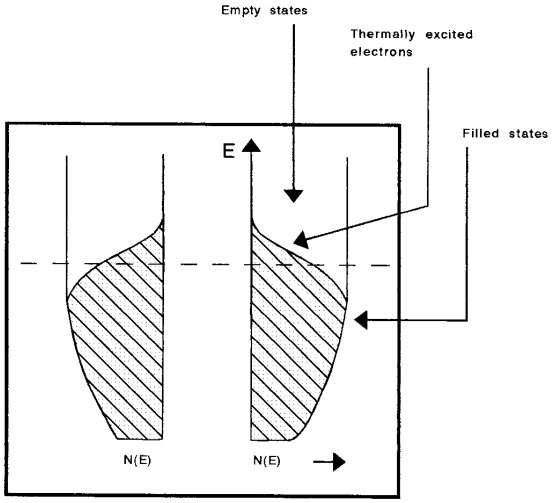

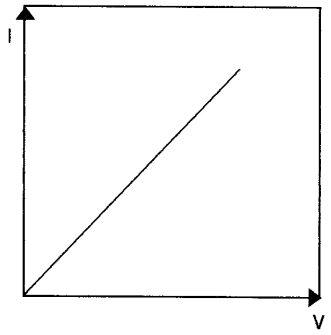

Figure 2.7a

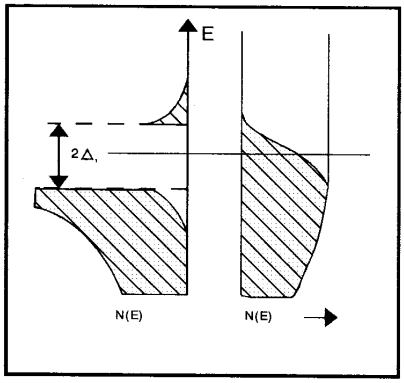

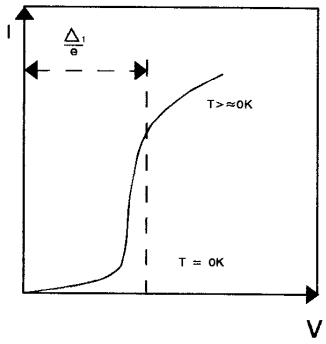

Figure 2.7b

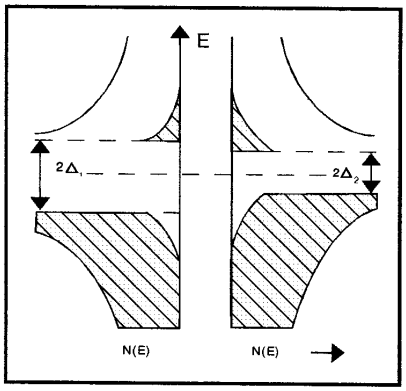

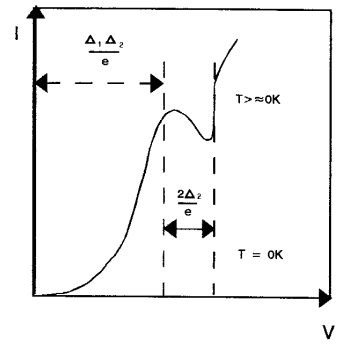

Figure 2.7c

Figure 2.7

An illustration after Giaever and Megerle [15] showing the density of states curves together with their respective I versus V characteristics of three junction electrode combinations close to zero Kelvin.

a) Both metals normal.

b) One metal superconducting.

c) Both metals superconducting.

See the accompanying text for a fuller explanation of the details.

to show that if the applied voltage is small the elastic tunnel current from metal 1 to metal 2 may be shown to be:

$$I_{1-2} = A\int_{-\infty}^{\infty} n_1\, n_2 \left[f(E) - F(E+eV)\right] dE \qquad (2.26)$$

Where n_1 and n_2 are the bensity states in the two metals forming the electrodes and A is a constant.

If one of the electrodes is superconducting and one normal, then at 0K, the conductance between superconducting and normal is directly proportional to the relative density of states in the superconducting metal. If the density of states in the two metals is constant over the range of the applied bias then Ohmic behaviour would be expected - see Figure 2.7b.

Figure 2.7b illustrates the situation where the Fermi level of the normal metal faces the forbidden energy gap of the superconducting metal. In this condition, at OK, the applied bias must be changed by ± half of the superconducting energy gap in order for current to flow. At temperatures other than OK thermal smearing of the electron energies around the Fermi levels will allow some current to flow.

Figure 2.7c shows a condition where both of the metals are superconducting, with energy gaps of $2\Delta_1$, and $2\Delta_2$. In this situation tunnelling can only occur when the applied bias $V = (\Delta_1 - \Delta_2)/e$. Upon increasing the applied bias the current will decrease because the density of states available for tunnelling into decreases with increasing energy above the gap. When the bias $V = ((\Delta_1 + \Delta_2) / e$, most of the unexcited electrons in one metal are brought opposite empty states in the other one and current will increase asymptotically towards the characteristics of two normal metals. At 0K no current can flow until $V = ((\Delta_1 + \Delta_2) / e$ has been applied. Therefore electron tunnelling in metal - insulator - metal structures can be identified by the dependency of the current

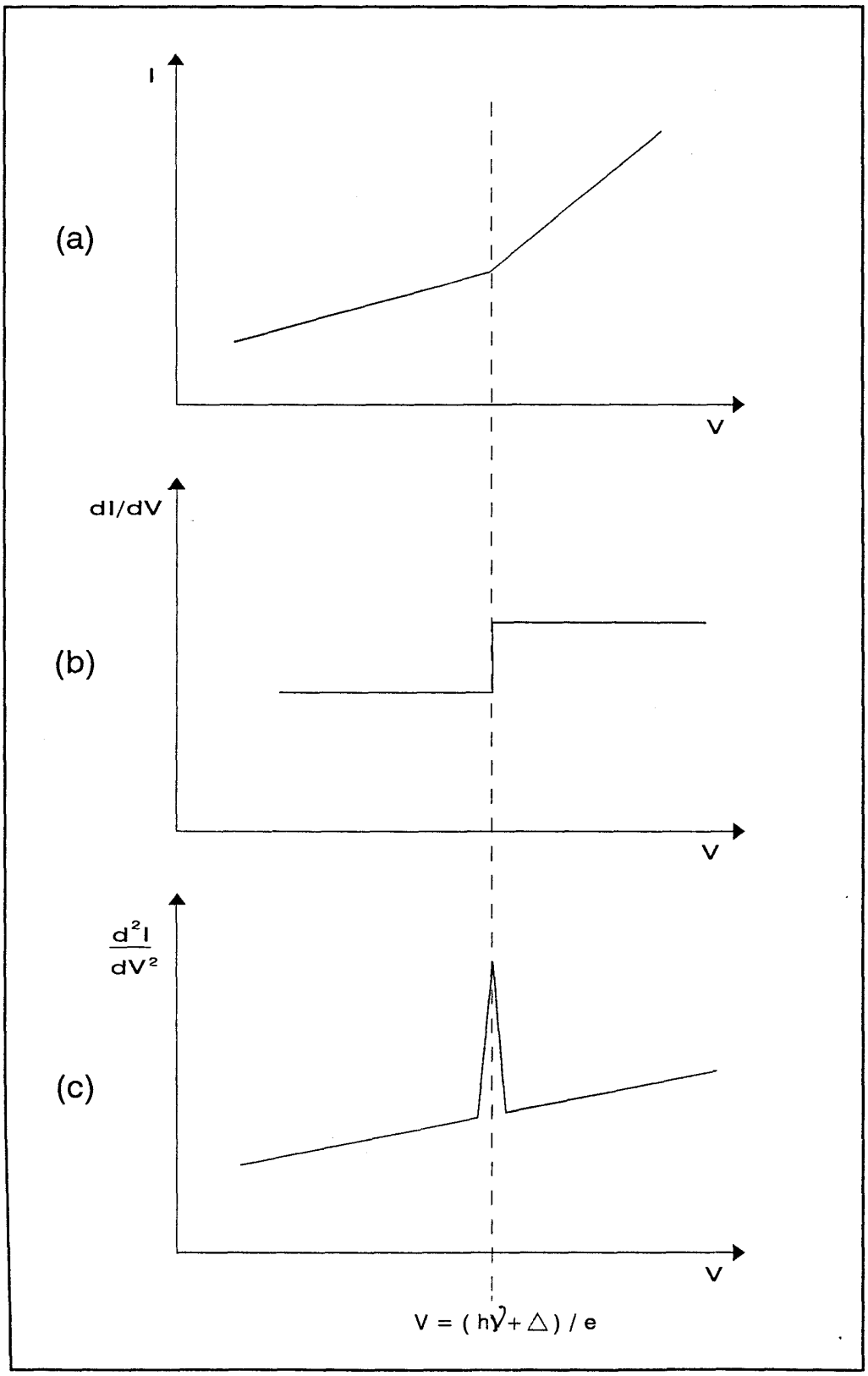

Figure 2.8.

Figure 2.8a

An inelastic interaction within the tunnel barrier will cause a small but significant increase in the total current flowing through the junction. this increase will reveal itself as an increase in the gradient of a plot of current versus voltage curve.

Figure 2.8b

The increase in the gradient as shown above in Figure 2.8a will be revealed as a step function in the first differential (dI/dV) versus V plot.

Figure 2.8c

Taking the second differential (d^2I/dV^2) and plotting the result versus V will reveal the changes due to the inelastic events as a delta function which has been smeared by thermal and other effects. It is these peaks positioned at $eV = h\nu + \Delta$ as shown in the figure which are referred to as the inelastic tunnelling spectrum. the energies are indicative of the energies involved in exciting the various molecular oscillators within the tunnel junction.

dependency of the current on the applied bias and the temperature of the experiment if one of the metals is allowed to go into a superconducting state.

2.4 Inelastic Electron Tunnelling

If the energy diagram for a MIM junction at absolute zero with one electrode superconducting as shown in Figure 2.7b is reconsidered, it can be seen that the electrons have an energy spectrum which is characterised by a band of forbidden energies. This band, denoted in the previous paragraphs by 2Δ, is centred on the Fermi level where at OK all of the electron energy states are filled below the gap and are empty above it.

Applying a bias voltage (V) across the junction will separate the two Fermi levels by eV. This will have the effect of placing empty states in one electrode opposite the filled states in the other and provided that the voltage being applied is greater than or equal to Δ / e electrons can tunnel isoenergetically from filled states on one side to empty ones on the other. If a molecular oscillator whose vibrational frequency is ν is now implanted in the barrier there exists a situation in which the electrons traversing the barrier could interact with and excite the oscillator. As a consequence of the interaction the electron would lose a quantum ($h\nu$) of energy and continue on to end up in a lower energy state in the opposite electrode. Whilst the elastic electron tunnelling begins at $V = \Delta/e$, the onset of the inelastic process described above will open up a conduction process which takes place at $eV = h\nu + \Delta$ as illustrated in Figure 2.8a. These inelastic electron tunnelling processes represent an opening up of extra conduction channels in the junction. The result of this is as each of these channels are opened up the inelastically tunnelling electrons will add to the total tunnel current thus producing a small increase in the total current at a specific bias voltage. These processes will be revealed as a step

function in the first differential (dI / dV) of the junction and 'peaks' in the second differential at eV = by + A. It is these peaks which are recognised as the inelastic electron tunnelling spectrum, their position in the spectrum being indicative of the energies lost by the electrons in exciting the various molecular oscillators within the IET junction.

A plot of the second differential of the current versus the applied bias is called an inelastic electron tunnelling spectrum and it is the basis of Inelastic Electron Tunnelling Spectroscopy (IETS) [20,21]. The inelastic processes which open up the inelastic tunnelling channels also include molecular vibrations which are analogous to Raman vibrational energies, infra-red molecular vibrations [22], electronic transitions, and phonon excitations within the metal electrodes [23]. The shape of the peaks will depend upon thermal smearing of the Fermi surfaces of the metals, effects in the density of states due to the use of superconducting electrodes, and the natural line-shape of the excitation.

The majority of tunnelling electrons suffer no loss of energy when traversing the barrier and constitute the majority of the tunnelling current with the inelastic tunnelling electrons making up typically 1 % or less of the total tunnelling current.

The tunnelling of electrons via inelastic interactions with the molecules within the barrier can be explained in terms of a one-electron model. This model was first proposed by Scalapino and Marcus in 1976 [23]. Later, in 1968, their theory was modified by Lamb and Jaklevic [24] to include electronic interaction with the polarizability of the molecule which would account for the Raman active modes which can be seen in the IET spectra. These molecules are discussed in the following section of this thesis.

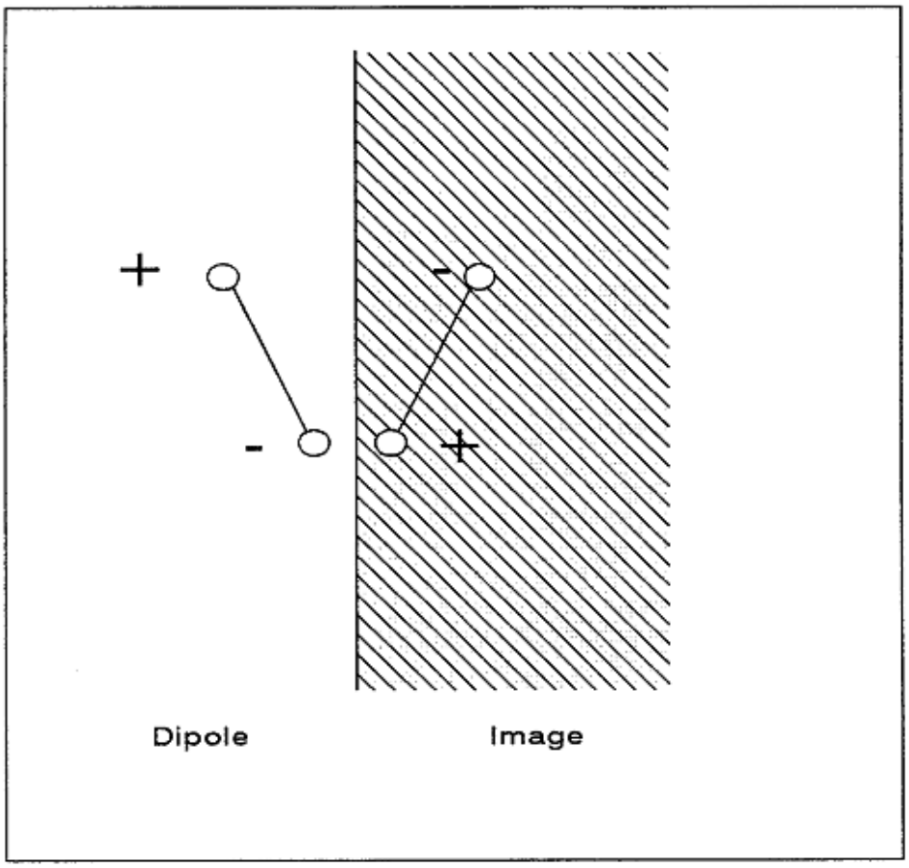

Figure 2.9a

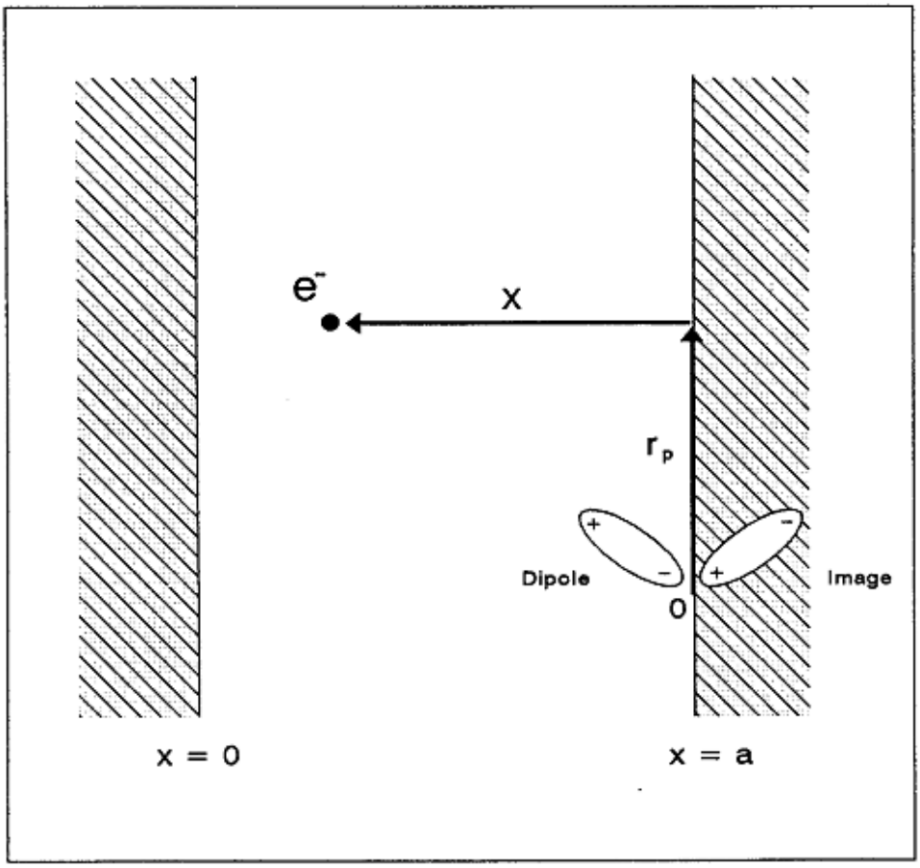

Figure 2.9b

Figure 2.9a

Scalapino and Marcus proposed that a molecular dipole which is situated near to one of the metal electrodes in a tunnel junction will induce an image of itself in the metal as shown in the figure. The component of the dipole which is parallel to the plane of the metal surface will be equal and opposite and therefore tend to cancel each other out, whereas the component which is perpendicular to the surface and its image will add together to give a net perpendicular sum.

Figure 2.9b

Using the coordinate system shown:

The parallel component will tend to be cancelled out by its image but the perpendicular component and its image add to give a net sum of $2p_x$. If the dipoles are - as assumed in the theory - points then the sum will act through the point shown by O in the diagram, and may interact with a tunnelling electron (e^-).

2.4.1 One - electron Model of Inelastic Electron Tunnelling

Scalapino and Marcus [23] considered the case in which the electric field of a tunnelling electron interacts with the Coulomb potential of an oscillating molecular dipole (and its image) which is situated near to one of the electrodes. They proposed that the image in the electrode would cancel the parallel component of the dipole moment and reinforce the perpendicular component of the dipole, relative to the plane of the junction - see Figure 2.9. The coupling of the dipole and its image was considered to be a perturbation of the barrier height.

Consider an oscillating point dipole situated inside the insulating layer and close to one of the electrodes in a metal - oxide - metal junction, as shown in Figure 2.9. The probability that a tunnelling will interact with a dipole can be obtained by utilizing the 'Golden Rule' of quantum mechanics [25]. The rule states that the probability per unit time that a tunnelling electron interacts with a dipole is proportional to the appropriate matrix element squared and so we can put:

$$P_{1\to 2} = \left(\frac{2\pi}{\hbar}\right) |M_{1\to 2}|^2 \, \delta\left(E_1 - E_2 - h\nu\right) \qquad (2.27.)$$

Where $P_{1\text{-}2}$ is the transition rate for inelastic tunnelling, $|M_{1\text{-}2}|$ is the matrix element for transmission and describes the electron - molecule interaction for the transfer of

electrons from metal 1 to metal 2, and $\delta(E_1 – E_2 - h\nu)$ is a delta or step function which ensures that $\delta(x) = 0$ unless $x = 0$ thus implying that $E_1 = E_2 + h\nu$. Scalapino and Marcus [23] approximated the electron - molecule interaction by the Coulomb interaction between the dipole moment of the molecule and the electron

$$U_i(x) = \frac{2ep_x x}{(x^2 + r_p^2)^{3/2}}$$

Where x, p, and r are defined as in Figure 2.9.

The interaction U_i (x) is treated as a perturbation on the barrier potential U(x) - assuming the barrier to be idealised as rectangular. Since the perturbation is assumed to be small for a simple rectangular barrier the initial and final wave functions can be evaluated by using a WKB approximation giving [24]:

$$|M_{1\to 2}| \propto \exp\left[-\int_0^s \left(\frac{2m}{\hbar}\right)\left[U(x) + U_i(x) - (E - E_p)\right]\right]^{1/2} dx$$

Where E is the total electron energy and Ep is the component of an electron's kinetic energy which is perpendicular to the direction of the current flow. Assuming that there are N molecular dipoles within the barrier Lamb and Jaklevic derived an expression for the inelastic tunnel current which is due to the electron - dipole moment interactions [24].

$$I_{inelastic} = N G_0 \frac{4\pi e}{\hbar \phi} \ln\left|\frac{s}{r_0}\right| \sum_m |\langle m|p_z|0\rangle| \times \int_{-\infty}^{\infty} f(E)[1 - f(E + eV - h\nu)](N_1(E)\, N_2(E + eV - h\nu)\, dE \qquad \textbf{(2.28.)}$$

Where the transition rate has been summed from 0 to m vibrational states. N, and NZ are the density of states of the two metals forming the electrodes, G_0 is the elastic conductance of the junction, and Φ is the maximum height of the barrier.

This expression embodies an important difference between elastic and inelastic electron tunnelling; the Fermi functions in the inelastic case are written assuming that the transitions are unidirectional - one-way only from metal 1 to metal 2. The term In $|s/r_0|$ represents a cross-section for tunnelling and r_0 a cut-off radius below which the dipole approximation no longer holds.

The reason for the difference in the Fermi factors is that in the case of elastic tunnelling it is equally likely that transitions will take place in both directions. The excitation energies and the low temperatures which give rise to the thermal smearing of the electron energy distribution in inelastic tunnelling ensure that all of the molecules are in their ground state and consequently no flowing of electron from 'final' to 'initial' states is possible. Therefore inelastic electron tunnelling is a one-way process [22].

This model by Scalapino and Marcus [23] predicts that the size of the increase in conductance due to the inelastic interactions is proportional to the square of the dipole matrix element - $|\langle m|p_2|0\rangle|^2$ The ratio of the inelastic junction conductance to the elastic conductance is given by:

$$\frac{G_{inelastic}}{G_{elastic}} = \frac{|M_{inelastic}|^2}{|M_{elastic}|^2}\,\delta(eV - h\nu)$$

where M is the matrix element for transmission.

An estimate of approximately 1% for the increase in conductance due to inelastic

interactions was made by Scalapino and Marcus [23], a figure which compares favourably with measured data taken by Lamb and Jaklevic [24]. In practice the intensities of peaks in IETS and IR generally show a good correlation with infra-red and orientation predictions except that there are extra peaks in IETS spectra. Lamb and Jaklevic extended the above model to include Raman interactions between the molecules and electrons through the polarizability of the molecule. The electrons electric field interacts with the molecule polarizing the molecule to induce a dipole moment in it, the electron then interacts with this induced dipole.

The interaction potential is given by [24]

$$U_{interaction}(\alpha) = -\left(\frac{4e^2\alpha x^2}{(x^2 + r_p)}\right)^3$$

Where α is the polarizability of the molecule and other symbols are as previously defined. The vibrational modes described by this interaction are those which are seen in Raman spectroscopy and are assigned, in IETS as being Raman active modes. Lamb and Jaklevic [24] derived a similar expression for the ration of elastic to inelastic conductance due to the excitation of these Raman modes by following the procedure of Salapino and Marcus [23]. Lamb and Jaklevic predicted conductance changes which were of the order of 1/10 the changes for infra-red modes - 0.1% to 0.5% c.f. 1% for infra-red.

2.4.2. The Kirtley Scalapino and Hansma (KSH) Theory

The theories of Scalapino and Marcus and Lamb and Jaklevic were able to

predict to within an order of magnitude peak intensities, but there were difficulties due to the assumptions they made when formulating their respective theories. These are highlighted in "Tunnelling Spectroscopy, Capabilities, Applications, and New Techniques " [7].

The full theory is beyond the scope of this work but the main points are listed below.

1. Kirtley, Scalapino, and Hansma [26] did not use the dipole approximation, instead they assumed that the molecular potential to be the sum of the Coulomb potentials due to a set of partial charges which were localized on each atom of the molecule. The partial charges arose from the uneven distribution of the bonding electrons.
2. Whereas both Lamb and Jaklevic and Salapino and Marcus only considered the nearest image in the metal electrode. KSH considered the images of partial charges.
3. KSH took into consideration the off-axis scattering by assuming that the momentum parallel to the interface is not conserved.
4. Bond polarizability was not considered.

5. All three groups defined the initial and final state wave functions using the WKB approximations, KSH used the transfer Hamiltonian formalism to transfer electron across the barrier, this meant that they could incorporate more complicated interaction potentials in their theory.

2.4.3. Predictions Arising from KSH Theory

A number of important predictions arise from the KSH theory, these are isted below:

1. They calculated the change in the ratio of elastic to inelastic tunnel junction conductance due to a monolayer of hydroxyl ions to be approximately 0.5%. Experimental determinations of this value put it at around 0.4%.
2. The selection rules due to orientation are the same for all three theories when the molecules are close to one metal electrode. Dipoles are oscillating perpendicular to the plane of the interface couple more strongly with tunnelling electrons and therefore should produce stronger IET spectral lines. KSH showed that contrary to this molecules which reside near to the centre of the barrier give rise to stronger IET spectral lines when their dipoles are oscillating parallel to the interface.
3. A consequence of number two above is that Raman active modes should be seen even if molecular polarizability is not included in the molecule - electron interaction.
4. It was shown that using reasoning similar to that used in 3 above, modes which are neither Raman or infra-red should also be observed; these are termed optically forbidden modes.
5. Certain vibrational modes show changes in the ratio of their elastic to inelastic conductances which are dependent upon the bias polarity.

The predictions of the Kirtley, Scalapino, and Hansma theory have, to some

extent, been born out by experiment. Kirtley and Hall [27] and Hall and Hamsma [28] using a range of adsorbates have shown qualitative agreement with KSH predictions of peak intensities and orientational behaviour. Hipps and Mazur [29] have shown some evidence for the existence of optically forbidden modes in the IET spectra.

The Kirtley, Scalapino, and Hansma theory [26] has proved to be reliable to date but there still exists plenty of scope for further work to extend the comparison to cover more complicated molecular species.

2.5 Resolution in IETS

The width of the natural lines in IETS are modified by a number of external factors. In addition to the natural width of the lines in IETS spectra, there are three contributions which contribute to the broadening of peaks and hence to the available resolution.

These are:

1. A broadening caused by thermal smearing of the electron energy distribution near to the Fermi energy.
2. Peaks are also broadened by the instrument and techniques used to detect and recover the vibrational modes.
3. The effect of superconducting electrodes.

25.1 Thermal Broadening

Thermal broadening was first discussed by Lamb and Jaklevic [24] and we will follow their method.

First consider an IET vibrational mode of energy hp. For T > OK electrons may be excited into states above the Fermi energy. As a consequence the applied bias voltage (V) required to excite a mode may be greater than by hν/e. Consider the diagram in Figure 2.10 in which is illustrated the situation where the Fermi function is shown thermally smeared where the density of electron states is slowly varying near to the Fermi energies in the two metals. In the illustration f(E), represent the filled states in metal on one side of a MIM junction and 1 - f(E) represent the unfilled states in metal on the opposite side of the junction. In this situation where the density of electron states is slowly varying near to the Fermi energies the inelastic tunnelling current can be expressed as:

$$I_{inelastic} = C \int_{-\infty}^{\infty} f(E)[1 - f(E + eV - h\nu)]\, dE \qquad \textbf{(2.29.)}$$

For simplicity the constant C contains all of the details of the electronmolecule interaction. The equation 2.30. expresses the condition that the electrons must tunnel from filled states in one metal to empty states in the metal opposite. Integrating gives from 2.31:

$$I_{inelastic} = C(eV - h\nu)\, \frac{e^x}{e^x - 1} \qquad \textbf{(2.30.)}$$

Where x = (eV - hν) / kT - k is the Boltzman constant.

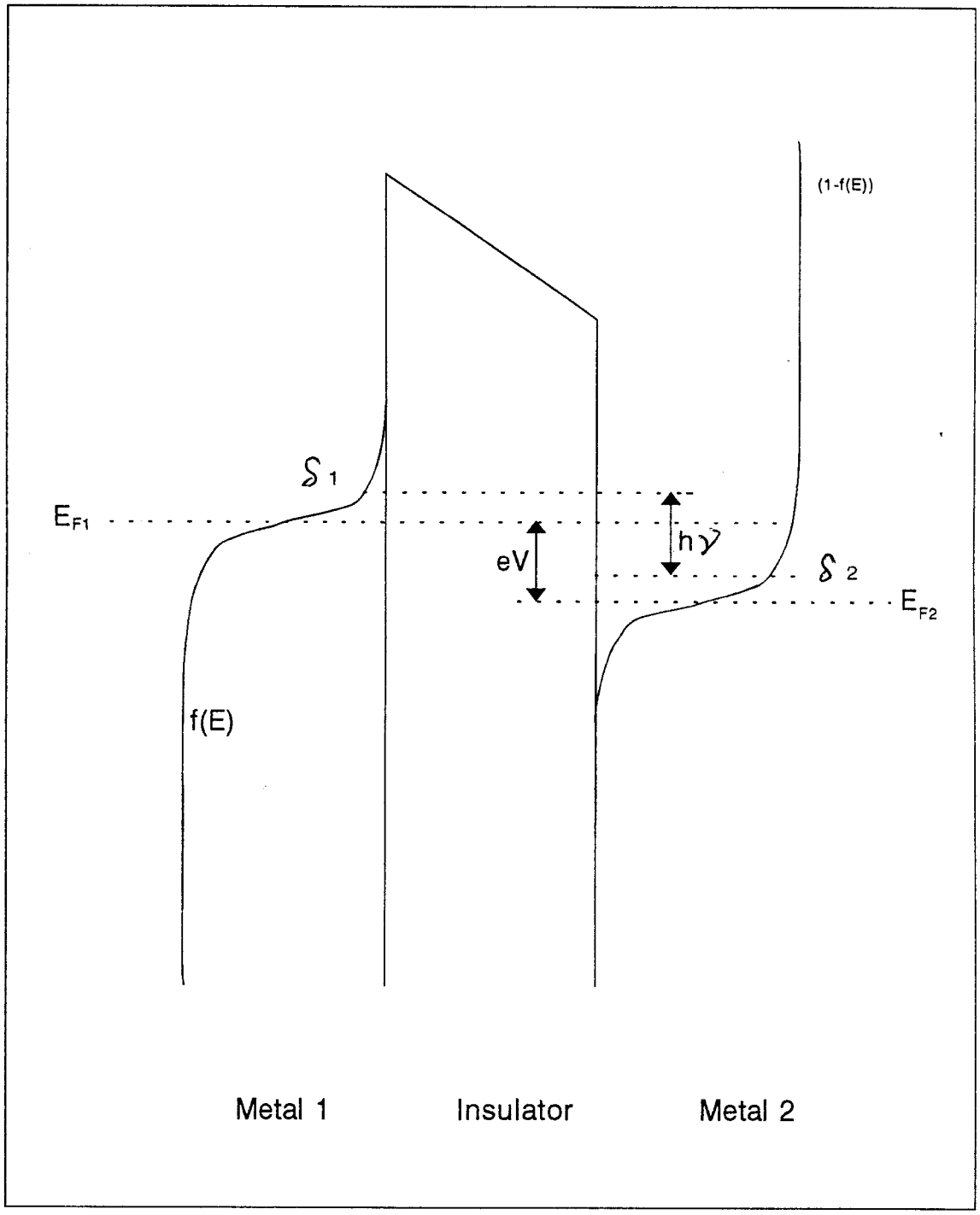

Figure 2.10.

Figure 2.10

The diagram shown here is to illustrate the origins of thermal broadening of the peaks in Inelastic Electron Tunnelling Spectroscopy and is after Keil et.al [20].

The illustration is of a metal-insulator-metal junction at zero Kelvin and under an applied bias of V volts. The region which is bounded by the Fermi function f(E) and the Metal I interface represents the filled states in metal 1. The region bounded by the insulator-Metal 2 and the Fermi function 1 - f(E) is representative of the empty states in Metal 2.

The positions marked by δ_1 and δ_2 are two possible initial and final energy states respectively which are due to the thermal smearing of the Fermi functions near to the Fermi levels in the two metals indicated by E_{F1} and E_{f2} respectively. As can be seen from the diagram:
$eV = h\nu - \Delta_1 - \Delta_2$.

To conform to the practice of displaying IET spectra as d^2I / dV^2 ; taking the second derivative with respect to voltage gives:

$$\frac{d^2 I_{inelastic}}{dV^2} = C \frac{e^2 e^x}{kT} \left(\frac{(x-2)e^x + (x+2)}{(e^x - 1)^3} \right) \qquad \textbf{(2.31.)}$$

Assuming that the natural linewidth is negligible, 2.33 above describes the linewidth expected at a finite temperature in an IET spectrum. This implies that the observed linewidth is due entirely to the smearing in the energy of the electron distribution in the two metals. The function is bell shaped and has a width at half the maximum height of 5.4 kT / e , in good agreement with experimental data [30] - see Figure 2.11a which illustrates the shape of the function. The linewidth varies from approximately 150meV at room temperature to about 2 meV at 4.2K.

2.5.2 The Effect of Superconducting Electrodes

When superconducting electrodes are introduced the situation is changed. Now the effect of changes in the tunnelling density of states must be taken into consideration. Below some critical temperature some metals become superconductors and their resistance to the flow of direct or low frequency a.c. current is reduced to zero [13]. The majority of IETS work is done at 4.2K by immersing the sample into liquid helium at atmospheric pressure. The main reason for the low temperature is the reduction of thermal noise but as most IET junctions contain one lead electrode and this electrode metal will become superconducting at 7.2K. As shown in the section on superconductivity the effect of this is an energy gap of 2Δ - the energy required

to break up a Cooper pair - centred on the Fermi level of the superconducting electrode. At a finite temperature below the superconducting transition temperature there will be a number of electrons thermally excited across the energy gap. The number of electron excited across the gap will be governed by the Fermi distribution. The Fermi distribution in the region of the 'tail' approximates to the Boltzman distribution, given by: exp - (E + Δ) / kT - (E is the electron energy). But because Δ >> kT at 4.2K there will be a sharp boundary in the energy profile between the filled and unfilled states reducing the extent of the Fermi tail.

The superconducting density of states is very large near to the gap as shown in Figure 2.6. and since the tunnel current is directly proportional to the superconductor density of states, and since E ≈ Δ the number of states in a small energy range is so large that tunnelling into these states will dominate. Therefore if either or both of the electrodes is superconducting the threshold of the inelastic tunnel current will be smaller require a narrower bias voltage range and thermal smearing is much reduced.

As stated above in the first paragraph the majority of IETS work is done at 4.2K by immersing the sample into liquid helium at atmospheric pressure and under these conditions the lead electrode will be in a superconducting state. The superconducting density of electron states possesses an energy gap of 2Δ centred on the Fermi level. For lead at 4.2K Δ is approximately 1.2 meV and kT is approximately 0.4 meV. There will, therefore be a significant decrease in the number of filled above and empty states below, the Fermi level in comparison with the normal metal electrode. Thus the effects of thermal smearing are reduced significantly. Above and below the gap the two density of states show a peaking effect which will further sharpen the onset if tunnelling - this does introduce

asymmetry into the curve also there is sometimes seen an undershoot on the high energy side of the peak. The aforementioned undershoot is illustrated in Figure 2.11 a later in the chapter, also shown in the figure is the shift of approximately Δ towards the high energy side in the top of the peak. The shift is an effect which is caused mainly by the amplitude of the modulation voltage [31]. Kirtley [32] has calculated that the thermal FWHM for a normal metal - superconducting lead configuration at 4.2K is 1.1 meV, which represents a useful improvement in resolution when compared to the situation when using two normal metals.

2.5.3 Modulation Voltage Broadening

The effects described above are not the only contributions to the width of the observed linewidth i.e. the resolution of lines in the spectra presented to the user. Spectra in IETS are obtained using a modulation technique using a lock-in amplifier and this results in significant effect on the second derivative linewidth. When IET spectra are taken an a.c. modulation voltage $V_\omega \cos \omega t$ is applied to the IET junction and superimposed upon the slowly increasing applied d.c. bias voltage (V) ; and d^2I/dV^2 is proportional to the second harmonic current response of the junction $I_{2\omega}$.

Klein et al were the first to discuss analytically the effect of a modulation voltage on the width of peaks in IETS [33]. The second harmonic is proportional to the second derivative averaged over interval of the modulation signal. Following Klein the tunnel current is expressed as:

$$\mathbf{I = f (eV + eV_\omega \cos \omega t)}$$

where V is the applied bias voltage and second harmonic response as:

$$I_{2\omega} = \frac{2}{t}\int_0^t f(eV_{eV} + eV_\omega \cos\omega t)\cos 2\omega t\, dt$$

putting $N = eV_\omega \cos\omega t$ gives:

$$I_{2\omega} \propto \int_{-eV_\omega}^{eV_\omega} f''(eV+N)[(eV_\omega)^2 - N^2]^{3/2}\, dN$$

The function is bell-shaped with a full width at half maximum height of 1.7 V_ω (rms). see Figure 2.11b.

Thermal broadening at 4.2 K is approximately 2 meV, with normal electrodes at this temperature the modulation broadening will be comparable to the thermal broadening if a modulation voltage of $1.2mV_{rms}$, is used. With superconducting electrodes at 4.2K the width at half maximum of the thermal broadening function is reduced to approximately 2.9kT [32]. Therefore in order to take advantage of the reduction of line width by using superconducting electrodes a modulation voltage of approximately 0.6 mV_{rms} is used. As the second harmonic signal varies as the square of the modulation signal and the signal to noise ratio varies as the square root of the averaging time, it would take a prohibitively long time to take a tunnelling spectrum with the same signal to noise ratio as that which would be obtained with a modulation voltage of 1.2 mV_{rms} Therefore broadening due to the modulation signal will be the major limiting factor as far as resolution in I.E.T.S. is concerned.

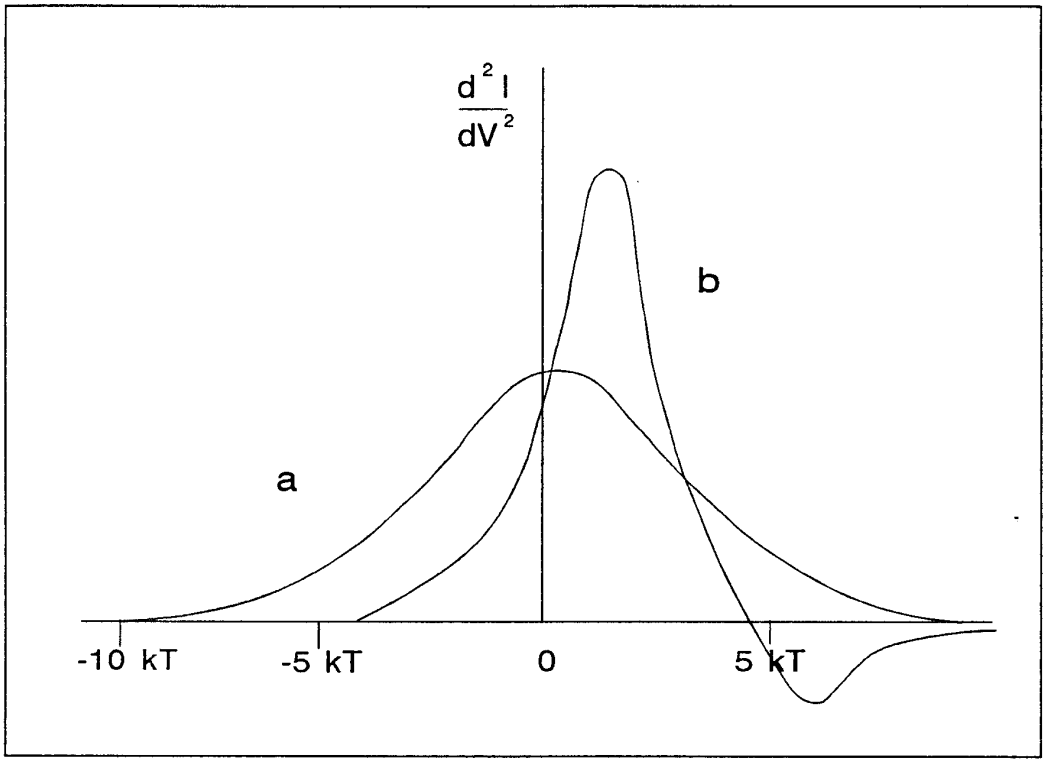

Figure 2.11a.

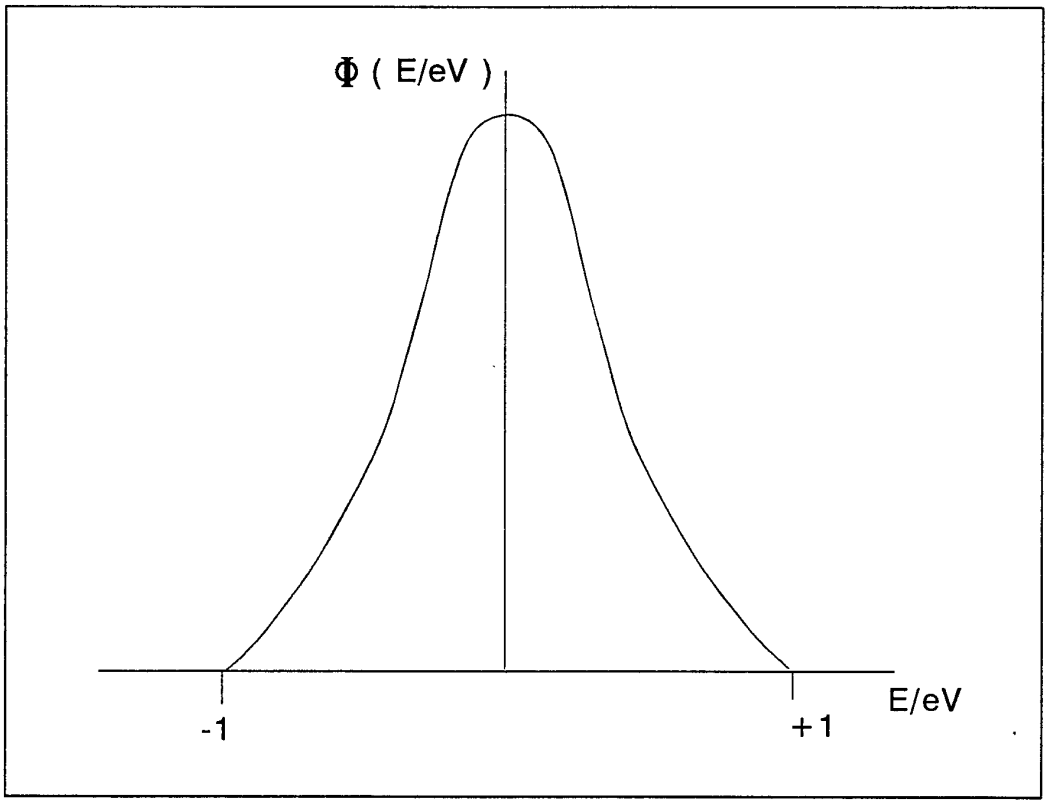

Figure 2.11b.

Figure 2.11a

An illustration of the thermal broadening function with both electrodes normal - after Hansma [21]

a) Both metals normal

b) One metal superconducting diagram based on an energy gap of 3kT which corresponds to a lead at a temperature of 4.2K the normal IET junction temperature. the offset of curve b is approximately 2.4 kT.

Figure 2.11b

An illustration of the modulation voltage broadening function redrawn after Kirtley [26]

Most spectra in IETS are taken using a modulation voltage of 1.7 mV_{rms} this gives a total broadening due to both the thermal and the instrumental effects combined, at 4.2K of approximately [32]:

$$\text{Total FWHM} = \left(\left(1.73\ V_{rms}\right)^2 \ \left(0.47\ T\right)^2\right)^{1/2} \text{meV} = 1.79 \text{ meV}$$

References

[1] Duke C B 1969 *Tunnelling in Solids Solid State Physics - Advances in Research and Applications* Supplement 10 (Academic Press NY).
[2] Gundlach K H and Simmons J G 1969 *Thin Solid Films* **4** 61.
[3] Cassels J M 1982 *Basic Quantum Mechanics* 2nd Edition (Macmillan London).
[4] Burnstein E and Lundqvist S (ed.) 1969 *Tunnelling Phenomena in Solids* (Plenum New York).
[5] Floyd R B and Walmsley 1978 J. *Phys. C* 11 4601.
[6] Sommerfield A and Bethe H 1933 *Handbook of Physics* ed. H Gieger and K Schnell (Julius Springer-Verlag, Berlin) Vol 24 2 450.
[7] Kirtley J 1982 *Tunnelling Spectroscopy Capabilities Applications and Techniques* ed. P K Hansma (Plenum Press - New York) 43.
[8] Bardeen J 1961 *Phys. Rev. Lett.* ***6*** 57.
[9] Giaever I 1960 *Phys. Rev. Lett.* ***5*** 4.
[10] Aldert Van Der Zeil 1968 *Solid State Physical Electronics* 2nd Edition (Prentice Hall Internation Editions).
[11] Enge H A, Wehr M R and Richards J A 1978 *Introduction to Atomic Physics (* Addison Wesley - Reading Massachusetts).
[12] Simmons J G 1971 J. *Phys. D* **4** 613
[13] Stratton R 1962 J. *Phys. Chem.* **23** 1177
[14] Ginnai T M 1982 *PhD Thesis* Leicester Polytechnic.
[15] Giaever I and Megerle K 1961 *Phys. Rev.* ***122*** *1101*
[16] Kamerlingh-Onnes H 1911 *Comm. Phys. Lab. Leiden* **120** 133
[17] Bardeen J Cooper L N and Schrieffer L R 1975 *Phys. Rev.* **108** 1175
[18] Roselnnes A and Rhoderick E H 1969 *An Introduction to Superconductivity* (Pergammon Press Oxford)
[19] Macmillan W L and Rowell J M 1969 *Superconductivity* ed. R D Parkes (Marcel Dekker NY)
[20] Keil R G, Graham T P, and Roenker K R 1976 *Appl.Spectroscopy* **30** 1
[21] Hansma P K 1977 *Phys. Rev.* **30C** 45
[22] Jaklevic R C and Lamb J 1966 *Phys. Rev.* 17 1133
[23] Saclapino D J and Marcus S M 1976 *Phys. Rev. Lett.* ***18*** 459
[24] Lamb J and Jaklevic R C 1968 *Phys. Rev. Lett.****165*** 821
[25] Schiff L I 1955 *Quantum Mechanics (* New York: McGraw-Hill) p153
[26] Kirtley J, Scalapino D J, and Hansma P K 1967 *Phys. Rev. B* **14** 3177
[27] Kirtley J and Hall J T 1980 *Phys. Rev.* ***B22*** 848
[28] Hall J T and Hansma P K 1978 *Surf.* Sci. **71** 1
[29] Hipps K W, Mazur U, and Pearce M S 1979 *Chem. Phys. Lett.* ***68*** 433
[30] Jennings R J and Merril J R 1972 J. *Phys. Chem.* **33** 1261
[31] Kirtley J and Hansma P K 1976 *Phys. Rev.* **B 13** 2910
[32] Kirtley J 1980 J. *Am. Chem. Soc.* ***80*** 217
[33] Klein J, Leger A, Belin M, Defoumeau D, and Sangster M J 1973 *Phys.Rev.* B **7** 2336

Contents

CHAPTER 3

JUNCTION FABRICATION, ASSESSMENT PROCEDURES AND CRYOGENICS

3.0 Procedures

This chapter outlines the cleaning and fabrication procedures followed by this group. Since these follow well established lines only brief descriptions are given, more detailed descriptions are presented in separate chapters when the information is relevant. The methods used by the author in fabricating, assessing and mounting the junctions used in this work mainly follows the well proven methods developed by previous workers in the School of Applied Physics [1-3]. Criteria for the minimum thickness of the bottom electrode in IET junctions were developed and implemented by this group; these will be described in chapter 5 of this thesis.

3.1. Cleaning and Preparatory Work

Cleanliness is essential if reproducibility is to be achieved and so prior to the manufacture of the junctions a rigorous cleaning procedure is followed. Throughout the processes of cleaning and manufacture, surgical gloves are worn to prevent contamination of the masks and slides by grease from the skin. After cleaning tweezers are used to handle and manipulate the slides throughout the manufacturing processes.

The substrate, which is a glass microscope slide cut to 70 x 11 mm is first cleaned by abrasion using a mild alkaline abrasive - Balzers No 1. The residue abrasive is then removed using a detergent/solvent degreaser - Balzers No 2. The slides are then placed, ten at a time, in a bottomless staining rack and ultrasonically cleaned in a 10% solution of the detergent Decon 90 for approximately 15 minutes. After this they are removed from the Decon and washed in running, filtered, mains water for approximately 30 minutes and then rinsed several times in Millipore water.

The brass masks are ultrasonically cleaned in the Decon solution previously used for the glass substrates. After a few minutes they are removed and scoured to remove any remaining metal, returned to the bath for a few more minutes and finally washed and rinsed along with the slides. After the 'Millipore' rinse both the masks and slides are dried in an oven at 100°C. Stored in the oven, the clean and dry masks and slides will remain uncontaminated for use throughout the day. It is also important to instigate a similarly strict cleaning regime for the glassware used in preparing the solutions used in the manufacturing processes.

The vacuum chamber which is kept at a low pressure when not in use is brought up to atmospheric pressure and the top removed. Aluminium wire is loaded onto a tungsten filament heating source and lead shot is placed in a resistively heated boat. Gloves are worn when working inside the bell chamber when handling the metals used in the evaporation process and when it becomes necessary to change either of the sources. The lid has built into it two fixing bolts which allow the masks to be attached to it so that when the top is replaced on the system the masks are

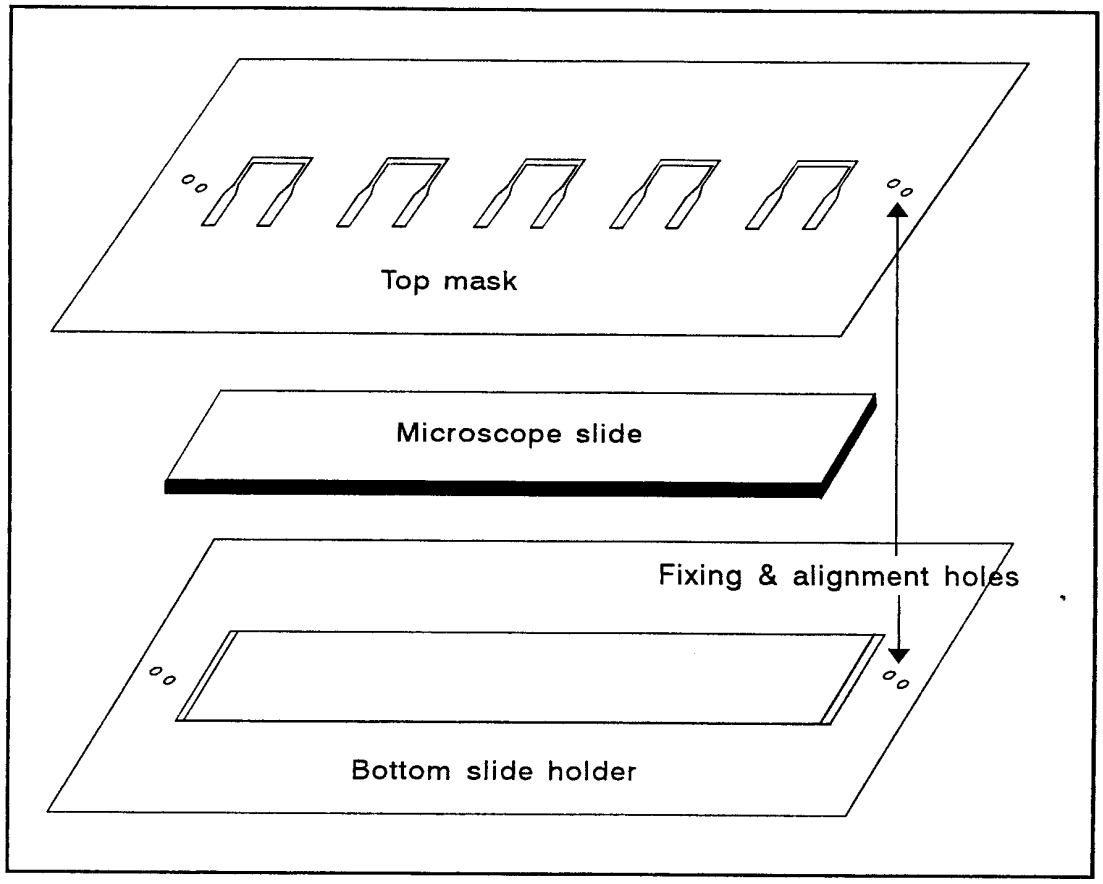

Figure 3.1a.

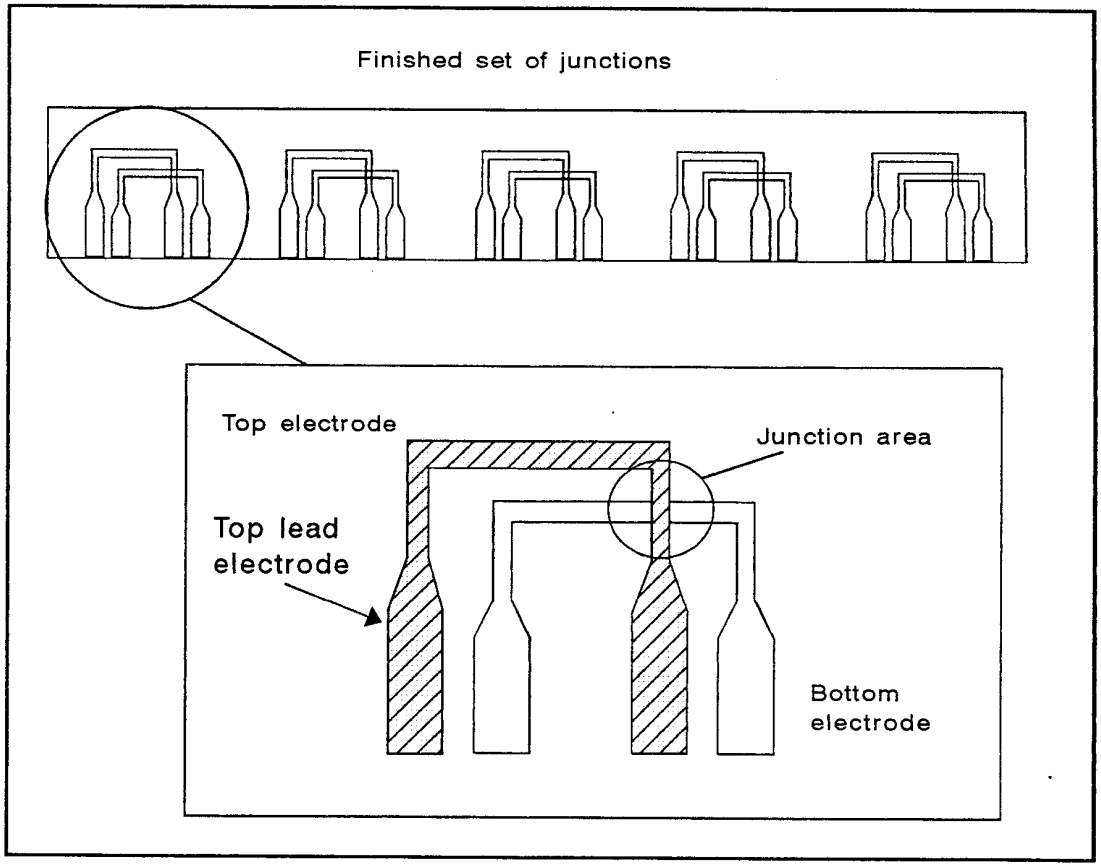

Figure 3.1b.

Figure 3.1 a.

This figure is an illustration of the masks used to produce IET junctions in this department. The top mask has slots cut into it, these slots allow the evaporated metals to pass through and be deposited on the glass microscope slid in the pattern defined by the slots. Thus forming the junction and its contacts to the spectrometer. Shown also are the dual purpose holes used for fixing the masks in the vacuum system and aligning them so that the two metal electrodes overlap each other to form a junction area. The lower set are used to forme the bottom electrode and the upper set to form the top.

Figure 3.1 b.

Show here is a diagram of a finished set of five IET junctions. The junction area is produced where the top and bottom electrodes cross over each other. Electrical contact is through the broad sections of the electrodes at formed by the evaporated metals at the edge of the microscope slide.

facing down towards the tungsten evaporation sources. Thus when a current is passed through either of the sources the aluminium or lead will be melted and evaporated to be deposited on the unmasked portion of the substrate - see Figure 3.1 a. The deposited layers of metal forms the patterns from which the junction are made.

3.2. ***Electrode*** Deposition and Oxidation

The junctions are made, five at a time, using brass masks see Figure 3.1 a. The masks are assembled with a cleaned glass slide and placed in the vacuum chamber as illustrated in Figure 3.2. The chamber is then evacuated to about 0.05 Torr. At this pressure a plasma glow discharge using a current of 50 mA is set up and maintained for several minutes in order to reduce the level of organic contaminants inside the chamber. The chamber is then pumped down to a pressure of approximately 10^{-S} Torr. The bottom electrodes are then deposited by passing a current through the filaments holding the aluminium wire. Throughout the deposition process both the deposition rate and thickness of the metal being deposited are monitored using a quartz-crystal film thickness monitor. The aluminium base electrodes are evaporated to a thickness of at least 300 nm after which the surface of the metal is oxidised. The oxidation is achieved either inside the bell chamber by a d.c. plasma glow discharge in air at approximately 0.05 Torr and 50 mA or by utilising the thermal oxidation which occurs naturally when the chamber is brought up to atmospheric pressure prior to the removal of the slides so that doping can take place.

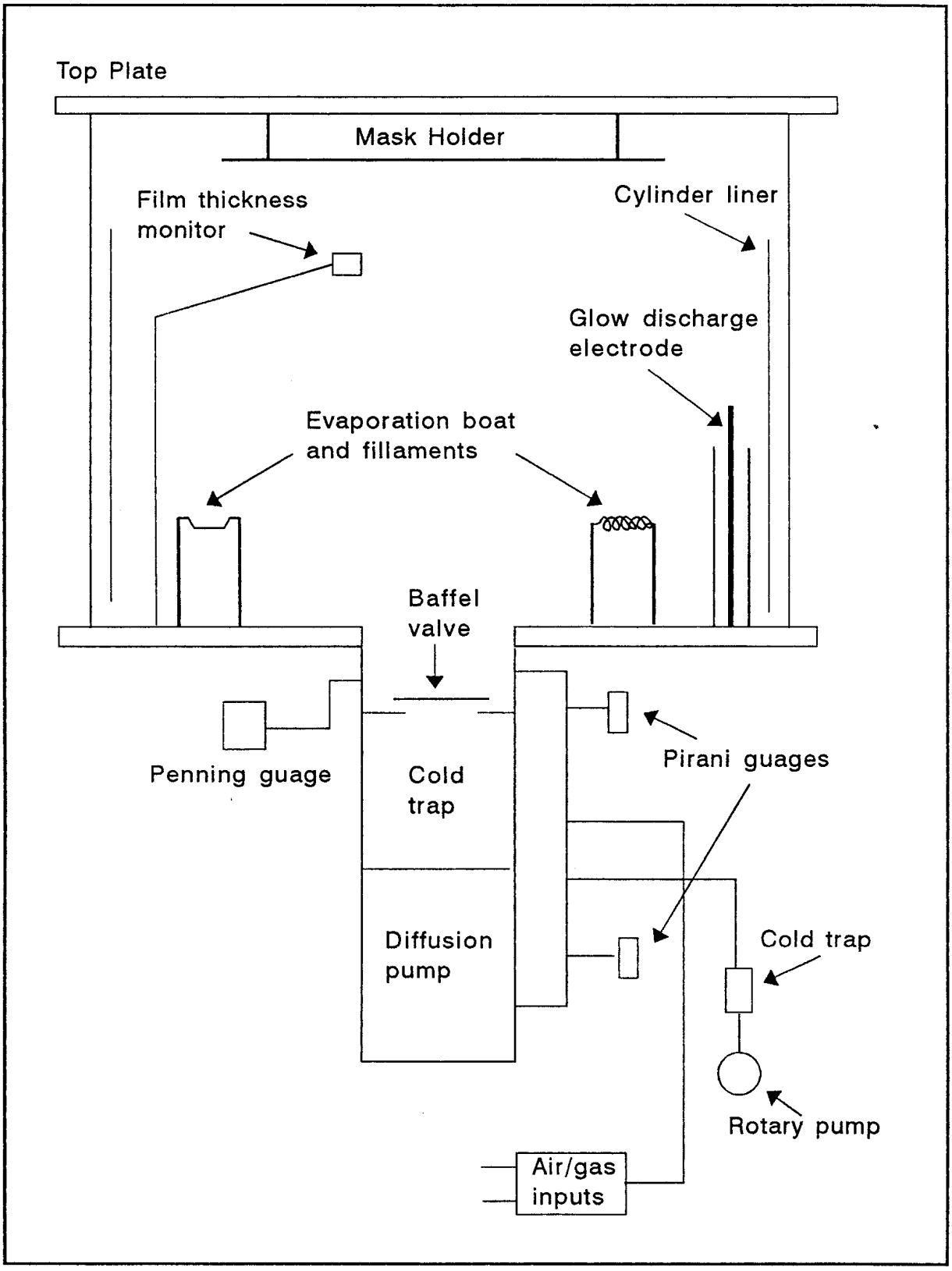

Figure 3.2.

Vacuum system and bell cylinder assembly

Figure 3.2

Shown here a schematic of the vacuum system used as standard by the IETS groups in this department for the fabrication of tunnel junctions. The illustration shows the approximate positions of the main components of the system.

1. The removable top plate is provided with a mask holder from which the masks are suspended prior to evaporation of the electrodes.

2. A molybdenum boat is used as the lead evaporation source and tungsten filaments as the aluminium evaporation source.

3. Liquid nitrogen cold traps are used in conjunction with Santovac - 5 rotary pump oil to reduce the possibility of hydrocarbon vapours backstreaming in to the evaporation chamber.

Immediately after oxidation the junctions are doped using one of the methods described in detail in section 3. 3. It is also convenient to note at this point that both undoped junctions and junctions doped with the solvents used to dilute the sample solutions were tested on a regular basis. These were used as control junctions to monitor for any contamination which might have occurred from the air during the oxidation process and/or the solvents being used.

After the slides have been doped they are replaced in the realigned masks returned to the vacuum system and the chamber is pumped down to about 10^{-5} Torr. The top electrode, which is usually made of lead, is then evaporated to a thickness of approximately 300 nm.

The newly completed junctions shown in Figure 3.1b are allowed to cool, the chamber is then vented to air and the slides removed. If the junctions are not going to be used immediately the completed slides are stored in a vacuum desiccator, where they can be kept for several days without any deterioration.

3.3 Doping Methods

After an oxide has been formed on the top surface of the base electrode metal, a means of depositing a controllable amount of the sample under investigation onto the surface must be devised. The present work has used two methods: Liquid phase doping and Langmuir Blodgett (L.B.) film transfer [4-6].

3.3.1. Liquid Phase Doping.

Liquid phase doping [7] is the simplest method and the most widely used by Inelastic Electron Tunnelling Spectroscopists for incorporating molecules into tunnel junctions. The materials under investigation were dissolved in a suitable solvent for example methanol or ethanol to form a solution of suitable concentration - usually about 1 mg mL^{-1}. All of the solvents used in this work were of 'Spectrograde' or 'Analar' grade. To test the reaction of the solvents with the oxide surface IET spectra were taken from junctions which had been doped with the pure solvent.

Liquid phase doping is performed by placing a glass slide, containing the five oxidised bottom electrodes on the axis of the vacuum chuck of a spinner; with the oxide surface uppermost. The doping solution is poured over the surface of the slide, left for a few seconds and then spun off. The doped slide is then returned to the vacuum chamber, and a top electrode is deposited after the chamber has been evacuated to approximately 10^{-5} T. During the pumping down process any excess dopant will be pumped off and exhausted to the air.

Studies with new dopants require that the optimum concentration of the dopant is ascertained. This is done on an empirical basis - a range of solutions of varying concentrations around 0.2 to 2 mg mL^{-1} are prepared and a series of junctions are doped with each of the solutions and each assessed in turn. Initial testing of the junctions is done by measuring their resistances. Once suitable resistances have been obtained junctions doped with the chosen concentration are placed in the spectrometer and spectra taken from them.

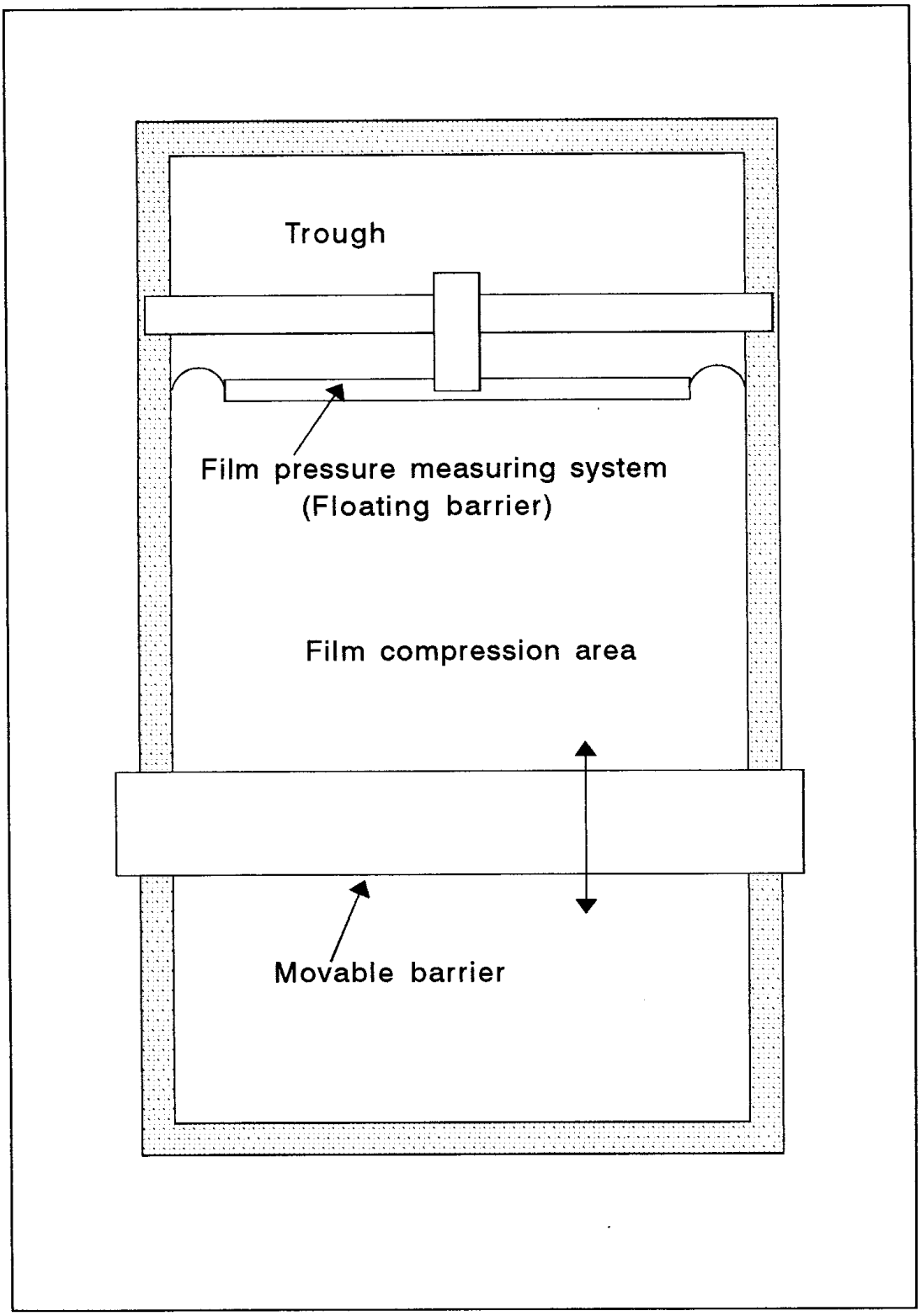
Trough
Film pressure measuring system
(Floating barrier)
Film compression area
Movable barrier

Figure 3.3.

Figure 3.3

Shown in this figure is a schematic of the MGW Lauda Langmuir Blodgett trough used for all of the Langmuir / Langmuir Blodgett film work done by the present group. The main features are illustrated, for a fuller discription of the apperatus see the appropriate section in this thesis.

The solvents to be used in the work must also be chosen carefully, with the following factors in mind. The dopant must dissolve in the solvent, leaving no residue. This was checked visually, a procedure followed by other groups [8]. If the dopant is not completely dissolved high junction resistances are encountered; this is perhaps due to pockets of high dopant concentration on the surface of the oxide. The solvents also carry low levels of contaminants into the junctions during the doping and their effect has to be monitored. They must also not contain any detectable amount of contaminants, react with or remain adsorbed on the oxide. The materials chosen for this study fulfilled this criteria; the IET spectra of their respective 'blank' junction showed no detectable signs of any contamination.

3.3.2. Using Langmuir Blodgett Films.

In the Langmuir Blodgett (LB) film technique [4-6] a solution of the material under investigation is spread upon the surface of a water bath - see Figure 3.3. The molecule under investigation must be amphipathic, possessing a hydrophillic and a hydrophobic end. Thus when the molecule is placed upon the surface of the water it will naturally orientate itself with the hydrophillic end towards the surface and the hydrophobic as far away as possible - see Figure 3.4a which show a diagrams of the amphipathic molecule stearic acid .

The amount to be placed on the surface must be calculated to give a film of well separated molecules after the solvent has evaporated. Once the concentration has been determined 20 - 30 μL of the solution is placed in 2 - 3 μL

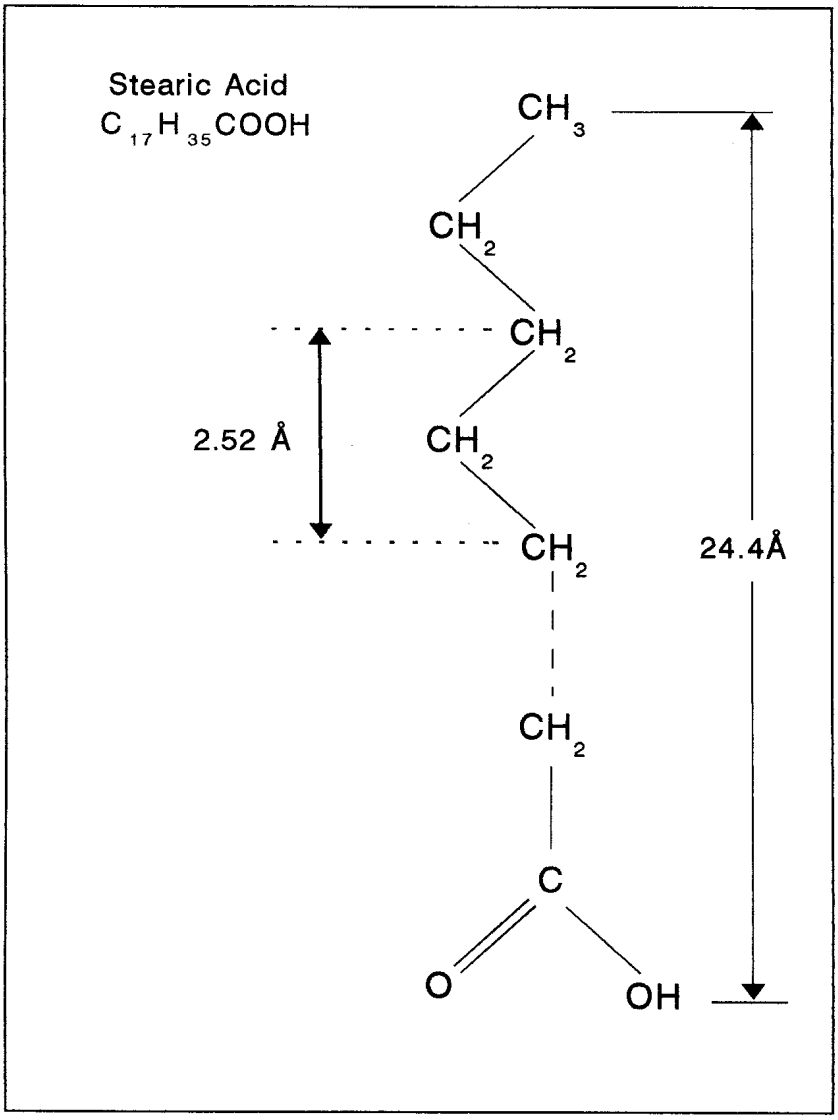

Figure 3.4a.

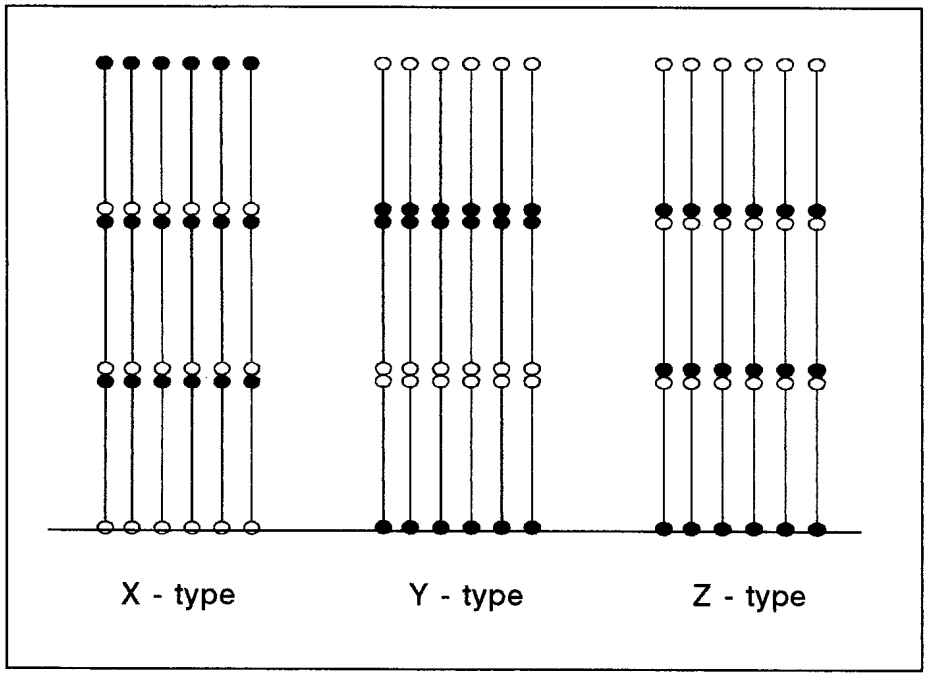

Figure 3.4b.

Figures 3.4a

The illustration shown opposite is Stearic acid the material used in the Langmuir - Blodgett work done by this group. By incorporating barium stearate into the subphase the H^{+} ion in the hydrophillic end group of the stearic acid was replaced by the divalent metal ion Ba^{2+}. The mixed films of steanc acid and barium stearate proved to have an increased stability - see the chapter on Langmuir - Blodgett films for details.

Figure 3.4b

Illustrated in diagram 3.4b are the three different modes of monolayer transfer. Depending upon conditions there will be transfer upon immersion of the substrate only (Y type), transfer on withdrawal only (X type), and transfer in both directions (Z type). The present series of experiments used only X-type monolayers.

The solid circles represent the carboxyl end groups and the open circles represent the methyl end groups in the molecule.

drops over the whole surface of the water . The bath is then left to stand for approximately 15 minutes in order to allow the solvent to evaporate, leaving the molecules spread over the entire surface of the subphase.

A computer controlled movable barrier situated on the surface of the subphase is then swept slowly across the water, pushing the molecules before it. At the opposite end of the trough there is a floating barrier which is connected to a transducer which is used to monitor the force on the layer of molecules as they are swept towards the barrier. The compression is performed with the subphase held at a constant temperature and a graph of pressure versus area then a p – A isotherm is taken as shown in chapter 5. At a predetermined pressure, corresponding to the solidus form of the layer the barrier stops advancing and the applied pressure is held constant. It is at this point the molecules are arranged in an ordered and compact monolayer, held together by van der Walls forces. The slide, which is mounted in a dipping device is then lowered slowly into and through the surface layer, held stationary for a few minutes and then withdrawn back through the layer usually at the same speed as the dipping speed.

The way in which the first and if the dipping is continued subsequent layers are arranged is determined firstly by the surface of the oxide and secondly by the nature of the exposed groups on the previous layer. There are three ways in which Langmuire Blodgett can be built up depending upon the conditions see Figure 3.4b. These are termed: X-type in which a layer of Langmuir film is transferred to the substrate on immersion only, Y-type in which a layer is transferred on withdrawal only, and Z-type where a layer is transferred in both directions.

Once the first layer (All of the work in this study used only one layer - a monolayer) had been deposited the sample is placed in a desiccator and left for at least 24 hours in order to remove any water molecules which may have been transferred with the monolayer. The slide is then placed into the vacuum chamber and the top electrode deposited over the junction in the same way as that for liquid phase doped junctions.

3.4. Junction Assessment

The completed junctions are evaluated immediately before use using an ohmmeter with a probe voltage of < lOmV. This low power ohmmeter is used to monitor the d.c. resistance of each of the five junctions. Junctions with a resistance between 50 and 400 ohms are considered suitable for IETS. A knowledge of the junction resistance can also give information about the quantity of the dopant present, allowing adjustments to the concentration of the doping solution to be made. Any junctions with resistances falling outside the above limits are normally discarded.

Once the evaluation process is completed any selected groups of junctions are mounted in a sample holder via a 32 way 0.1" PCB edge connector. This connector provides a means of overcoming the problems of connecting the spectrometer to the sample which have been encountered by other workers; the gold-plated contacts of the edge connector provide excellent electrical and mechanical contact with the sample. This sample holder is constructed so that it can be placed into a standard 50 litre Helium storage Dewar vessel via the neck of the vessel. The procedure is carried out very slowly in order to avoid rapid cooling and violent

boiling of the helium. The top of the dewar is sealed using an 'O' ring arrangement thus preventing icing within the neck. Once the sample holder is completely immersed in the helium it can be connected to the spectrometer via a 25 pin D plug at the top of the assembly.

3.4.1. Assessment of Junctions at 4.2 Kelvin

Several tests are performed with the sample immersed in the liquid helium. The modulation voltage at low bias (= 5mV) is monitored on an oscilloscope, lead is superconducting at this temperature and a non-linearity in the current to voltage characteristics caused by tunnelling into the superconductor should be observable - reference chapter 4. If the effect is small or not present the junctions are not used.

The second test is to take fast, low resolution spectra of each of the acceptable junctions to assess the signal to noise ratio of each of selected junctions using an X-Y plotter. This process also highlights junctions which have abnormal behaviour such as creeping and breakdown.

Creepers are junctions which are unable to sustain the applied bias; breakdown occurs in one of two ways. The first is a sudden large excursion current which then returns and continues normally and the second is a sudden complete breakdown of the junction. Suitable junctions are then chosen to be scanned at high resolution to produce IET spectra.

3.5. Materials

The materials used in this work were of the purest grade available, this is especially true of the L.B. chemicals where particular attention was paid to the concentrations of surface active contaminants.

3.5.1. Solvents and Water

All the solvents used were Spectrograde' or 'Anal ar' grade, supplied by BDH, and used without any further purification. A check was kept upon the condition of the solvents by regularly running 'blank' junctions - junctions doped only with solvent. The solvents used were n-hexane, ethanol, methanol and methoxy ethanol. The materials used for cleaning the L.B. trough are dealt with in Chapter 6.

All water used in the L.B. trough and for the final rinsing of the glassware and substrates was supplied from a Millipore plant providing water with a conductivity of 18 MΩ cm^{-1}. The water used for the washing stages is mains water filtered through a 30 micron filter followed by a 5 micron filter.

References

[1] Ginnai T M 1982 PhD *Thesis* Leicester Polytechnic.
[2] Langley A J 1982 *PhD Thesis Leicester* Polytechnic.
[3] Tunnicliffe D L *PhD Thesis* Leicester Polytechnic.
[4] Blodgett K B 1934 J. Am. *Chem. Soc.* **56** 495.
[5] Blodgett K B 1935 *ibid* **57** 1007.
[6] Langmuir 1 1920 *Trans. Faraday Soc.* **15** 62.
[7] Simonsen M G, Coleman R V and Hansma P K 1974
[8] Reynolds S 1983 PhD *thesis* Leicester Polytechnic.

Contents

CHAPTER 4

THE SPECTROMETER

4.1 Instrumentation and Accuracy

The spectrometer used in this work was originally built by Tunnicliffe [1], developed by Oxley [2] with improvements by Reynolds and co-workers [3,4]. It was reviewed in 1987 by Reynolds [5] where it was shown for the first time that the instrument is capable of resolving peak shifts of 0.39 meV in the OH mode of the benzoate ion with an accuracy of ± 0.02 meV.

4.2 Technique

Inelastic Electron Tunnelling Spectroscopy (IETS) is a surface technique which enables the vibrational modes of small amounts of molecules adsorbed upon an oxide to be determined. As stated earlier in chapter two the tunnelling current in a MIM junction is made up from two components. The first and by far the largest is the contribution made by electron which have tunnelled through the potential barrier without loss of energy, this is termed the elastic tunnelling current. The second contribution, making up less than 1% of the tunnelling current, is from electrons which have lost some of their energy by exciting molecular vibrations within the barrier before tunnelling continuing through the barrier - this contribution is termed the inelastic tunnelling current. The onset of each of these inelastic events produces a slight increase in the current versus voltage characteristic

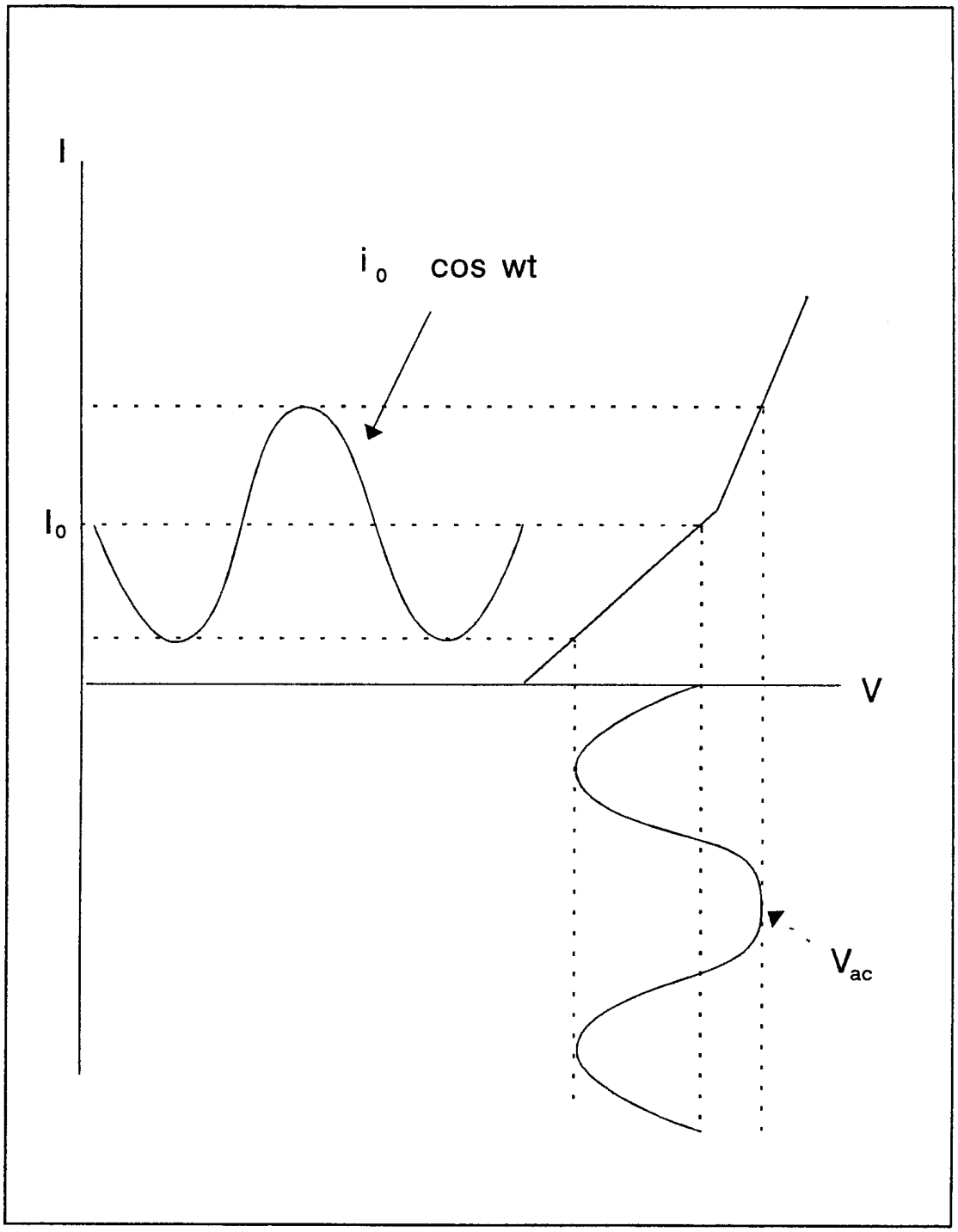

Figure 4.1

Figure 4.1

This figure is an illustration which represent the current versus voltage characteristic of a tunnel junction at the position where a conductance change due to an inelastic event has occurred. A modulation current $i_o \cos \omega t$ is superimposed upon the standing current I_o , this produces a distorted voltage response V_{ac} due to the non-linearities in the I - V curve.

at a particular voltage (V) given by V = hν/e where h is Plank's constant, e is the electronic charge, and ν is the frequency of the particular vibrational mode within the barrier. Detection of these small changes is usually done by applying a varying voltage to the junction and then taking the second derivative d^2I/dV to reveal the changes in conductance as a series of 'peaks' on the smoothly sloping elastic background and in essence an IET spectrum consists of a plot of d^2I/dV^2 versus V. Therefore an IET spectrometer must be able to detect any inelastic events against a very much greater background of elastic conduction and be able to present the results as a plot of d^2I/dV^2 versus V. Modulating the d.c. bias current with a small sinusoidal signal and measuring the second-harmonic voltage response of the junction is the most convenient way of doing this and most spectrometer designs use this technique.

The non-linearities in the I versus V characteristics resulting from the inelastic tunnelling events will mean that the a.c. response of the junction will be distorted. The I versus V characteristic of a tunnel junction in the vicinity of an inelastic event is shown in Figure 4.1. The response will contain harmonics of the fundamental frequency applied to it which will be proportional to the first and second derivatives of the I versus V characteristics as shown in the following analysis.

Denoting the peak amplitude and angular frequency of the modulation current to be i_o and ω respectively, then the voltage response of the junction, V(I) can be expanded as a Taylor series

$$\mathbf{V(I) = V(I_o + i_0 \cos \omega t)}$$

expanding gives:

$$= V(I_o) + i_o \cos\omega t \frac{dV}{dI}(I_0) + \frac{1}{2!}(i_o \cos\omega t)^2 \frac{d^2V}{dI^2}(I_0) + \ldots\ldots$$

$$= V(I_0) + i_o \cos\omega t \frac{dV}{dI}(I_0) + \frac{1}{4} i_o^2 (1 + i_0^2 \cos\omega t) \frac{d^2V}{dI^2}(I_0) + \ldots \quad \textbf{4.1}$$

Where the higher order terms have been neglected. From equation 4.1. it can be seen that the voltage (V_ω) at the first harmonic frequency is proportional to the fast derivative:

$$V_\omega \propto \left(\frac{dV}{dI}\right)(I_0)\ \delta \cos\omega t \qquad (4.2)$$

and the Voltage($V_{2\omega}$) at the second harmonic frequency is proportional to the second derivative:

$$V_{2\omega} \propto \left(\frac{d^2V}{dI^2}\right)(I_0)\ \delta^2 \cos\omega t \qquad (4.3)$$

Each of these voltage are available across the tunnel junction and can be recovered using a lock-in amplifier.

Using a similar analysis and expanding the steady state current as a function of the steady state voltage , it can be shown that the current response of the junction is also given by a series of harmonic terms involving dI / dV and d^2I / dV^2 - ignoring the higher orders.

Although constant voltages are possible it is easier to achieve conditions which approximate to constant current merely by use of passive components - as in this spectrometer. The derivatives are related through the identities:

$$\frac{dI}{dV} = \frac{1}{(\frac{dV}{dI})} \quad \cdots\cdots\cdots \quad (4.4)$$

$$\frac{d^2I}{dV^2} = -(\frac{dI}{dV})^3 \frac{d^2V}{dI^2} \quad \cdots\cdots\cdots \quad (4.5)$$

And the conversion of d^2V/dI^2 to d^2I/dV^2 is done conventionally by computer software.

4.3 Bias and Modulation

The d.c bias current is supplied through a series combination of resistors. The ohmic drop across Ra is used to monitor the bias current. R_b is used to set the range bias voltage - usually 0 to 0.5 V. The bias supply is 10V and so R_b will be twenty times the value of the junction resistance; thus if the junction resistance varies by less than 100% the current will change by less than 5%. Similar reasoning applies to R. where this resistor is more than one hundred times the value of the junction resistance. The modulation generator supplies IV peak to peak which is dropped to I mV peak to peak across the junction.

A four point probe technique is used to determine the second-harmonic voltage. Also provided that the differential input voltmeter used to measure the junction resistance has an input impedance far greater than the resistance of the connecting leads, the voltage drop across these will be negligible. It should be noted here that there will usually be a small parasitic ohmic drop across the junction due to its finite area. The importance of this effect has been observed by others and studied by this present group [6 - 8] - see Chapter 5.

4.3.1 a. c. Signal Recovery

An IET spectrometer must be able to detect the amplitude of the second-harmonic signals; these are proportional to the square of the modulation current (or voltage) amplitude appearing across the junction. The modulation voltage cannot be increased to too high a level otherwise modulation broadening will reduce the resolution of the spectrum - see Chapter 2. Routinely a modulation voltage of 1mV peak to peak is used, this is of the same order as the effect of thermal smearing of the signal from a junction held at a temperature of 4.2K. Using these parameters changes as small as 10nV in the value $V_{2\omega}$ have to be detected by the second harmonic recovery system. If the phase of the signal is known - as it is here - a powerful recovery technique known as phase-coherent or lock-in detection can be used. In simple terms the phase sensitive detector consists of two unity gain amplifiers connected to a switch which is controlled by the phase of a reference signal. When the signal is positive the input signal is directed to the input of a unity

gain amplifier and when the reference signal is negative the input signal is sent to the input of an inverting unity gain amplifier.

Thus if the input and reference signals are exactly in phase the output from the phase sensitive detector will be a full-wave rectified version of the input signal. The signal from the output is then applied to a low-pass filter to smooth the waveform to give a d.c. level proportional to the mean amplitude of the input. If, however, the input has a 180° phase difference with the reference signal the output will still be full-wave rectified but the output from the detector will now be negative. And if the two signals have a 90° phase difference the output from the filter will contain no net d.c. response.

Thus the signal and reference must have a constant phase relationship for the phase sensitive detector to give a d.c. output. It is therefore necessary to derive the signal and the reference from the same source. Signals or noise from other sources will have a random phase relationship to the reference signal and will appear as a.c. fluctuations on the output signal.

The lock-in amplifier used by this team is a Brookdeal 9503 with a factory modification to increase the high-frequency cut-off from 100kHz to 200kHz. The reference signal is provided a Brookdeal 5021F oscillator which is powered by the 9503. The 5201F is also used to provide a high purity sine wave for the modulation supply. Typically the sensitivity range corresponds to a $V_{2\omega}$ signal of about 300 nV; this allows the peaks to be displayed within the full scale deflection of the LIA ± 10 V d.c.).

The lock in detector requires two inputs, the input signal V, and the reference input V, The reference input is derived from the modulation supply and therefore the

frequencies of the two inputs are identical. Also, an internal doubling circuit is used to double the reference signal frequency which enables the second harmonic signals (d^2I/dV^2) to be processed.

Usually data from the spectrometer are transformed into digital form to enable the processing to be performed on a dedicated computer. The spectrometer can also be used in an analogue mode with the bias being ramped by a motorised potentiometer. The spectrum is produced by applying the bias to the x-axis of a chart recorder and the output from the lock-in amplifier to the y-axis.

4.3.2 Noise

The detection system in the IET spectrometer provides a very high degree of noise rejection, which is limited only by the time allotted to the scan of the junction. However, there are constraints placed upon the experimenter by the inherent long term d.c. stability of the lock in amplifier. Long time scans may encounter drift in the expected operating parameters of the LIA introducing unacceptable errors.

There are three areas where noise reduction is essential if satisfactory results are to be obtained in IETS. These are: junction, environmental and instrumental. The contributions from each of these are discussed in the following paragraphs.

Junction noise arises from shot [9,10] and 1/f noise [10 - 13], The first, shot noise, is a direct consequence of the particulate nature of charge and is the major contributor to the noise profile in a well prepared junction. The spectral

distribution of shot noise has a wide frequency range and is random, containing many frequencies - 'white noise' - and therefore its reduction cannot be achieved by operating at a particular frequency.

The magnitude of flicker or 1/f noise decreases with frequency and its origins are not well understood. To reduce its effect the spectrometer is operated at a fundamental frequency of 50 kHz. This figure was chosen for the operating frequency of the a.c. modulation with particular regard to the 1/f noise from the junction and to the thickness of the screening material of the room. In a recent paper by Speakman and Adkins [14] it has been proposed that if the aluminium barriers in IETS junctions are grown in the presence of water there is a large contribution to noise which could be attributed to ionic motion causing fluctuations of the tunnelling conductance.

The d.c. bias supply to the junction is fed through an LC filter to minimise noise at the signal frequency. The preamplifier has a low a noise as possible - the design was adjusted to have acceptable parameters by previous workers.

The noise created by the digital equipment required to operate the spectrometer, the computer and DVMs etc, can be a problem; to overcome this the spectrometer is housed in a separate room from the signal recovery equipment.

Environmental noise in the form of transients, mains interference and other electromagnetic interferences has been reduced to acceptable levels by filtering the mains input to the room with a Belling Lee filter type L1822 which provides 100 dB attenuation from 0.1 Hz to 10 GHz with a notch at 50 Hz also the spectrometer is housed in a screened room. The electromagnetic screening is in

the form of a cladding of aluminium sheet 1.6 mm thick. The design of the cladding involved the choice of an operating frequency of 50 kHz for the a.c. modulation frequency [2].

4.4 The Spectrometer Circuit.

The basic circuit chosen followed a design by McMorris et al [15], a schematic diagram is shown in Figure 4.2.

The spectrometer has 10 basic components:

1. The control box.
2. Lock-in Amplifier and Oscillator.
3. Second-harmonic preamplifier.
4. Computer and associated hard/software.
5. Digital voltmeters.
6. Digital to analog converter.
7. X-Y chart recorder.
8. Printer.
9. Plotter.
10. oscilloscope to monitor modulation input and second harmonic waveforms.

These units are briefly reviewed in the following sections.

- The spectrometer control box was built by Tunnicliffe [1,2] and modified by Reynolds [3]. The box enables the operator to select any one of the five junctions for appraisal. The d.c. bias for the junction, up to ± 5v, is supplied by a solid state

current source feeding through a set of adjustable series resistors with a standard resistor to allow the measurement of current followed by an LC filter.

- The modulation supply is filtered prior to being applied to the junction to ensure that the measured second-harmonic signal, detected by the spectrometer, are indeed caused by non-linearities in the junction.

- The control box also contains a motor driven potentiometer - a Rayleigh MP 120. This unit is used, during the set up procedure to control the input to the current source and to sweep the junction independent of the computer.

- The lock-in amplifier is a Brookdeal 9503 modified by the manufacturer to have a high frequency cut off of 200 kHz (the standard instrument has a cut-off frequency of 100 kHz). Housed in, and powered by, the LIA unit is a Brookdeal 5012F oscillator. This oscillator is used to provide both the reference signal and the modulation supply. It has a total harmonic distortion of 0.05% with a second harmonic content of 0.005%. The second harmonic preamplifier is based upon an integrated amplifier supplied by RS Components . It is fed via a series LC circuit which is resonant at 2w. The arrangement using the preamplifier improves the noise performance [2], although it is not certain why. The design of the circuit has been described in detail elsewhere [2].

- The computer which controls the logging of data, processing and the peripherals is a Digital Electronics Corporation (DEC) LS-11/2. Interfacing with the computer is conducted via a 9.6 Kbaud serial RS232 line. A Badel single density

dual floppy drive provides the means for storage for programs and data; each floppy disc will store 128 K bytes of data.

- The voltmeters which are used to record the values of the bias voltage, junction current or lock-in amplifier output are two Solatron 7055 DVMs. Their accuracy is 1 μV on the 200 mV range, l0 μV on the 2V and 100μV on the 20V range. They have a built-in option which provides increased noise rejection at the expense of integration times. The minimum input impedance of the instruments is greater than 1GΩ and therefore no significant loading problems occur. The two DVMs are interfaced with the computer through a serial RS232 port operating at 9.6 Kbaud.

  The one problem with noise is encountered with the DVM which is connected directly across the junction to measure the bias. A built-in clock caused a.c. interference resulting in unacceptable levels of second-harmonic distortion. To overcome this an RC low-pass filter is placed between the junction and the voltmeter input; this does result in some loss of accuracy in measuring the bias but which is acceptable. To further reduce the noise the screens of the connecting leads to the voltmeters are earthed at the spectrometer end.

- The digital to analogue converter (DAC) provides a computer controlled 0 to 10 volt d.c. voltage which is used as a reference for the bias current driver; this enables the computer to control the bias voltage. The twelve bit conversion provides 4096 steps of increasing voltage thus enabling the bias to be scanned in 0.1 mV steps over a 500 mV range. The DAC is controlled via a 16 bit parallel interface and the analogue fed to the control box through a screened cable.

- A Bryans 2500 A4 chart recorder is used to monitor the output from the LIA as a function of applied bias. IET spectra may be obtained directly on the recorder by driving the bias with the motorised potentiometer built into the control box.

- The plotter employed to output the spectra is a Tektronix 4662 digital plotter. The plotter provides high quality graphical images up to A3 size with a maximum resolution of 4096 on the X axis and 2731 on the Y. It is also possible to digitise points on the plotted graphs, allowing accurate determination of positions of features on previously plotted data. The plotter is interfaced via a 600 baud RS232 line. The stylus is controlled by a joystick and the co-ordinates of the position fed into the computer by pressing a button to accept the reading.

- A printout of header files etc. are produced on a Data Systems IDS-440 impact dot matrix printer.

- The oscilloscope used to monitor and set up the spectrometer is a Phillips PM3251 dual beam.

A schematic diagram of the complete spectrometer is shown in Figure 4.2.

4.5 Software

The software used to drive the spectrometer, collect and process the data and provide hard copies of spectra etc was designed and written by S.Reynolds[2].

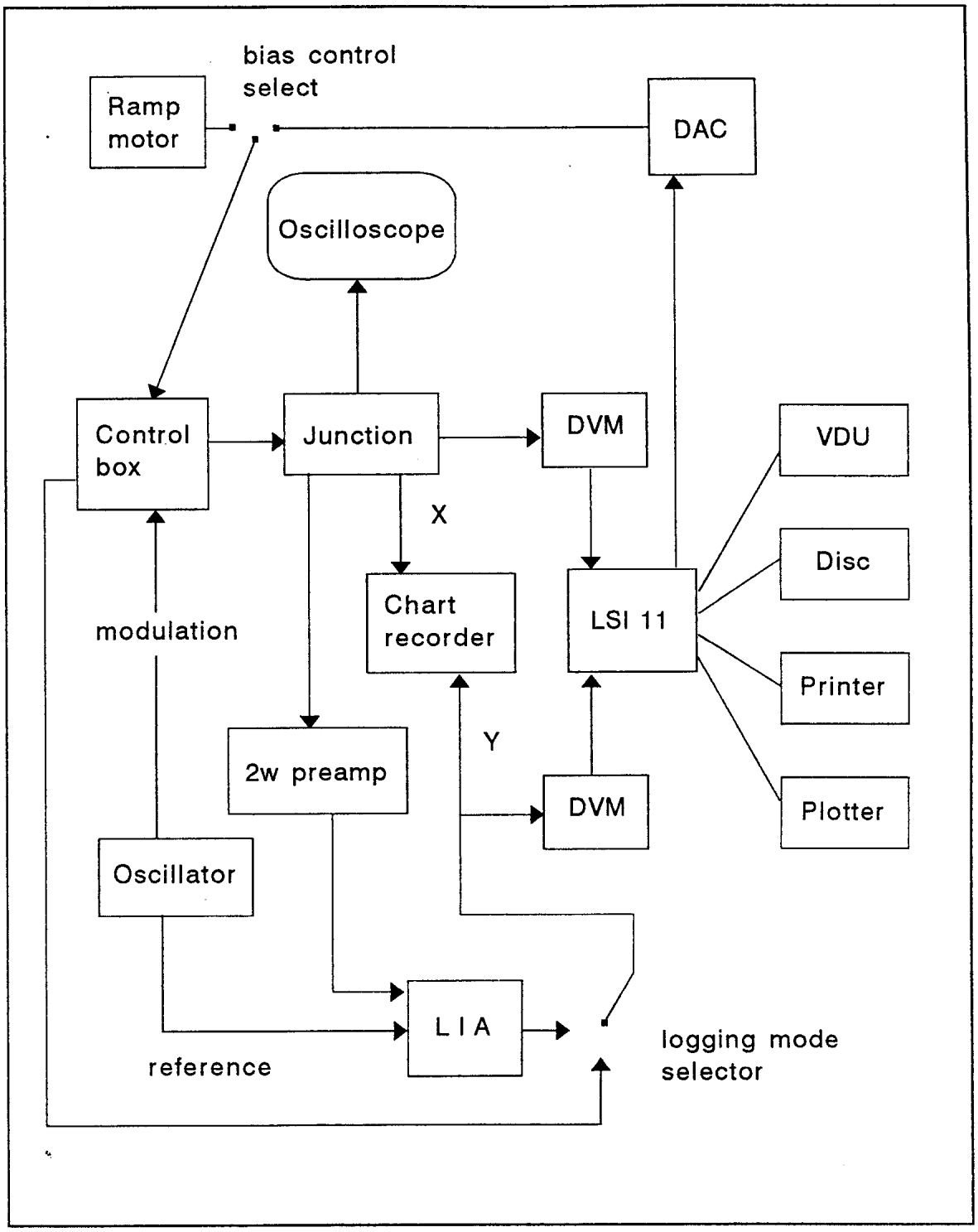

Figure 4.2

Shown in this figure is a schematic of the inelastic electron tunnelling spectrometer used by the group for all of the IETS work presented in this thesis.

References

[1] Tunnicliffe D L 1983 *PhD Thesis* Leicester Polytechnic.[2] Oxley D P, Bowles A J, Horley C C, Langley A J,Pritchard R G and Tunnicliffe D L. 1980 *Surf. Interface Anal.* ***2*** 31.

[3] Reynolds S 1983 *PhD thesis* Leicester Polytechnic.

[4] Reynold S, Gregson L D, Horley C C, Oxley D P, and Pritchard R G 1980 *Surface and Interface anal.* ***2*** 217

[5] Reynolds S, Peasgood A, Oxley D P and Pritchard R G 1987 J. *Phys. C: Solid State Phys.* ***20*** *Soc.* ***15*** 62.

[6] Giaever 11969 *Tunnling Phenomina in Solids* ed. E Burstein and S Lundqvist, (New York:Plenum) Chapter 3

[7] Ginnai T M 1982 *Ph.D. Thesis* Leicester Polytechnic.

[8] Line M J, Pritchard R G, Oxley D P 1989 J.Phys.Condens. Matter **1** 6835.[9] Lamb J and Jaklevic R C 1968 *Phys. Rev.* ***165*** 821

[10] Kirtley J 1980 J. *Am. Chem. Soc.* ***80*** 217.

[11] King R 1983 *Integrated Electronics and Systems.* (UK:Van Nostram) [12] Van de Ziel A 1968 *Solid State Physical Electronics* (New Jersey: Prentice-Hall) 619

[13] Van de Ziel A 1954 *Noise* (New Jersey:Prentice-Hall) 219

[14] Speakman A M and Adkins C J 1992 J. *Phys. Condens. matter* ***4*** 8035

[15] Mc Morris I W N 1977 J. *Chem. Phys.* ***66*** 3952

Contents

CHAPTER 5

RESISTIVE AND BIAS-POLARITY-DEPENDENT EFFECTS ON VIBRATIONAL MODE ENERGY

5.1 Introduction

The material presented in this chapter covers an investigation into two of the phenomena which affect measured peak positions in IETS spectra. The first part of the chapter deals with the effect that the resistance of the electrodes forming the junction has on measured peak positions. The second part of the chapter deals with top-metal and bias polarity effects in undoped tunnel junctions.

5.1.2 The Effect of Electrode Resistance

in order to understand fully the conditions under which one may be confident that electrode resistances are not significant a series of experiments were performed using Al-AlOx-Benzoate-Pb junctions. In this work the resistance of the bottom electrode was varied in a systematic way by altering the thickness of the aluminium forming the bottom electrode.

Measurement of vibrational modes with optimum precision requires careful design of the tunnel junction geometry even when four point probe measurement techniques are employed [1,2]. Care must be taken to avoid the finite electrode resistance causing unwanted potential variations along the electrode material forming the actual junction area.

Mask and Junction Layout

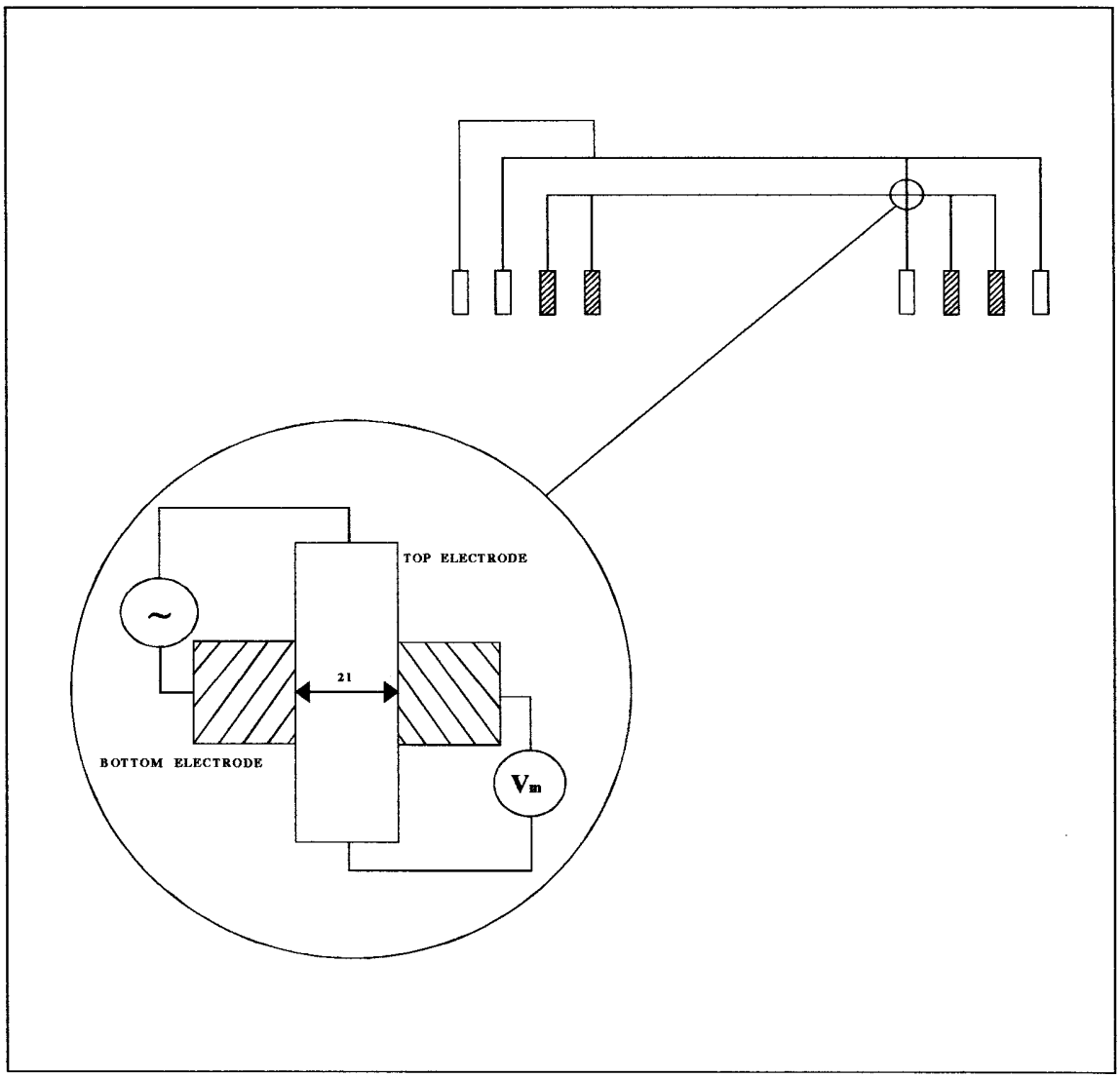

Figure 5.1.

Figure 5.1

An illustration of mask design showing the modified form used in this set of experiments. Also shown is a schematic diagram of the junction area illustrating the positions of the applied bias and the meter used to monitor the voltage across the junction. It can be seen from this diagram that the applied p.d. and the meter are at opposite ends of the junction.

Schematic of Tunnel Junction (After Giaever)

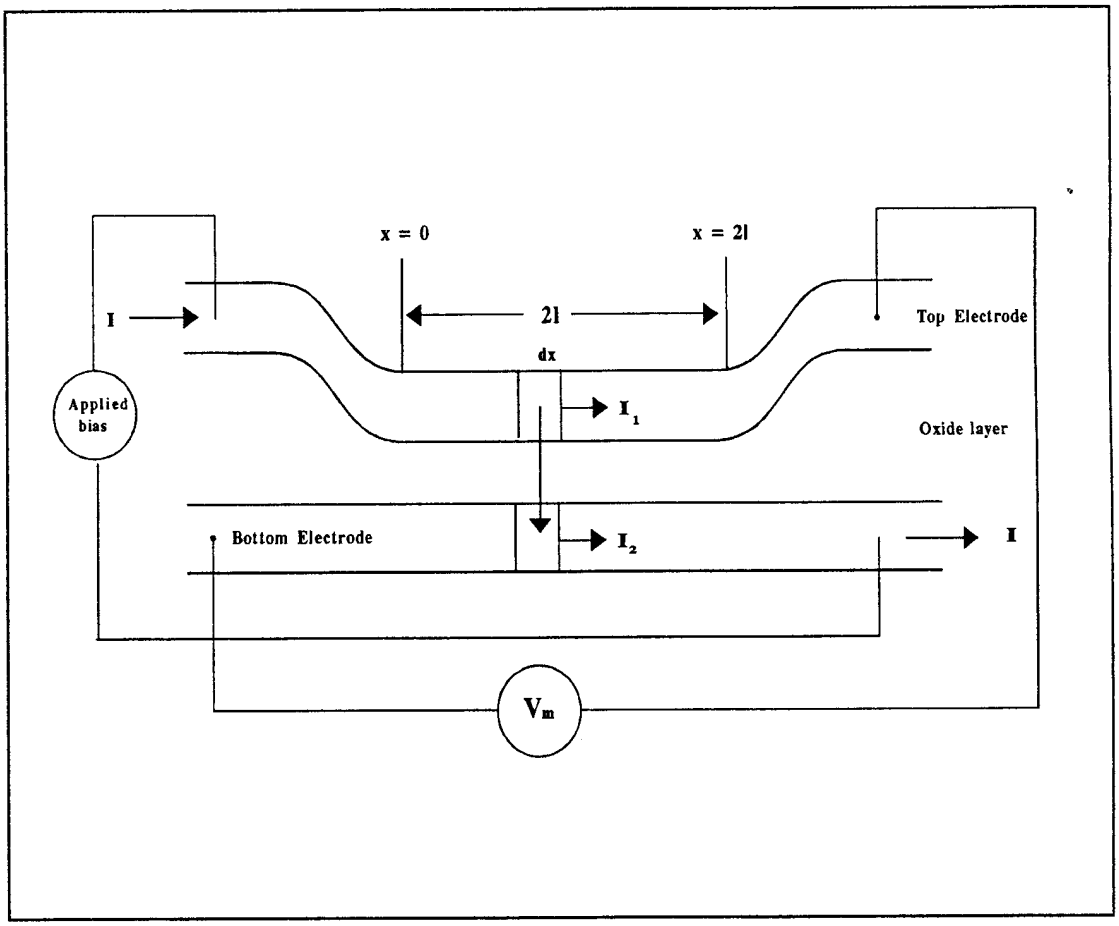

Figure 5.2.

Figure 5.2

A schematic representation of an undoped tunnel junction. The currents and their associated potentials will be functions of position along the junction. The measured resistance will only be a measure of the junction resistance as long as the resistance of the electrodes is very much less than that of the junction.

In the context of this the junctions used in this study are cross shaped, the electrodes being evaporated at right angles to each other - see figure 5.1. An examination of figures 5.1 & 5.2 will show that because the voltmeter and power supply are connected to opposite ends of the electrodes forming the junction, the voltmeter will indicate a measured voltage that is less than that applied. As a consequence of this the vibrational modes will appear to be initiated at apparently lower applied bias and a commensurate line broadening occurs - see figure 5.3.

In the set of experiments conducted into the effect of electrode resistance on measured peak positions the top electrodes were made exclusively from lead. This metal is chosen because lead becomes superconducting at around 7K and as all the .work is conducted with the samples immersed in liquid helium at 4.2K to reduce thermal noise.

The effect of the resistance of the top electrode is eliminated and therefore plays no role in shifting measured peak positions.

It is shown that the positions of spectral lines in IETS can be modified if the resistances of the electrodes which form the junction become too large. The aluminium electrode which forms the junction bottom area is inherently resistive and therefore the applied bias will produce a potential gradient across the junction. This potential variation across the junction manifests itself in two ways. Firstly the measured positions of the spectral lines are shifted and secondly the lines themselves are broadened. These two effects are in addition to the thermal and modulation broadenings and peak shifts described elsewhere in this thesis. The small shifts in peak position and peak broadening caused by electrode resistance are isolated from these other contributions and a simple correction procedure is developed.

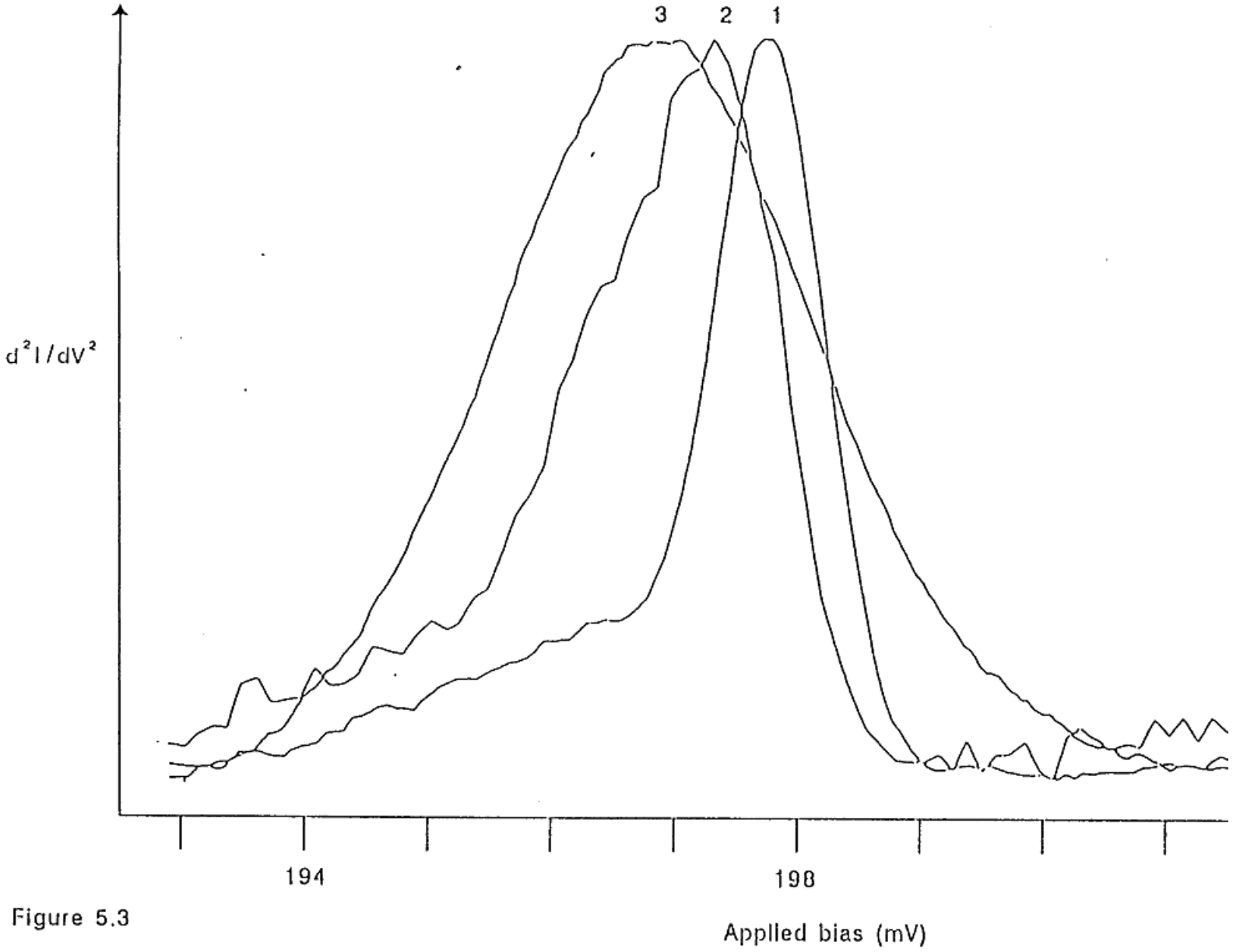

Figure 5.3

Figure 5.3.

IET spectra of the 198 meV region of the benzoate spectrum, for three thicknesses of bottom electrode, with the top electrode biased positively. All spectra were obtained at a junction temperature of 4.2 K, and at a modulation amplitude of 1.0 mV. A smooth background, corresponding to the change in elastic conductance with applied bias voltage, has been subtracted. A down-shift of 1.9 mV occurs when the thickness of the electrode is reduced from 548 nm to 31 nm.

Key to peak numbering

Peak No	Electrode Thickness (nm)	Position (mV)
1	548	198.3
2	80	197.7
3	31	196.4

5.1.3 Top Metal and Bias Polarity Effects

The second part of the chapter deals with top-metal and bias polarity effects in undoped tunnel junctions. The top electrode metals used in this part of the work were: lead, tin and silver respectively. It is important to realise that molecules incorporated in tunnel junctions are under the influence of three fields:

(i) From the barrier structure.

(ii) From the image charges.

(iii) From the applied^{-} bias.

The measurements presented in this section reveal that the peak shift is independent of the metal being used as an electrode material - within the experimental errors of this work. This result is consistent with a simple superposition of the three electric field acting on the hydroxyl group due to the tunnel barrier, the image charge and the applied bias respectively. The implication of this is that so far as the subtle effects on peak shift on reverse bias are concerned, the tunnel junction environment of the adsorbed species is essentially benign.

Using typical values for barrier heights and the distance of the proton in OH from the top electrode together with an expression for image potential [3], the relative orders of magnitude of these three fields are readily shown to be 10^{10} Vm^{-1} for (i) and (ii) and 10^{8} Vm^{-1} for (iii). This clearly shows that in the case of the proton of an OH group, both the barrier and image contributions to the resultant field are considerably greater than that arising from the applied bias.

As IETS has progressed and measurements have been refined to the current level (mode energies can now be reproducibly measured to within 0.03 meV in 150 meV), subtle effects have emerged. Recent work [1] has highlighted the role of the electric field within the junction, suggesting that it interacts via anharmonic effects to perturb the vibrational frequencies of adsorbed molecules. Other workers have examined the effect of image charges in the metal electrodes of the junction on peak positions [3] and significant peak shifts due to the nature of the metal in the top electrodes have also been reported [4-6] It is clear that there is a need to distinguish these effects from the equally important peak shifts associated with the chemical aspects of the adsorption of dopant molecules to the oxide surface [7-9].

It is also important to recognise that the potential barrier associated with the metal oxide work functions produces a significant electric field at a dopant molecule as does the image charge. The net electric field referred to above can be varied in two ways. The first is by alteration of the potential barrier associated with the metal oxide work functions by the use of different metals as counter-electrodes. The second approach is a simple reversal of the applied bias for a given top electrode.

The material presented here extends previous measurements on reverse-bias peak shifts [1] to include different top metal electrodes. These data are then used to examine the relative roles of the electric field contributions outlined above.

5.2 Notation

In this chapter the terms forward and reverse bias refer to the lead top electrode being biased positively and negatively with respect to the aluminium bottom electrode respectively. The peak shift, ΔV, is the numerical difference between the

measured position of a given peak under forward bias and its position under reverse bias.

5.2.1 Glossary of Terms

2l = the width of each of the electrodes assuming both are identical.

$\mathbf{1_1}$ and $\mathbf{1_2}$ are the currents flowing in the top and bottom electrodes respectively.

$\mathbf{V_1(x)}$ = the potential at position x in the top electrode.

$\mathbf{V_2(x)}$ = the potential at position x in the bottom electrode.

$\mathbf{R_e}$ = The resistance of the electrode.

$\mathbf{R_j}$ = the resistance of the junction.

$\mathbf{V_{app}}$ = the applied bias.

$\mathbf{\Delta V}$ = the numerical difference between the applied and measured p.d.

$\mathbf{V_m}$ = the measured potential difference.

$\mathbf{\Delta V_\omega}$ = the excitation voltage of a particular molecular oscillator of frequency ω.

$\mathbf{\Delta V_R}$ = The numerical difference between the measured position of a given peak under forward and reverse bias.

5.2.3 Junction Fabrication

The junctions were prepared as described in detail in chapter. The exceptions to this procedure were the junctions with silver top electrodes.

These initially proved to be very unreliable, exhibiting breakdown below 250mV, and excessive noise or no OH peak at 450mV. A subsequent private communication from

Professor P.K.Hansma suggested the use of a lower evaporation rate for the aluminium and thermal oxidation at temperatures higher than ambient (instead of plasma glow discharge) together with thinner top electrodes. The adoption of these procedures resulted in silver junctions having greater reproducibility and reliability.

5.3 Electrode Resistance Effects.

These experiments establish clearly that even when four-point-probe measurements are used, it is necessary to be aware of the effects of parasitic potential variations along the electrode material forming the actual junction area.

The importance of this is illustrated in figure 5.3 which presents a detailed examination of the normal mode of the 198.3 meV peak in the benzoate spectrum, where the mode is substantially down shifted and broadened when the Al electrode is reduced in thickness below the normally used level of 300nm. A relatively straightforward model described below allows one to establish criteria that allow such effects to be avoided.

The preparation of tunnel junctions essentially similar to those used in this work have been described in detail [11] However as discussed below, modifications to the geometry have been introduced. These facilitate both measurement of the top- and bottom-electrode resistance and performance of simultaneous four point probe IETS at 4.2K.

5.4 Resistive Errors

The theory is developed in the following ways: First a simple theory is developed. This is then followed by two detailed analyses of a tunnel junction first with both electrodes normal and secondly with the top electrode superconducting. These last two more rigorous treatments following an analysis performed by Giaever [12].

5.4.2 The Simple Theory

In this analysis the junction under consideration is Al-oxide-Pb The top Pb electrode will be superconducting, the more usual state in PETS, and therefore have zero resistance. Referring to figure 5.2. and assuming that the top electrode is biased positively with respect to the bottom; conventional current will therefore flow as shown in the figure. Assuming a uniform current density through the oxide, the current in the aluminium electrode at any position for x > 0 is given by:

$$I_2 = \frac{Ix}{2l}$$

for (0 < x <_ 21), for x > 21, Ix = I, and for x < 0, Ix = 0

To calculate the potential drop ΔV along the electrode, consider the voltage drop δV across a small element δx at x.

$$\delta V = \left[\frac{I R}{2l}\right] x \quad \delta x$$

Therefore the total change in potential difference AV in the electrode between x = 0 and x = 21 is given by integrating over the total length, 21, of the electrode.

$$\Delta V = \frac{IR}{2l}\int_0^{2l} x\,dx$$

$$\therefore \Delta V = \frac{IR2l}{2} \qquad \textbf{(5.1a)}$$

The current through the junction is given by: $\mathbf{I = V_{applied} / R_j}$ and the resistance per unit length of the aluminium electrode is: R_e / 2L where L is the total length of the aluminium electrode. Substitution into equation for ΔV gives:

$$\Delta V = \frac{V_{applied}}{2}\frac{R_e}{R_j}\frac{2l}{L} \qquad \textbf{(5.1b)}$$

Equation 5.1. shows that AV is dependent upon the ratio of the total resistance of the aluminium electrode (R_e) - a parameter measured during selection of junction which are suitable for IETS - and the resistance of the junction (R_j). Because of the positioning of the voltmeter - see figure 5.1 - the measured potential difference across the junction is less than that being applied. As a consequence of this as the bias is increased, molecular oscillators nearer to the applied bias end will be excited at an apparently smaller applied bias. Thus neglecting thermal and modulation effects the changes in conductance associated with each

oscillator will appear to commence at a bias voltage reduced by ΔV from the true value. This will produce a downward shift in the measured positions of the spectral lines.

5.4.3 Resistive Peak Shift after Giaever

In this part of the analysis both electrodes are assumed to be formed from the same material and are not in a superconducting state. Referring to figure 5.2. The currents and voltages along the electrodes will be functions of position. The total resistance of each of the electrodes is R_e, and the tunnelling resistance is R_j. The voltage drop across the element due to the current, I_1, in the top electrode is:

$$\frac{R_e}{2l} I_1 = -\frac{dV_1}{dx} \qquad \textbf{(5.2)}$$

and the voltage across the element of length dx due to the current, I_2, in the bottom electrode is given by:

$$\frac{R_e}{2l} I_2 = -\frac{dV_2}{dx} \qquad \textbf{(5.3)}$$

I_1 and 1_2 being functions of position x along the electrode. It is apparent that the sum of these currents gives the total current:

$$\mathbf{I_1 + I_2 = I} \qquad \textbf{(5.4)}$$

The potential drop across the across the junction element dx at x is given by:

$$V_{1(x)} - V_{2(x)} = R_j \, 2l \, \frac{dI_2}{dx} \qquad (5.5)$$

Where $V_1(x)$ is the voltage at position x in the top electrode, V_2 (x) is the voltage at position x in bottom electrode and I_2 is the current flowing in the bottom electrode, see figure 5.2. Equations 5.2 to 5.5 are the starting point for the more rigorous treatment, the initial step is to differentiate equation 5.5 giving:

$$\frac{dV_1}{dx} - \frac{dV_2}{dx} = R_j \, 2l \, \frac{d^2I_2}{dx^2} \qquad (5.6)$$

From 5.1 and 5.2

$$\frac{dV_1}{dx} = - \frac{R_e}{2l} I_1$$

$$\frac{dV_2}{dx} = - \frac{R_e}{2l} I_2$$

Also $I_1 = I_1 - I_2$ and from 3 $(I_2 - I_1) = (I_2 - I + I_2)$

$$\therefore \quad \frac{d^2I_2}{dx^2} = \frac{R_e}{R_j} \frac{2}{(2l)^2} \left[I_2 - \frac{I}{2} \right] \qquad (5.7)$$

Equation 5.7 is of the form:

$$\frac{d^2I_2}{dx^2} = K_1 I_2 + K_2$$

Where

$$K_1 = \frac{R_e}{(2l)^2}\frac{2}{R_j}$$

and

$$K_2 = -\frac{R_e}{R_j}\frac{I}{(2l)^2}$$

Trying a solution of the form:

$$I_2 = Ae^{ax} + B^{-ax} + C$$

$$\frac{d^2I}{dx^2} = a^2 (I_2 - C)$$

Therefore from equation 5.7

$$C = \frac{I}{2}$$

and so

$$I_2 = Ae^{ax} + Be^{-ax} + \frac{I}{2} \qquad (5.8)$$

also using equation 5.7

$$\therefore \qquad a = \frac{1}{2l}\left(\frac{2\,R_e}{R_j}\right)^{\frac{1}{2}}$$

The boundary conditions are:

at $\mathbf{x = 0}$ $\mathbf{I_2 = 0}$ and noting that $\mathbf{e^0 = 1}$ and $\mathbf{e^{-0} = 1}$

Substituting into equation 5.8 gives:

$$A + B + \frac{I}{2} = 0 \qquad \textbf{(5.9)}$$

At $\mathbf{x = 2}$ $\mathbf{I_2 = I}$ substitution into equation 8 gives:

$$I = Ae^{2la} + Be^{-2la} + \frac{I}{2} \qquad \textbf{(5.10)}$$

Let $\alpha = \mathbf{A + B} \rightarrow \mathbf{-(I/2)}$ from equation 5.9.

and $\beta = \mathbf{Ae^{2la} + Be^{-2la}} \rightarrow \mathbf{I / 2}$ from equation 5.10.

From 5.9

$$B = -\left(\frac{I}{2} + A\right)$$

Substituting into 5.10 gives:

$$Ae^{2la} - \left(\frac{I}{2} + A\right) e^{-2la} = \frac{I}{2}$$

$$Ae^{2la} - Ae^{-2la} = \frac{I}{2}\left(1 + e^{-2la}\right)$$

Since $\mathbf{(e^x - e^{-x})/2 = Sinh\ x}$, $\mathbf{e^x - e^{-x} = 2\ sinh\ x}$

Therefore $\mathbf{2(e^x - e^{-x}) = 4\ sinh\ x}$ and therefore

$$A = I\left(\frac{1 + e^{-2la}}{4 \sinh 2la}\right) \qquad \textbf{(5.11)}$$

from 5.9 **B = (I/2) - A** giving:

$$B = -\frac{I}{2} - A = -\frac{I}{2} - \left(\frac{I\,(1 + e^{-2la})}{2\,(e^{2la} - e^{-2la})} \right)$$

$$\therefore \qquad B = -I\,\frac{(1 + e^{2la})}{4 \sinh 2la} \qquad \textbf{(5.12)}$$

Also from 5.5:

$$V_{1(0)} - V_{2(0)} = R_j\, 2l \left(\frac{dI_2}{dx} \right)_0$$

and from equation 5.8

$$\left(\frac{dI_2}{dx} \right)_0 = a\,(Ae^0 - Be^{-0}) = a\,(A - B)$$

Therefore

$$V_1(0) - V_2(0) = R_j\, 2la\,(A - B)$$

$$V_1(2l) - V_2(2l) = R_j\, 2l\, a\,(Ae^{2la} - Be^{-2la})$$

$$V_1(2l) - V_2(0) - V_2(2l) + V_1(0) = \qquad \textbf{(5.13)}$$

$$R_j\, 2l\, a\,(Ae^{2la} - Be^{-2la} + A - B)$$

working on the right-hand side term and substituting for A and B using 5.11 and 5.12

gives:

$$= \frac{I}{4 \sinh 2la} \left(4 + 2e^{2la} + 2e^{-2la} \right) \qquad \textbf{(5.14)}$$

$\cosh x = 1/2 (e^x + e^{-x})$, therefore dividing $2e^{2la} + 2e^{-2la}$ by 2 will give:

$$\frac{I}{\sinh 2la} \left(1 + \cosh 2la \right)$$

From equation 5.13 and referring to figure 5.4 we see that

$$2 V_m = - IR_e + 2l\, a\, R_j\, I \left(\frac{1 + \cosh 2la}{\sinh 2la} \right) \qquad \textbf{(5.15)}$$

and

$$\frac{V_m}{I} = R_j\, l\, a \left(\frac{1 + \cosh 2la}{\sinh 2la} \right) - \frac{R_e}{2} \qquad \textbf{(5.16)}$$

From equation 5.7

$$a = \frac{1}{2l} \left(\frac{2 R_e}{R_j} \right)^{1/2} \qquad \therefore \qquad la = \frac{1}{2} \left(\frac{2R_e}{R_j} \right)^{\frac{1}{2}}$$

substituting for 5.la gives:

$$\frac{V_m}{I} = R_j \left(\frac{1}{2} \left(\frac{2 R_e}{R_j} \right)^{\frac{1}{2}} \frac{1 + \cosh 2al}{\sinh 2al} \right) - \frac{R_e}{2 R_j}$$

giving:

$$\frac{V_m}{I} = R_j \left(\frac{1}{2} \left(\frac{2\,R_e}{R_j} \right)^{\frac{1}{2}} \left(\frac{1 + \cosh \left(\frac{2\,R_e}{R_j} \right)^{\frac{1}{2}}}{\sinh \left(\frac{2\,R_e}{R_j} \right)^{\frac{1}{2}}} \right) - \frac{R_e}{2\,R_j} \right) \qquad (5.17)$$

let $\varepsilon = (2R_e / R_j)^{1/2} = \sqrt{2}\,(R_e / R_j)^{1/2}$, and $\mu = (R_e / 2R_j)^{1/2} = 1/\sqrt{2}\,(R_e / R_j)^{1/2}$ therefore $\varepsilon / \mu = 2$ and so $\varepsilon = 2\,\mu$. Also noting that $\cosh^2 x = 1/2\,(1 + \cosh 2A)$ and that $\sinh 2x = 2 \sinh x \cosh x$.

Therefore

$$\frac{1 + \cosh 2\,\mu}{\sinh 2\,\mu} = \frac{2 \cosh^2 \mu}{2 \sinh \mu \cosh \mu}$$

cancelling gives :

$$\frac{\cosh \mu}{\sinh \mu}$$

substituting this result into equation 5.15 and cancelling results in the equation obtained by Giaever [12]

$$V_m = I\,R_j \left(\left(\frac{R_e}{2R_j} \right)^{\frac{1}{2}} \left(\frac{\cosh \left(\frac{R_e}{2R_j} \right)^{\frac{1}{2}}}{\sinh \left(\frac{R_e}{2R_j} \right)^{\frac{1}{2}}} \right) - \frac{R_e}{2\,R_j} \right) \qquad (5.18)$$

The measured voltage is thus dependent upon the ratio of the electrode and junction resistances. If $R_e > R_j$ the result may be negative and therefore we should be very critical of all results where $R_e \approx R_j$. Forming the electrodes from superconductors, $R_e = 0$ will eliminate the problem.

5.5 Giaever with Top Electrode Superconducting

The usual configuration of the tunnel junctions used in this work is Al - AlOx - dopant - Pb. To bring the theory more into line with the practice the above mathematical treatment will be applied to a junction of the form Al - AlOx - Pb. Here the top electrode is evaporated from lead and so will be superconducting at the temperatures used in the experiments - 4.2K thus equation 2 will become:

$$- \frac{dV_1}{dx} = 0$$

The equations numbered 5.3 to 5.5 will remain the same for this analysis.

differentiating equation 5.5 gives:

$$\frac{dV_1}{dx} - \frac{dV_2}{dx} = R_j \, 2l \, \frac{d^2 I_2}{dx^2}$$

but $\mathbf{dV_1 / dx = 0}$ and so

$$\frac{dV_2}{dx} = - R_j \, 2l \, \frac{d^2 I_2}{dx^2}$$

also

$$-\frac{dV_2}{dx} = \frac{R_e}{2l} I_2$$

substituting gives:

$$\frac{R_e}{2l} I_2 = R_j \, 2l \, \frac{d^2 I_2}{dx^2}$$

and so

$$\frac{d^2 I_2}{dx^2} = \frac{R_e}{R_j} \frac{1}{(2l)^2} I_2 = K I_2$$

A solution must be of the form:

$$I_2 = Ae^{ax} + Be^{-ax}$$

leading to:

$$\frac{d^2 I_2}{dx^2} = a^2 \left(Ae^{ax} + Be^{-ax} \right) = a^2 I_2$$

$$\therefore \quad \frac{d^2 I}{dx^2} = a^2 I_2 = K I_2 \Rightarrow a^2 = K$$

$$\therefore \quad a = K^{\frac{1}{2}} = \frac{1}{2l} \left(\frac{R_e}{R_j} \right)^{\frac{1}{2}}$$

as before, with top electrode normal.

Also $\mathbf{I_1 = I - I_2 = I - (Ae^{ax} + Be^{-ax})}$

and so from equation 5.3

$$\frac{dV_2}{dx} = -I_2\left(\frac{R_e}{2l}\right) = -\left(\frac{R_e}{2l}\right)\left(Ae^{ax} + Be^{-ax}\right)$$

Integrating between 0 and 2l

$$\int_0^{2l} dV_2 = -\left(\frac{R_e}{2l}\right)\int_0^{2l}\left(Ae^{ax} + Be^{-ax}\right)dx$$

Boundary conditions are:

At x = 0, $I_2 = 0$ giving 0 = A + B therefore A = - B

At x = 2l, $I_2 = I$ giving $I = Ae^{2al} + Be^{-2al}$

Substituting for B gives:

$$I = Ae^{2al} - Ae^{-2al} = A\left(e^{2al} - e^{-2al}\right)$$

giving

$$I = 2A \sinh 2al$$

therefore

$$A = \frac{I}{e^{2al} - e^{-2al}} = \frac{I}{2 \sinh 2al}$$

and since **B = - A**

$$V_2(2l) - V_2(0) = -\left(\frac{R_e}{2la}\right)\left(Ae^{2al} + Ae^{-2al} - A - A\right)$$

Giving:

$$V_2(2l) - V_2(0) = -\frac{R_e A}{la}\,(1 - \cosh 2al)$$

Noting that

$$A = +\frac{I}{2 \sinh 2al} \qquad also \qquad a = \frac{I}{2l}\left(\frac{R_e}{R_j}\right)^{\frac{1}{2}}$$

Substituting for A and a gives:

$$V_2(2l) - V_2(0) = \frac{R_e}{l}\left(\frac{I}{2 \sinh 2al}\right) 2l \left(\frac{R_j}{R_e}\right)^{\frac{1}{2}} (1 - \cosh 2al)$$

$$V_2(2l) - V_2(0) = (R_e R_j)^{\frac{1}{2}} I \left(\frac{1 - \cosh 2al}{\sinh 2al}\right) \qquad (5.19)$$

And

$$\frac{1 - \cosh y}{\sinh y} = \frac{-\frac{y^2}{2!} - \frac{y^4}{4!}}{y + \frac{y^3}{3!}}$$

cancelling gives:

$$\frac{-\frac{y}{2!} - \frac{y^3}{3!}}{1 + \frac{y^3}{3!}} \qquad (5.20)$$

If y is small sinh y tends to y and so equation 20 will tend towards - y / 2, where

y = 2al substituting into 5.19 gives:

$$\Delta V = V_2(2al) - V_2(0) = (R_e R_j)^{\frac{1}{2}} I - \frac{2al}{2}$$

Cancelling gives:

$$\Delta V = R_e^{\frac{1}{2}} R_j^{\frac{1}{2}} - I\, al$$

But:

$$a = \frac{1}{2l} \left(\frac{R_e}{R_j} \right)^{\frac{1}{2}}$$

substituting for **a** gives:

$$\Delta V = R_e^{\frac{1}{2}} R_j^{\frac{1}{2}} - I \frac{1}{2l} \left(\frac{R_e}{R_j} \right)^{\frac{1}{2}} l$$

$$\Delta V = - R_e \frac{I}{2}$$

In terms of resistance per unit length (R)

$$\Delta V = \frac{R\, I\, 2l}{2} \qquad \textbf{(5.21)}$$

Comparing this equation for the potential drop along the electrode with equation 5.1a shows them to be exactly the same.

5.6 Comparison With Previous Work

It is interesting to note at this juncture that Kirtley and Hansma [4] using different metals as top electrodes, found a strong correlation between peak position and widths for the OH and OD stretch modes in Al-AlOx- Pb junctions. It might be envisaged that this correlation is due to a resistive effect since their results are quoted for electrodes approximately 200 nm thick. However, they found no thickness dependence of the effect they observed, and thus their shifts cannot be explained by the effects discussed in § 5.3. But, for given tunnel junctions and bottom electrode materials and thicknesses, it is readily shown that ΔV is proportional to $(21)^2$.

5.6.1 Dependence of Peak Shift on Electrode Width

The resistance of the aluminum electrode is given by:

$$R_e = \frac{\rho_e L}{2l\ t} \qquad (5.22)$$

Where L is the total length of the bottom electrode and assuming that the thickness of the electrode is constant. The resistance of the junction is given by:

$$R_j = \frac{\rho_j\ t_j}{2l\ 2l} \qquad (5.23)$$

Where tj is the length of the junction - i.e. the thickness of the insulating oxide layer.

Incorporating these equations into equation 21 results in:

$$\Delta V = \frac{V}{2} \frac{\rho_e L}{2l\ t} \frac{(2l)^2}{\rho_j\ t_j} \frac{2l}{L} \qquad (5.24)$$

Cancelling gives:

$$\Delta V = \frac{V}{2} \frac{\rho_e}{\rho_j} \frac{(2l)^2}{t\ t_j}$$

Assuming constant electrode and junction thickness and all other parameters remaining constant

$$\Delta V \propto (2l)^2 \qquad (5.25)$$

Thus the peak shift is dependent upon the square of the width of the electrodes forming the junction. The electrodes used by Kirtley and Hansma were 140μm wide compared with ours which were 500μm wide. This would indicate that the expected resistive shift of KH would be of the order of a twelfth of those in this study. This confirms that the resistive effects in the shifts reported by Kirtley and Hansma would have been outside the resolution of their experiments.

5.7 Top-metal and Polarity Effects in Undoped Junctions

By repeating the work of Kirtley and Hansma and then extending the investigation to incorporate junctions under reverse bias, this study investigates the effect of the metal used as a counter-electrode on the polarity shift of the 450 mV OH peak.

Table 5.1 lists the results from a series of experiments conducted on AL-AL- Ox-M tunnel junctions, where M = Pb, Sn, Ag. This table brings together the work of two other groups, Kirtley and Hansma [4,5] investigated the effect on the position of the OH peak at 450mV of using metals other than lead as a top electrode under forward-bias conditions and Reynolds and co-workers [1] revealed a small, polarity dependent shift on the position of the 144mV peak in the benzoate spectrum using a lead top electrode, this result being in agreement with similar work on OH at 450mV by Adkins and Sleigh [3].

Table 5.1.

Results for the 450 meV peak. Forward bias and reverse bias refer to the counter-electrode being biased positively and negatively with respect to the bottom aluminium electrode. ΔV *refers to the numerical difference in peak position, for a given peak, under forward and reverse bias.*

Counter-electrode	Forward bias (mV)	Reverse bias (mV)	ΔV(mV)	Kirtley and Hansma (mV) †
Pb	445.6 ± 0.1	447.8 ± 0.1	2.2 ± 0.2	446
Sn	444.3 ± 0.1	446.4 ± 0.1	2.1 ± 0.2	444
Ag$	435.3 ± 0.5	438.2 ± 0.5	2.9 ± 1.0	438

† *Forward bias only.*

As seen in §5.2 the use of silver as a counter-electrode material necessitated adopting different manufacturing procedures for the junctions, which resulted in thinner top electrodes. This has the effect of introducing an error due to the resistance of the electrodes. This is treated using the procedures of §5.4 and yields $\Delta V = 2.7$mV *which when added to the forward-bias result gives 438.0 mV in good agreement with Kirtley and Hansma [4].*

Adkins and Sleigh [3] by assuming, in line with other workers, that the component of the potential of the oscillating system due to the applied field as a linear form, obtained an expression for the top electrode shift in terms of the interaction of the molecular system with its electrical image:

$$\frac{\Delta\omega}{\omega_0} = -\left(\frac{q^2}{16\,\pi\,\epsilon_r\,\epsilon_0\,d^3\,m\,\omega_0^2}\right)\left(1 + \frac{3}{2}\,d\,\beta\right) \qquad \textbf{(5.26)}$$

Here, m is the mass of the proton in the OH group, q is the partial charge on the atom of the adsorbed species, d is the distance from the terminal hydrogen to the top electrode and β is a constant equal to:

$$\omega_0\sqrt{\frac{m}{2D}}$$

Where D is the dissociation energy and ω_o is the frequency of the unperturbed system. A corresponding expression was obtained by Kirtley and Hansma [4] in their analysis. Examination of equation 26 shows that because the last term in the second parentheses has a value of approximately eight, this term dominates and thus the frequency shift is seen to have a $1/d^2$ dependence on d. This would have the effect of producing changes of a few per cent in peak position, a result borne out by the present experiments.

Data from the present work are shown in table 1: columns 2 and 5 show that there is a close correlation between the forward-bias results of our work and the data from Kirtley and Hansma's experiments. Clearly shown is the downward shift in peak position observed when different metals other than lead are used as top electrodes.

The approximation of regarding the electric field acting on a dopant molecule as arising merely from the external bias applied to the junction would appear to be an oversimplification since it is located in a region where one might expect the potential near the edge of the barrier to vary rapidly. The use of different top metal electrodes should offer a means of modifying this latter contribution. However, if a simple superposition of the three field contributions is assumed one would predict that the peak shift on reversing the applied bias should be relatively insensitive to top metal material. This is borne out by the results of the present work; examination of column 4 in table 1 shows that the shift due to reverse bias polarity is insensitive to the metal used to form the top electrode, within the errors of our experimental work.

A comparison of the molecular and image potentials, in this simple one dimensional model, will show that the spatial variation of the force due to the molecular potential is always much greater than the restoring force due to the image potential. By selecting the dominant terms, Adkins and Sleigh obtained an expression for the nolarity shift:

$$\frac{\Delta \omega_{polarity}}{\omega_0} = \frac{3qh\beta\gamma}{\varpi S} \qquad (5.27)$$

Here $\gamma = \varepsilon 1 S/(\varepsilon 2 + \varepsilon\, 2 S 1)$ is the factor by which the field in the adsorbate exceeds the mean field across the barrier. The permittivities of the oxide and the adsorbate are respectively ε1 and ε2; S, S 1 and S2 are the thicknesses of the tunnel barrier, oxide and the adsorbate respectively and ω is the measured frequency.

By considering equation 5.27 we see that it is unlikely that any of the parameters other than γ and S could be affected by changing the top metal; ω is determined by

experiment and β is a constant from the Morse potential:

$$U_0 = D\,(1 - e^{-\beta x})^2$$

Also q is given the value of free OH in this case following Adkins and Sleigh. The total thickness S is the sum of S 1 and S2 and incorporated into S2 is d, the distance of the top hydrogen to the metal surface. Thus it can be seen that the polarity shift is weakly dependent upon d through γ.

Using observed frequency shifts and assuming a value for d, Adkins and Sleigh calculated a value for q/e. In the case of lead the value selected for d was 200 pm, which corresponds to a figure slightly larger than the radius of a lead atom. The figures S1 = 2 nm, S2 = 0.2 nm, ε1 = 7.6, ε2 = 1, hω = 450 meV and Δω = 1.1 meV gave a result of -0.32 for q/e compared with -0.2 in the case of free OH [13]

The radii of tin and silver atoms are smaller that of tin being 140 pm and that of silver being 144 pm, which raised the question of whether or not using these metals as counter electrodes would reduce the value of d from that of the lead value and thus change the peak shift by an observable amount.

Handy [14] found that smaller metal atoms gave thinner effective barriers, suggesting that the small atoms penetrated further into the oxide. This would have the effect of reducing d in our simple model, which would increase -y and therefore Δω. In this study we have assumed that d would be, in each case, rounded up to a value slightly above the radius of the atoms of the metal used as a counter electrode in line with the assumption above. The validity of this assumption is, perhaps questionable but since the whole area of theoretical calculation of charge distribution is somewhat unreliable the assumption is as good a starting point as any to provide order of magnitude comparisons.

We substitute values of d Ag = 155 pm and d Sn = 150pm to give q/e = - 0.28 for silver and q/e = - 0.27 for tin. The results compare well with the calculated value of -0.2 cited above but, given the unreliable nature of calculating charge distributions and the low signal to noise ratio for the OH mode, it would be naive to draw exact conclusions from these results.

By substituting the values for the radii of the atoms of the various metals used as counter electrodes ΔV can be calculated roughly. The results of these calculations are listed in table 5.2.

Table 5.2.

Calculated variations in the peak shift, for three values of atomic radius.

Top Metal	γ	|ΔV| /(mV)
Pb	4.7	2.2
Ag	4.99	2.34
Sn	5.04	2.36

An examination of column 3 in table 5.2 shows that the calculated variation in peak shift will not be resolved in this work. A maximum variation between lead and tin of 0.16 mV is calculated, compared with errors of ± 0.2 mV in the experimental results listed in table 5.1.

It may prove more advantageous with such small shifts to focus attention onto other, better resolved peaks. The 144mV peak in the benzoate spectrum, for example, has been shown to exhibit a small shift on polarity change [5]. A detailed study, using different top electrodes, of both the normal and deuterated form of the benzoic acid spectrum, may provide the data that will pinpoint any differences in polarity shift caused by the use of different top metal electrodes.

5.8 Conclusions

Examination of the peak shift of the 450 meV OH mode on reversing the applied bias reveals that any dependence on the nature of the top metal electrode used is too small to be revealed with the accuracy of the present work. This is in accordance with existing theoretical work and of related interest is the result that we can treat the relatively large and non uniform barrier and image contributions to the resultant field by superposition with the applied field and show that the effect of the former two upon bias reversal is negligible. Thus, in quite subtle ways, the tunnel junction environment remains benign in so far as the vibrating species are concerned.

Calculations of the ratio q/e for the hydroxyl group on alumina within a tunnel junction performed originally by Adkins and Sleigh for a lead top electrode have been extended to include other electrode materials. The results are again roughly consistent with those obtained for free OH by other workers.

The ratio of width to thickness of the electrodes in IET junctions is shown to influence both the apparent position and breadth of spectral lines. This

phenomenon is a result of finite electrode resistance and can be significant even when four point probe conditions pertain. A simple treatment after Giaever allows such effects to be corrected for even when they are difficult to avoid experimentally.

5.9. References

[1] Reynolds S, Peasgood A, Oxley D P and Pritchard R G 1987 *J.Phys. C: Solid State Phys.* ***20*** 2497.

[2] Tunnicliffe D L 1983 *PhD Thesis* Leicester Polytechnic.

[3] Adkins C J and Sleigh A K 1987 *J. Phys. C: Solid State Phys.* ***20*** 4037

[4] Kirtley J R and Hansma P K 1975 *Phys. Rev. B* ***12*** 531.

[5] Kirtley J R and Hansma P K 1976 *Phys. Rev. B* ***13*** 2910.

[6] Lamb J and Jaklevic R C 1968 *Phys. Rev.* ***165*** 821.

[7] Hair M L 1967 *Infrared Spectroscopy in Surface Chemistry* (New York: Dekker) p141.

[8] Bowser W M and Weinberg W H 1977 Surf. *Sci.* ***64*** 377.

[9] Gundlach K H and Kadlec J 1974 *Chem. Phys. Lett* ***25*** 293.

[11] Oxley D P, Bowles A J, Horley C C, Langley A Pritchard R G and Tunnicliffe D L 1980 *Surf. Interface Anal.* ***2*** 31.

[12] Giaever 1 1969 *Tunnelling Phenomena in* Solids ed. E Burnstein and S Lundquist (New York: Plenum) p 27.

[13] Lee T and Schaefer H F 1985 *J. Chem. Phys.* ***83*** 1784.

[14] Handy R M 1962 *Phys. Rev.* ***126*** 1968.

Contents

CHAPTER 6

AN IETS STUDY OF A MONOLAYER LANGMUIR BLODGETT FILM OF STEARIC ACID ON ALUMINIUM OXIDE

6.0 An Overview of Langmuir - Blodgett Films

The diversity of the applications of organic thin films bears witness to the fact that they have an ever increasing role to play in a wide diversity of applications. For example, such films are being used as, photoresists and electron resists for very large scale integration, as photo conductors for printing and copying, as liquid crystal displays, protective coatings and for surface modifications such as adhesion promoters and lubricants.

Attention has also been directed towards their applications in the fields of thin film sensors, transducers and optical devices. Biomedical interest is centred around thin film sensors of various biological processes, such as testing for antibodies. Thin films also have a role to play in the preparation of biocompatable surfaces; implants, for example, need to have an affinity with the fluids of the body such as blood to prevent attacks by antibodies. Much of the early work on these type of films has been done with amorphous organic or polymeric films but the demand for thinner and thinner films increased the need to produce more ordered and well-defined films.

Reducing the thickness of conventional films increases the likelihood of pinholes and defects and led to the conclusion that more ordered films, i.e. those approaching crystallinity, needed to be even more defect free. These requirements naturally led to a re-evaluation of the work done on thin films by I. Langmuir and

K.Blodgett [1-4]. Films made by the Langmuir - Blodgett (LB) technique are highly anisotropic and densely packed. Also by modifying the functional end groups they can be engineered for specific uses. The way in which such films attach to the substrate can be dictated, the structure of the film established and the end groups made functionally appropriate for the chosen application.

The simplicity and versatility of the technique underlies its potential importance for molecular electronics. The ability to design and construct organised systems of molecules that interlock and interact, like the parts of a machine, presents an exciting challenge. Materials can be designed which have properties which depend upon the exact location of each of their component molecules. The building of such molecular assemblies is of great importance and interest in the developing field of microelectronics.

The terminology used to label these films is generally accepted to be as follows:

1. Langmuir Film

A monolayer of material which has been compressed to form a two dimensional solid on the surface of a liquid subphase.

2. Langmuir - Blodgett Film

Langmuir film which as been transferred from a liquid subphase onto a solid substrate. Langmuir - Blodgett films can be composed of one layer of material or built-up multi-layers of one or more materials.

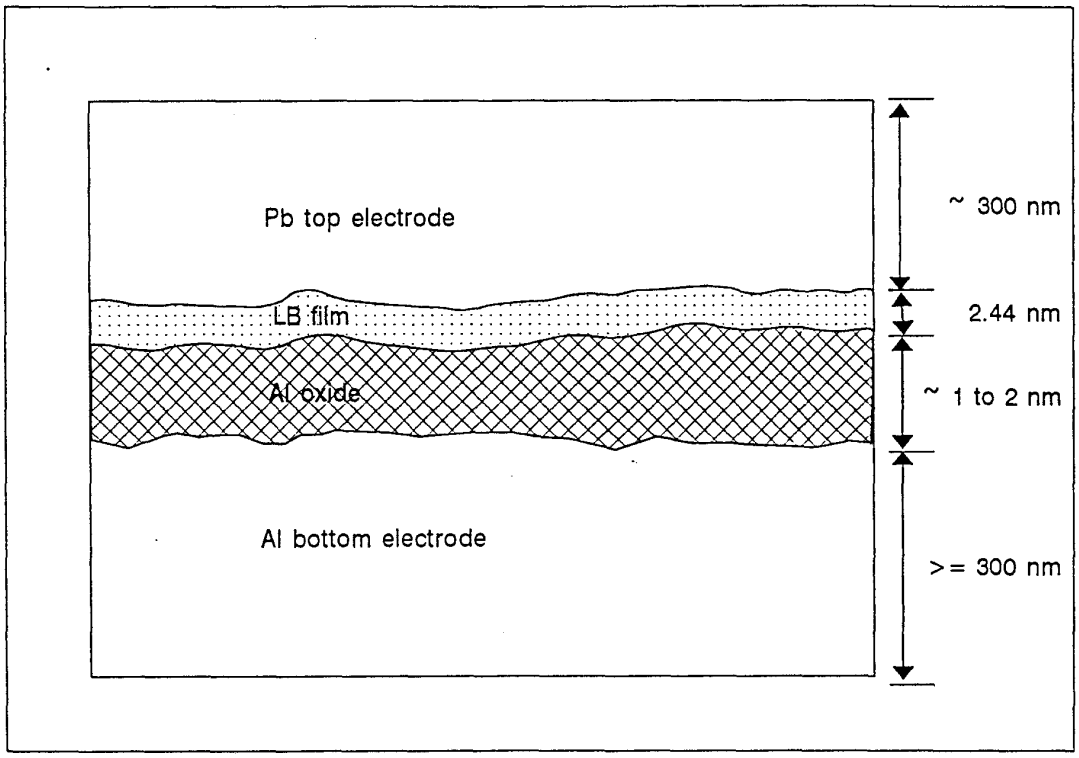

Figure 6.1

Illustrated in this figure is schematic representation of a cross-section through a completed tunnel junction of the type used in this set of experiments. Also shown are typical dimensions of the layers forming the junction sandwich.

6.1. Introduction

The work presented in this chapter builds on work done in this department by Ginnai [5]. Ginnai studied electron tunnelling and conduction methods in single and multi-layer Langmuir - Blodgett films using IETS. The films were fabricated using a trough and dipping mechanism designed and manufactured in the department. His investigations used mixed films of stearic acid and barium stearate and were conducted using tin as a substrate for the Langmuir - Blodgett film and bottom electrode of the IET junctions.

Three of the conclusions drawn from the groups work were:

1. The group found that it appeared not to be possible to manufacture an IET junction using aluminum as a substrate material.
2. The manufacture of defect free films was very difficult to achieve.
3. If non reactive metals such as gold were used as base electrode materials it was impossible to manufacture defect free devices.

An important aim of the present work is to re-investigate the possibility of performing IETS using aluminium -aluminum oxide - LB film - Lead and tin - tin oxide - LB film - Lead junction constructions. Figure 6.1 is a schematic cross section of a tunnel junction. The difference between the present group's work and that of Ginnai's is centred on the manufacture of the films. The group now has access to state-of-the-art film manufacturing facilities in the form of a new tank supplied by Lauda which is housed within a class 100 clean room. It is hoped that these sophisticated facilities will eliminate any of the contamination and monitoring errors which may have been present in the equipment used by the first group and increase the chances of producing good defect-free films. These facilities and equipment are described in detail in the following sections.

6.2 An Introduction to Film Fabrication

Langmuir - Blodgett film fabrication although simple in concept requires careful and sophisticated techniques and procedures. The first parts of the following sections outline the techniques which need to be understood and the preparatory work which had to be done in order to be confident that the Langmuir - Blodgett films produced by this group were coherent and reproducible.

6.2.1 Langmuir Films

The fabrication of a Langmuir film entails the spreading of a small amount of material on the uncontaminated surface of a liquid subphase and then compressing it to form a monomolecular sheet. The subphase most usually used is water. The subphase liquid must be pure especially with respect to surface active contaminants as these may influence the properties of the monolayer. Monolayer forming molecules usually posses both hydrophobic and hydrophillic end groups, such as long alkyl and carboxylic groups respectively. If the amphiphillic balance - the balance between the end groups - is appropriate the molecule will be adsorbed at the air-water interface. A volatile solvent is often employed to assist spreading on the surface.

A monolayer on the surface of a liquid is a two dimensional system. The application of a suitable lateral pressure may result in a monomolecular sheet being formed with all the molecules aligned approximately normal to the surface see figures 6.2a to 6.2c. With the molecules aligned and touching, Van der Waal's interactions can take place along the molecules length and the molecules form into a 2dimensional solid. Figures 6.2a - c illustrate the way that a Langmuir film is formed on the surface

of the subphase. The letters a, b and c identify three of the main components of the tank and subphase.

a. The fixed, floating, barrier which is connected to the monitoring sensors.

b. The moveable barrier - this is driven forwards to compress the film.

c. An area of clean subphase surface which remains uncontaminated and is sealed from the rest of the surface. The sensor uses this surface as a benchmark against which it measures the pressure being applied to the Langmuir film.

Obviously it is of great importance that the film is not over-compressed to a point where it collapses and no longer consists of a well ordered monomolecular sheet. If a suitable solid substrate is then dipped through the film, provided the conditions are suitable, part of the monolayer of molecules will be transferred to the surface of the substrate.

The state of the compression of the film is defined in terms of its surface pressure (π), which is defined as $\pi = \gamma_0 - \gamma$. Where π is defined as the surface pressure or differential surface tension, γ_0 is the surface tension of the gas / liquid interface and γ is the surface tension of the gas / film interface. If the surface area available to the layer of molecules is monitored at the same time as the compressing force it is possible to plot the surface pressure of the monolayer versus the surface area available per molecule. From this curve the behaviour of the spread film can be determined. A plot of pressure versus area for a constant temperature is termed a π/A isotherm - see figures 6.3a & 6.3b.

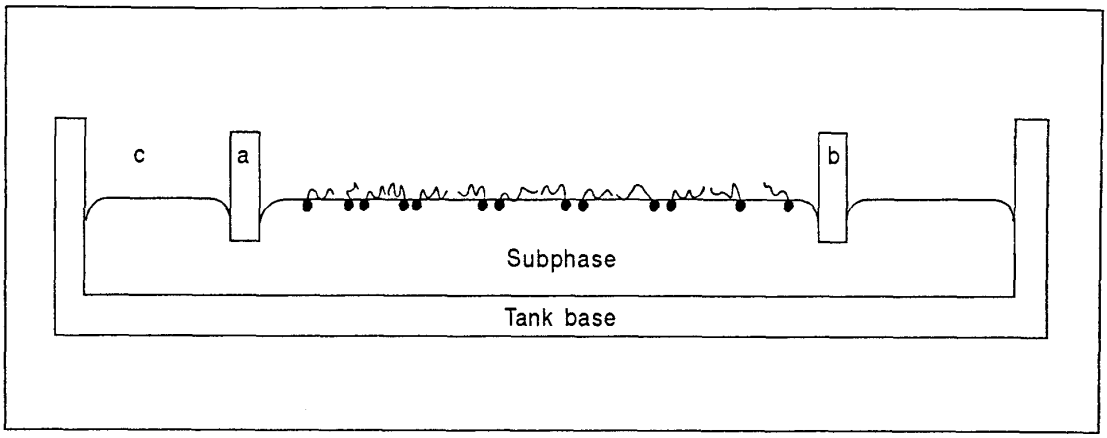

Figure 6.2a.

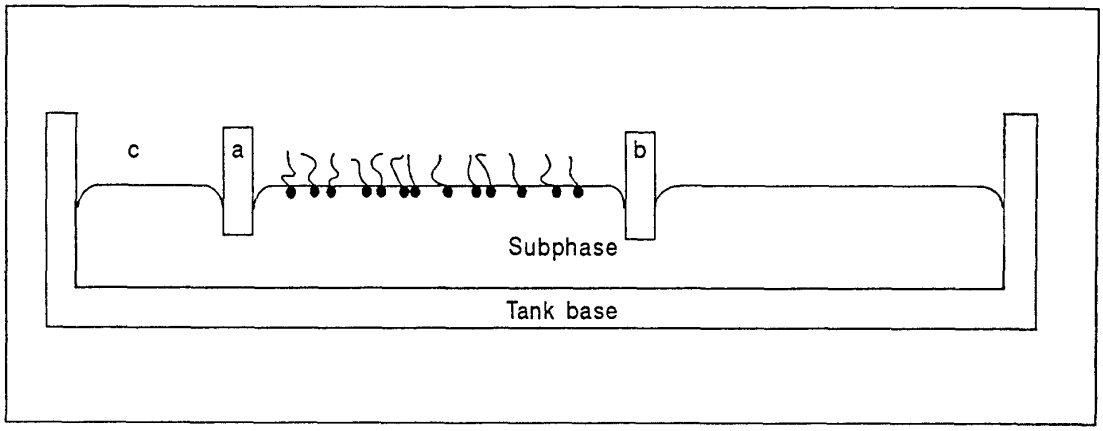

Figure 6.2b.

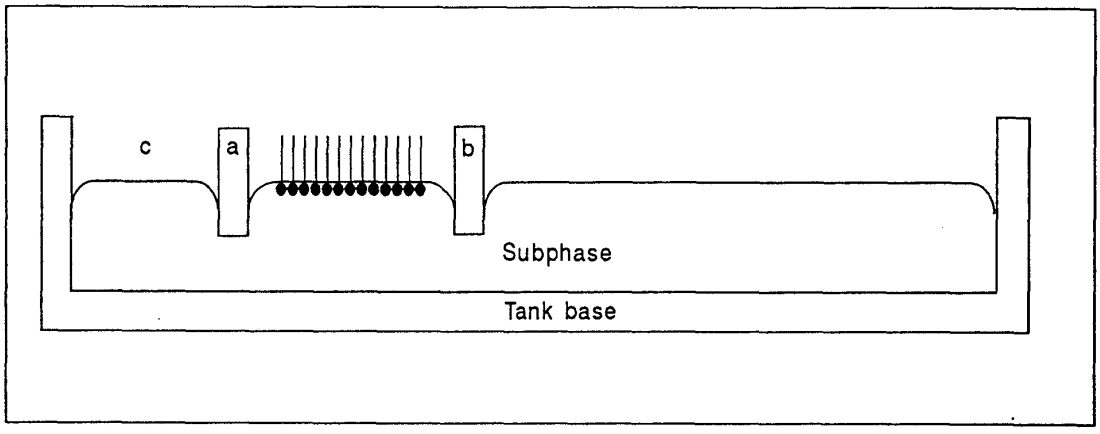

Figure 6.2c.

Figure 6.2a.

Illustrates the gaseous phase of a monolayer. The molecules have spread out to occupy the maximum area available to them. The hydrophillic ends are in the surface of the subphase and the hydrophobic chains are distributed near to the surface.

Figure 6.2b.

Shown here is a representation of the liquids phase of a Langmuir monolayer. As the moveable barrier is moved slowly towards the fixed one the surface area available to the molecules is reduced. This reduction in available area causes the hydrophobic chains to be lifted away from the surface. The surface pressure at which this phase occurs is usually very small (< 1mN m^{-1}) owing to the weak interaction between the tailgroups and the water.

Figure 6.2c.

The last figure in the series is a schematic of the final phase change which takes place. This represents a transition to an ordered solid-like arrangement of the two-dimensional array of molecules. This occurs at a pressure of about 25 mN m^2 and an area per molecule of 0.22 nm^2 $molecule^{-1}$. This is close to that occupied by stearic acid molecules in a single crystal of the acid.

By analogy with an ideal gas three distinct regions can be identified on the curve. These three regions correspond to the gaseous, fluid and solid phases of the monolayer. Beyond the solid phase the layer collapses and the molecules pile up on top of each other. Transfer of the layer to a solid substrate is normally undertaken with the monolayer held in the solid phase and with the surface pressure being held constant during the transfer.

The junctions used in this study were made from mixed films of stearic acid and barium stearate sandwiched between metal electrodes. The metal electrodes were produced using the same methods as described in chapter 3. The criterion developed in chapter five regarding the thickness of the metal films is also applied during their manufacture. The difference between these junctions and those used in the rest of the IETS work covered in this thesis lies in the way that the dopant material is incorporated in the junction. In this work the dopant layer is incorporated into the junction as an L-B film prior to the evaporation of the top electrode.

Figures 6.3 a and 6.3b are stylised surface pressure / area (π/A) curves and are a representative sample of the curves obtained for stearic acid / barium stearate using the LB trough. By analogy with a normal gas undergoing a compression three distinct regions can be distinguished on the curve. These correspond to the gaseous, liquid and solid phases of the monolayer. Each of the three regions are a result of a sudden change in the configuration of the molecules forming the layer on the surface of the subphase as described below.

Gaseous phase

In the gaseous phase the molecules are floating on the surface of the water forming the subphase. The hydrophillic heads of the amphipathic molecules get bound

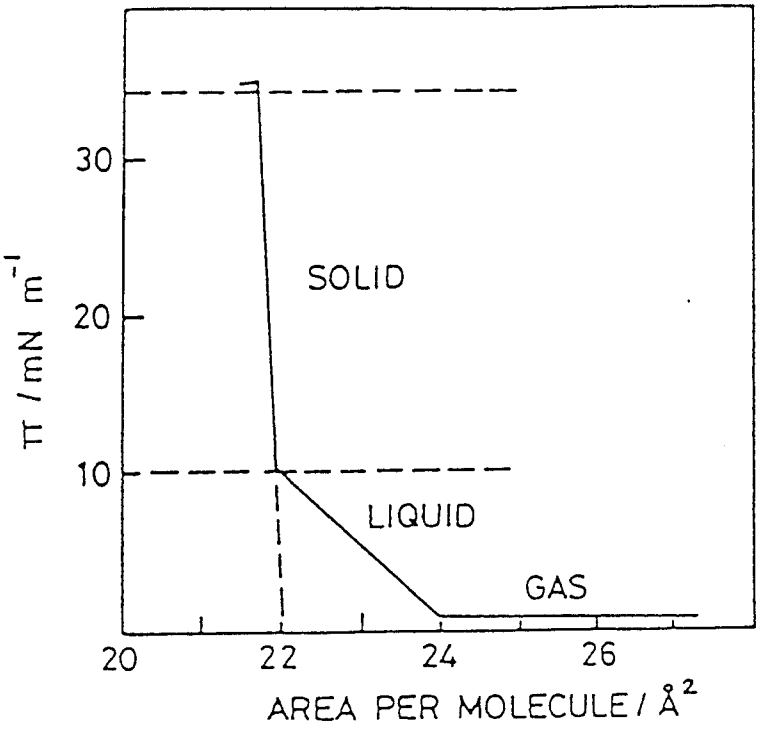

Stylised phi versus area curve

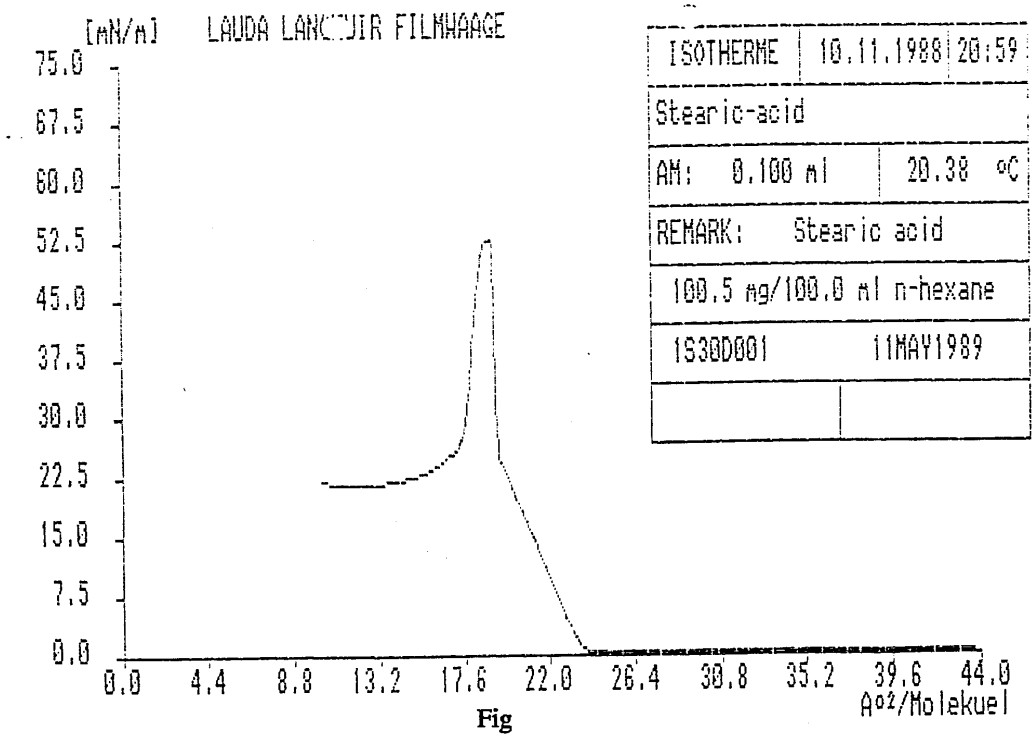

Fig

Phi versus area curve for stea ric acid

Figure 6.3.a

Is a stylised phi versus area curve illustrating the three regions within the curve - gas, liquid, and solid.

Figure 6.3b

Illustrated here is a plot taken from the Lauda trough using a stearic acid / barium stearate monolayer. Comparison with the diagram in 6.3a shows the close correlation between the theory and raw data.

into the subphase and their hydrophobic tails float on the surface with no long-range order discernable.

Liquid phase

As the movable barrier is moved forward, the area available to the molecules is reduced and the pressure on them is increased. When the area of the surface is reduced to a point where there is not enough space to accommodate all of the hydrocarbon tails on the surface the tails will be forced into various standing positions and there will be some short range order. This condition corresponds to the liquid phase in a compressed gas.

Solid phase

If compression of the monolayer continues a limit for the lateral compression of the film is reached when the surface area is approximately 20Å^2 per molecule. In this situation van de Waal's forces come into operation and all of the molecules are formed into well ordered, two dimensional sheet. This phase is termed the solid phase and the sheet has long range order. Further compression of the monolayer will result in collapse of the sheet into a three dimensional crystal-like form with molecules piled on top of each other.

6.3 L-B Film Materials

The general rules-of-thumb for any materials used in conjunction with Langmuir film production are as follows; note that no order of precedence is placed upon the sequence of the following limitations.

l. It is essential that only the purest grades of materials are selected to be used; the levels of surface active contaminants are especially important in this work.

2. Other materials which may come into contact with the subphase/film should not be prone to oxidation.

3. It is also important that the materials used in the manufacture of the tank are not prone to leaching. In this process chemicals which become entrapped during the manufacture of the material are released into the subphase causing contamination.

The tank used in this department was supplied by Lauda their expertise and testing ensure that the materials used in the construction of the tank comply with the rigorous standards outlined above. Other materials such as glassware and handling equipment etc. undergo the rigorous cleaning procedure developed by this department and have been described in chapter three of this thesis.

6.3.1. Subphase Water

When selecting the subphase liquid particular care must be taken in reducing surface active contaminants to the absolute minimum. The water used as a subphase in this set of experiments was supplied by a dedicated system manufactured by Millipore.

The process of purifying the water used in this set of experiments starts with water taken from the mains. This was passed through a thirty micron particulate filter to remove solids. The filtered water was then pumped through a softener to remove carbonates and then through an activated carbon filter to remove salts. Next it is forced through a reverse osmosis filter after which its conductivity has increased to 0.5 to 1 x 10^{-2} $M\Omega^{-1}$ m^{-1}. The water is then pumped through two inorganic chambers

and an organic scavenger cartridge and finally through a five micron filter to give a output

supply of water which has a conductivity of 18 x 10^{-2} $M\Omega^{-1}$ m^{-1}. All tap water used for washing of glassware etc was passed through a thirty micron filter followed by a five micron filter to remove solids from the supply. The supply was piped directly into the clean room where the L.B. trough was housed. Regular maintenance of the piping was required to eliminate the build up of organic contaminants which could have occurred in the pipe when the tank remained unused for any extended periods of time. This was carried out by a qualified technician who also monitored and maintained the quality of the Millipore water.

6.4 Instrumentation

The instrument used to manufacture the Langmuir - Blodgett films used in this study was a Lauda Filmbalance FW2 manufactured by Lauda 1251, Pfarrstraβe 16/43, 6970 Lauda - Königshofen. The MGW Lauda Filmbalance is a highly sophisticated precision instrument capable of manipulating monolayers of molecules over a wide range of film and subphase conditions. A measuring range of - 5 to 95 mN/m, a resolution of < 0.04 mN/m and accurate temperature control over the range from 0° to 60° ensure that the static and dynamic characteristics of a wide range of films can be interpreted, with great accuracy. Transfer of the films from the subphase to substrate is done under computer control using an integral dipping mechanism.

Figure 6.4 is a diagram of the trough showing the main features. The trough is fabricated from brass and then coated with a thin sheet of Teflon (ptfe). The coating has a number of advantages; first the hydrophobic nature of the ptfe allows the subphase surface to form a meniscus which extends above the level of the top

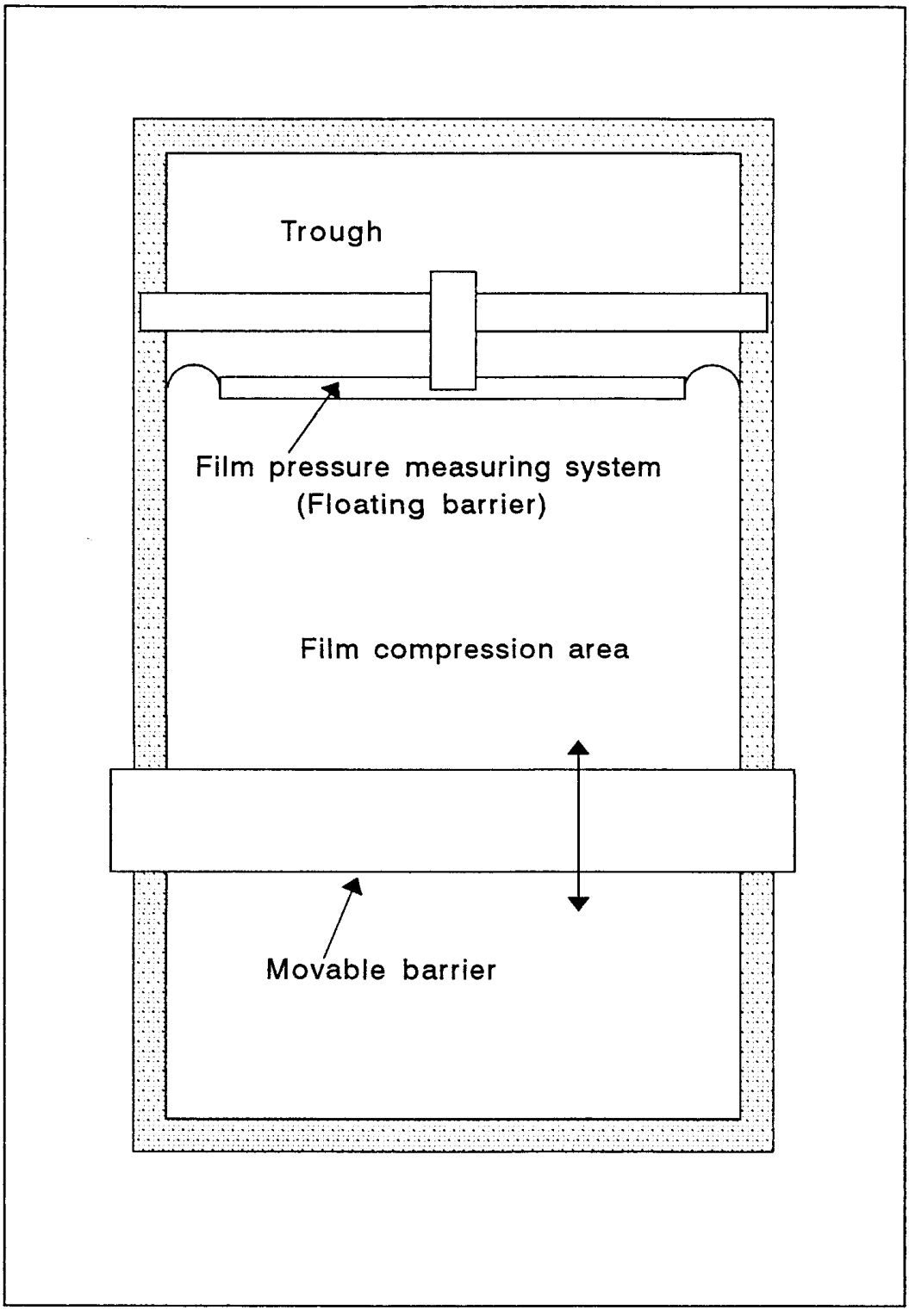
Trough
Film pressure measuring system
(Floating barrier)
Film compression area
Movable barrier

Figure 6.4.

Figure 6.4

This figure is an illustration of the Lauda Langmuir Blodgett trough used throughout the series of experiments conducted on Langmuir films. Indicated on the diagram are the main components; the film pressure measuring system which consists of a floating barrier, the compression system which consists of a moving barrier, and the film compression area which is contained between these two barriers.

surface of the tank. This prevents any films which have been deposited on the surface of the subphase slipping under the measuring or moving barrier during compression. Secondly the hydrophobic nature of the ptfe makes the tank easy to clean and easy to empty when changes of subphase are required. Thirdly Teflon is resistant to most organic substances and fourthly the coating of ptfe prevents the ingress of any metal ions from the brass to the subphase.

The trough which contains the subphase has dimensions 700 mm long, 150 mm wide and 6mm deep. Incorporated in the trough near to the measuring barrier is a well which measures 80mm wide, 30 mm long and 60 mm deep; the total volume of the subphase is therefore about 700cc. The well is there to allow substrates up to approximately 60 mm long by 75 mm wide to be coated by passing them wholly in and out of the subphase.

The trough is clamped in good thermal contact to thermostatically controlled base through which thermostatically controlled heated or cooled liquid can be passed thus allowing the temperature of the subphase to be controlled. The temperature of the base and the subphase are monitored using two Platinum resistance thermometers.

The sample film is spread between two ptfe barriers, one fixed and one movable. The movable barrier rests on the sides of the tank preventing leakage of langmuir film around its two ends and thus defining the surface area available to the film. Controlling the separation of these barriers controls the area over which the film is allowed to spread. The movable barrier can be driven towards or away from the fixed barrier at continuously variable speeds of between 0.9 cm / min and 65 cm / min. Feedback electronics also allow the barrier o be used to maintain a specific pressure on the film. Two limit switches dictate the extremes of the movable barrier positions thus limiting the minimum and maximum surface area. When the barrier makes contact

with either of the switches its direction of motion is automatically reversed.

The fixed barrier is a floating barrier. It consists of a ptfe boat which is attached to the sides of the trough via two ptfe sealing foils which prevent leakage of the film past this barrier and onto the clean surface of the area of clean subphase behind the barrier. This barrier is situated below a bridge which extends over the width of the tank resting on the metal sides being firmly fixed in place by two thumb screws thus ensuring that it does not move in relation to the rest of the tank. Built into this bridge is the measuring sensor. Extending from the sensor are two metal prongs which locate in two holes in the floating barrier. It is through the two prongs that the sensor transducer is actuated. In its zero position the pressure on both sides of the barrier will be equal and the barrier will be in a rest position and the transducer output will be zeroed. As the movable barrier is forced against the surface film pressure is transmitted through the film to the floating barrier. The floating barrier responds by moving back into the clean area of subphase and this movement is detected by the transducer. The output from the transducer is fed to an Amstrad 1512. computer which is used to control the tank and its ancillary equipment. A dedicated software package controls the instrument, the dipping device, gathers and processes the data, and produces a hard copy on a dot matrix printer. Technical details of the tank are incorporated in an appendix at the back of the thesis.

Environmental control of the gas above the surface of the subphase is two fold. Firstly a sealable cover on the tank enables the whole volume above the subphase to be flooded with a gas other than room air, thus providing the capability of putting inert atmosphere above the subphase. Secondly the air in the clean room is filtered to provide class 100 clean room conditions and the room is isolated from the outside atmosphere by maintaining a slight positive pressure within the room.

6.5 *Vibration* and Contamination Precautions

Vibration is a major problem in any work with Langmuir films. The input of energy into the surface layer from outside sources should be guarded against at all costs. The measuring range of the sensor incorporated in the tank is – 5 to 81.96 mN/m and forces below the maximum covered by the sensor can destroy a film. The Lauda tank is housed in a purpose constructed room. The location of the facility was chosen to minimise vibrations. Being situated at the corner of the building next to a massive wall any transverse and lateral vibrations of the building inner steel frame are reduced to a minimum. The tank itself is located upon a massive purpose built table which in turn is attached to the wall. The table is built from steel and has a top made from a large flat slab of slate covered by a sheet of 10 mm thick plate glass. The glass enables the surface of the table to be kept clear of contamination caused by any spillage of chemicals. Possible absorption of spilt liquids into the slate and their subsequent slow evaporation into the atmosphere is also thus avoided.

Airborne contamination of the clean room is controlled in a number of ways. First prior to entering the room all personnel must don protective outer garments consisting of: clean-room boots, coveralls, hats, masks, and rubber gloves. This clothing has been prepared to clean-room standards and is kept in a locked cupboard sealed in plastic bags until required.

Secondly a sticky-mat which removes dust from the soles of the boots must be crossed prior to entering a set of double doors - effectively an air-lock. A strict procedure is followed when using these doors, after entering the outer door must be closed before opening the inner door to the room proper. The room is fed exclusively by pumped and filtered air. The pumping maintains the air in the room at a slight

positive pressure with respect to the rest of the building and therefore when the inner door to the room is opened the only movement of air will be clean air from the clean room to the outside thus preventing the ingress of airborne contaminants. Finally the tank itself has a lid which when closed provides a last resort protection. These measures ensure that level of particulate contamination within the clean room are kept down to a very low level.

6.5.1 Monitoring of Airborne Contamination

Regular monitoring of the contamination with a Calmet particle size meter shows that when the room has been left unused overnight the standard is class 100. This means that there are no more than 100 half micron particles per cubic metre of room air - see figure 6.5. When the room is in use the standard is between class 300 and 600, i.e. there are between 300 and 600 half micron particles per cubic metre of room air. As a matter of course the floors and walls are cleaned regularly by trained staff following a specialised cleaning procedure.

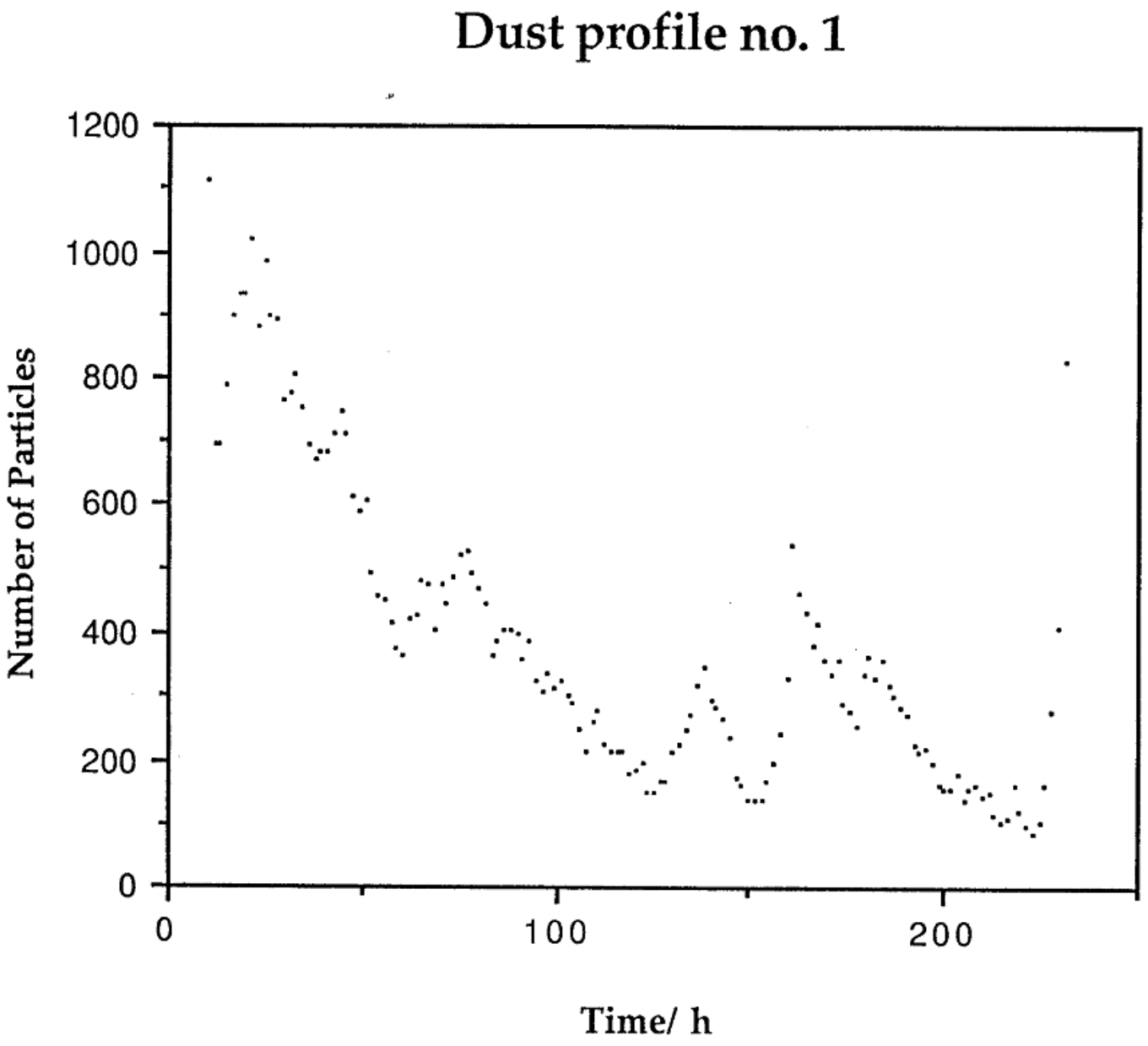
Dust profile no. 1
Number of Particles
1200
1000
800
600
400
200
0
0
100
200
Time/ h

Figure 6.5.

This figure is a reproduction the results of one of the many dust monitoring sessions. The dust profile shows that after an initial settling down period the numbers of particles per cubic metre fall to within the range 300 to 600. This sample was taken over a 200 hour period using a Calmet dust Monitor. The profile represents normal working conditions within the environment of the clean room.

6.6 Rigorous Cleaning of LB Trough

Even though all work was carried out using a Lauda trough which is housed in a class 100 clean room, it was necessary to instigate a rigorous cleaning routine. Multiple users and the wide range of chemicals under investigation necessitated that this routine was stringently followed. Liaison with the other users has resulted in the following system being developed. This procedure was followed at the start of any work on the tank when it had previously been used by another worker or when it was considered that the instrument required more rigorous cleaning.

a) Before use, the tank is emptied and then filled with a solution of water and acetone, in approximate equal proportions.

b) The temperature of the water in the bath is then raised to 50° C, following an automatic routine built into the dedicated software.

c) At the end of the above cycle the water/acetone solution is removed from the tank and the system flushed a number of times - at least twice - with clean water.

d) The last change of pure water is left in the tank and the temperature is then allowed to reduce to the selected working temperature. Once this temperature has been reached an isotherm of the clean surface is taken. The criterion used to detect a clean surface was:

   A change in the surface area of about 95% had to result in a negligible change in the surface pressure.

6.6.1 Standard Cleaning Procedures

When using the tank for extended periods as a single user any cross contamination is of course eliminated. Following an initial cleaning as described above a less stringent and time consuming method was used for the second and subsequent cleaning during these work periods.

Initially the subphase was cleaned by using a fine stainless steel tube which was built into the tank. The tube was connected to a flexible pipe and then to a water vacuum pump. This device was used to sweep the surface and suck from it any floating contaminants or old film layers. It is essential in the Lauda system that the height of the water at the measuring barrier is maintained at a predetermined level. To achieve this there are built into the tank a number of nozzles which are attached to an extraction system. These nozzles are set just behind and to the sides of the barrier. When the pump to which they are connected is switched on the nozzles extract water from the surface of the subphase, reducing the level of the surface to its optimum position. These nozzles are also used initially to clean the surface of the subphase. Following a menu driven option in the software 200 to 250 mL of subphase water are added to the tank. The water pump is then actuated and water is extracted by the nozzles as the driven barrier is moved towards the measuring barrier. The effect is to clean the surface and reduce its height to the working level.

The cleanliness of the subphase surface was checked, as it is before depositing any surface film, by sweeping the surface with the movable barrier and monitoring the residual surface pressure, once again using an option from the software menu. For film spreading it was required that for a change in surface area of about 95% the pressure change had to be negligible. This translates to a horizontal line on the

pressure / area graph along the X axis. Very often the above procedure had to be repeated several times before the criterion was met.

6.7 Monolayer Materials

Some compounds produce stable monomolecular films when they are deposited in the gas/liquid interface at the surface of a liquid, as a result of their amphipathic, or amphiphillic nature, of the molecules. Each amphipathic molecule has one part which is capable of forming strong van der Waal's interaction with the liquid molecules. This part of the molecule is lyophilic and specifically hydrophillic if the liquid is water. It should be noted here that with the work of this group the hydrophillic end of the molecule is responsible for the spreading of the molecule over a large surface area - for only water was used as a subphase liquid. Another part of the molecule has a much weaker ability to form any stable interactions with the liquid molecules. This part of the molecule is lyophobic and specifically hydrophobic if the liquid is water. Most of the work to date has been performed on fatty acids and their salts which fulfil the requirement outlined above.

In summary the fatty acids used by this group can be described as amphipathic compounds having a highly polar head group which is attached to a hydrocarbon chain (hydrocarbon tail) of ten carbon atoms or more. If a very dilute solution of one of these compounds in an organic solvent which is insoluble in water (around one milligram per millilitre) is dropped onto the surface of pure water and the solvent evaporates, an insoluble film is spread across the top of the water surface.

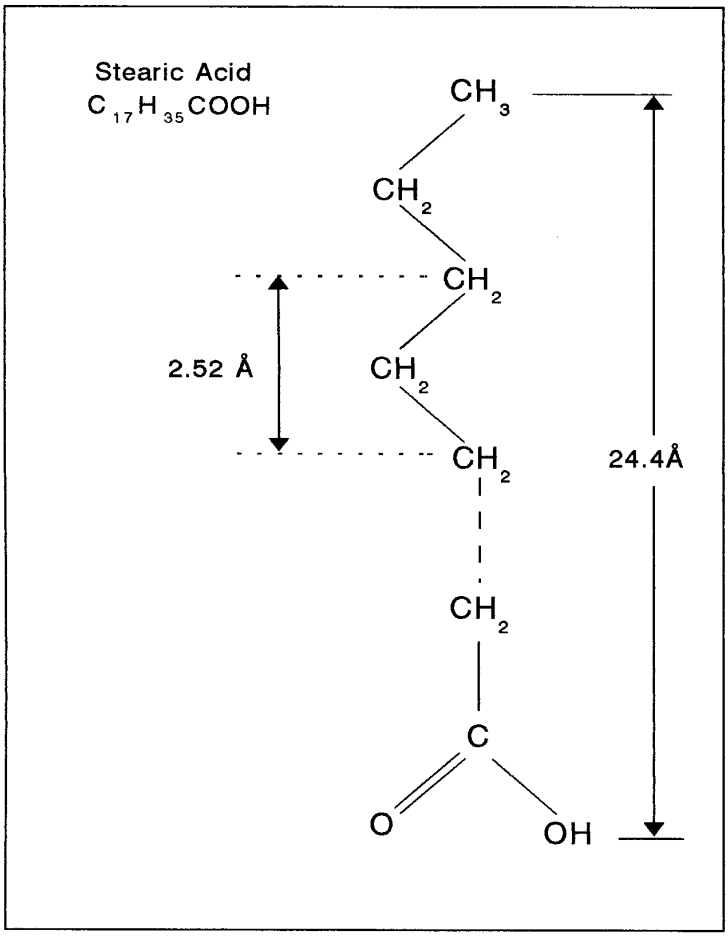

166

Figure 6.6a

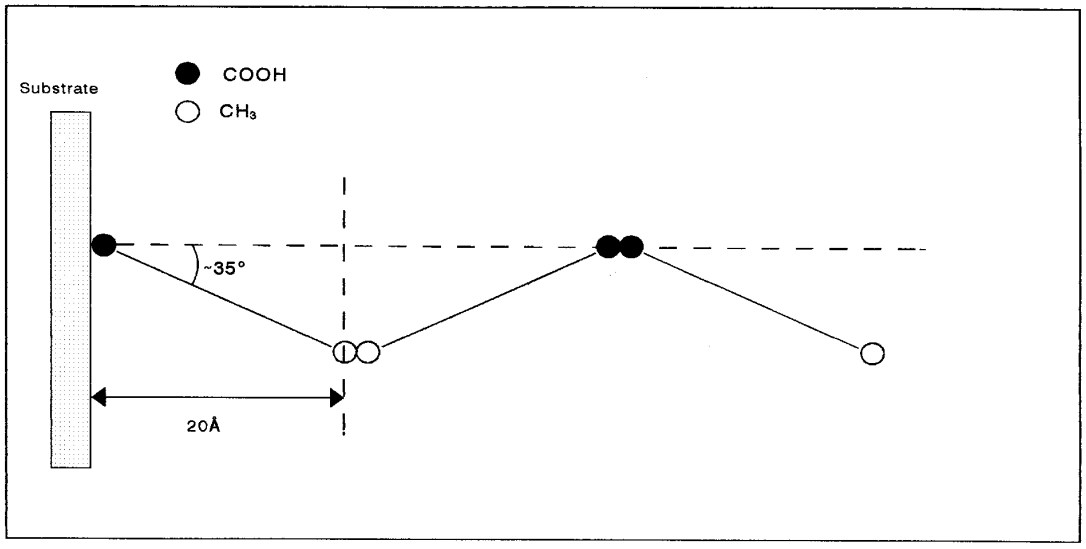

Figure 6.6b

Figure 6.6a.

The chemical structure of stearic acid and its barium salt are shown in this figure. It is usual in Langmuir Blodgett film production to replace the H^+ ion in the hydrophillic end group with a divalent ion by introducing into the subphase a soluble salt of the desired metal. Barium chloride or cadmium chloride are the most usual choices. The reaction converts stearic acid into barium (or cadmium) stearate. The extent of the conversion depends upon the pH of the subphase. The inclusion of the metal ion increases the stability of the monolayer but its rigidity is increased and with it a greater risk of transferring defects.

Figure 6.6b.

An illustration of a possible arrangement of a mixed Langmuir Blodgett film of stearic acid and barium stearate after Dr. T. Ginnai. The configuration of the molecule with respect to the substrate surface is presented as a solution to the differing lengths of the molecule. When it is measured in its crystal form a length of 2.44 nm is recorded and when measured in a Langmuir Blodgett film its length is calculated to be approximately 2 nm. Tilting the molecule at an angle of 35° to the surface of the substrate as illustrated would account for the different lengths.

6.7.1 Stearic Acid

The stearic acid - and the barium chloride - used throughout this study was Fisons analar grade nominally 99.5%. The structure of stearic acid is illustrated in Figure 6.6a. In this series of experiments the H+ ion in the hydrophillic end group was replaced by a divalent ion by introducing the latter into the subphase as a soluble salt of the desired metal. Barium chloride or cadmium chloride are the most usual choice; barium chloride was used in this study. The reaction with the metal ion converts the stearic acid to barium stearate.; the reaction takes the form

$$2(C_{17}H_{35}COOH) + M^{2+} \rightleftharpoons M^{2+}(C1_{17}H_{35}COOH^{-})_2 + 2H^{+}$$

The subphase additive - barium chloride - was used at a concentration of 2.5×10^{-4} M. At this concentration precipitation of metal oxides and carbonates is avoided [4]. This reaction and the extent of the conversion of the acid to the salt depends critically upon the pH of the subphase. If it was required to adjust the pH in the present work a few drops of sodium citrate or acetic acid solutions were added to the subphase. The solutions for use in adjusting pH levels were prepared at a concentration of 0.1 M strength. The inclusion of metal ions into the subphase has the advantage of increasing the stability of the monolayer but it does have the disadvantage of increasing the rigidity of the film and therefore the possibility of transferring defects is higher [3]. It is therefore, as with most experimentation, necessary to optimize the balance by selecting a suitable subphase pH in the range - 5.7 to 6.0 in this series of experiments.

X-ray studies done on single crystal stearic acid have shown the length of the molecules to be 2.44 nm [7] which would give spacings and angles as shown in figure 6a. Other X-ray work done on Langmuir Blodgett films of stearic acid give a length of 2.00 nm for the molecule [8]. It was suggested by Gnnai [5] that this apparent difference could be explained by assuming that the molecules within the LB film are not aligned perpendicularly to the substrate surface. Taking this line of reasoning as one possibility puts the molecules at an angle of 35 degrees from the perpendicular. An illustration of this possible arrangement for the molecules as proposed by Dr. Ginnai also shown in figure 6.6b.

6.7.2 Solvents

Stearic acid is supplied in the form of a crystalline powder and therefore does not spread spontaneously on the surface of the water forming the subphase. To improve the spreading, the stearic acid is spread from a solution of a suitable solvent. The criteria for the solvent were three fold: firstly it should have the ability readily to dissolve the stearic acid. Secondly it should not react with any of the other materials it might come into contact with in the Langmuir Blodgett film production and deposition and thirdly it should evaporate completely in a reasonable length of time after dispersion of the film on the subphase. In this study the solvent used was n-Hexane 60° - 80° (special for spectroscopy grade) supplied by BDH.

6.8 Substrate Preparation

The preparation of the substrates and the evaporation of the aluminum electrodes has been described elsewhere in this work (see chapter 3) and exactly similar procedures were followed in the production of tunnel junctions for this group of experiments. The difference occurs in the way that the dopant layer was incorporated in the tunnel junction. As outlined in section 6.1. of this work the dopant layer is pre-formed into a well defined layer prior to its incorporation in the tunnel junction. The methodology of this process is described in the following section.

6.8.1 Langmuir Film Fabrication

Langmuir films are fabricated by depositing a solution of the material under examination onto an uncontaminated surface of a liquid subphase (water containing barium chloride). The sample being a fatty acid will if the conditions are suitable spread out to form a monomolecular layer on the surface - see Figure 6.2a. This layer should have no long-range order. This disordered layer can be ordered into a monomolecular sheet by applying an appropriate lateral pressure via a movable computer-driven barrier. As the pressure is slowly applied, eventually all of the molecules will be organized into a solid sheet. In this situation this close proximity of the individual molecules with each other allows van der Waal's forces to pull the layer into a well ordered solid which being one molecule thick is effectively a two dimensional solid sheet- see figure 6.2c.

Some of the sheet can then be transferred to a solid substrate by dipping the substrate through the surface and then withdrawing it. Multiple layers can be formed by repeating the dipping procedure, transferring the sample to the substrate one layer at a time. As the material is stripped from the surface of the water it is necessary to

maintain the pressure on the surface layer to preserve the integrity of the layer. This is achieved via the barrier which compresses the layer under computer control. The pressure within the layer is monitored and as material is removed the barrier is pushed forward to keep the pressure constant at the value required to maintain the monolayer on the surface in its solid form.

The main advantages of films constructed using this technique in electrical studies are accurately known thickness, high dielectric strength, highly ordered, controlled orientation of constituent molecules, a defect free and uniform film even for layers as thin as 2.5 nm.

The Langmuir - Blodgett technique lends itself well to inelastic electron tunnelling spectroscopy where the tunnel junctions are required to be less than 10 nm thick. Studying the electrical properties of thin insulating layers such as those forming tunnel junctions is fraught with many pitfalls. To achieve reproducible results the films must be uniform and defect free. Defects in the insulating layer - pinholes through which conduction can take place - as low as one in a million can significantly modify results so as to render them useless [9] . Films deposited in the conventional way by evaporation or oxidation can suffer from pinhole defects which lead to data which are not reproducible. These defects have been shown to be a consequence of the fabrication process [10]. The Langmuir - Blodgett technique appears to have many advantages over conventional processes. The films are well ordered with a known structure and have a uniform and controllable thickness.

As discussed earlier the disadvantages mainly lie in two fields. Firstly the fabrication of the films requires meticulous care if reproducibly good layers are to be made. Secondly every device made using an LB film has a metal oxide built into it. If

non-reactive metals such as gold are used to form the electrodes it appears to be impossible to manufacture defect free devices [5].

6.8.2 Film Spreading

Once the tank had been cleaned a semi automatic procedure was followed which prepared the subphase temperature and surface conditions. The subphase was heated up to a predetermined temperature - usually between 20 and 22 $^{\circ}$C. Generally temperature has a crucial effect on film transfer. The main one is to limit the rate of transfer of the monolayer to the substrate [10] and the range 20 -22 has been shown to be the optimum for good transfer. Once the temperature has stabilised the movable barrier is withdrawn to expose the maximum area of subphase - 927 cm^2. Doing this ensures that there is sufficient surface area available to allow the film to spread out and form a monolayer which is in the gaseous phase (see next section). Using 20 micro litres of stearic acid / n-hexane solution gives an area per molecule of 80 Å^2 [5].

A pressure versus area curve was then taken to check the condition of the surface of the subphase. If the resulting graph indicated a constant pressure of zero, within experimental error, the subphase was assumed to be clean and uncontaminated and a sample of dispersant solution was then applied to the surface of the subphase. The sample - in this work stearic acid - was formed into a suitable dispersion solution by diluting it in n - Hexane at a concentration of 1 mg ml^{-1} . A bulk solution of 10 ml was made up in the clean room using a 10 ml volumetric flask kept specifically for the purpose.

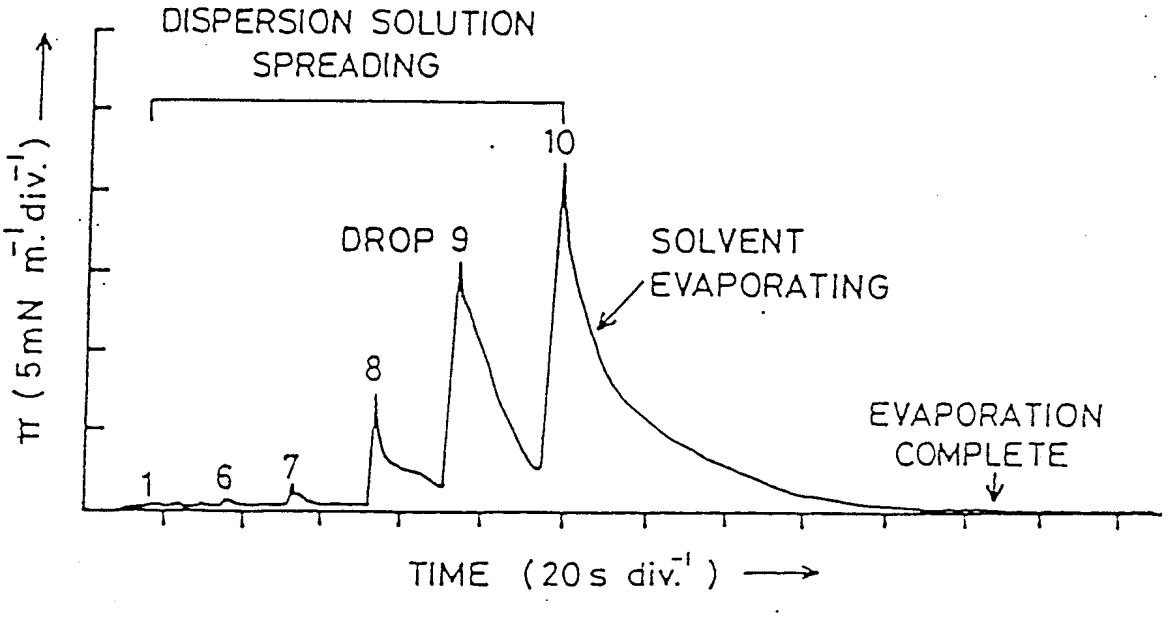

Figure 6.7

Typical surface pressure versus time plot obtained curing film spreading.

The solvent n-Hexane was chosen because, as with all solvents used in the preparation of dispersion solution in L-B film production, it is insoluble in the subphase. This concentration was chosen as an optimum; higher concentrations tended to result in agglomerations of the sample in patches on the surface due to the fast evaporation of the solvent whereas lower concentrations might result in entrapment of solvent molecules within the monolayer.

As only 20 to 30 pd of the sample were spread at any one time the sample was dispensed from a 50 µl syringe (Hamilton Microlitre Syringes 50µl). Some of the solution was poured into a clean measuring cylinder, and taken into the syringe from this container. The syringe was filled and emptied three times with pure solvent and twice with the dispersion solution before being used to dispense the sample onto the surface.

The sample was applied, through an aperture in the lid of the Lauda tank, one drop at a time and very close - about 2 mm - to the surface of the subphase. The drops themselves were applied over the whole area of the surface after which a time was allowed for the solvent to evaporate from the dispersant solution. The time allowed followed guidelines set up by previous workers in the department [5,12] - see Figure 6.7. For the amount of solution used in this work the minimum evaporation time is 5 minutes. However it was usual to allow 30 minutes to elapse before compressing the film.

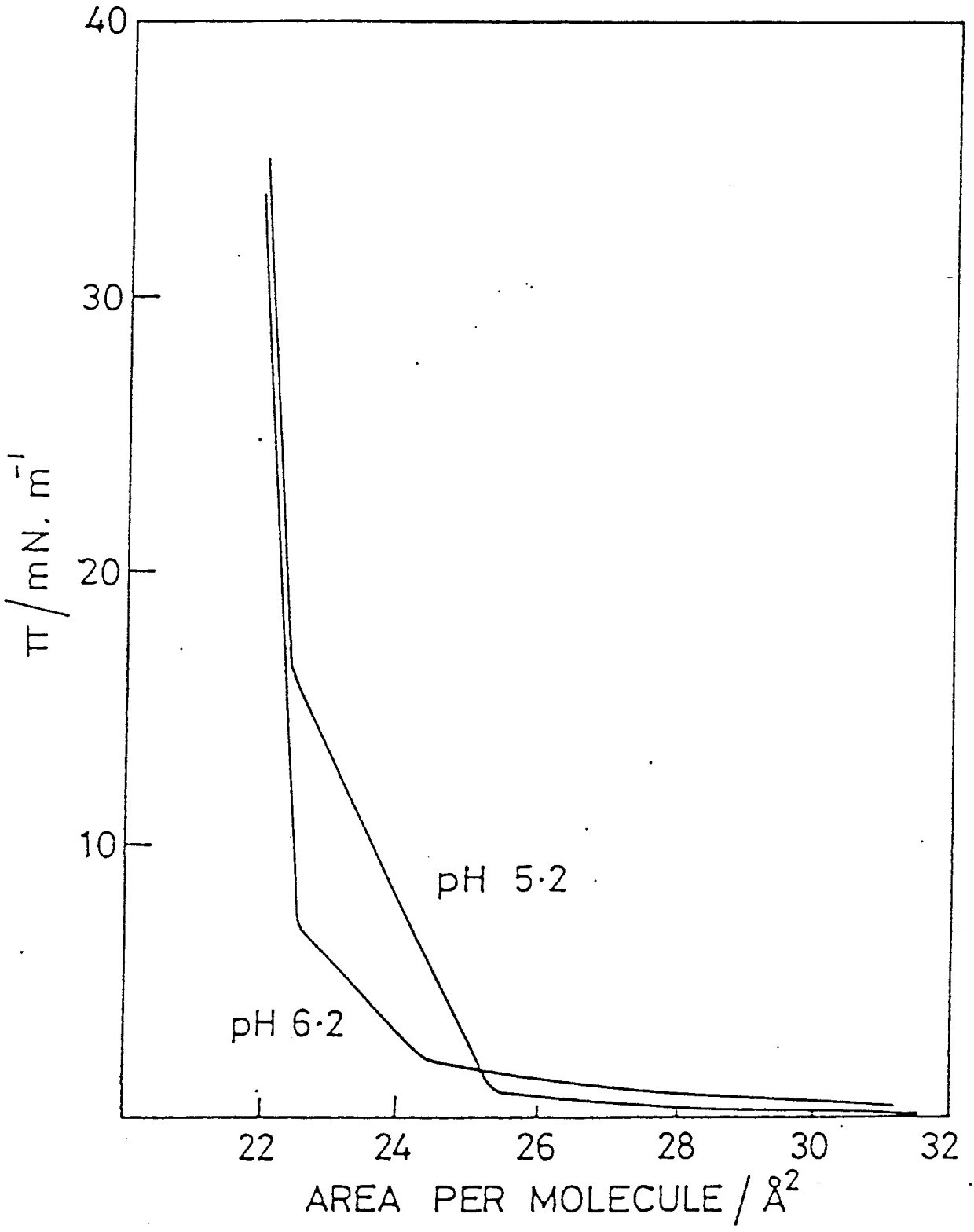
40
30
20
10
$\pi / mN.m^{-1}$
pH 5·2
pH 6·2
22
24
26
28
30
32
AREA PER MOLECULE / Å^2

Figure 6.8

Figure 6.8

This diagram illustrates the way in which the phi versus area curve varies when the pH os the subphase is changed between 5.2 and 6.2. Varying the pH of the subphase dramatically alters the shape of the isotherm. As pH is increased the area under the liquid-phase portion of the curve gradually reduces until if disappears completely at a ph of 6.5.

6.8.3 Deposition Conditions

After the solvent has evaporated the movable barrier is driven towards the measuring barrier thus reducing the area available to the monolayer. The barrier is driven forward at a very slow rate - 2 - 5 cm^2 per minute - to ensure that the layer remains in equilibrium during this period of reforming [13]

During this compression of the film the most commonly measured property is the surface pressure $\pi = \gamma_o - \gamma$. Plots of surface pressure versus area are the most commonly used and are termed compression isotherms and it is this type of plot which is used throughout this section. Using the convention suggested by Langmuir [14], the compression isotherm can be regarded as made up of three linear regions which can be regarded as Gas, Liquid and Solid; all fatty acids undergo essentially similar behaviour [15].

When transferring parts of the film onto solid substrates the dipping is done whilst the film is held in its solid phase. It is important to note here that the pH of the subphase has a bearing on the shape of the curve which of course reflects differences in the monolayer's physical characteristics. Referring to figure 6.8, increasing the pH of the subphase modifies the curve. As the pH is increased the area under the liquid phase portion of the curve is progressively reduced until it is effectively eliminated at pH 6.5, and there is a sudden transition from the gaseous to the solid phase. It has been shown, in earlier work at this establishment [5], that the ideal range of subphase pH is 5.2 to 6.5. Optimising the pH between these limits results in several benefits. The mixed films fabricated in this range produce an acceptable proportion of stearic acid and its salt to give a flexible monolayer and good adhesion. Also using a pH of around 5.7 to 6.0 avoids the precipitation of metal hydroxide and carbonates [4].

Finally this middle range roughly corresponds to the pH of the water used in the tank in equilibrium with air and so effectively eliminates the need to adjust the subphase

6.9 Monolayer Transfer

Once the Langmuir film has been fabricated it is usually necessary, no matter what the application, to transfer it from the liquid subphase onto a solid substrate so that its properties can be exploited. In this work the film was incorporated in a tunnel junction for examination by inelastic electron tunnelling spectroscopy. The junctions used in this work are produced in exactly the same way as those used and referred to in the rest of the thesis. The major difference comes in the way that the organic material is incorporated in the junction. Whereas all of the other work was conducted using liquid phase doping the junctions in this work were 'doped' using a Langmuir Blodgett film.

The films are transferred by dipping or pulling the solid substrate through the film when the monolayer in compressed to its solid phase whilst maintaining the pressure constant at the chosen value - between 25 and 30 mN m^{-1} . The three different modes of monolayer transfer are as follows:

X type Transfer of the film onto the substrate by passing the substrate from the air (gas) through the monolayer into the subphase only.

Y type Transfer of the film onto the substrate by passing the substrate from the air (gas) through the monolayer into the subphase and a successive transfer by returning from the subphase through the monolayer to the air (gas).

Z type Transfer of the film onto the substrate by passing it from the subphase through the monolayer into the air (gas) only.

The above view of monolayer deposition is an oversimplification. In practice the mode of the transfer will be chiefly governed by the surface of the substrate and its pre-conditioning. These are factors which will be governed by the parameters set for the functional requirements of the finished device.

It is also important to realise that the mode describes the way in which the first and any successive layers are taken from the surface onto the substrate. Multi-layers containing combinations of these deposition types can be made by a number of methods, all of which involve processing the surface of the substrate, the surface of the film or the transferred layer to dictate the orientation of the molecules in the next layer of the series. These multi layer methods are beyond the scope of the work.

The material used in this study was a mixed film of stearic acid and barium stearate. No film will be transferred on the first downstroke (immersion) of the substrate through the monolayer because the clean surface of the glass and the freshly produced aluminium bottom electrode are both hydrophillic surfaces. These surfaces will attract the hydrophillic ends of the molecules but as the substrate is moving down into the subphase the molecules will remain on the surface of the subphase On all subsequent strokes through the film there will be monolayer deposition onto the substrate. During the first withdrawal the hydrophillic surfaces will attract the COON end group of the molecules within the surface layer and a Y- type layer is deposited on the surface of the electrodes and the glass as shown in Figures 6.9a and 6.9b. Subsequent immersions and withdrawals would stack the layers on top of each other.

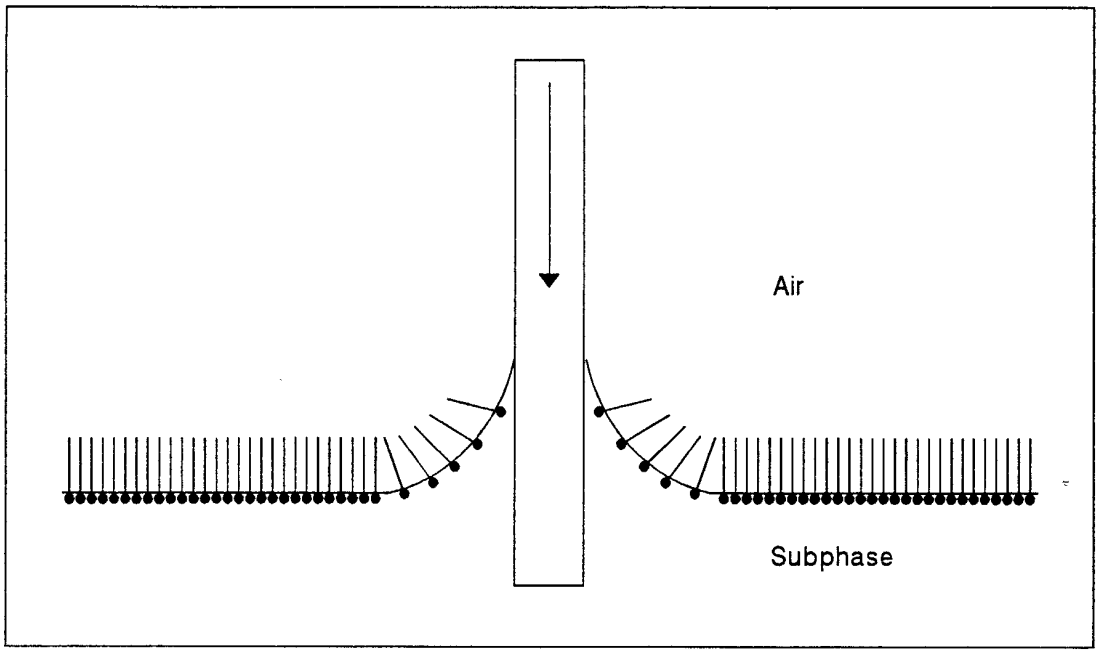

Figure 6.9a.

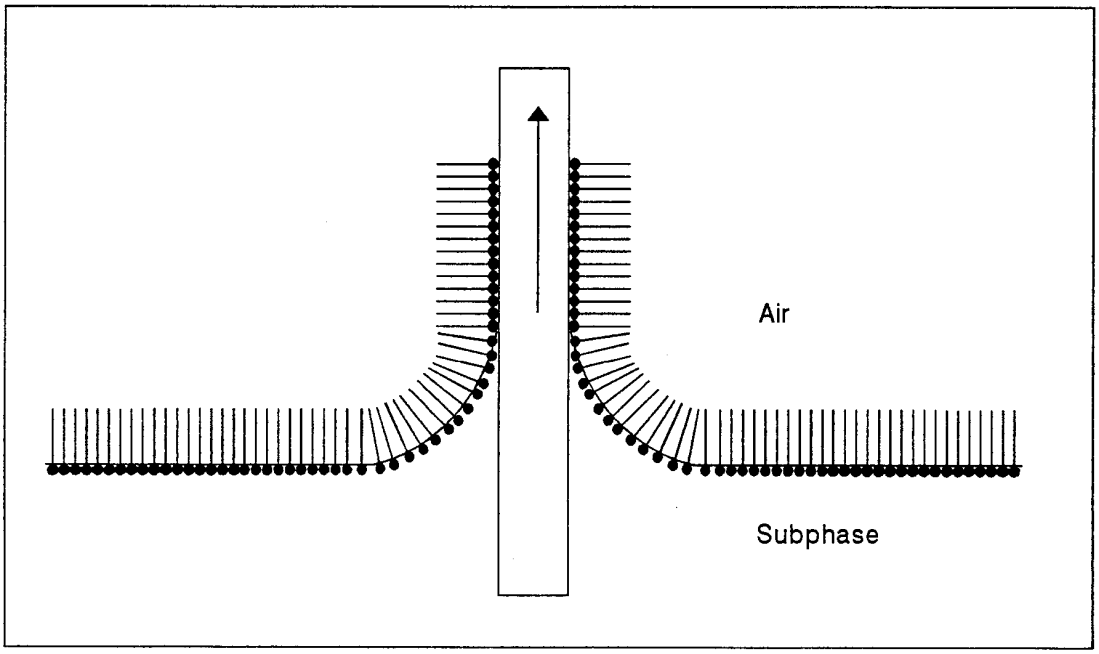

Figure 6.9b.

Figure 6.9a

Illustrates the first immersion of a hydrophillic substrate into a Langmuir film which has been compressed to the solid phase and is maintained under constant pressure. As the substrate passes down through the film for the first time there will be no transfer from the monolayer to the substrate.

Figure 6.9b

Shown here is the first withdrawal of the substrate from the body of the subphase. For a hydrophillic substrate material will be transferred to it from the surface layer to form a Langmuir Blodgett film on the substrate.

The orientation of these subsequent layers would depend upon the exposed surface of the previous layer and the Langmuir film, both of which could be conditioned to pre-determine the Langmuir - Blodgett film structure.

6.9.1 Transfer Ratio

IETS requires that the monolayer deposited on the substrate is unbroken and continuous. To this end a series of experiments were conducted into determining the transfer ratio of the dipped area of the substrate to the area removed from the film during deposition. The tests were conducted using microscope slides of nominal dimensions 73 mm long x 22 mm wide x 1 mm thick - for each of the tests each slide was measured to determine its dimensions.

To test if the ratio of glass to aluminium or the pattern of the aluminum had any effect on the transfer ratio a variety of configurations of evaporated aluminium / glass were prepared. These ranged from no aluminium to complete coverage of the slide. Differing patterns of aluminium were also tried - including the pattern used to produce the junctions. The dipping pattern was also varied; some slides were passed down through the film and then withdrawn while others were only withdrawn up through the film from the subphase. Multiple dips were also performed to compare subsequent depositions with the first. Although it must be emphasised that only single layers of Langmuir Blodgett film were used in the present work.

Table 6.1. lists a representative sample of the results. These results compare very favourably with previous work done in the department; Grinnai [5]

Aluminium Coverage	**Dipping procedure**	**Area of subphase removed cm^2**	**Transfer ratio ± 0.02**
One surface completely covered	Down & up	16.01	0.99
	Up only	16.58	1.02
	Down only	00.10	0.01
Top half of slide covered	Down & up	16.21	1.00
	Up only	16.30	1.01
	Down only	0.001	0.00
Left side of slide covered	Down & up	16.22	1.00
	Up only	16.20	1.00
	Down only	0.000	0.00
Pattern used to produce junctions	Down & up	16.28	1.00
	Up only	16.20	1.00
	Down only	0.010	0.00
Clean glass slide	Down & up	16.21	1.00
	Up only	16.30	1.01
	Down only	0.021	0.00
Completely covered slide	Down & up	16.22	1.00
	Up only	16.20	1.00
	Down only	0.002	0.00
Average transfer ratio excluding down only dips			**1.00 ± 0.02**

Table 6.1.

Transfer ratio of a Langmuir film of mixed stearic acid and barium stearate. All parameters appertaining to the cleaning of the tank, subphase, and substrate and the production of the electrodes were as outlined elsewhere in the thesis.

obtained transfer ratios of unity with an error of 10%. The present work shows transfer ratios of unity with an error of 2% .

6.9.2 Parameters used in Transfer Ratio Tests

Dipping speed	***10 mm min*** $^{-1}$	**pH of subphase**	***5.9***
Subphase temp.	***20.0*** ^{0}C	**Room temp**	***23.0*** ^{0}C
Surface pressure	***25 x*** 10^{-3} Nm^{-1}	**Total area dipped on each run**	***16.217*** cm^2

Table 6.2.

The various parameters used during the determination of the transfer ratio are listed below in Table 6.2. These parameters were selected from the results of work done and outlined in the previous sections of this chapter. All conditions appertaining to the cleaning of the tank, subphase, substrate and the production of the electrodes were as outlined elsewhere in the thesis.

6.9.3 Comments on Using LB Films as a Dopant in IET Junctions

The above results show that by using the parameters a transfer ratio of one can be achieved. This infers if a substrate containing a pattern of evaporated aluminium which defines the bottom electrodes of a set of five tunnel junctions is dipped each of the electrodes will receive a coherent monolayer of film. These results apply to the partially constructed junction, prior to the evaporation of a top lead electrode. As with other doping methods (liquid phase for instance) it is assumed that application of the lead top electrode does not compromise the integrity of the dopant monolayer. The resulting sandwich construction is metal - oxide - LB film - lead. The LB film being a coherent insulating monolayer approximately 2.5 nm thick.

6.10 Processing Parameters for L - B Films

The data gathered in the previous sections have been brought together in table 6.3 below which outlines the parameters for the production of Langmuir films at this establishment. These parameters ensure that the films produced and their subsequent transfer to a substrate are optimised.

Film Material	Stearic Acid $C_{17}H_{35}COOH$	**Subphase temperature**	20 ^{0} C
Solvent	n - hexane (60 - 80 ^{0}C)	**Surface pressure (solid phase)**	25 - 30 mN m^{-1}
Concentration	1 mg ml $^{-1}$	**Dipping speed**	2 - 5 mm min^{-1}
Metal ion	Ba^{2+}	**Subphase**	Water
Ion concentration	2.5 x 10 $^{-4}$ M	**pH of subphase**	5.8 - 6.1

Table 6.3.

Summary of the deposition conditions of the Langmuir Blodgett films incorporated in Al- AIOX - LB film - Pb IETS tunnel junctions.

6.11 Experimental

Using the parameters outlined above a series of IETS junctions were manufactured. These were of form tin - tin oxide or aluminium - aluminium oxide - mixed LB monolayer of stearic acid and barium stearate - lead construction. The cleaning of the

glass substrate and the evaporation of the electrodes followed the well proven methods outlined elsewhere in this thesis.

Once the bottom aluminium electrode had been evaporated it was taken in a clean petri dish to the clean room where a monolayer of mixed stearic acid and barium stearate had been freshly prepared. Once dressed and in the clean room the slide containing the set of five bottom electrodes was removed from the petri dish using tweezers. It was then placed between the jaws of a mini bulldog-clip, ensuring that the clip only touched the glass and not the aluminium electrodes. This type of holder was chosen after many trials with various designs to be the most reliable. The clip was then fixed to the arm of the dipping mechanism using its integral magnet. The dipping mechanism was placed over the hole in the lid of the tank and the arm lowered until the bottom edge of the slide was approximately .5 mm above the surface of the subphase. This was done by observing the reflection of the bottom edge in the surface - the positioning is not critical. The only criterion is that the slide is positioned so that the dipping mechanism is able to immerse all of the evaporated electrodes in the subphase so that on withdrawal each of them will receive a coating of the film. Once this had been done it was necessary to leave the clean room to operate the dipping mechanism. The dip then proceeded automatically under computer control. When the cycle of dipping was complete (one immersion and withdrawal) the slide was removed from the holder and placed in a desiccator overnight.

The next day the slide was brought down to the vacuum system in a clean petri dish. The slide was removed from the dish and placed in the masks which defined the electrodes and then put into the vacuum system to have the top lead electrode

evaporated . Once the lead electrode had been evaporated the finished set of five junctions was taken to the spectrometer room for initial assessment. The assessment procedures, criteria for selection and the IETS procedures followed exactly those described in chapter 3.

It is important at this point to realise that although adopting the parameters outlined above resulted in transfer ratios of unity, the ratio of the numbers of working junctions to the numbers produced was not as high as expected. It was thought that by having a suitably thin - a few nanometres - and coherent dopant layer a large number of junctions would be suitable for IETS. It was expected therefore that many junctions would exhibit a d.c. resistance within the range 50 to 500 Ω therefore fulfilling the first criterion for good IET junctions for use in this spectrometer. But contrary to this expectation only a small (but we felt a significant) number of junctions had a resistance of less than 5000Ω.

Previous workers in the department had been unable to obtain any working junctions using aluminum as a base electrode material and resorted to using tin as a bottom electrode metal [5]. The junctions with aluminium bottom electrodes prepared by Ginnai generally had resistances of >1MΩ and showed an I-V characteristic which was markedly non-linear even at applied biases as low as 50 mV. However some of the junctions with aluminium bottom electrodes in this present work had resistances of a few hundred Ohms. The use of aluminium as a base electrode material was successful, although it must be recognised that the percentage of working junctions was very small in comparison with junction using other doping techniques.

The questions posed by the statistically small number of working junctions obtained when doping with L-B films - a disturbing phenomenon experienced by both Ginnai's group and the present one - is addressed later on in this chapter.

6.11.1 Junction with Tin Base Electrodes

It appeared not to be possible in the present series of experiments to obtain spectra from junctions constructed using tin as a base electrode metal. Experiments using tin-tin oxide-LB film-Pb junctions were conducted over a period of ten months - hundreds of junctions were manufactured - none of these produced spectra. All of the devices produced using tin as a bottom electrode metal either had very low junction resistances (of the order of a few Ohms) or very high junction resistances (of the order of tens of kilohms). The very few junctions which did have resistance of the order of 1000 Ohms were either creepers - junctions which would only temporarily support an applied bias or broke down during the setting up of the spectrometer. Several modifications to our technique were suggested by Dr. Ginnai after a private communication with him. These involved increasing the glow discharge times and using a wet O_2 atmosphere for the oxidation. Using the modifications suggested did increase the resistance of the oxide in blank junctions slightly - on average the junction resistance of blank junctions went up from around 5 Ohms to around 10 Ohms. But after the junctions were completed and tested there was no perceivable effect on the finished junctions.

6.11.2 Interpretation of Spectra

Figure 6.10. shows an IET spectrum obtained by this present group using an Al-A10,, - mixed stearic acid / barium stearate Langmuir Blodgett film - Pb tunnel junction. There are a number of regions in the infra-red spectra of carboxylic acids which can be used for the characterisation of IET spectra [18], and these will be used to assign peaks in the IET spectrum.

Figures 6.10, 6.11, and 6.12 have been transcribed to compare with the results obtained from this study. Figure 6.10 is from this study figure 6.11, after Kiel et al [17], compares the data for the fingerprint region from IETS with other spectroscopy techniques for liquid phase doped stearic acid, and figure 6.12 is a reproduction of an IET spectrum obtained from an IETS study of LB films of stearic acid by Ginnai [5].

Carbonyl group absorption takes place at 213 mV (1716 cm^{-1}) in the infra red spectrum see figure 6.11. Dissociation of the acid has a significant effect on this band. The band corresponding to carbonyl group absorption usually disappears to be replaced by two new bands at 180 and 200 mV (1440 and 1600 cm^{-1}). These two new bands result from the resonance stabilised COO^- group and correspond to symmetrical and antisymmetrical vibrations of the COO^- structure respectively.

IET spectra obtained from Langmuir Blodgett film junctions have very little or no features at around 213 mV (1716 cm^{-1}). Instead there is a broad band at 199 mV (1600 cm^{-1}) which corresponds to the antisymmetrical stretching of the COO^- group - see figures 6.10 and 6.12. The band at 178 mV (1440 cm^{-1}) corresponds to the symmetrical stretch of this group. As was stated in the previous paragraph most IET spectra of carboxylate acids do not show any features which indicate that carbonyl group vibrations are taking place within the sample. Chemisorption of carboxylic

acids normally proceeds through the formation of the salt of the acid with the base electrode [19]. If the adsorbate is a Langmuir film the situation is more complicated because before transfer to the substrate the monolayer is partially converted to the salt of any divalent cation in the subphase solution - barium chloride in this work. Therefore the presence of a C=O vibration would imply that not all of the carboxylic acid had been chemisorbed onto the surface. If this were so it would indicate that some of the material was only physisorbed onto the surface. This would have adverse implications regarding the adhesion of Langmuir Blodgett films onto aluminium surfaces but the C= O peak was small - see figures 6.10 and 6.12.

The free hydroxyl OH stretch at 450mV is clearly visible in the spectra from both groups. This peak is weaker than the corresponding peak in liquid - phase doped samples but this is possibly due to the overnight desiccation of the LB doped samples. Other evidence for O-H absorption occurs between 312 and 345 and at 375 mV in infra red spectra of carboxylic acids. In the tunnelling spectra - figure 6.10 there is a broad shoulder discernable between 320 and 340 mV but this is very weak, the other peak at 375 is, as is usual in IET spectra of carboxylic acids, overlaid by the very strong CH absorption at 360 mV.

In infra red spectra there is also a doublet 159 - 168 mV see figure 6.11; the higher frequency is linked with CO and CH in-plane deformation the origin of the lower peak is unknown. Coupled CO and OH will often give rise to another band between 172 and 180 mV (1375 - 1440 cm'), this is most often found at 179 mV.
A peak assigned to CH_2 deformation is also found at approximately 180 mV. Features corresponding to these effects can be determined in the tunnelling spectrum shown in figure 6.10. Reinforcing the assignment of in-plane deformation of the hydroxyl of the carboxylate group is a peak at 120 mV which is assigned to the out-of-plane

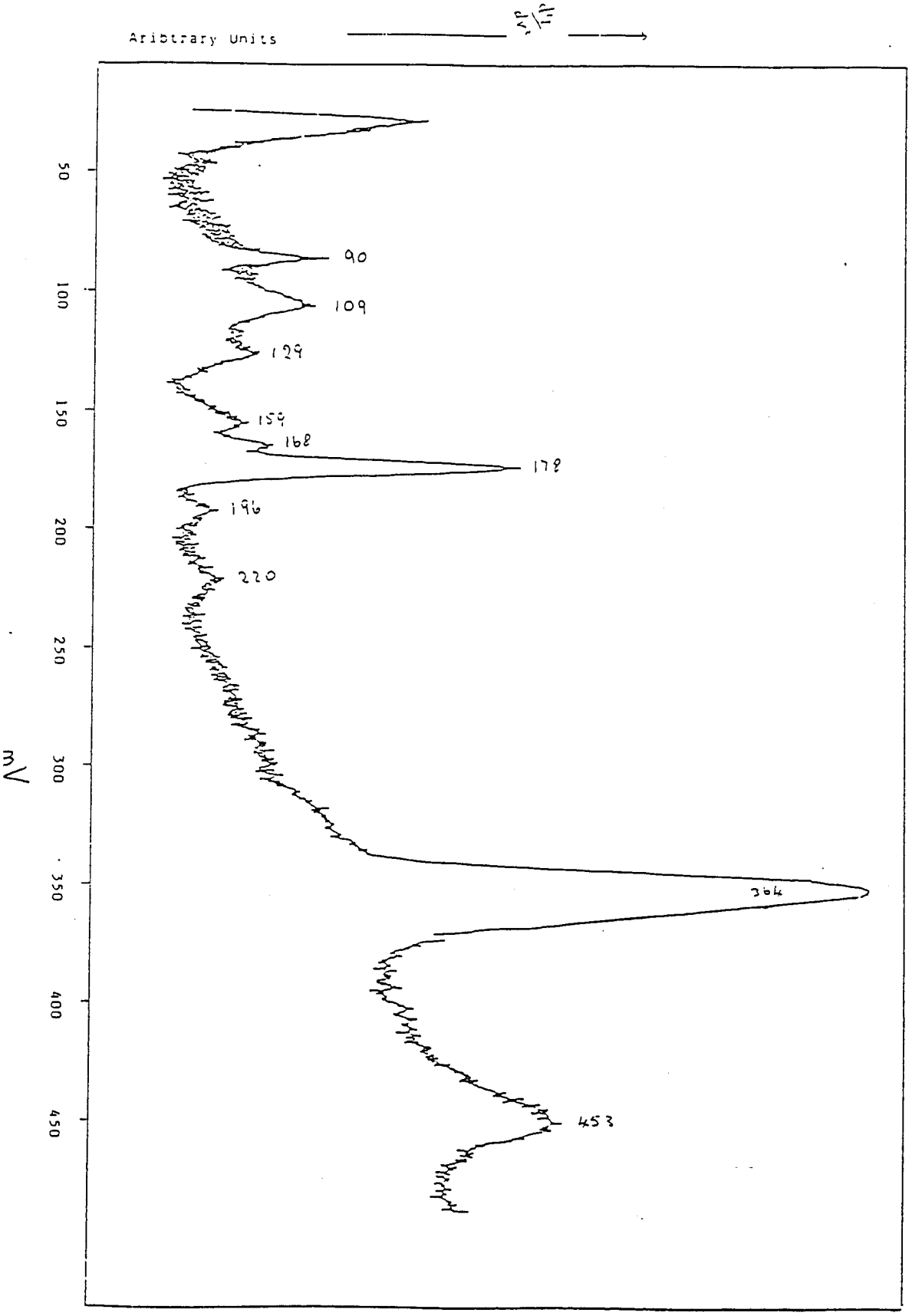
Arbitrary Units
m/z
50
100
150
200
250
300
350
400
450
90
109
129
159
168
178
196
220
364
453

Figure 6.10

Figure 6.10.

An inelastic electron tunnelling spectrum obtained by the author from a tunnel junction incorporating a Langmuir Blodgett film. The film was composed of a mixture of stearic acid and barium stearate. A modulation voltage of 2 mV peak to -peak was applied to the junction and the lead top electrode was biased positively.

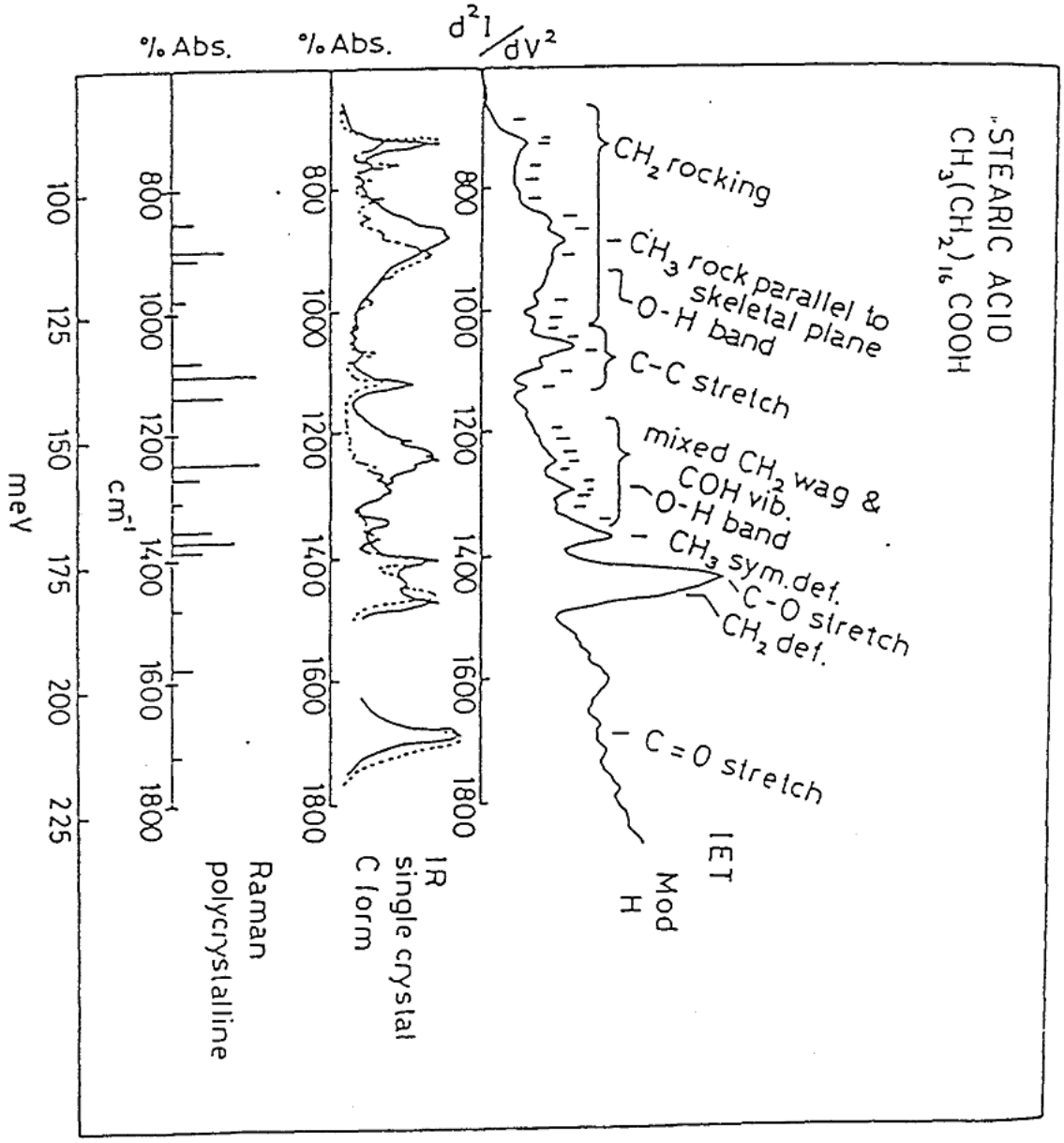
STEARIC ACID
$CH_3(CH_2)_{16}COOH$
d^2I/dV^2
CH_2 rocking
CH_3 rock parallel to skeletal plane
O-H band
C-C stretch
mixed CH_2 wag & COH vib.
O-H band
CH_3 sym. def.
C-O stretch
CH_2 def.
C=O stretch
IET
Mod H
% Abs.
% Abs.
IR
single crystal
C form
Raman
polycrystalline
cm^{-1}
meV
800
1000
1200
1400
1600
1800
100
125
150
175
200
225

Figure 6.11

Figure 6.11

Show for comparison are the fingerprint regions of the inelastic electron tunnelling, infra red and Raman spectra of stearic acid. The IET spectra was taken using a liquid-phase-doped junction of of aluminium - aluminium oxide - stearic acid - lead construction held at 4.2 K., other spectra were taken at room temperature. The spectra transcribed here were after Kiel et al.

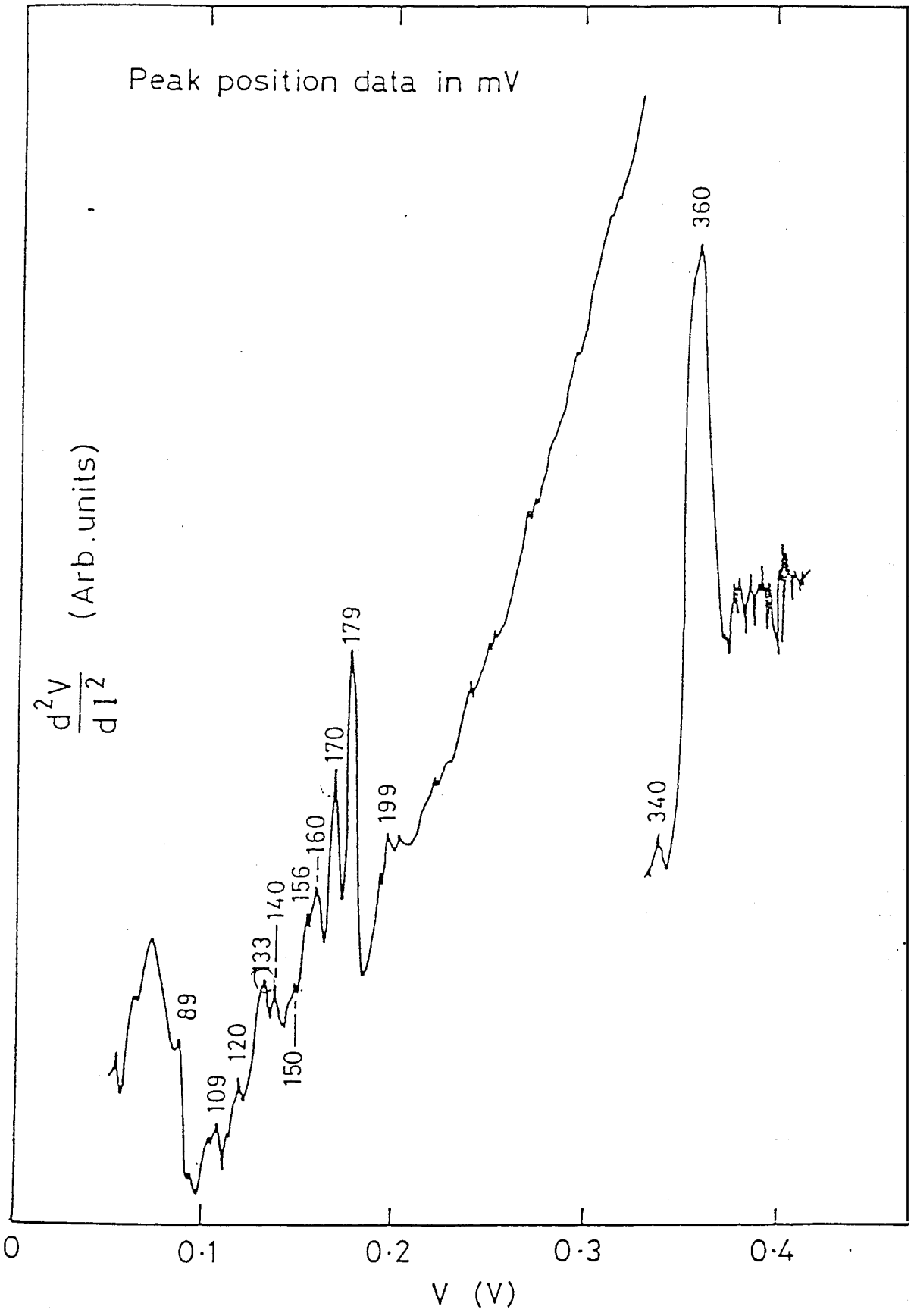
Peak position data in mV
$\frac{d^2V}{dI^2}$ (Arb.units)
89
109
120
150
133
140
156
160
170
179
199
340
360
0
0·1
0·2
0·3
0·4
V (V)

Figure 6.12

Figure 6.12

Reproduced here for comparison purposes is a inelastic electron tunnelling spectrum of a Langmuir Blodgett film of a mixed stearic acid - barium stearate film. The spectrum is after Ginnai et al.

deformation of this group. Various Raman modes can also be associated with some of the features. The strong structure at 90 and 109 mV can be assigned to a Raman CH_2 rocking modes and 129 mV to Raman C - C stretch.

Lastly the strong feature at approximately 38 mV is assigned to aluminium phonons.

Table 6.4. lists the comparisons between the IET spectra from a liquid phase doped junction and a junction produced with a Langmuir film as the dopant layer together with infra red data. It is important to take into account the temperature at which these techniques are applied when interpreting tunnelling spectra. Both infra red and Raman are taken at very much higher temperatures giving rise to changes in positions, widths and intensities of the bands.

6.12 Comparison with Previous Work

These results represent data from one of the very few inelastic electron tunnelling spectra obtained from junction incorporating a Langmuir Blodgett film layer. Comparison with the other work done in this department [5] confirms many of the conclusions drawn by Ginnai.

The spectra obtained in the present work were similar to Ginnai's except the present spectra had a little more background noise but were cleaner at higher energies allowing resolution of the OH peak at approximately 450 mV - see figure 6.12.

IETS LB film	liquid phase	**Infra red**	**Assignments**
90	90	90	CH_2 rock
		100	
109	110		CH2 rock
120	121	118	OH deformation
129	132		C - C stretch
	140	138	
	147	150	
	155		
160	161	161	coupled CO / OH
170	170		C - O / CH in plane
178	179		symmetric COO - / CH2 deformation
199	200		anti-symmetric COO - stretch
215	219	213	C = O stretch
230`	229		
335	340	330	OH absorption
360	360	355	CH
453	450		Free OH

Table 6.4

Comparison of peak assignments for liquid-phase and L-B film doped IETS junctions.

M.Line et al Peak positions / meV	**T.Ginnai et al Peak positions / meV**	**Peak Assignments**
90	89	CH2 rock
	96	CH2 rock
109	110	CH2 rock
120	120	OH deformation
129	132	C - C stretch
	140	C - C stretch
	147	Mixed CH2 and COH vibrations
	156	
160	161	Coupled CO / OH
170	170	C - O / CH in plane
178	179	Symmetric COO- / CH2 deformation
199	199	Anti-symmetric COO- stretch
215		C = O stretch
230		
335	340	OH absorption
360	350 - 360	CH stretch
453		Free OH

Table 6.5

Comparisons of peak data from T.Ginnai et al and this group.

Table 6.5 compares the peak positions obtained by Ginnai for IET of mixed stearic acid - barium stearate Langmuir Blodgett film with the results from the present group using an exactly similar material but a different substrate.

The Raman modes characterising the vibrations of the carbon chain at 90, 109 and 129 mV are represented in both spectra. Various CH_2 modes can be ascribed to peaks in both spectra and the antisymmetric and symmetric COO^- bands can be determined from either spectra. One extra feature in the data from the present work is the resolving of the peak corresponding to surface OH stretch - this was masked by noise in the spectra obtained by Ginnai.

6.13 Evidence for Tunnelling Through L-B Films

There is a correlation between the spectra obtained with repeat runs on the same sample. It is however very much more difficult to produce a tunnel junction using a Langmuir Blodgett film than with liquid phase doping. The main problems were concerned with two effects. The first was that there was a very small proportion of junctions which had a junction resistance of less than a few tens of kilohms and secondly when the junctions did have a suitably low resistance, 100 -500 ohm, most of them had propensity to fail at a very low voltage. The vast majority of these failures tended to break down with the junction suddenly developing a very low resistance. In a few cases the opposite applied and junctions would break down with the junctions developing very high resistances, measured as infinite resistance on the instruments used to monitor this parameter. The majority of these cases appeared to have had large transient features appearing before failing . Some of the junctions exhibited these features during a run without failing and upon a re-run these features were nearly always reproducible.

It has been suggested that these features are attributable to traps in the oxide layer [20] or impurities picked up from the subphase or atmosphere [21]. It seems unlikely that the inclusion of impurities within the layer could be the cause because of the clean-room conditions prevailing during manufacture of the junctions. As Ginnai points out [5], for tin based junctions there is good correlation between I.R. and tunnelling spectra. The inclusion of an oxide layer in the completed junction complicates the issue. The data could been interpreted as a process whereby the electrons tunnel through the oxide and then via defects in the insulating layer to the top electrode. Junctions made with only tin oxide as an insulating layer showed very low junction resistances - less than one ohm and tended to break down below 20 mV. The oxide in these junctions therefore plays a much less significant role in the tunnelling process. He concluded therefore that his studies on the role of the oxide layer in IET junctions doped with a Langmuir Blodgett film did underline the fact that a tunnelling mechanism of charge transfer cannot be assumed simply on the observations indicated above and those undertaken by other workers [10,23]. he did finally conclude that electron tunnelling is the predominant conduction mechanism through Langmuir films.

The oxide used in these experiments was alumina which produces a blank junction with a resistance of tens of ohms, this therefore is a different situation from tin which rules out the low junction resistance part of the argument. The rigorous procedures the present group have developed and adopted together with the environmental control also virtually eliminate contamination of the Langmuir Blodgett layer.

The main evidence for tunnelling through the organic layer which

constitutes the L-B film is provided by the observations of signals which can be attributed to inelastic interactions between the tunnelling electrons and the molecules of the organic film forming the insulating layer. Only a very small proportion of electrons undergo inelastic collisions - around 1% of the total number which constitute the tunnelling current. Features within the IET spectra which can be attributed to the energy losses produced by these rare events provide very good evidence for a tunnelling mechanism based upon electron tunnelling within the organic layer.

Additional evidence is apparent in the strong correlation between IETS spectra and those produced by infra red and Raman techniques. These latter techniques have no oxide layer to complicate the issue and therefore further substantiate the proposal that the structure observed in IET spectra is indicative of electron tunnelling through the Langmuir Blodgett film incorporated in the junction.

6.14 Comments

Despite all the preparations and precaution taken, the fact that the vast majority of tunnel junctions produced using LB films had a very high junction resistance is both disturbing and interesting.

The electrical properties of thin insulating films are very sensitive to the uniformity of their thickness and to their structural perfection. Defects to an extent as low as one part in 10^5 can modify results to a significant extent [10]. Studies on insulating thin films - metal oxides and vacuum deposited thin films - have suffered from irreproducibility as a consequence of the fabrication process [9]. Indeed many of the factors which determine the conductivity of these films are extrinsic in nature. Using a Langmuir Blodgett film should fulfil many of the requirements for good reproducible tunnel junctions.

The thickness of the insulating layer in a tunnel junction i.e. < 10 nm should be

well catered for by using Langmuir Blodgett technique. The thickness of the insulating layer is determined by the length of the molecule and its apparent orientation on the substrate and so choice of molecule should predetermine the thickness for a coherent film. The coherence of the film is determined during the fabrication of the Langmuir film prior to transfer to the substrate and monitored during transfer. Thus by using a Langmuir Blodgett film to produce the insulating layer of a tunnel junction the two important criteria of thickness and coherence should be well satisfied. But, by far the greatest proportion of tunnel junctions doped with LB films of stearic acid/ barium stearate have a measured d.c. resistance greater than 5000 Ohms. This together with the fact that when stearic acid is liquidphase-doped onto a similar substrate the resistance of the junction falls dramatically to lie within a suitable range for IETS with our instrument namely 50 to 500 Ohms begs an explanation.

The assumptions made about the structure of the insulating layer when a junction is liquid phase doped are identical to those made for LB films. When a junction is liquid-phase-doped it is assumed that the insulating layer is a coherent, well ordered monolayer. Furthermore the monolayer is thought to be oriented such that the molecules within it are arranged in ordered manner with the hydrophillic End towards the oxide layer. These two assumptions cover coherence and thickness respectively and fulfil the basic requirements of a tunnel junction insulator. We will look at each requirement in turn in the light of our knowledge of Langmuir / Langmuir Blodgett films and liquid-phase-doped films.

6.14.1 Film Coherence

Langmuir films are fabricated using a well controlled environment. Their structure and integrity is monitored and is well known through their isotherms. Transfer ratios were determined to ensure that a l : l ratio was achieved thus ensuring a defect and pin hole free layer, within experimental error.

Liquid-phase-doped films are assumed to be coherent monolayers. Their coherence is implicit in their ability to produce tunnelling spectra which are analogous to infra red and Raman spectra, because tunnelling is particularly sensitive to pinholes and defects.

6.14.2 Film Thickness

Langmuir Blodgett films have a known thickness - assuming that the length of the molecule forming the film is known. Their orientation and therefore the thickness of the film is monitored and controlled during their transfer to the substrate.

The thickness of liquid-phase-doped films has been measured by several methods which produce dimensions which correlate well with expected molecular dimensions. It is assumed that the dopant layer is orientated approximately perpendicular to the substrate surface to give an appropriate tunnelling thickness.

The main difference between liquid phase doped and Langmuir blodgett films first reveals itself as a difference in the d.c. resistance of the completed junctions. As stated above the d.c. resistance of LB films is very much greater than the resistance of a junction liquid phased doped with an exactly similar molecule.

This difference could be attributable to one of two things or a combination of both. First the oxide layer in the LB film junctions could be thicker due to its immersion in the subphase thus increasing a junctions resistance. Second the film layer in the liquid-phase-doped junction may not be as coherent as that in the LB film junctions due to the dispersed nature of the molecules within the solvent prior to doping.

6.14.3 Oxide Thickening.

Turning our attention first to the thickening of the oxide. The fact that the aluminium oxide is (by the mere nature of the LB film technique) immersed into water during junction manufacture might point to oxide thickening as a factor.

In order to test this possibly a number of experiments were carried out by the present group. These involved dipping bottom aluminum electrodes into a clean subphase (without a monolayer) at the same speed as that used for transferring the Langmuir film to the substrate. The electrodes were then stored in conditions similar to those used for storing Langmuir Blodgett doped films for a similar time. The junctions were then either liquid phase doped in the normal way or used to produce blank junctions.

Dipping the bottom electrode into the subphase and then placing it in a desiccator for 15 hours did result in an increase in the thickness of the oxide layer. Experiments with blank junctions have shown that the resistance of the junction increases from between 1 to 20 Ohms for an undipped bottom electrode to to between 50 and 500 Ohms for a dipped one. The finished junctions produced spectra which

were indistinguishable from each other and from blank junctions which had been made in the usual way.

Other junctions were completed by liquid phase doping the aluminium oxide after the treatment outlined above. These junctions exhibited junction resistances between 300 and 1.5K ohms. Suitable junctions were selected using the criteria previously outlined for selecting junctions and these junctions produced spectra which were exactly similar to those produced by junctions produced using the 'normal' procedure outlined earlier in this thesis.

Assuming that LB films produce junctions in which the arrangement of the layer of dopant molecules is not far removed from the arrangement of a layer produced by liquid phase doping. It would be expected therefore that a junction doped with an LB film should in the worst case have a junction resistance of roughly 1.5K ohms. This value is far below the many 10s of kilohms obtained in practice for LB film junctions. This leads us to suppose that oxide thickening is not responsible for the high junction resistance of junctions doped with LB films.

The inevitable inclusion of an oxide layer within any completed IET junction complicates the picture of the tunnelling process. It is possible to describe the process as one which is dominated by electrons tunnelling through the oxide layer and then through thin areas and other defects in the organic layer. This picture appears to contradict the transfer ratio data which indicates a coherent layer but the errors in measuring the area of the transferred layer cannot rule out the possibility of small defects in the film.

Other workers in the department have attempted to prove that the dominant charge transfer mechanism through LB films is electron tunnelling [5]. Using tin as a bottom electrode Ginnai produced evidence to show that conduction in single layer films was by direct tunnelling between metal electrodes.

A definitive test of tunnelling is to use at least one superconducting electrode and try to observe that only a small current flows for a bias eV less than the energy gap of the electrode [22] - see chapter 2. This test has been applied to Langmuir Blodgett films by other workers [23] but their results also were suspect because of the presence of an oxide layer.

The close correlation between the spectra obtained by this author and the previous group is strong evidence for quantum mechanical electron tunnelling in the Langmuir Blodgett films incorporated into the present junctions. But, the question of why so many of the junctions produced using LB films have very high junction resistances and those which have been liquid-phase-doped do not, remains unanswered unless the integrity of the liquid phase and the L-B films are questionable.

The answer may lie in the fact that many workers have produced IET spectra of polymers. R. R. Mallik [24] did work on a number of polymers producing spectra from materials of relatively high molecular weight.

A short list follows to illustrate the range of materials he used:

Polymer	Molecular weight
PVA	45,000
PVOH	72,000
PEOX	$5x10^6$
PEG	370

All of these materials are far too long to be oriented perpendicular to the oxide surface and still produce IET spectra. An answer to the enigma is maybe that the polymers are adsorbed onto the surface like a pile of spaghetti on a plate. In this configuration the polymer chain is adsorbed in a tail - train loop - tail pattern which would allow some of the polymer to be adsorbed via interactions between the train segments, as shown below in figure 6.13.

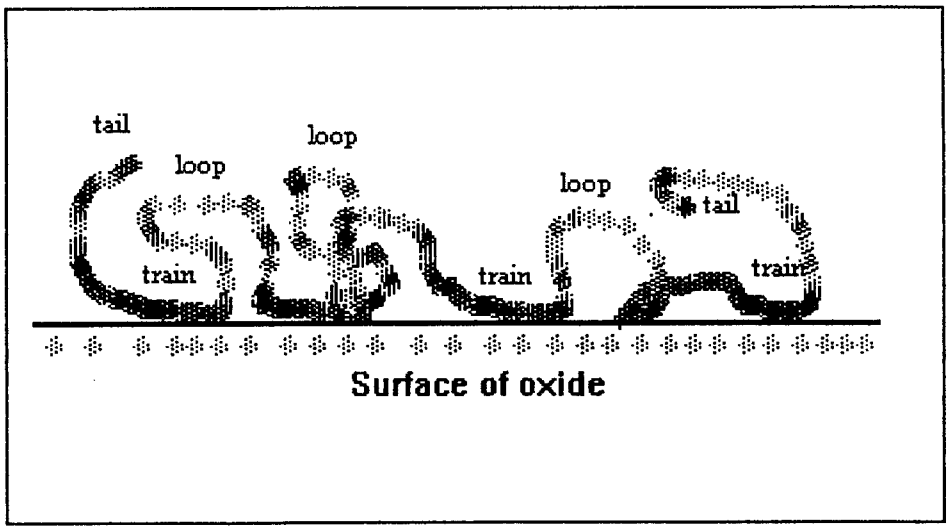

Figure 6.13

This model would give rise to a situation where portions of the polymer layer were thinner than others; significant tunnelling could take place through these thin spots in the dopant layer.

It is proposed that a similar situation exists in liquid phase doped junctions where the disordered nature of the doping procedure is conducive to the formation of faults and thin spots in the dopant layer. This model can explain the success rate achieved with liquid phase doping. The failure of LB films produced as a suitable dopant method can also be explained. If the Langmuir Blodgett films produced in this department are as coherent and uniform as the experiments seem to imply, it could be that their perfect structure is the cause of our inability to produce IET spectra from them.

The spectra produced by T.Ginnai were obtained from junctions dipped in a tank made at Leicester Polytechnic whereas the tank used in the series of experiment was a state-of -the-art instrument capable of producing fine quality LB films. These observations, whilst not degrading the quality work done by Ginnai, lead us to propose that the early films were more prone to imperfections than those produced in the Lauda trough and therefore produced more spectra by tunnelling via these imperfections.

It may be possible to resolve the points on film coherence and thickness made above if the surfaces of LB and liquid-phase doped junctions could be mapped and compared by using (STM) or (AFM). Also modifications to the spectrometer to enable high resistance junctions to be catered for would enable spectra to be obtained from the at present unusable junctions. Data from these junctions might highlight the role of the oxide layer and or defects within the overlaying film.

6.14.4 Tunnelling Probability versus Junction Thickness

The height and width of the potential energy barrier are critical factors in modifying the tunnelling processes. Starting with a simple rectangular barrier it can be shown that under conditions of small bias and low temperature it can be shown that the tunnel current density (j) is given by:

$$j = \frac{3}{2}\sqrt{2m}\left[\frac{e}{h}\right]^2 \frac{\sqrt{\phi}}{s} V \exp\left[\frac{-2s}{\hbar}\sqrt{2m\phi}\right]$$

Where the symbols have their usual meanings.

Note:

$$\mathbf{j \propto V}$$

$$j \propto V \exp\left[\frac{-2s}{\hbar}\sqrt{2m\phi}\right]$$

i.e.

$$\mathbf{j \propto e^{-2ks}}$$

Where the inverse decay length k is:

$$k = \frac{\sqrt{2m\phi}}{\hbar}$$

In fact :

$$2k \,/\, \text{Å}^{-1} \approx 1.025\sqrt{\frac{\phi}{eV}}$$

For a typical barrier height of 4 eV, $k = 1\text{Å}^{-1}$

Therefore there is a marked dependency on the width of the barrier. Inserting nominal values gives:

For $s = 20$ Å

$$e^{-2ks} = 4.2\ e^{-18}$$

For $s = 21$Å

$$e^{-2ks} = 5.7\ e^{-19}$$

and for $s = 40$ Å

$$e^{-2k} = 1.8\ e^{-35}$$

As can be seen from the above calculations there is a very strong dependence of j upon s. J decreases by an order of magnitude if s is increased by just 1Å. Therefore we can conclude that if there are defects or 'thin spots' within the Langmuir Blodgett film (or indeed any film) forming the dopant layer in an IETS junction they have a vitally important role to play in the tunnelling process.

References

[1] Langmuir I 1920 *Trans. Faraday* Soc. **15** 62
[2] Blodgett K B 1934 J. *Am. Chem. Soc.* **56** 495
[3] Blodgett K B 1935 *ibid.* **57** 1007
[4] Langmuir I and Schaefer V J 1937 J. *Am. Chem. Soc.* **59** 2400
[5] Ginnai T M 1982 PhD *Thesis Leicester Polytechnic*
[6] Lamb J and Jacklevic R C 1968 Phys. Rev. **B5** 821
[7] Miiller A 1927 Proc. *Royal Soc.* ***114 A*** 542
[8] Careem M A 1976 PhD *Thesis University of London*
[9] Simmonds J G 1971 J. Phys. D. Appl. Phys. **4** 613
[10] Mann B Kuhn H 1971 J. *Appl. Phys.* **42** 4398
[11] Blodgett K B and Langmuir 1937 *Phys. Rev.* 51 964
[12] Dinnez G 1988 M Phil. *Thesis Leicester Polytechnic*
[13] Gershfield N 1972 *Techniques of Surface and Colloid Chemistry and* Physic eds. Good, Stromberg, and Patrick (Marcel - Dekker : N.Y.)
[14] Langmuir I 1916 J. *Am. Chem. Soc.* **39** 1848
[15] Gaines G L 1966 *Insoluble Monolayers at Liquid - Gas Interfaces* (Wiley Interscience : New York)
[16] Vold M J 1952 J. *Colloid Sci.* **7** 196
[17] Keil R G, Graham T P and Roenker K R 1976 App. *Spectroscopy* **30** 1
[18] Bellamy L J 1975 *The Infrared Spectra of Complex Molecules (* Chapman and Hall : London)
[19] Hall J T and Hansma P K 1978 *Surf.* Sci. **76** 61
[20] Skarlatos Y, Barker R C and Yelon A 1976 J. Appl. *Phys.* **22** 106
[21] Gundlach K H and Kadlek J 1974 *ibid* 25293
[22] Giaever I and Megerle K 1961 *Phys. Rev.* **122** 1101
[23] Leger A, Klein J, Berlin M and Deforneau D 1971 *Thin Solid Films* ***8*** R51
[24] Mallik R R 1985 PhD Thesis Leicester Polytechnic

Contents

CHAPTER 7

A STUDY OF 2- HYDROXYETHYL METHACRYLATE

7.1 Introduction

The group of synthetic polymers termed hydrogels consist of a matrix of hydrophillic macromolecules which are cross-linked to form a three-dimensional network. The hydrophillic nature of the gels means that they will imbibe water spontaneously until an equilibrium hydration is reached. This equilibrium will depend upon the density of the crosslinks and the number and nature of the sites. All hydrogels, except p-HEMA, are constructed from a matrix of water-soluble polymers. At equilibrium these gels can contain over 95% water and the water is assumed to spread spontaneously over the surface of hydrogels, assuming the surface is fully hydrated.

Hydrogels have many applications in the field of prosthetics. For instance these materials are widely used in the fields of, surgical and dental implants, blood bags, tubing, syringes, etc. Most synthetics have properties which differ widely from the tissue with which they are interfaced or are replacing [1], the major difference is that except for bones, nails, and the outer layers of skin, mammalian tissues are highly aqueous, having water contents ranging up to 90% in blood plasma.

The bio-compatibility of hydrogels lies in their ability to absorb, and retain within their structure, large quantities of water. The outermost layer of water is exposed on the surface of the polymer structure where it interfaces with the tissues surrounding the implant; thus a compatible surface is presented to the tissue [2].

These polymers are covalently or ionically cross-linked three dimensional networks which are generally hydrophillic [3,4]. They interact with aqueous solutions by swelling to some equilibrium volume. The networks can be relatively strong as in the case of the membranes used in dialysis machines or weak as in the case of implants which are inserted in a dehydrated state into and then swell to fill a body cavity. It can be said that generally the strength of the hydrogel becomes less as the water content increases [5]. The mechanical behaviour of the network is dependent on such variables as the nature of the cross-linker, the polymer network and its crystallinity; features which are beyond the scope of this work. Thus the bulk properties of synthetic hydrogels can be tailored to suit a particular application. Poly hydroxyethyl methacrylate (p-HEMA) is a very important and one of the most widely used biomedical polymers. The hydrogel studied in this work is Poly-2-hydroxyethyl methacrylate a version of p-HEMA which is tailored to have an end use as a contact lens material.

7.2 Solution Polymerisation - General Protocol

Polymers were produced by conventional free radical polymerisation. The polymerisation was carried out in a five necked, 500cm^3 resin flask in a water bath at 65°C. This flask was equipped with an overhead stirrer, a condenser fitted with a drying tube, a thermometer, a pressure equalised dropping funnel and finally a nitrogen bleed. In a typical reaction 300 cm^3 of methanol or ethanol were added to the flask. The temperature was raised to 65°C and the solvent degassed for 15 minutes. 30gms of the monomer HEMA and 1% initiator AZBN

were weighed out and dissolved in 100 cm' of the solvent. This mixture was then added dropwise to the flask and the resulting mixture refluxed for 12 hrs. under a blanket of nitrogen. The contents of the flask were then allowed to cool. If the polymer precipitated out it was redissolved before the solution was added dropwise to approximately 1 litre of diethyl ether which had been cooled with solid CO_z. The finely precipitated polymer was then filtered and after being washed three times with diethyl ether, dried in a vacuum over at 60°C.

All details of polymerisation supplied by Dr. H. Oxley and all the samples used in this IETS study of the hydrogel p-HEMA were kindly donated by Professor Brian Tygh, Dr. H. Oxley, and Dr. P. Corkhill, all of whom also provided invaluable assistance during a number of discussion sessions and subsequent communications. HEMA - 2 -Hdroxy ethylmethacrylate was supplied by Ubichem and AZBN azobisisobutyronitrile supplied by Aldrich. Figure 7.1 is an illustration of one unit of poly 2-hydroxylethyl methacrylate (p-HEMA).

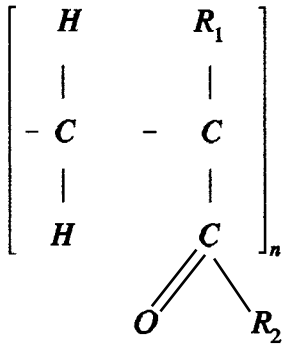

Figure 7.1

p-HEMA or Poly 2 - Hydroxy ethylmethacrylate

Where $R_1 = CH_3$ and $R_2 = OCH_2\,CH_2\,OH$ and n = 9

7.3 Water in the Hydrogel p-HEMA

The nature of water in hydrogels has been the subject of many studies [6 -15], and an hypothesis which infers a structure within liquid water has been proposed [12]. The model put forward is based upon the results obtained from a number of experiments which investigated some of the physical properties of water: calorimetry, bulk conductivity, NMR, dilatometry, dielectric relaxation, etc. Using the data provided by these techniques inferences were made concerning which macroscopic details of liquid water were reflected in any given microscopic property.

There exists a consensus of opinion which believes that there is bulk of evidence which substantiates the hypothesis that entrapped water within hydrogels may be significantly different from bulk or normal water. It is hypothesized that hydrogels may contain three classes of water: X water (a free water-like phase), Y water (an interfacial water-like phase), and Z water (a bound water-like phase). The phase of the individual groups of water molecules is influenced by their proximity to the p-HEMA molecules forming the hydrogel. The water will consists of a fraction which is significantly affected by the polymer network (Z water - bound water), a fraction which is relatively unaffected by the polymer molecules (X water - free water), and an intermediate fraction (Y water - interfacial water).

7.4 Rationale of the Experiments

In this chapter the results from two important studies of hydrogels will be presented. In the first part, the way in which water is incorporated into an

ultra-thin layer of p-HEMA will be investigated. This study is unique in that it follows the way in which an ultra-thin layer of hydrogel swells during the time water is infused into it. There have previously been many studies of the swelling behaviour of hydrogels but all of these earlier studies dealt with bulk samples - the author references a representative sample of reports [4,5,16-18].

In the second part of the chapter inelastic electron tunnelling spectroscopy (IETS) is used first to study p-HEMA and its parent monomer hydroxyethyl methacrylate (HEMA). IETS provides us with an insight into the way in which both the monomer and the polymer respectively adsorb onto an aluminium oxide surface. This study is the first IETS investigation of the way in which a coating of hydrogel one monolayer thick is adsorbed onto the surface of aluminum oxide.

The remaining sections of this chapter outline the theory, the experimental procedures and conclusion drawn from the data collected during experiments conducted on the p-HEMA.

7.5 Development of Experimental Procedures

All of the work done previously on these important and interesting materials has been performed using bulk samples of the hydrogel in question. These samples are usually constructed as a cylinder, cube, or sheet of a few cubic centimetres volume. This group decided to investigate a much thinner and smaller sized sample. It was decided that the many important applications in which hydrogels are used as thin coatings warranted an investigation into both the swelling of very thin films of the material and the interfacial bonding.

In the conductance experiment the constant current was supplied by a Keithley constant current source and the potential monitored via a Keithley programmable Digital Voltmeter (DVM). These instruments were chosen because of the accuracy of the constant current source and the high input impedance of the DVM (>1GΩ on any dc range). The high input impedance ensures that any potential drop across the voltage probe leads is negligible in comparison with those across the junction. These instruments are also capable of being interfaced to a computer via an IEEE 488 serial line thus enabling the data logging to be completely under the control of a Phillips 286 computer. This facilitated rapid and accurate gathering of data from the conductance and time measurement.

7.5.1 The Swelling of p-HEMA

Measuring the dimensional change which occur as water infuses into a thin (effectively a monolayer) sample of p-HEMA presented some problems and required a novel monitoring technique. For the method we turned to some earlier work which was done in the department [19]. Mallik had done some work on the way in which water is adsorbed onto the aluminium oxide surface within an IETS junction. He introduced the water to the surface by infusing it through the lead top electrode of the tunnel junction. The technique was used to overcome the problems associated with the liquid phase doping of tunnel junctions when using certain volatile monomers and solvents e.g. Propan-2- ol, 2-methylpenton-2- one and Phenol.

It was decided that the method of infusion doping used in some earlier work by Mallik could serve our purpose if employed as outlined in the following text. By

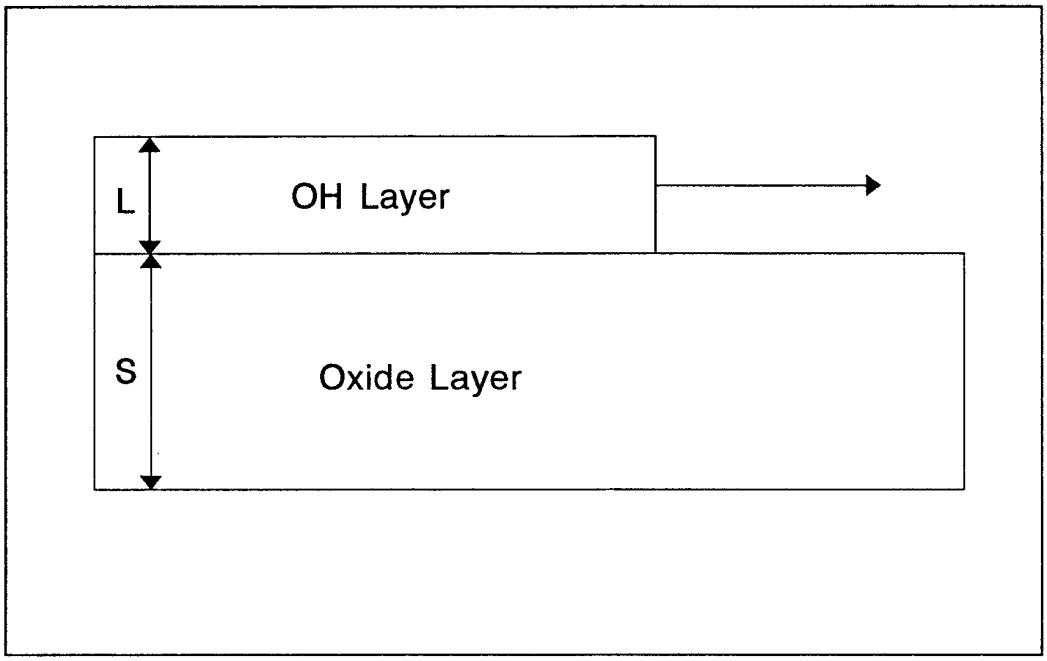

Figure 7.2a

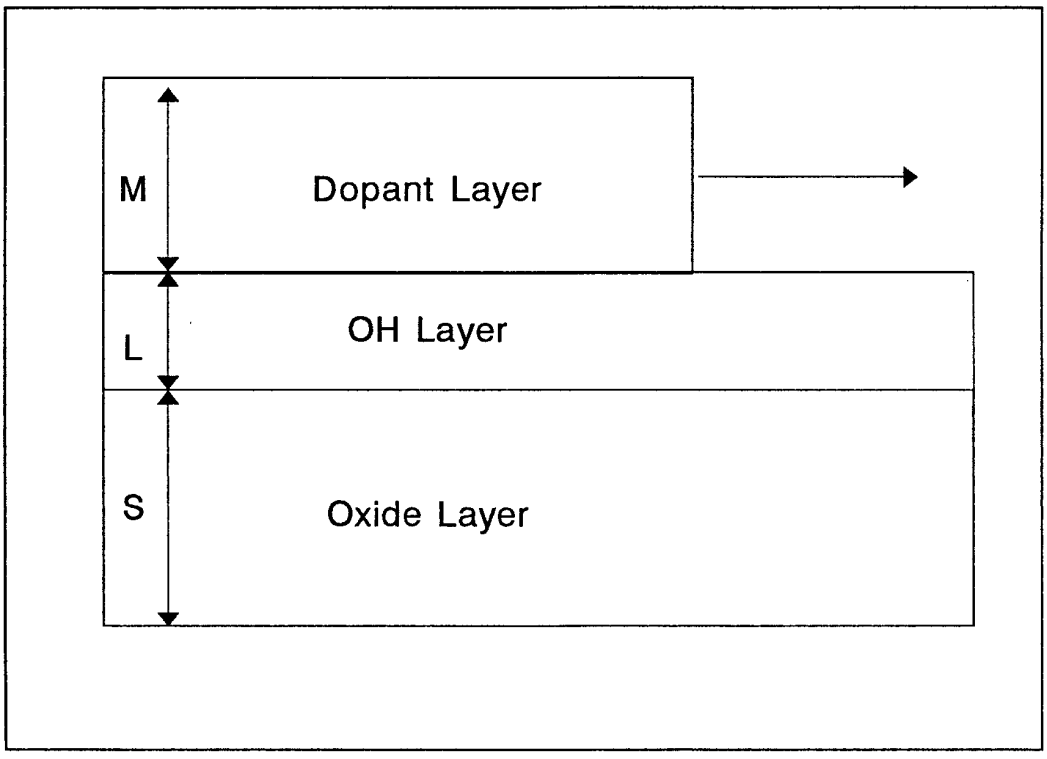

Figure 7.2b

Figure 7.2a

A schematic representation of the growth of the first monolayer onto the surface of aluminium oxide as water is infused into the junction - after Mallik. The first layer consists of a monolayer of hydroxyls and it is assumed that this layer will be completed before the second monolayer is deposited on top of the hydroxyls.

Figure 7.2b

Illustrated here is a representation of the way in which the second monolayer is assumed to be deposited upon the completed hydroxyl layer. The dopant in the case of the present group's study is exclusively water. Again the simple theory proposes that this second layer is completed before the next and so on with each subsequent monolayer as they are deposited.

These two figures represent an idealised view of monolayer growth onto an aluminium oxide surface, after Mallik.

using the technique of liquid-phase doping a monolayer of the hydrogel could be incorporated within an IETS junction - see chapter on junction construction for details. Once a lead top electrode had been evaporated over the top of the doped junction the physical dimensions of the junction would be fixed. Therefore, the conductance of the junction would be dependent mainly upon the thicknesses of the two insulating layers formed by the aluminium oxide and the monolayer of p-HEMA respectively. If water was now allowed to infuse through the top electrode it would be taken up by the hydrogel. As a result of the inclusion of the water in the hydrogel the polymer would swell producing changes in the thickness of the insulating layer formed by it, and consequently changing the conductance of the junction. Therefore the conductance changes would mimic the swelling of the hydrogel and by monitoring the changes in conductance we concluded that we might make inferences about the way in which hydrogels swell as water is incorporated in them.

7.5.2 Infusion Doping

The technique of infusion doping which was first reported in 1977 by Jacklevic and Gaerttner [20,21] involves dopant molecules being introduced onto the Aluminium oxide surface of a completed Al-Alox-Pb tunnel junction by penetration of the lead counter electrode. Mallik [19] verified the effect by using the simple technique of applying vacuum grease to selected areas of the top electrode to preclude the ingress of the dopant to the selected areas. His work concluded that the dopant did indeed infuse through the lead of the top electrode and not through the edges of the Junctions. Illustrated in figures 7.2a and 7.2b

are schematic representations of monolayer growth as proposed by Mallik. The rate at which the infusion occurs is critically dependent upon two variables. These are the rate at which the deposition of the lead takes place and the thickness to which it is deposited [20-22]. Also investigated was the use of other top electrode materials since lead is generally unstable under infusion doping where water-rich vapours adsorb upon the metal and attack it. However, of the metals tried Ag, Cr, and Cu proved to be ineffective but there was some limited success with Sn and Au. For the work in this chapter lead is exclusively utilised as a counter electrode material. The diffusion rate and the thickness of the lead electrode were chosen to correspond to the optimum values of 300 nm thick of lead deposited at a rate of 1 nm s^{-1} obtained by Mallik.

Contamination by formic acid is a problem which is often encountered in infusion doping experiments [22]. The close proximity of its boiling point, 100.5°C, to that of water means that it is often a low level - ppm - impurity in water. Also the production of formic acid (HCO_2H) through a catalytic reaction of the lead in the top electrode by atmospheric carbon dioxide and water is another source of contamination. This being so, an apparatus was built which allowed completed junctions to be sealed in it and the surrounding atmosphere purged with nitrogen gas to exclude CO_2 thus preventing the reaction with the lead taking place a schematic of the apparatus is shown in Figure 7.3. The chamber also allows the changes in conductance which occur during the infusion process to be monitored accurately and the data collected via a computer link.

The main body and the lid of the chamber were constructed from very high grade stainless steel. The chamber enabled measurements to be made in real

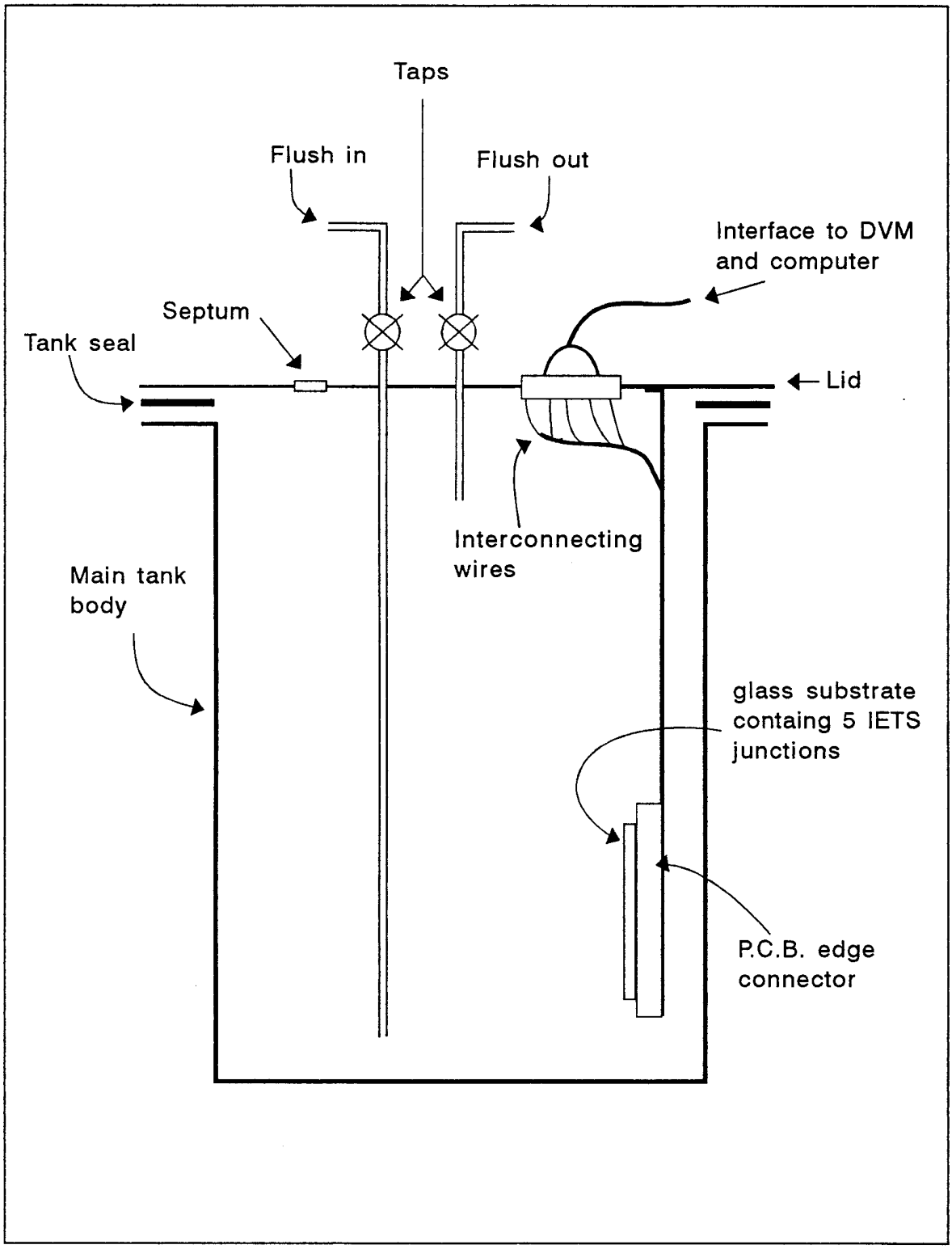
Taps
Flush in
Flush out
Interface to DVM
and computer
Septum
Tank seal
Lid
Interconnecting
wires
Main tank
body
glass substrate
containg 5 IETS
junctions
P.C.B. edge
connector

Figure 7.3

Figure 7.3

An illustration of the chamber designed and constructed for infusing water into an IETS Junction. The design enabled measurement in real time to be made of the conductance changes which occurred during the time the infusion was takeing place. Interconnections to a computer allowed complete control of the monitoring and storage of the data collected.

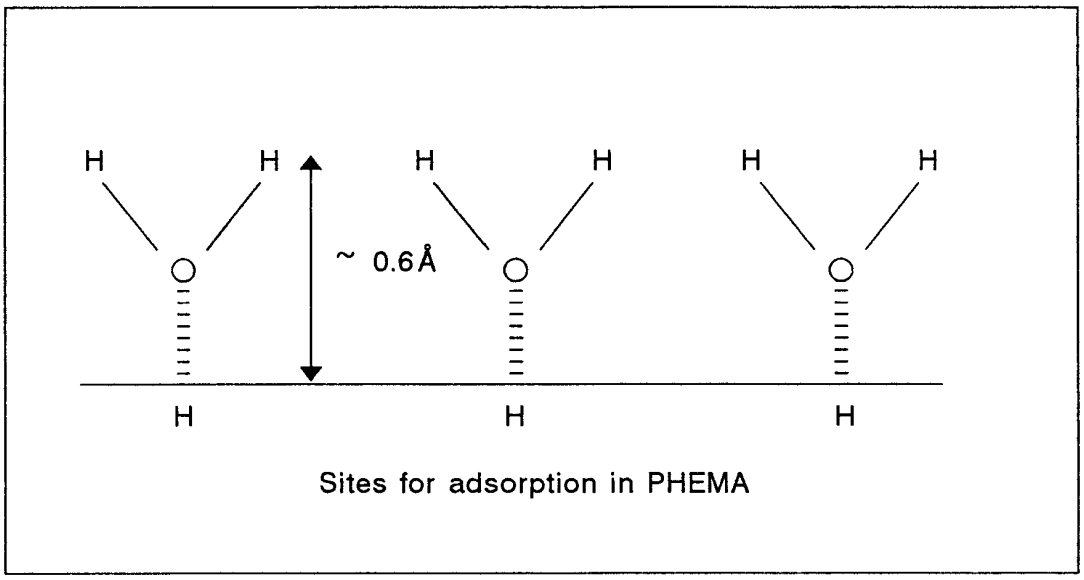

First layer of water

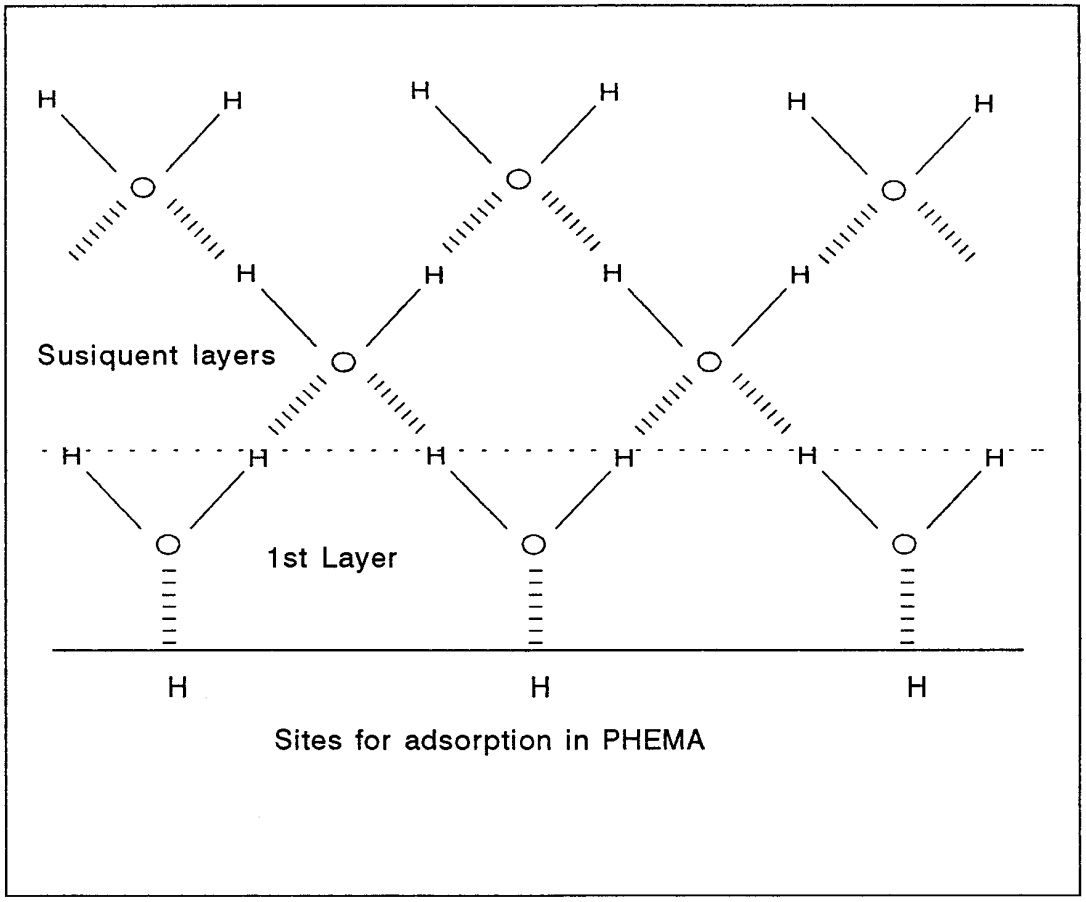

Second and subsiquent layers of water

Figure 7.4a

Figure 7.4

Illustrated in this diagram is an idealised representation of the way in which it is proposed that the first two layers of water are adsorbed onto the surface of poly 2 - hydroxyethylmethacrylate (p-HEMA). Indicated on the top diagram is the approximate thickness of the first layer of water adsorbed onto the polymer. The lower diagram shows a highly stylised two-dimensional representation of the way in which the subsequent layers of water are adsorbed in a tetrahedral structure.

time of the conductance changes which occurred during the infusion of water into an IETS junction doped with p-HEMA. The cable marked 'Interface to DVM and computer' served as an umbilical to provided the interface for the constant current source and the wires for the four point probe measurement. All facets of the monitoring and storage of data were controlled by an IBM compatible 286 computer. A constant current was applied to the junction and the conductance of the junction monitored as water was infused into the hydrogel. Any changes in conductance were considered to be indicative of changes in the thickness of the junctions insulating layer. Illustrated in Figure 7.4 is an idealised picture of the way in which the first two layers of water are adsorbed onto p-HEMA.

The experiments performed with the apparatus described above have provided some evidence of structure within the layers of water which were sequentially assimilated by the hydrogel within the IETS junction. These data further substantiate a consensus of opinion which proposes that when water is incorporated in p-HEMA it has an order imposed upon it by the polymer [23-26]. The first and most intimate layer being tightly bound to the polymer is the most structured and ice like in its characteristics. The following layers exhibit a degree of structure which diminishes with distance from the surface, until a 'normal' unstructured water is encountered in the main body of the incorporated water.

7.6 Elastic Tunnelling at Low Bias During Infusion Doping

Using a trapezoidal barrier model and the approximation of Wentzel-Kramers-Brillouin (WKB), Brinkman, Dynes and Rowell [27] have shown that the

conductance of a tunnel junction at low bias is given by:

$$G = \gamma' \frac{\bar{\Phi}^{1/2}}{S} A_j \exp\left(-K S \bar{\Phi}^{1/2}\right) \qquad (7.1)$$

Where:

G is the conductance of the junction.

Aj is the junction area.

γ' is a constant.

ÅΦ (eV) is the mean barrier height.

S (Å) is the thickness of the barrier.

K is ≈ 1 for the units quoted.

For the region of interest in the present work the pre-exponential factor is smoothly varying and can be considered to be approximately constant. Burnstein and Lunquist [28] expressed the junction conductance to a good approximation by:

$$G \approx \gamma A_j \exp\left(-S \bar{\Phi}^{1/2}\right) \qquad (7.2)$$

Mallik normalised the conductance to the conductance of the aluminium oxide and using this approximation he was able to interpret his data in terms of a sequential growth of monolayers water molecules, with the first layer adsorbed on the aluminum oxide and subsequent layers stacking on top of each other. This approximation will be taken as a starting point when modelling the swelling of thin layers of p-HEMA.

The low-bias current versus voltage characteristic of a tunnel junction is linear up to around 100mV. There are slight deviations due to inelastic tunnelling events taking place but these are outside the experimental errors of this conductance study. Applying a small constant current to the junction at low bias and assuming that $\Phi^{1/2}$ was not so important as S changes in barrier thickness can be monitored via the approximately ohmic changes in junction potential.

It is essential that the monitoring of these changes is done using a four-point-probe technique.

7. 7 Experimental Details

A number of criteria were observed when preparing IET junctions for these experiments. The thickness and rate of depositing the lead electrode is thought to play an important role in the rate at which the infusion occurs [20-22,29], with the fastest infusion taking place in thin slowly evaporated films. Thin films give rise to a problem in that although they speed up the infusion time they are more likely to allow the transmission of contaminants into the junction. Thicker lead electrodes reduce the chances that any contaminants will reach the junction through the top electrode. However, if the lead is made too thick the time taken for the experiments to take place is prohibitively long. A compromise of a lead electrode thickness of 300nm was chosen; this gave a reasonable time for the infusion to take place and an adequate protection against the penetration of contaminants.

The slides onto which the junctions were evaporated were prepared and cleaned using the procedures developed to provide IETS samples - see Chapter 3 of this thesis.

Immediately after the top lead electrode had been evaporated the slide was mounted in a printed circuit board edge connector and transferred to the infusion chamber. The chamber was then sealed and then flushed with nitrogen. The chamber was interfaced via an IEEE link to the computer and logging started. After a few seconds the chamber was flushed with room air to purge the nitrogen. The dopant 'Millipore' water was introduced into the chamber via a septum - a self-sealing plug - using a clean hypodermic syringe and the resulting changes in junction conductance monitored, assuming $\Phi^{1/2}$ doesn't have much effect, using the techniques outlined previously in section 7.6.

Measurements were made at low bias with V_b « Φ to ensure that the junction will remain on the approximately linear region of its I vs V characteristics. The measurement were made by passing a constant current of 1 mA through the junction whilst monitoring the potential of the junction .

The data were processed in a spreadsheet - Supercalc 5 - where the graphical analysis capabilities of the software were used to display the data in a visual form to aid interpretation and to print out hard copies of the graphs.

7.8 Assumptions

In order to interpret the results a number of assumptions must be made at the outset. A resume of these assumptions is as follows.

- As the dopant is infused into the IET junction it will in general modify the nature of the potential barrier, which wall result in local variations in its height and width. These changes will result in a

decrease of the conductance of the junction - as a consequence of equations 7.1 and 7.2 .

- The water molecules are assumed to infuse into the junction to form uniform and sequential monolayers on the dopant p-HEMA. These monolayers are also assumed to be formed sequentially in that one layer is assumed to be completely formed before initiation of the next.
- The time for each monolayer to be adsorbed is constant and the layers are adsorbed in a uniform manner. The function is also assumed to be planar in its composition. This implies that the oxide surface formed during the manufacture of the IET junction is a smooth or smoothly undulating surface with no topographical defects - i.e. holes etc.

Clearly these initial approximations are very broad; the time taken for a layer to be adsorbed will depend upon how the first and subsequent monolayers interact with each other. The initial layer will have adsorption sites on the polymer surface to adhere to, whereas subsequent layers will be presented with the surface of the previous monolayer which may not be so conducive to bonding as readily as the initial one.

7.9. An Overview of the Results

Show in figure 7.5 is a graph of conductance in siemens versus time for a 'blank' junction during the infusion of water through the top lead electrode. Shown for comparison in figure 7.6 is the graphical representation of a set of data taken by R.R. Mallik, during the infusion of water into an exactly similar junction.

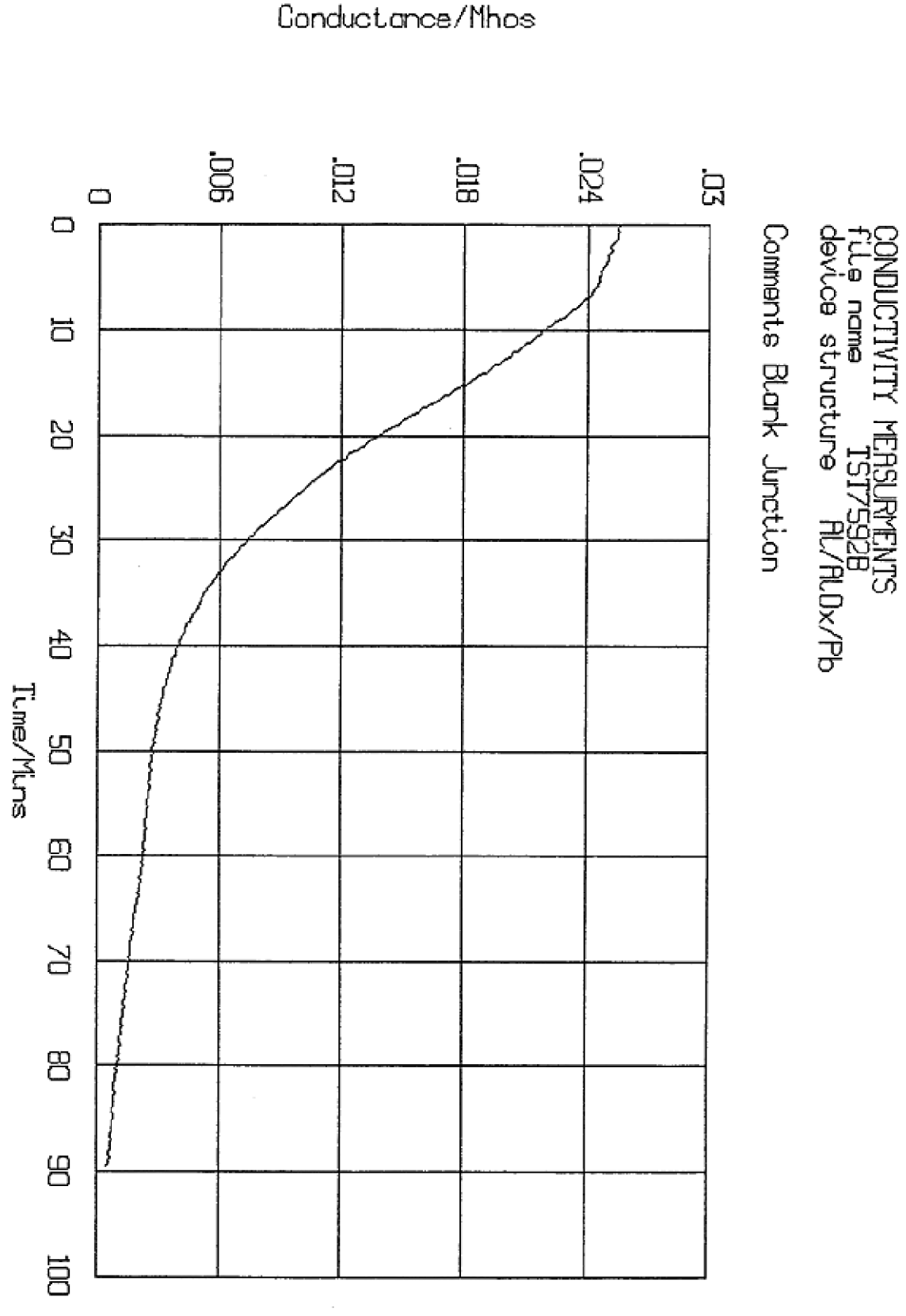
Conductance/Mhos
0
.006
.012
.018
.024
.03
0
10
20
30
40
50
60
70
80
90
100
Time/Mins
CONDUCTIVITY MEASURMENTS
file name TST7592B
device structure Al/AlOx/Pb
Comments Blank Junction

Figure 7.5

Figure 7.5

A reproduction of representative plot taken by this present group during the infusion of pure water into an aluminium - aluminium oxide - lead IET junction. The graph is shown for comparative purposes and is to be compared with the figure overleaf of a plot taken by a previous group with a similar junction configuration.

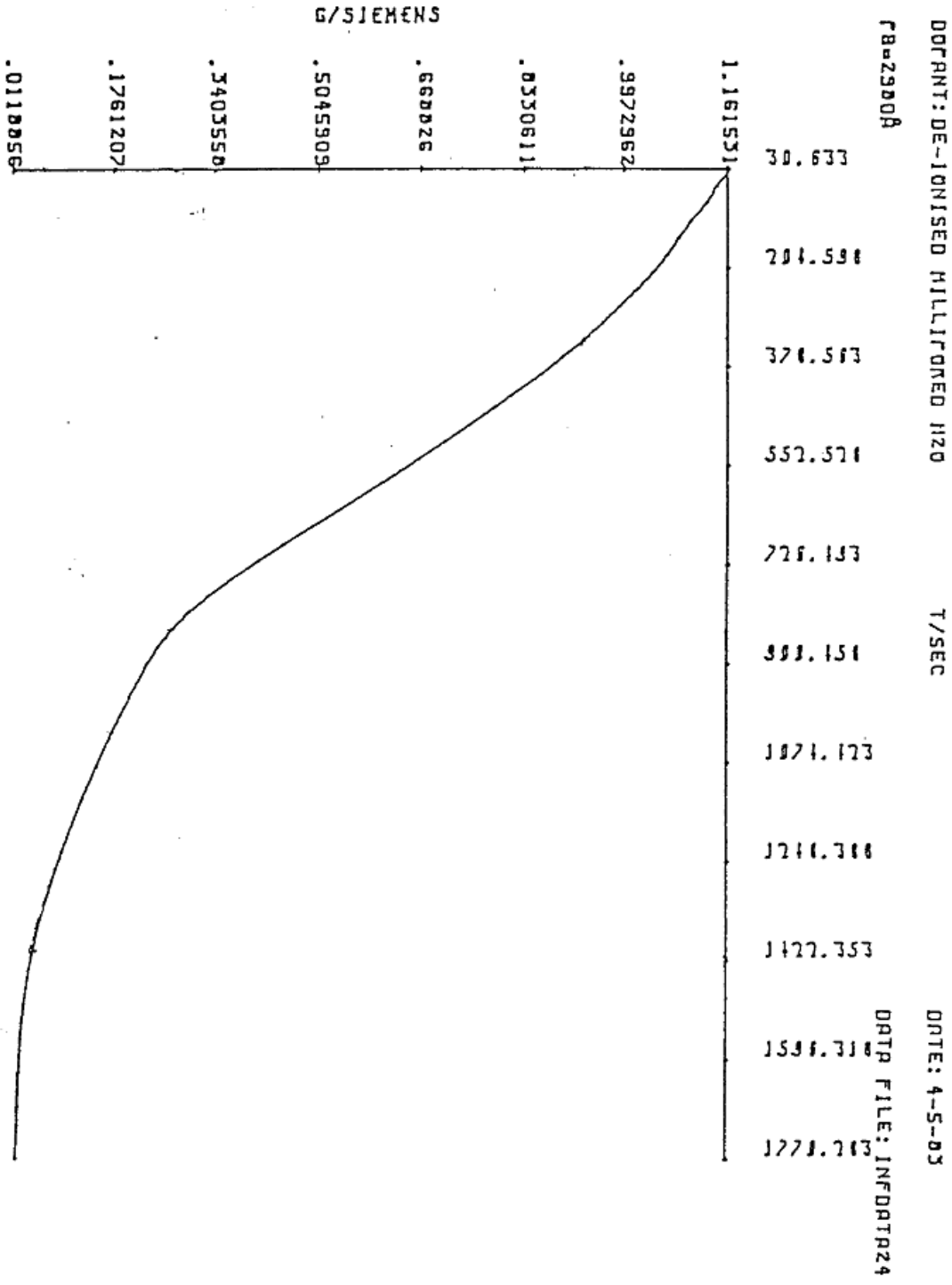
G/SIEMENS
.0118856
.1761207
.3403558
.5045909
.668826
.8330611
.9972962
1.161531
DOPANT: DE-IONISED MILLIPORED H2O
T/SEC
DATE: 4-5-83
DATA FILE: INFDATA24

Figure 7.6

Figure 7.6

A reproduction of a plot taken by a previous group during the infusion of water in to a blank (undoped) IET junction. The form of the graph is similar to the one illustrated in figure 7.5 and is shown for comparison only.

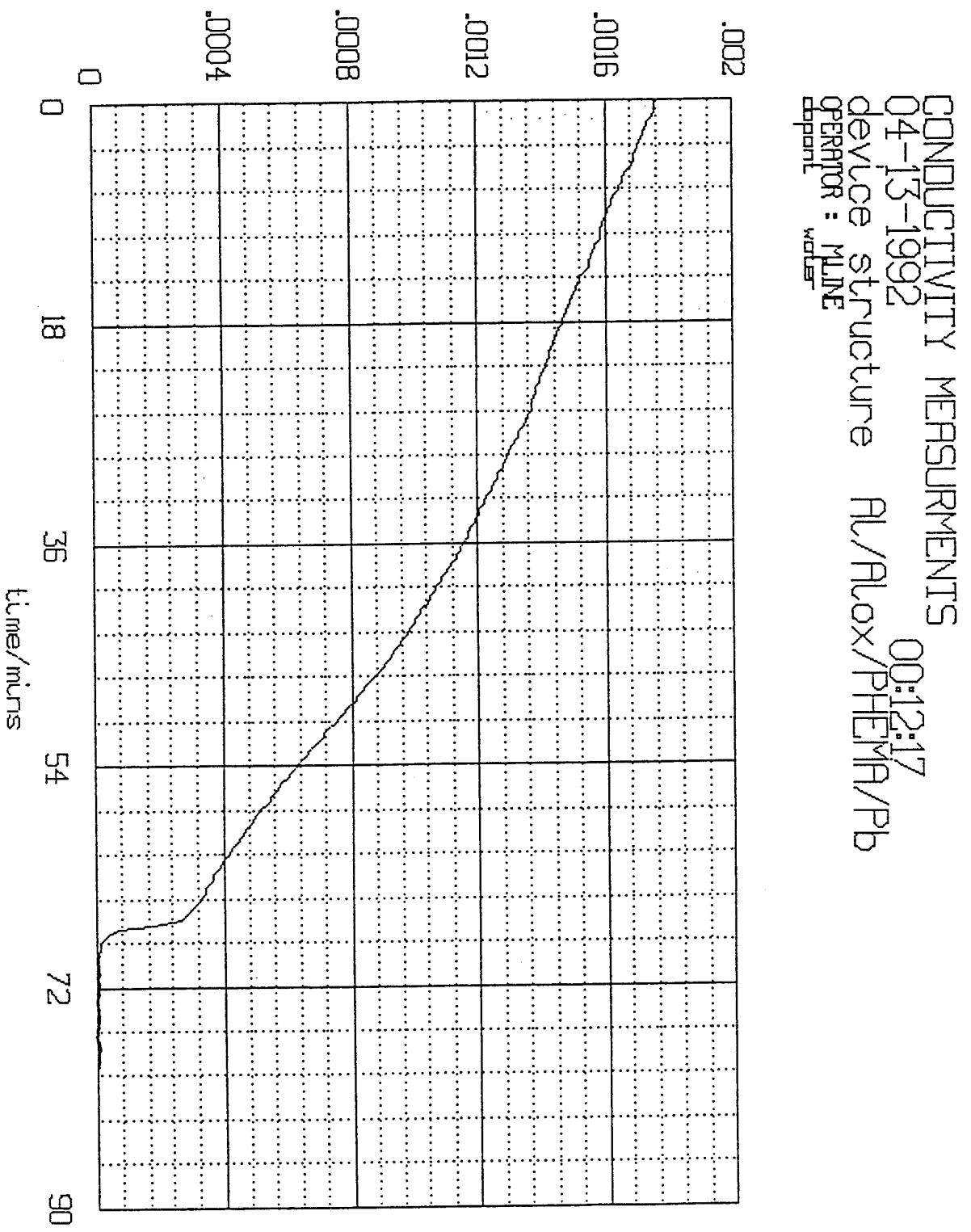
Conductance / Siemens
CONDUCTIVITY MEASURMENTS
04-13-1992 00:12:17
device structure Al/Alox/PHEMA/Pb
OPERATOR : MLINE
dopant water
0
.0004
.0008
.0012
.0016
.002
0
18
36
54
72
90
time/mins

Figure 7.7

Figure 7.7

The plot illustrated here is a representative sample of data taken during the infusion of water vapour into an aluminium - aluminium oxide - p-HEMA - lead IET junction. Comparison with figures 7.4 and 7.5 will highlight the inverted form of the graph. When the junction has been doped with the polymer, subsequent infusion of water results in an increasing gradient in the conductance versus time curve contrary to the decreasing gradient observed during the infusion of water into blank IET junctions.

Figure 7.7 is a representative graph of the data obtained from a series of experiments carried out by the present group on conductance changes in IET junctions doped with pHEMA during the infusion of water through the top lead electrode. A study of these graphs will show that the forms of graphs shown in figures 7.5 and figure 7.7 differs greatly. Graph 7.5 has a gradient which decreases as the infusion progresses - mimicking the results obtained by R. R. Mallik whereas the graph shown in figure 7.7 shows a trend which reveals itself as an increase, in a certain region, of the gradient of the graph as the infusion progresses, contrary to Mallik's results. Other regions of the graphs also show marked differences from Mallik's. These might be due to the way in which p-HEMA swells after the initial layers of water have adsorbed into the polymer. Other workers using bulk samples have shown that as hydrogels absorb water the shape of the volume versus time curve takes on a sigmoidal shape [12]. The latter parts of the conductance versus time graphs taken by the author may reflect this behaviour.

Mallik used his results to show that the water molecules infused through the top electrode of the junction to form an hydroxyl layer on the surface of the aluminium oxide coating the bottom electrode followed by a mono-layer of water. The subsequent mono-layers of water were then formed, one at a time, on top of each other. He produced an equation based on 7.2 above on which he modelled his results. Starting with the premise that the water molecules will infuse through the top electrode in that same way as suggested by Mallik gives a starting point for our interpretation of these results. Using the equation developed by Mallik - see equation 7.3 below - we will compare the conductance of the first layer, g_1 with that of the second layer g_2.

$$\frac{g_2(t)}{g_1(t)} = \frac{e^{-L\phi^{1/2}}(e^{-M\phi^{1/2}} - 1)}{(e^{-L\phi^{1/2}} - 1)} \qquad 7.3$$

Where L is the thickness of the first layer and M is the thickness of the second and subsequent layers of water molecule - which are assumed constant; $g_1(t)$ and $g_2(t)$ are the conductances of the first and subsequent layers respectively where each layer is assumed to be deposited in the same time (t). The thickness (M) of the second and subsequent layers is taken to be 2Å. The figure of 2Å is chosen to be the approximate diameter of a water molecule in line with the models proposed by Eisenberg and Kauzmann [29]. For the gradient of the graphs to increase the ratio $g_1(t) / g_2(t)$ must be greater than unity. Inserting values where L = M, L < M, and L > M respectively indicates that the thickness of the first layer is important in determining the slope.

Letting

Φ = 1eV, L = 2Å, M = 2Å

gives a ratio of conductances of **0.14**

Whereas letting

Φ = 1eV, L = 3Å, M = 2Å

gives a ratio of conductances of **0.045**

Lastly with

Φ = 1eV, L = 0.5Å, M = 2Å

gives a ratio of conductances of **1.46**

These few calculations show the critical dependence of the magnitude of the ratio of successive gradients of the conductance versus time graphs upon the

thickness of the first layer deposited. The part of the graph considered in this analysis covers the time period from zero to approximately one hour. Reducing the value of the thickness of the first layer to around 0.42Å produces a ratio of 1.76. which approximates to experimentally obtained ratio of successive gradients in the aforementioned section of graph - see Figure 7.6. This thickness of 0.42Å is half the expected layer thickness of 1Å for an hydroxyl layer and around 1/5 of the approximate 2 Å thickness of a layer of water molecules as assumed above.

The first layer of water adsorbed onto p-HEMA is hydrogen bonded to the hydroxyl groups and there would also be some bonding carboxyl groups and to oxygen. This first layer would be under the influence of the oxygen and hydroxyl groups and this influence leads to a tightly bound initial layer. The influence diminishes with distance from the polymer surface and so the water would be less tightly bound as we move in space from the polymer surface into the body of the material. Each of the layers could be considered to be 'thicker' than the previous one until at a large distance from the polymer surface the influence would tend to zero and the structure of the water would correspond to bulk water.

7.10 Conclusions from Conductance Data

The equipment designed and built by the author enables IETS junctions to be infusion doped with water (although other liquids could be used) routinely and simply with a minimal risk of contamination. The provision of input and output taps allows the purging of the chamber with an inert gas such as dry nitrogen.

Flushing the chamber with an inert gas minimises formic acid contamination by excluding atmospheric carbon dioxide.

Automatic collection and monitoring of the conductance data is achieved in situ by means of a Keithly digital multimeter which is interfaced to a computer. The program running the system is listed at the back of the thesis in an appendix. The changes in the conductance of a junction approximately follow changes in the thickness of the insulating barrier and therefore inferences appertaining to the mechanisms by which water is adsorbed into the polymer can be made via the changes in the junctions conductance. The data collected intimate that when water is incorporated within a hydrogel it has some limited structure. There is some evidence to suggest that the first layer of water adsorbed into the polymer is significantly thinner than subsequent layers.

A simple model of sequential monolayer growth is proposed and used with success to suggest the thickness of each of the monolayers as they are adsorbed into pHEMA. The model, using reasonable assumptions, can be made to predict which are in fairly good agreement with the experimental data .

The present group's experiments where IETS junctions were used to investigate the way in which water is incorporated into a hydrogel are the first of their kind. The swelling of these important polymers has been studied before by other groups but in all of those other studies data have been collected using bulk samples whereas this work has investigated the effect water has on a monolayer of the polymer. The preliminary results show evidence for suggesting that the water once adsorbed within the polymer has a limited structure imposed upon it by its proximity to the polymer with the initial monolayer of water being

thinner than the subsequent monolayers. It is suggested that the initial layer of water absorbed to the p-HEMA is hydrogen bonded to the hydroxyl groups and there would be some bonding carboxyl and to oxygen.

Thus in the initial layer, the influence of the oxygen and / or hydroxyl groups in the polymer leads to a tightly bound initial layer. As the influence of the polymer diminishes through an increase of distance from its surface so the thickness of the subsequent layers would increase. This supports a consensus of opinion that water within polymers has a structured or layered form close to the polymer surface [23-26,31].

The shape of the graphs also suggest that after the first few layers of water have been adsorbed the shape of the curve deviates from the simple model proposed by the author. Although the swelling behaviour of the gel after the initial layers has not been investigated by this group an initial inspection of the data suggest that it follows a sigmoidal shape seen by others in work done on bulk samples [12].

7.11 An IETS Study of the Monomer and Polymer of 2-hydroxyethyl methacrylate

Inelastic electron tunnelling spectroscopy in conjunction with other spectrographic techniques is a powerful tool for studying the nature of the interface between polymers and the surface of metals and oxides [19-32].

Although it is impossible to resolve all of the vibrational modes of molecules having more than a hundred atoms or so using IETS [33], it is believed that IET spectra reflect the nature of the adsorption due to interactions

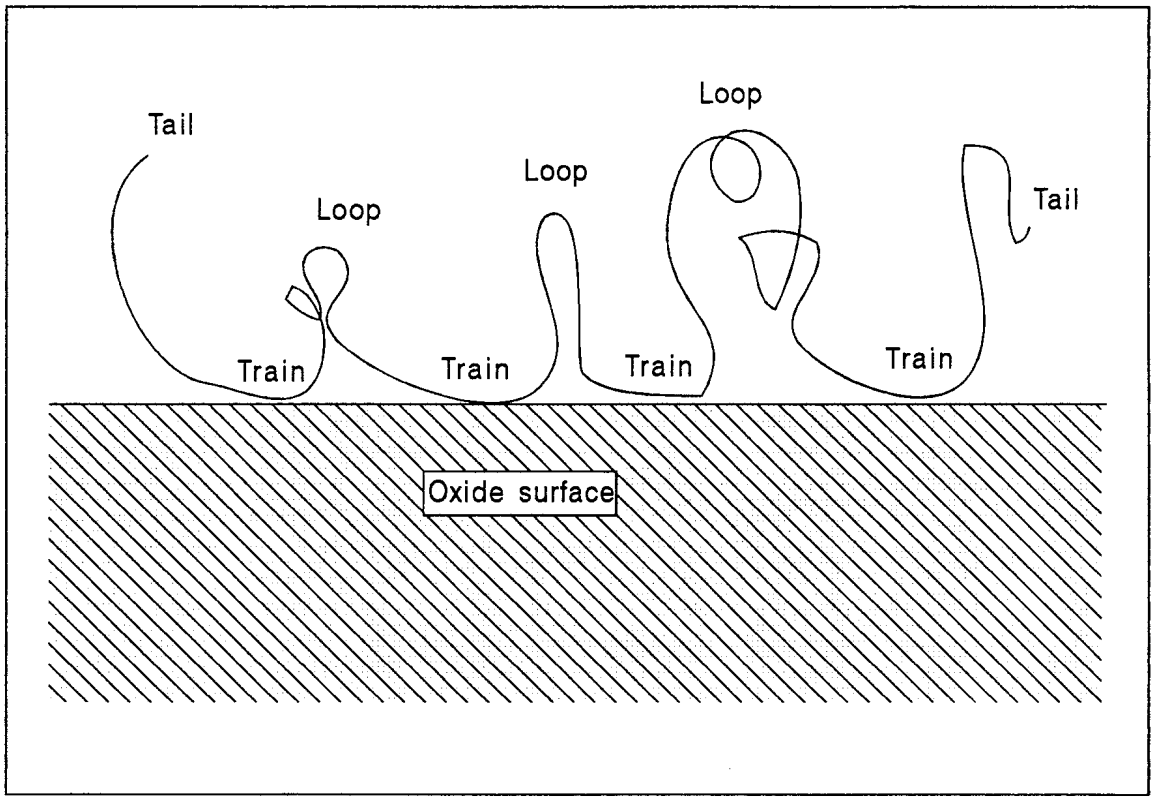
Tail
Loop
Loop
Loop
Tail
Train
Train
Train
Train
Oxide surface

Figure 7.8.

Figure 7.8

Illustrated in this figure is a representation of the spaghetti tail - loop - train type of adsorption of high molecular weight polymers onto surfaces as proposed by Lal and Stepto [39].

between reactive segments of the polymer and adsorption sites on the surface of the metal forming the bottom electrode of the junction [34].

Using the instrument and procedures developed in this department [35-38] an investigation into the adhesion of 2-hydroxyethyl methacrylate (HEMA) and poly 2-hydroxyethyl methacrylate (p-HEMA) adsorbed on aluminium oxide was conducted. As is the usual practice infrared spectra of bulk samples of the monomer and polymer were also taken to provide a comparison of peak positions. Calculations by Lal and Stepto [39] which describe the conformational nature of polymer adsorption took into account factors such as chain structure, polymer - surface, and polymer - solvent interactions. It was proposed that polymers were adsorbed in a tail - train - loop - tail configuration; rather like a pile of spaghetti tossed onto a plate see - figure 7.8. Adsorption of the material takes place along the 'train' segments and potential adsorption sites on the surface of the oxide.

7.12 Experimental

The tunnel junctions used in this set of experiments were exclusively of the type Al - AlOx -Dopant polymer - Pb, the layer of aluminium oxide was produced thermally in air at room temperature. Comprehensive descriptions of junction fabrication, quality assessment, and general manufacturing protocols are given in Chapter 3 of this thesis.

Infra-red spectra - see Figures 7.9a and 7.9b - were obtained using a Nicolet spectrometer. All the solvents used in the preparation of the IETS samples were either Spectrograde or Analar quality. In order to ascertain whether

DATE _____
SPECTRUM NO. _____
SAMPLE _____

ANALYST _____
PATH _____
SOLVENT _____
CONCENTRATION _____

Figure 7.9a

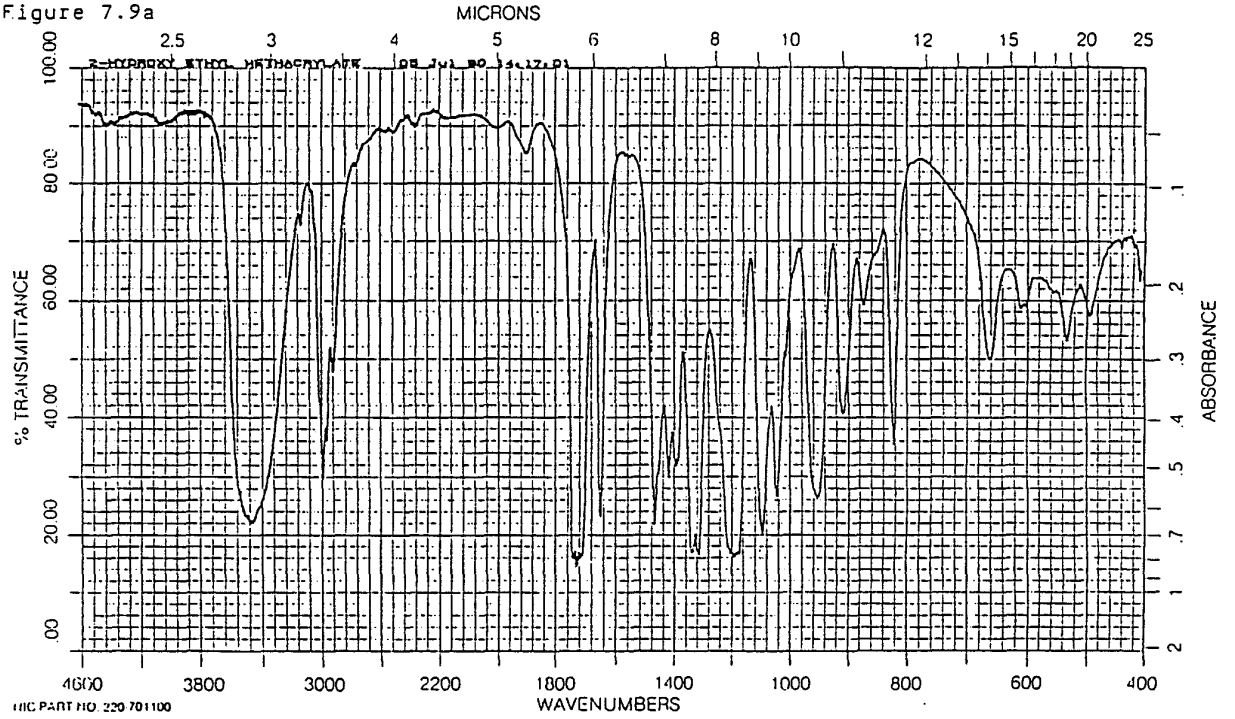

Figure 7.9b

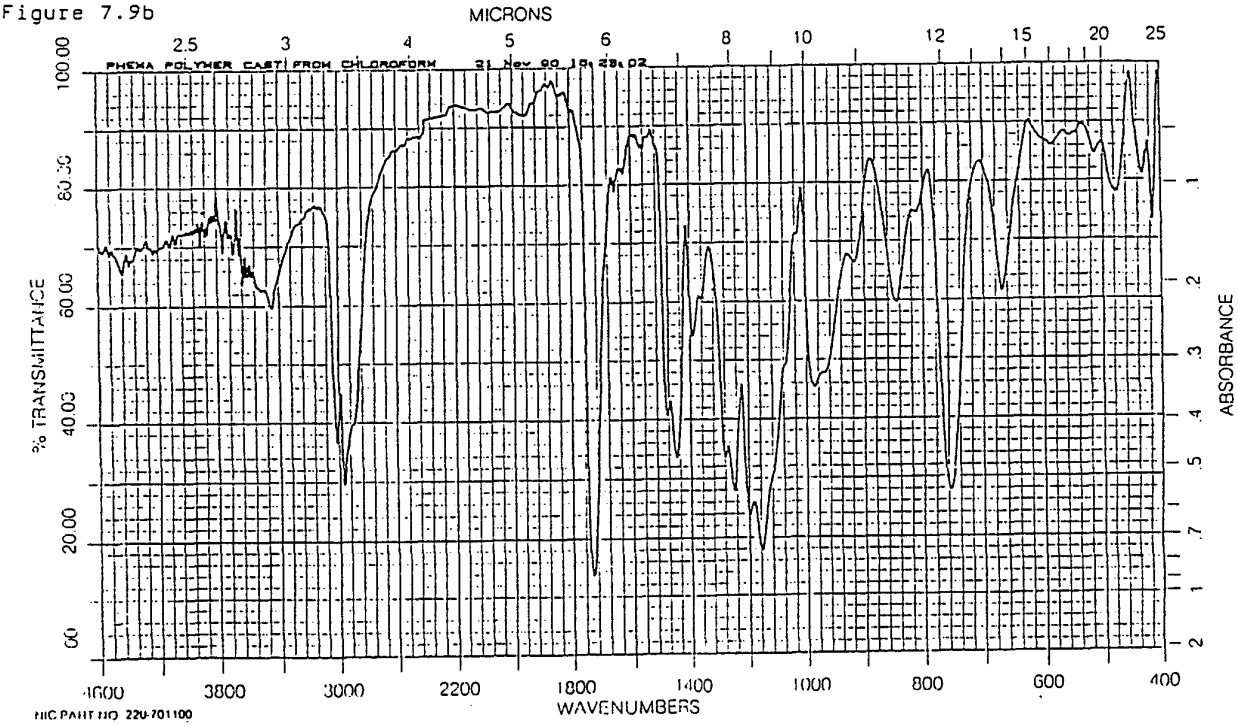

Figure 7.9 a

Infrared spectrum taken from a sample of 2-hydroxyethyl methacrylate. Note the strong peak at 205.85 mV (1655 cm^{-1}) which is assigned to the stretch mode of C = C , indicating an unpolymerised sample.

Figure 7.9 b

In this infrared spectrum of poly 2-hydroxylethyl methacrylate where the feature at 205 mV has been reduced down to a very small peak indicating that the sample of p-HEMA has been polymerised.

any solvent or solvent born contaminants remained adsorbed after liquid-phase doping of the junction the usual practice of testing several 'blank' junctions was followed. All these junctions had a low do resistance and the IET spectra produced were consistent with a clean oxide surface.

7.13 Results and Discussion

Both the monomer and the polymer produced strong, reproducible, IET spectra. Once the spectra had been obtained - see figures 7.10 and 7.11, the peak positions were taken from the plots using 'Digit' which is a digitizing routine developed by Dr. S. Reynolds [32] - see Tables 7.1 & 7.2.

7.14 Comparison and Interpretation of IET Spectra.

An initial comparison of the IET spectrum taken from the monomer and that taken from the polymer shows that they have a number differences the main ones occurring at around 200 - 250 mV and 60 - 100 mV.

The main features and differences will be dealt with starting from the high frequency end of the spectra. Both spectra exhibit features around 450 to 500 mV which correspond to the stretch modes of surface OH. The monomer shows a peak at 378 mV which is assigned to = CH_2 stretch and there is a very noisy feature around 370 mV in the polymer spectrum. Both spectra shown strong peaks around 360 mV which are due to CH_2 / CH_3 vibrational modes. The peak in the monomer at 211 mV is assigned to the stretching mode of C = O.

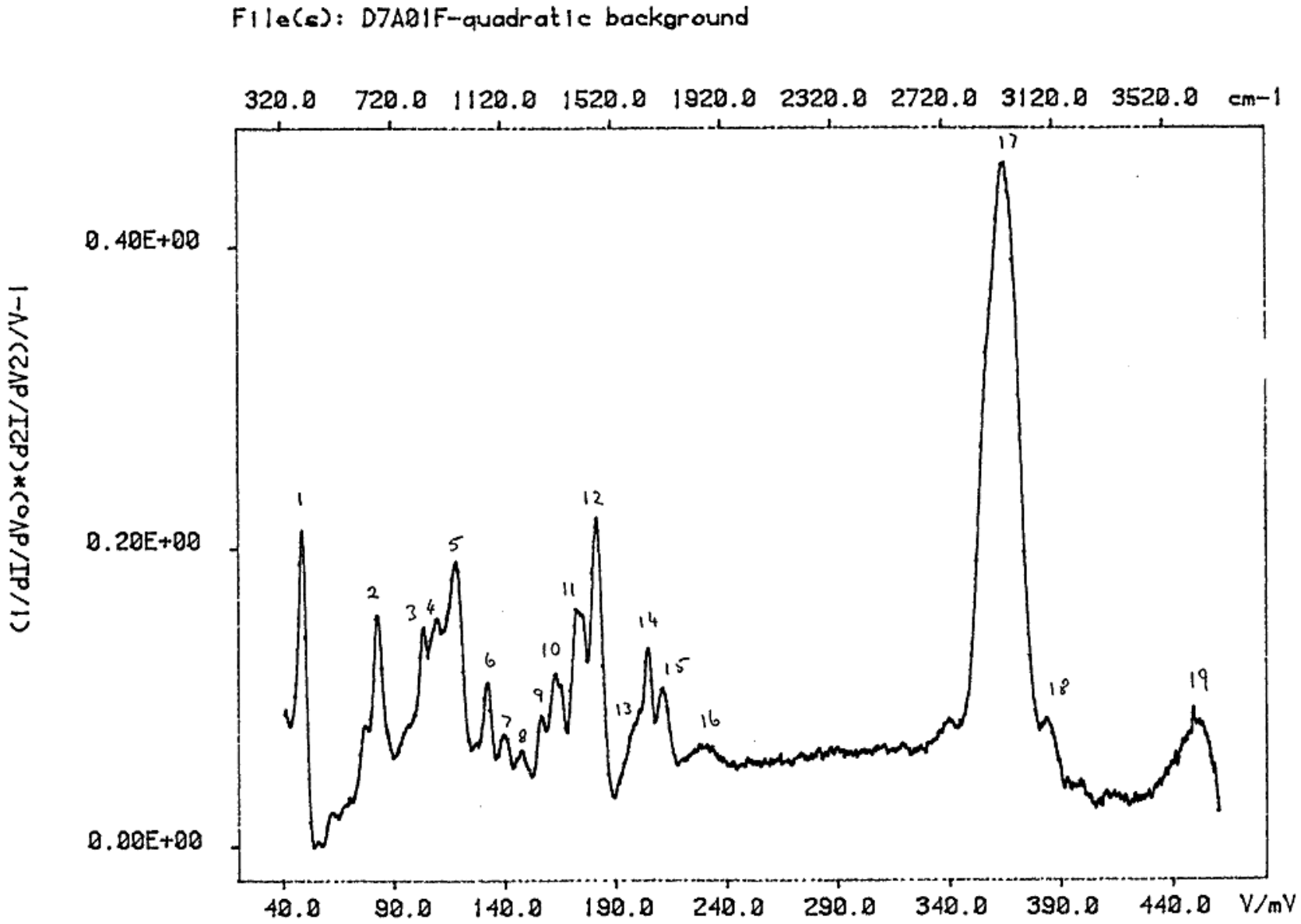
File(s): D7A01F-quadratic background
320.0 720.0 1120.0 1520.0 1920.0 2320.0 2720.0 3120.0 3520.0 cm-1
0.40E+00
0.20E+00
0.00E+00
(1/dI/dVo)*(d2I/dV2)/V-1
1
2
3
4
5
6
7
8
9
10
11
12
13
14
15
16
17
18
19
40.0 90.0 140.0 190.0 240.0 290.0 340.0 390.0 440.0 V/mV

Figure 7.10

Reproduced in this figure is a representative sample of one of the first IET spectrum taken from a junction doped with a sample of the monomer 2hydroxyethyl methacrylate.

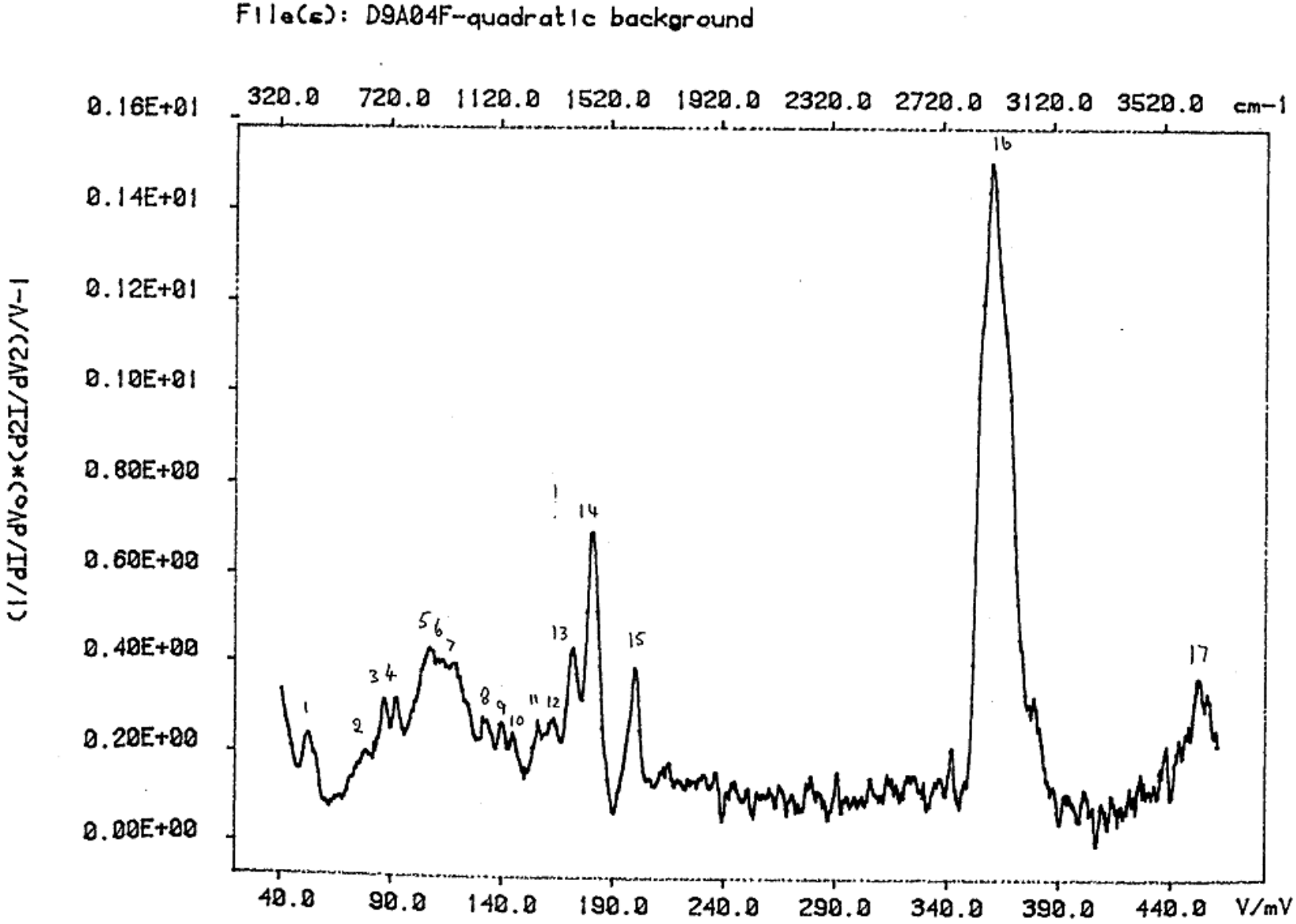
File(s): D9A04F-quadratic background
0.16E+01
0.14E+01
0.12E+01
0.10E+01
0.80E+00
0.60E+00
0.40E+00
0.20E+00
0.00E+00
(1/dI/dVo)*(d2I/dV2)/V-1
320.0
720.0
1120.0
1520.0
1920.0
2320.0
2720.0
3120.0
3520.0
cm-1
40.0
90.0
140.0
190.0
240.0
290.0
340.0
390.0
440.0
V/mV
1
2
3
4
5
6
7
8
9
10
11
12
13
14
15
16
17

Figure 7.11

This illustration is of the spectrum taken from an IETS junction doped with the hydrogel poly 2-hydroxylethyl methacrylate. It is a representative sample of the spectra taken by the author in this first series of experiments using IETS to examine the adsorption of p-HEMA onto aluminium oxide.

A comparison with the region around 211 mV in the spectrum taken from the polymer reveals that the peak assigned to the C = O stretch has disappeared to be been replaced by two peaks at 178.29 mV and 198.33 mV. Peaks in IETS spectra at these positions are assigned to the symmetric and the antisymmetric stretching modes of the carboxylate anion COO^- respectively. Hall and Hansma [40] proposed that carboxylic acids dissociate on the surface of the aluminium oxide after which they are chemisorbed by the formation of a bidentate bridging complex between the ion in the aluminium oxide surface and the carboxylate anions. These peaks present strong evidence that the R_2 end group of the polymer must has been cleaved from the rest of the molecule leaving the carboxylate anion be adsorbed onto the aluminium oxide surface as a resonance stabilised bi-dentate bridging arrangement.

There is a weak shoulder at 201.4 mV in the spectrum of the monomer which is assigned to a C=C stretch mode. It was expected that there would be a strong feature in the spectrum at around 200 mV to indicate an unpolymerised sample. The infrared spectrum of the monomer shows a strong peak at 205 mV which indicates the presence of the double bond in the monomer see figure 7.10a and 7.10b.

It is inferred from the weak peak in the IETS data that the dipole moment of the C = C is not orientated near to perpendicular with the oxide surface see explanation in Chapter 2 of this thesis.

Both the monomer and the polymer show similar peaks in the region around 170 mV to 147 mV, these features as assigned to mixed CH and COH vibrations. Skeletal deformations of the polymer backbone is indicated by the

Peak No	Peak Positions mV	Peak Positions cm^{-1}	Assignment
1	49.96	399.68	
2	80.72	648.99	OH bend hydrogen bonding
3	85.84	686.72	
4	115.31	927.09	Al-O phonon
5	125.62	1,009.98	OH bend
6	131.2	1,054.85	CH_3 rock
7	139.66	1,122.87	C - C stretch
8	147.34	1,184.61	Mixed
9	156.31	1,256.73	CH_2
10	166.56	1,339.14	and
11	171.69	1,380.39	COH Vibrations
12	181.94	1,462.80	CH_3 deformation
13	201.4	1,619.26	very weak shoulder C=C
14	211.03	1,696.68	C = O stretch
15	222.94	1,792.44	
16	233.44	1,876.86	Al-O 2x overtones
17	369.17	2,968.13	CH_2 / CH_3 stretch modes
18	378.25	3,041.13	$=CH_2$ stretch
19	479.19	3,852.69	OH surface

Table 7.1

2 - hydroxyethyle methacrylate (HEMA)

Table 7.1

Listed in table 1 are the peak positions and assignments for the data taken from a representative IETS graph of the monomer HEMA. All peak positions are in mV and have been adjusted for the superconducting energy gap of lead.

Peak No	*Peak Positions mV*	*Peak Positions cm^{-1}*	Assignments
1	53.09	426.84	
2	78.09	627.84	COO^- out of plane rock
3	87.62	704.46	OH lattice water
4	92.85	746.51	
5	107.85	867.11	C - C stretch
6	112.62	905.46	CH_3 rock
7	119.28	959.01	
8	132.86	1,068.19	
9	140.00	1,125.60	
10	144.76	1,163.87	Skeletal C-C-O / C-O stretch
11	155.48	1,250.06	CH_3 deformation
12	162.62	1,307.46	CH_3 sym deformation
13	170.95	1,374.44	CH_3 asym deformation
14	178.29	1,433.45	COO^- asymmetrical stretch
15	198.33	1,594.57	COO^- symmetrical stretch
16	359.05	2,886.76	CH_2 / CH_3 stretch modes
17	451.9	3,633.28	OH stretch

Figure 7.2

Poly 2- hydroxyethyl methacrylate (p-HEMA)

Table 7.2

Listed in table 7.2 are the peak positions and assignments for the data taken from a representative IETS graph of the monomer HEMA. All peak positions are in mV and have been adjusted for the superconducting energy gap of lead.

peak at 144.76 mV in the polymer spectrum. C - C stretch modes are evident in both of the spectra at 140 mV. The peak at 125 mV in the spectrum of the monomer which does not appear in the polymer spectrum is assigned to an OH bend. Two features corresponding to CH, rock appear in both spectra at around 115 mV. There is a peak at 107.85 mV in the polymer spectrum which is assigned to a C-C stretch mode. At 80.72 mV in the spectrum of the monomer a peak appears which has been assigned to OH bend. There is a peak located at a similar position (78.09 mV) in the polymer spectrum together with another at 53.09mV. These two peaks are thought to reflect either COO^- in plane and out of plane rock respectively or possibly librational modes of lattice water within the polymer. Librational modes are due to the rotational motions of water molecules restricted by the lattice of the polymer [43].

Hydrogels entrap water and the water is incorporated as lattice or coordinated water. Water trapped within organic salts also is incorporated as lattice or coordinated water and work by Fugita et al [41] and Gamo [42] highlighted a number of low frequency modes at around 75 to 95 mV which were assigned to the wagging, rocking, and twisting modes of water coordinated to a metal ion. The polymer spectrum shown above also features an extra peaks at 87.62 and 92.85 mV it is proposed that these peaks are due to vibrational modes of coordinated water within the hydrogel.

7.15 Conclusion from IETS Data

It is concluded that the polymer sample (p-HEMA) has the ester group labelled R_Z in Figure 7.1 above cleaved by a reaction when it is adsorbed onto the aluminium oxide surface of the bottom IETS junction electrode. It is proposed

that the polymer is adsorbed onto the aluminium oxide via a resonance stabilised bidentate bridging complex formed by the carboxylate anion COO^- and the surface. There is also some evidence of coordinated water entrapped within the polymer - in line with the result obtained from the conductivity data given above.

The monomer shows little evidence of C = C modes in the spectrum and it is proposed that the monomer is adsorbed onto the aluminium oxide surface via mainly hydrogen bonding of hydroxyl and carboxyl groups, and with some bonding to oxygen. The lack of a strong C = C peak can be explained by assuming that the dipole moment of the C = C is oriented approximately parallel to the oxide surface thereby reducing the intensity if its peak in IETS. It is suggested that the apparent confliction arising from the fact that the R_2 group is cleaved in the polymer and not in the monomer might be explained by conformational restrictions imposed by the rigidity of the monomer molecule.

References

1] Kiraly R J and Nose Y 1974 *Biomat. Med. Dev.* **2** 207
[2] Bruck S D 1973 *Biomed. Mat. Res.* ***7*** 387
[3] Wichterle O and Lim D 1960 *Nature* ***185*** 117
[4] Refijo M F and Yasuda H 1960 *J. App/. Polymer Sci.****9*** 2425
[5] Wichterle O and Chromecek R 1969 *J. Plymer Sci.* Part C **16** 4677
[6] Frank H S and Wen W Y 1957 *Discuss. Faraday Soc.* **24** 133
[7] John M S Andrade J D 1973 *J.Biomed. Matter Res.* ***7*** 509
[8] Sunhee C Mu Shik Jhon and Andrade J D 1977 *J. Colloid and Interface Sci.* **61 (1)** 1.
[9] Eui Hwan Kim et.al. 1983 *Bulletin of Korean Chem. Soc.* **4 (6)** 251.
[10] Hazelwood C F Nichols B L 1969 *Nature* **222** 747.
[11] Hai Bang Lee Mu Shik Jhon and Andrade J D 1974 *J.Colloid and interface Sci.* ***51 (2)*** 225.
[12] *Hydrogels for Medical and related Applications* J.D.Andrade Editor ACS Syposium Series Washington D.C. 1976.
[13] Koreeda et. al. 1973 *J.Amer. Chem. Soc.* ***95*** 239.
[141 Ryback G 1972 JCS *Chem. Comm.* 1190.
[15] Ling G N 1969 Department of Molecular Biology - Pensilvania Hospital 1.
[16] Rafter B D and Miller I F 1972 *J. Polymer Sci.* Part A-1 **10** 2425
[17] Refojo M J 1967 *J. Polymer Sci.* Part A-1 ***5*** 3103
[18] Janacek J 1973 *J. Macromol. Sci.* ***C9*** 415
[19] Mallik R R 1985 *PhD Thesis Leicester Polytechnic.*
[20] Jaklevic R C and Gaerttner M R 1977 *Appl. Phys. Lett.* ***30*** **(12)** 646.
[21] Jaklevic R C and Gaerttner M R 1978 *Applications Surf.* Sci. **l** 479.
[22] Nelson W J, Walmsley D G and Bell J M 1981 *Thin Solid Films* ***79*** 229.
[23] Hai Bang Lee, Mu Shik Jhon and Andrade J D 1974 *J. Coll. and Interface Sci.* ***55 (2)*** 225
[24] Sunhee Choi and Mu Shik Jhon 1977 *J. Coll. and Interface Sci.* **61 (1)** 1
[25] Hazelwood C F and Nichols B L 1969 *Nature* **222** 747
[26] Eul Hwan Kim et al 1983 *Bull. of Korean Chem. Soc.* **4 (6)** 251
[27] Brinkman W F, Dynes R C and Rowell J M 1970 *J. Appl. Phys.* **41 (5)** 1915. [28] *Tunnelling Phenomena in Solids* E.Burnstein and SLundgvist (Editors) (Plenum Press N.Y.) 1969.
[29] *Tunnelling Spectroscopy, Capabilities, Applications, and New Techniques P* K Hansma (Editor) ((Plenum Press N.Y.) 1982.
[30] D.Eisenberg and W. Kauzmann 1969 *The Structure and Properties of Water* Clarendon Press Oxford. 1969.
[31] *Personal communication* Dr. Phil Corkhill, Dept of Chemistry Aston University.
[32] Reynolds S 1983 *PhD Thesis Leicester Polytechnic.*
[33] Walmsley D G and Nelson W J *Tunnelling Spectroscopy, Capabilities Applications and New Techniques* Ed. P K Hansma (Plenum Press NY) 1982 311
[34] Lal M and Stepto R F T 1977 *J. Polym. Symp.* **61** 401
[35] Langley A J 1982 *PhD Thesis* Leicester Polytechnic.

[36] Ginnai T M 1982 *PhD Thesis* Leicester Polytechnic.
[37] Tunnicliffe D L 1983 *PhD Thesis* Leicester Polytechnic.
[38] Oxley D P et.al. 1980 *Surf. Interface Anal* ***2*** 31
[39] Kirtly J Scalapino D J and Hansma P K 1976 *Phys. Rev.* ***B14*** 3177
[40] Hall J T and Hansma P K 1978 *Surf. Sci.* ***71(14)*** 1537
[41] Fugita J, Nakatnoto K and Kobayashi M 1956 J. *Am. Chem. Soc.* ***78*** *3963*
[42] Gamo J 1961 Bull. *Chem. Soc. Japan* ***34*** 760, 1430
[43] *Infrared Spectra of Inorganic and Coordinated Compounds* Nakamoto N 1963 p156

Contents

CHAPTER 8

A STUDY OF ZINC CHLORIDE IN POLY(ETHYLENE GLYCOL) BY INELASTIC ELECTRON TUNNELLING SPECTROSCOPY (IETS)

8.0 Introduction

In this chapter inelastic electron tunnelling spectroscopy (IETS) [1-3] has been used for the first time to compare the behaviour of poly (ethylene glycol) with poly (ethylene glycol) containing zinc chloride adsorbed onto an aluminium oxide surface.

Poly (ethylene glycol) is a low molecular weight analogue of poly (ethylene oxide) the common parent polymer used in polymeric electrolytes, see Figures 8.1a and 8.1b. An understanding of the mechanisms by which these materials adhere to a surface can provide a valuable insight into the electrode/electrolyte processes which take place in thin film devices incorporating ionic polymers.

A wide range of organic materials and polymers adsorbed on aluminium oxide [4-6] have been studied previously in this department and this work has provided a valuable insight into the detailed mechanisms at a molecular level of the adhesive and other properties of ultra-thin layers. Materials ranging from simple molecules to complex polymers have been studied [4-6]. IETS has also been used to investigate the incorporation of synthetic polymers into IET junctions [7,8]. These previous worker have shown that IETS, used in conjunction with other spectroscopic techniques, is a powerful tool for investigating the adsorption mechanisms of both small and large molecular weight molecules onto aluminum oxide.

Schematics of Poly (ethylene oxide)

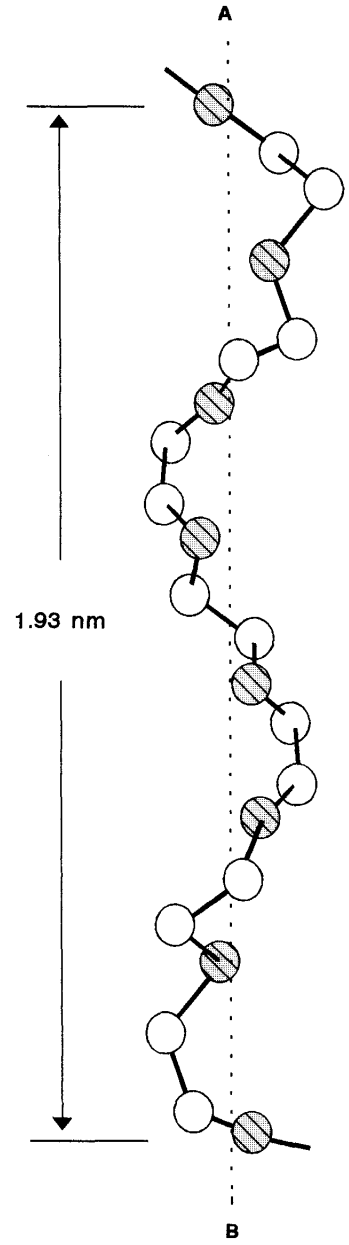

Figure 1a.

Shows the spatial structure of poly (ethylene oxide)

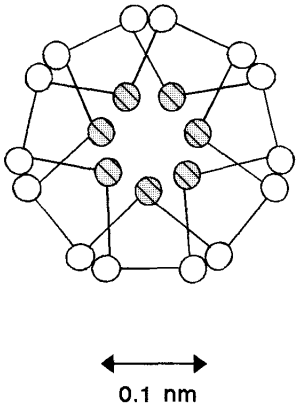

Figure 1b.

Poly (ethylene oxide) looking along the axis AB, as indicated in diagram 1a, illustrating the arrangement of the oxygen atoms along the axis of the spiral.

= CH_2

= O

Figures 1 a and 1 b are schematic drawings of poly (ethylene oxide) showing the spatial arrangement of the molecule. Not to scale)

Therefore when an insight into the adhesion of PEG onto a surface was required. The features listed previously suggested that IETS would be a suitable ideal technique to be used in the investigation. For although the spectra obtained from IETS do not necessarily reflect the behaviour of the polymer as a whole - Walmsley and Nelson showed that it is impossible to resolve the vibrational modes of molecules with more than a hundred or so atoms [9]. The data may be extrapolated to enable some adsorption mechanisms to be proposed as possible explanations for the way in which the polymers are attached to the surface. One view is that the polymer is adsorbed via interaction between specific segments of the polymer and active sites on the surface of the oxide [10] - steric hinderance may have a role to play in the way these interactions take place. Another view put forward is that the polymer lies on the surface like a pile of spaghetti which has been randomly thrown there and is adsorbed in a tail - loop - tail manner [10] - see Figure 8.2. Which allows Adsorption to take place through interactions between the tail segments and adsorption sites on the oxide surface. Therefore IETS can provide vibrational spectra of polymeric materials from which the adsorption mechanisms of ultra thin layers of polymers can be inferred.

The IET spectra presented in this chapter are believed to reflect the way in which the two polymers are adsorbed onto the surface of the aluminium oxide. This study extends the range of materials investigated by Inelastic Electron Tunnelling Spectroscopy to include an analogue of an important polymeric electrolyte materials.

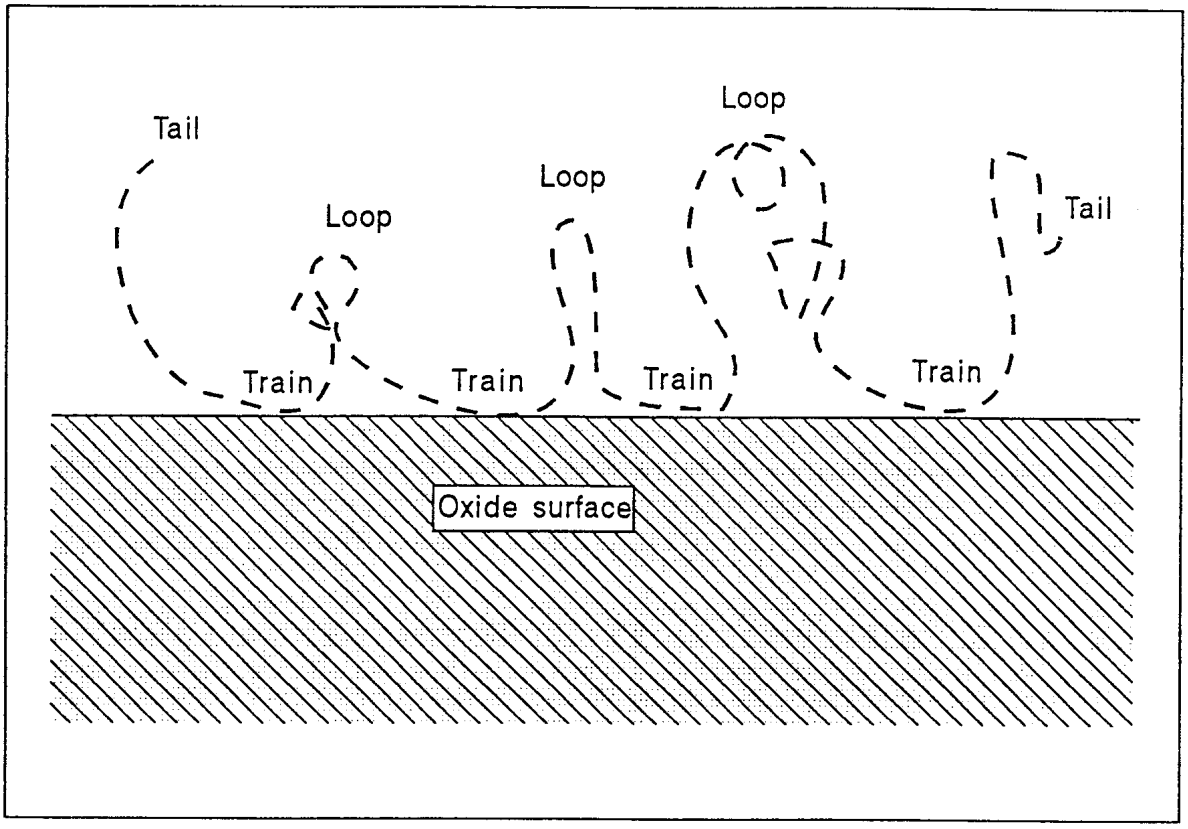

Figure 8.2.
An illustration of a proposed mechanism for the adsorption of a polymer onto the surface of the bottom electrode of a tunnel junction - after Lai and Stepto. the adsorption takes place through interactions between the train segments which are in intimate contact with the surface and active sites on the surface of the aluminium oxide.

8.1 Experimental Details

The preparation of the junctions used in this work followed well proven methods developed by workers in this university over a number of years [5] Unwanted effects on peak positions and widths were avoided by use of bottom electrodes of thickness of at least 300 nm in line with previous work [11]. These methods ensure that in each of the batches of junctions produced there is a high proportion which are suitable for IETS.

The samples used were based on poly(ethylene glycol) of relative molar mass 400 in this form the polymer being a liquid. The solutions were produced by mixing 25g of anhydrous zinc chloride (BDH analar grade) with 100 cm^3 of the poly (ethylene glycol). The resulting mixture was then stirred for twenty four hours at room temperature. For IETS the solutions of both the PEG_{400} and PEG_{400} / $ZnCl_2$ were diluted in the ratio of 1 part of PEG_{400} to 50 parts of ethanol (spectroscopy grade). This dilution was necessary in order to effect liquid phase doping of the oxidised aluminium forming the bottom electrode of the junction, producing junctions with d.c. resistances of the order of fifty to three hundred ohms, an ideal range for IETS.

After evaporating the top lead electrode each junction was assessed using a standardised procedure developed in this laboratory. Suitable junctions were then immersed in liquid helium prior to scanning by the spectrometer.

PEG_{400} (mV)	PEG_{400} : $ZnCl_2$ (mV)	Peak Assignment
	37.03	Al oxide phonon
	52.19	
68.35	68.44	Skeletal Twist
79.83	80.16	Skeletal Twist
	89.38	
102.90	100.80	
113.50	111.60	
133.10	131.90	
141.20	140.50	C-O Stretch
155.10	155.00	C-H_2 Wag
171.80	172.40	C-H Bend
180.00	179.50	C-H Bend
196.40	196.40	
212.30		
233.40		
270.40		
338.20	341.70	C-H Stretch
354.20	358.30	C-H Stretch
	439.80	O-H stretch

Table 8.1

Results and IETS peak assignments for poly (ethylene glycol) uncoordinated and coordinated with zinc chloride

8.2 Instrumentation

The design, development, and resolving power of the IET spectrometer used in this work [12-15] has been described in detail elsewhere in this thesis.

8.3 Comparison of IET Spectra

Figures 8.3 and 8.4 are examples of the reproducible IET spectra obtained from junction doped with PEG_{400} (sample 1) and a solution of zinc chloride in PEG_{400} (sample 2). The two spectra show a marked difference at around 450 mV. This feature which corresponds to an excitation of an OH stretch mode [16] is prominent in the spectrum of zinc coordinated samples but is absent in the spectra of the uncoordinated samples. There is also some difference to be seen in the two spectra in the range 180 mV to 250 mV. The remaining peaks are the same, within the experimental error of the work. - Table 1 lists the peak positions of the two spectra.

8.4 The Adsorption of PEG on Alumina

Koubek *et al* [17] in work carried out on the adsorption of aliphatic amines on alumina suggested that very strong adsorption occurs on aluminum ions in the surface via coordinated nitrogen - aluminium bonds. Chemically there are some similarities between amine and hydroxyl end groups. It is therefore proposed here that when the PEG is incorporated in a tunnel junction it adheres to the oxide surface

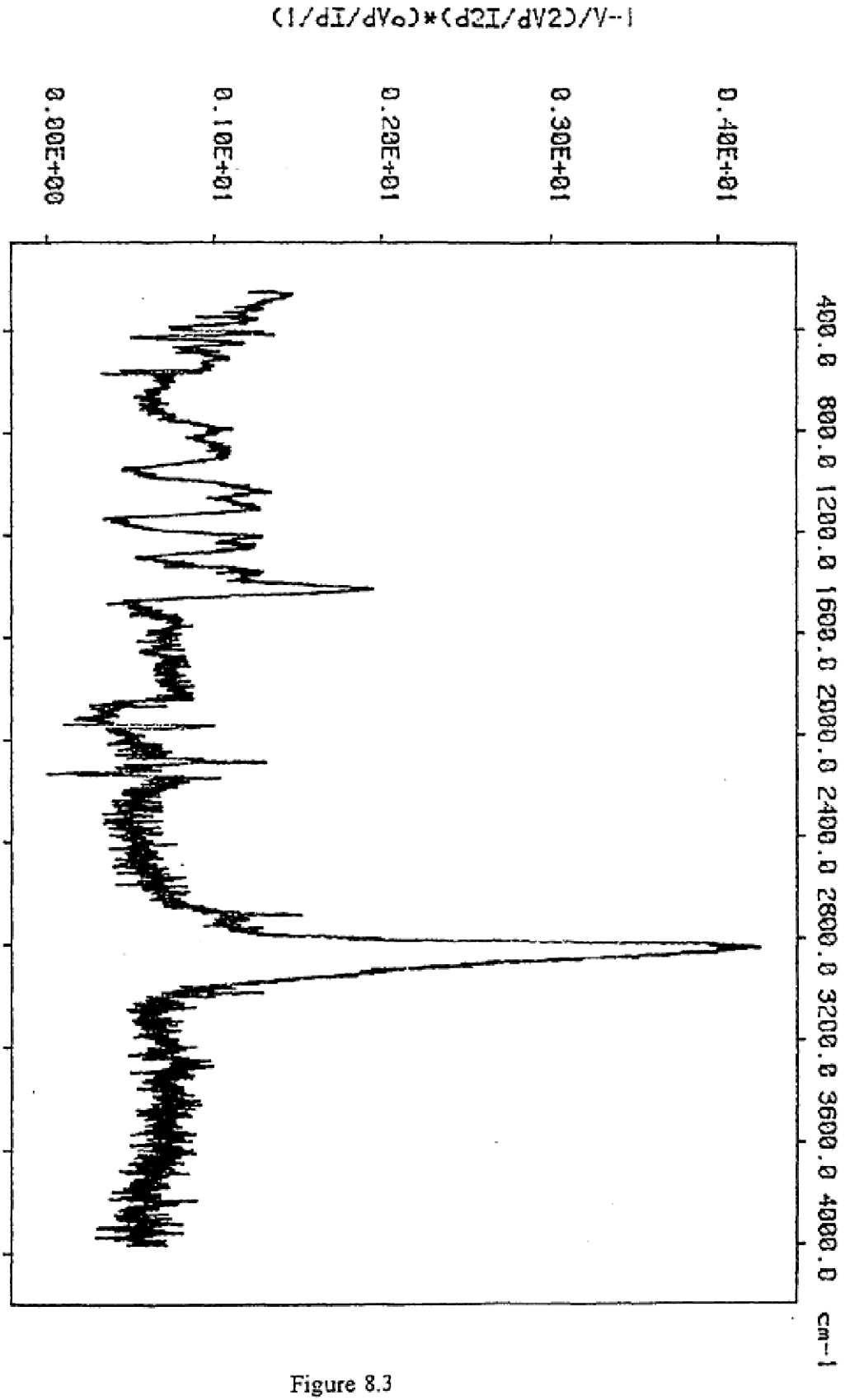
PEG 400
(1/dI/dVo)*(d2I/dV2)/V-1
0.40E+01
0.30E+01
0.20E+01
0.10E+01
0.00E+00
400.0 800.0 1200.0 1600.0 2000.0 2400.0 2800.0 3200.0 3600.0 4000.0 cm-1
50.0 100.0 150.0 200.0 250.0 300.0 350.0 400.0 450.0 500.0 V/mV

Figure 8.3

Figure 8.3.

Shown in this figure is a representative sample of a spectrum taken from a junction which was liquid phase doped with PEG_{400} .

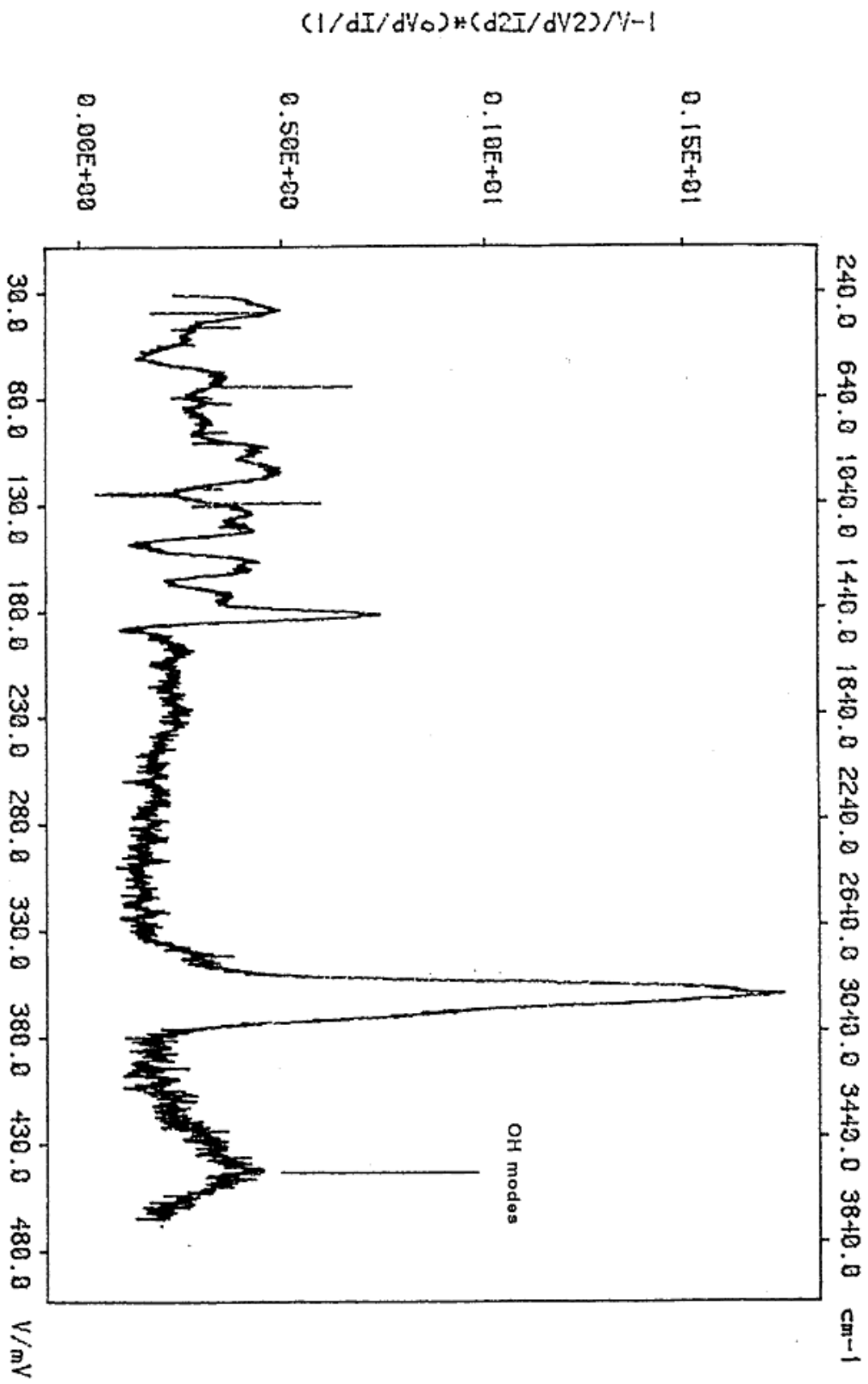
(1/dI/dV)*(d2I/dV2)/V-1
0.15E+01
0.10E+01
0.50E+00
0.00E+00
240.0 640.0 1040.0 1440.0 1840.0 2240.0 2640.0 3040.0 3440.0 3840.0 cm-1
30.0 80.0 130.0 180.0 230.0 280.0 330.0 380.0 430.0 480.0 V/mV
OH modes
PEG 400 : ZnCl2

Figure 8.4

Figure 8.4

An illustration of the IET spectrum obtained from junction doped with samples of PEG coordinated with zinc chloride. An extra peak correspondingn to an OH mode is clearly seen at around 450 mV.

via coordinate oxygen - aluminium bonds as shown in figure 8.5. Oxygens in the polymer donate two electrons to form a bond with an aluminum ion in the surface of oxide.

In the solvent sample there is free rotation of the end groups and therefore these groups can be orientated with respect to the surface over a large range of positions. Some of these orientations will, of course, be conducive to the adsorption of the group onto the oxide. But there are only two end OH groups in each polymer molecule. Some of these end groups will be bonded to the oxide but their numbers will be small and so it is proposed that their effect will remain unresolved in the spectra.

8.5 The adsorption of PEG_{400} / $ZnCl_2$ on Alumina.

An initial comparison of the spectra obtained from the two samples reveals that there are very few differences. The spectra from sample 1 contains some features at around 200 to 280 mV which do not appear in the spectra of sample 2. Whilst there is an extra peak at 439.8 mV in the spectra from sample 2, the rest of the two spectra are essentially the same.

Turning our attention to the peak at 450 mV, the presence of the peak at around 450 mV, which is normally assigned to an OH stretch mode, would seem to indicate that there are more hydroxyl groups coupled with the surface of the oxide in the zinc coordinated sample than in the pure sample This could come about in two different ways.

Firstly if many more of the end groups of the polymer were presented to the surface in a manner conducive to bonding their incorporation and orientation would

Adsorption of PEG_{400} onto aluminium oxide

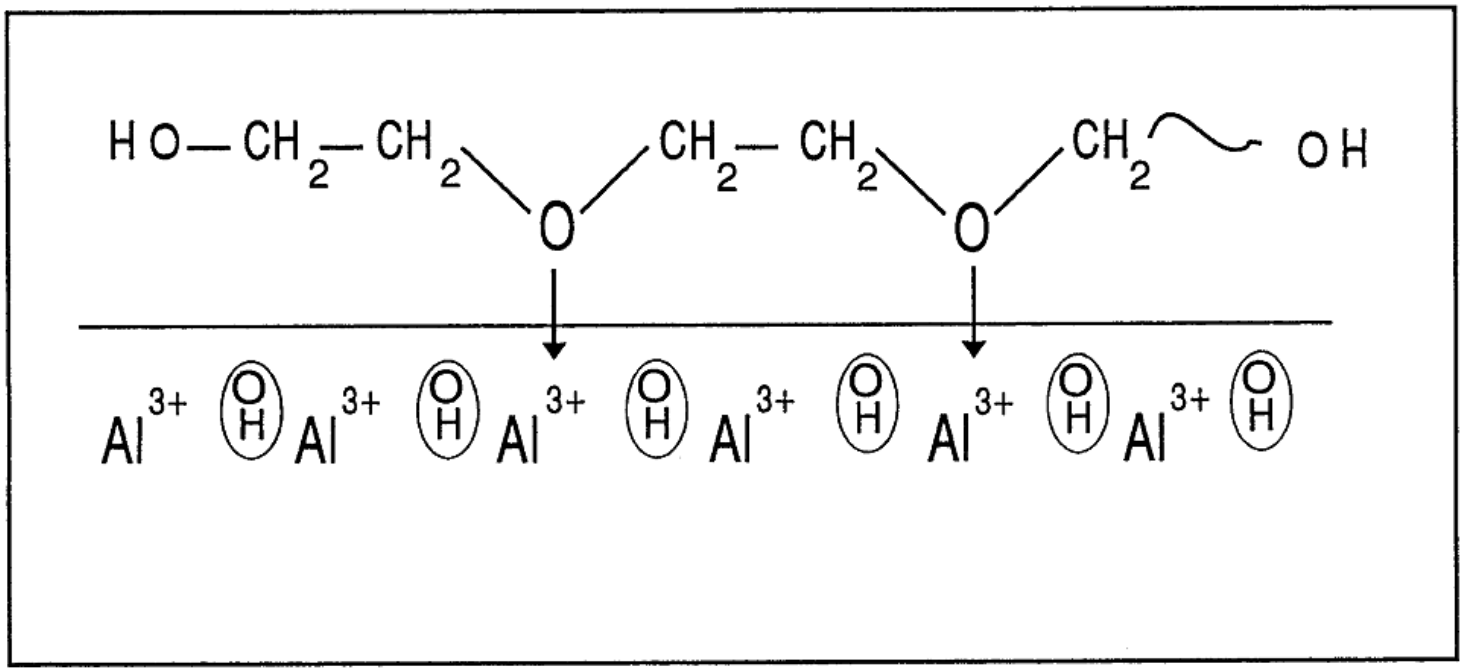

Figure 8.5.

When the solvent PEG_{400} is incorporated in a tunnel junction it it adheres to the surface via co-ordinate oxygen/aluminium bonds.

bring about a peak at around 450 mV. The incorporation of zinc into the polymer might sterically hinder the free rotation of the terminal groups of the polymer and this being so it would reduce the numbers of positions that the end groups could assume. The realignment of the molecule might favour hydrogen bonding between the OH terminal groups and hydroxyls on the oxides surface - see Figure 8.6a. Figure 8.6b illustrates a simplified schematic model by which PEG_{400} / $ZnCl_2$ could be adsorbed onto an aluminium oxide surface. The coordination of zinc with the ether oxygens of the polymer leave only the hydroxyl end groups available for bonding to the surface. Figure 8.6b shows a more realistic view of the incorporation of the zinc which also leads to the second, and more likely, explanation of why there is an extra peak at about 450 mV in the spectra of sample 2.

Secondly zinc chloride is highly hydroscopic and although 'dry' samples are purchased and packaged together with an inert gas to prevent hydration, as soon as the packaging is opened water is absorbed onto the sample from the moist air in the lab. The materials affinity with water can be observed through the immediate change in the colour of the sample when it is first exposed to the atmosphere, darkening within a few seconds of the exposure. The incorporation of the water into the zinc would ensure that there were many more hydroxyl groups within the junction and therefore these groups could bond with the surface through hydrogen bonding with surface hydroxyls - as illustrated in Figure 8.7.

8.6 Infrared and Thermographic Analysis (TGA) Data

In order to quantify and compare the amount of water present in a fresh sample of zinc chloride with that present in a sample which had been opened, used to produce

A Schematic of a Proposed Adsorption mechanism of a solution of Zinc Chloride In Poly (ethylene glycol) onto Aluminium Oxide.

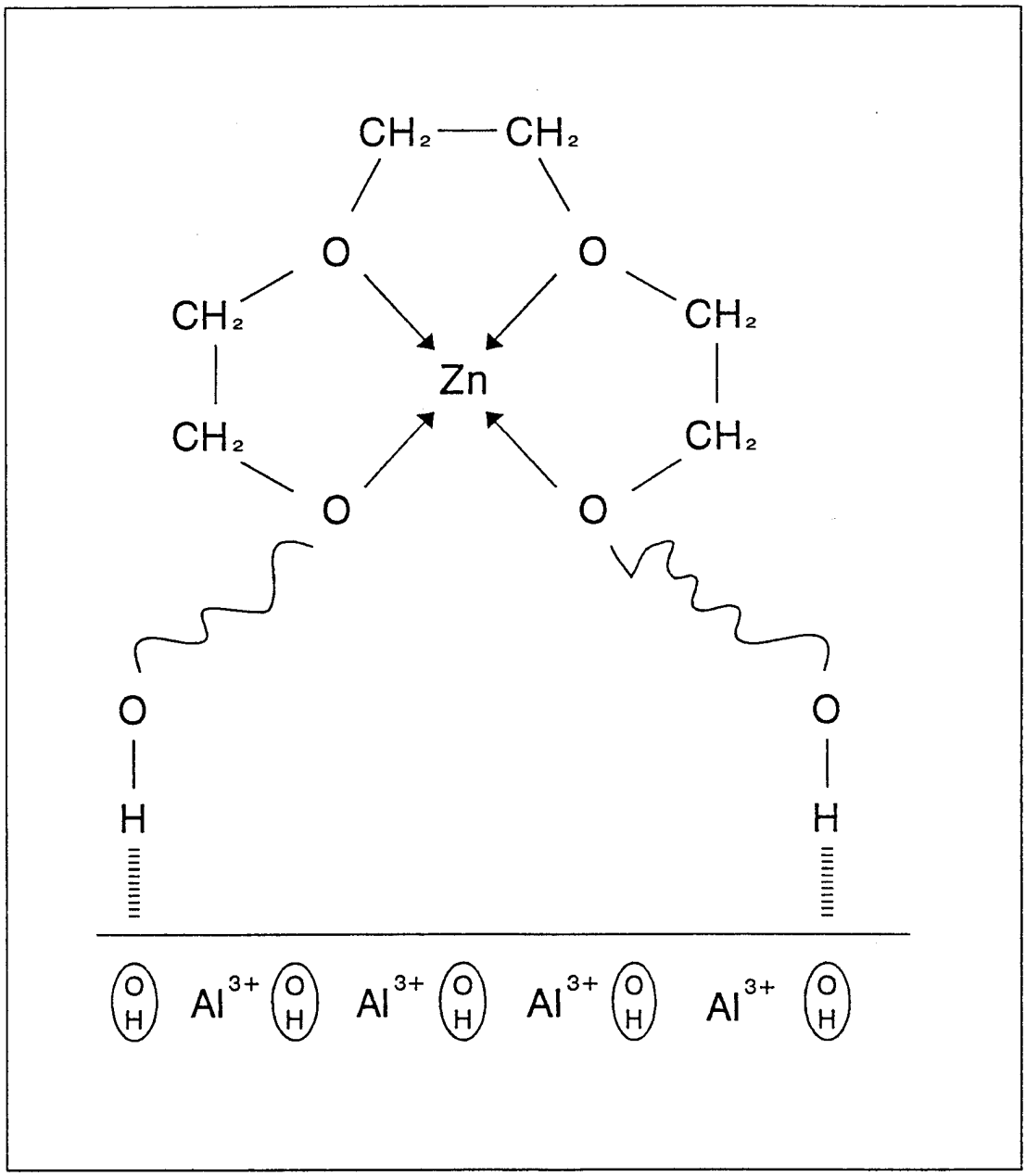

Figure 8.6a

When a solution of zinc chloride in poly (ethylene glycol) is adsorbed onto aluminium oxide it could adhere to the surface via hydrogen bonding of the end groups.

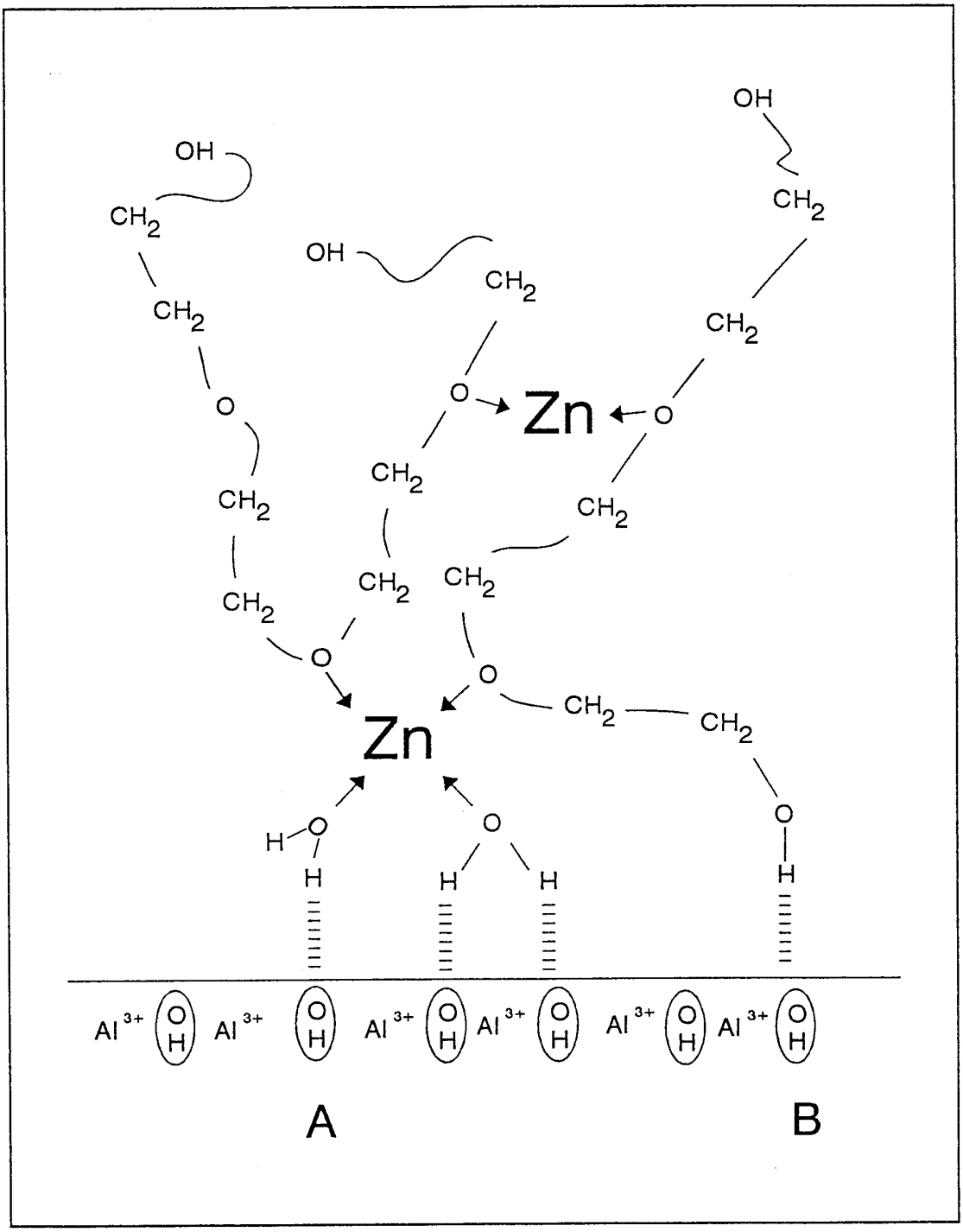

Figure 8.6b

A proposed mechanism for the asorption of zinc chloride onto aluminiumoxide. Asorption can occur through hydrogen bonding to an end group as in A and via hydrogen bonding with water which is bonded to the zinc as in B.

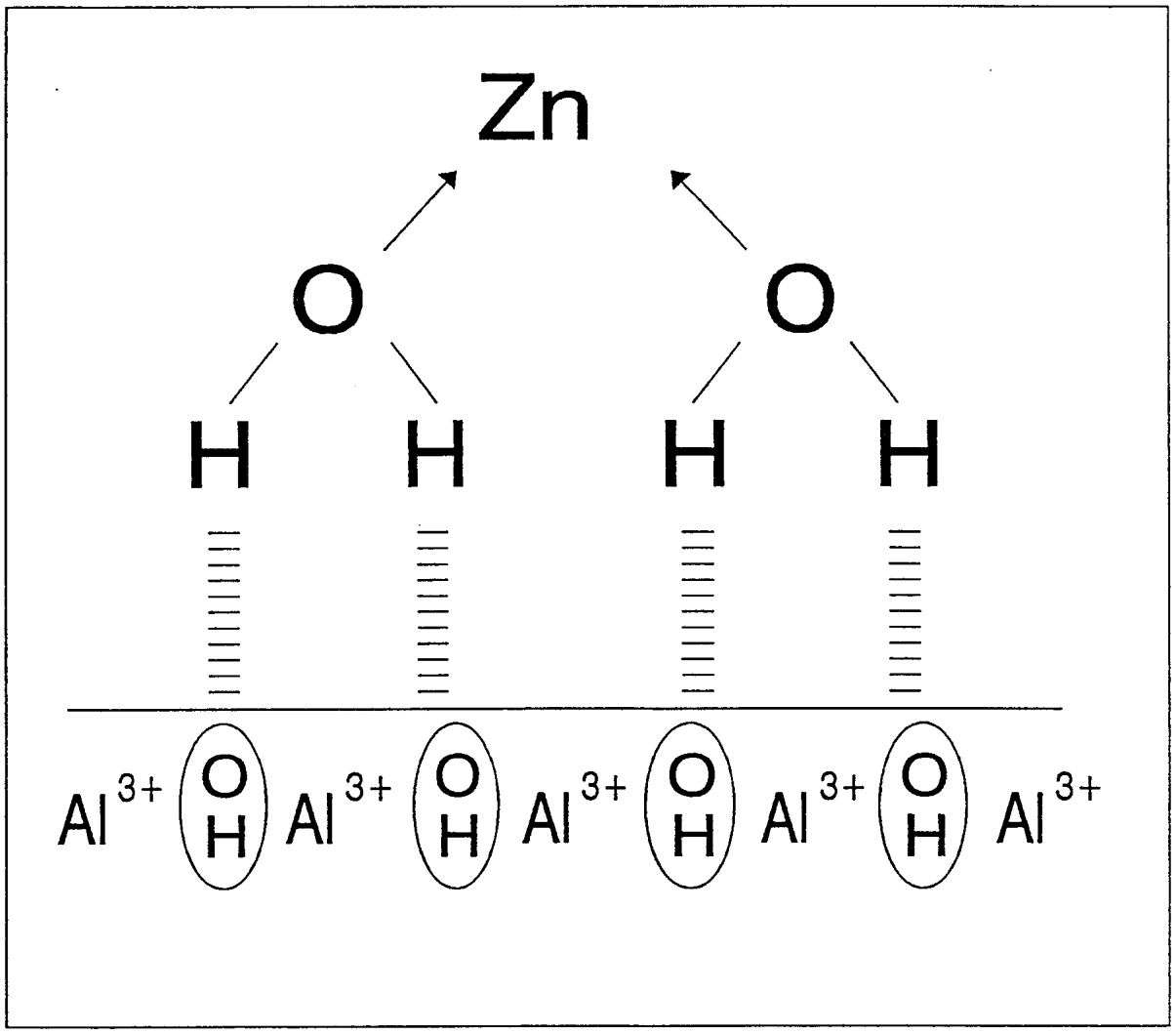

Figure 8.7.

The diagram in this figure is a stylised represenataion of the hydrogen bonding of PEG_{400} / ZnCl to aluminium oxide. It is proposed that bonding takes place between the water incoporated in the zinc and the hydroxyls in the surface of the aluminium oxide.

samples for doping, and then stored in the laboratory for some time infrared spectroscopy and thermographic analysis were performed on each of the samples. Figures 8.8 to 8.11 are reproductions of representative samples of the graphs produced by each of these techniques.

8.6.1. Infrared Data.

Taking the infrared data first, Figures 8.8 and 8.9 are the spectra obtained from the fresh batch of zinc chloride and the used sample respectively. The area of importance in this investigation is between 2400 cm^{-1} and 3800 cm^{-1}, it is in this region that the peaks due to vibrations of the OH modes occur. The peaks in this area of the spectrum will be indicative of the amount of water present in the sample. Water in inorganic salts can be classified either as lattice or coordinated water, although there is no definite borderline between the two [18]. Lattice water is water entrapped within the lattice of the metal and coordinated water is water coordinated with the surface of the material.

Figure 8.8 shows a strong feature in the spectrum at about 3600 cm^{-1} , this would seem to indicate that water was present in the sample during the spectrographic analysis. Turning our attention to the infrared spectrum taken from the used sample, Figure 8.9 we see that there is also a feature in the region under investigation. Only this time the feature is much broader and more complex in form with much more differentiation of the energy levels. This displays clear evidence that the used sample contains much larger amounts of water compared from the new and unused sample. The rest of the spectra are very similar, with just some reduction in intensity of the weaker peaks.

From these data it can be inferred that a fresh sample of zinc chloride will contain significant amounts of water and it will continue to absorbe more water during

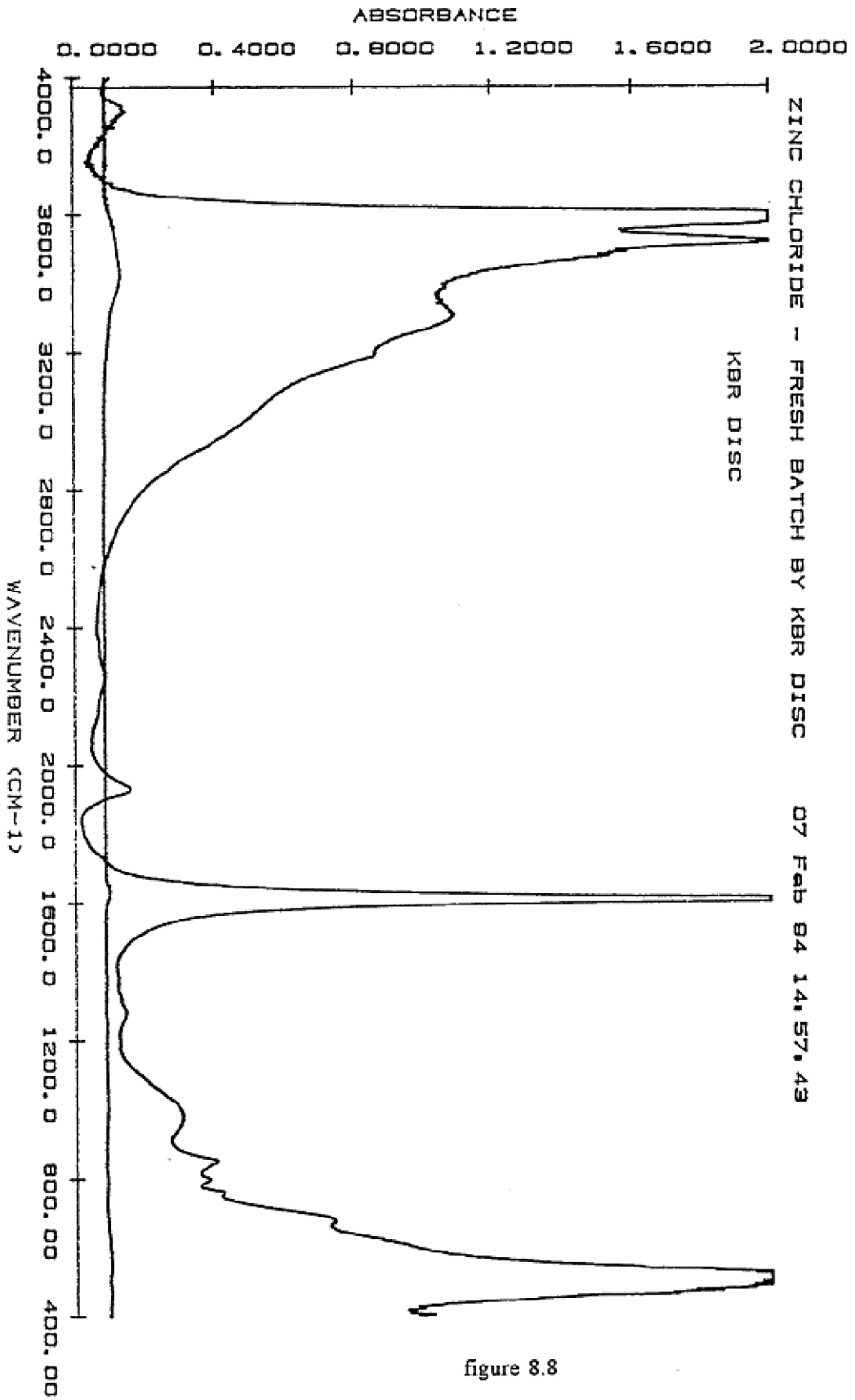
ABSORBANCE
0.0000
0.4000
0.8000
1.2000
1.6000
2.0000
4000.0
3600.0
3200.0
2800.0
2400.0
2000.0
1600.0
1200.0
800.00
400.00
WAVENUMBER (CM-1)
ZINC CHLORIDE - FRESH BATCH BY KBR DISC
KBR DISC
07 Feb 84 14:57:43

figure 8.8

Figure 8.8

Reproduced in this figure is the infra red spectrum taken from a fresh batch of zinc chloride. The sample was opened and a sample placed in the i.r. spectrometer immediately.

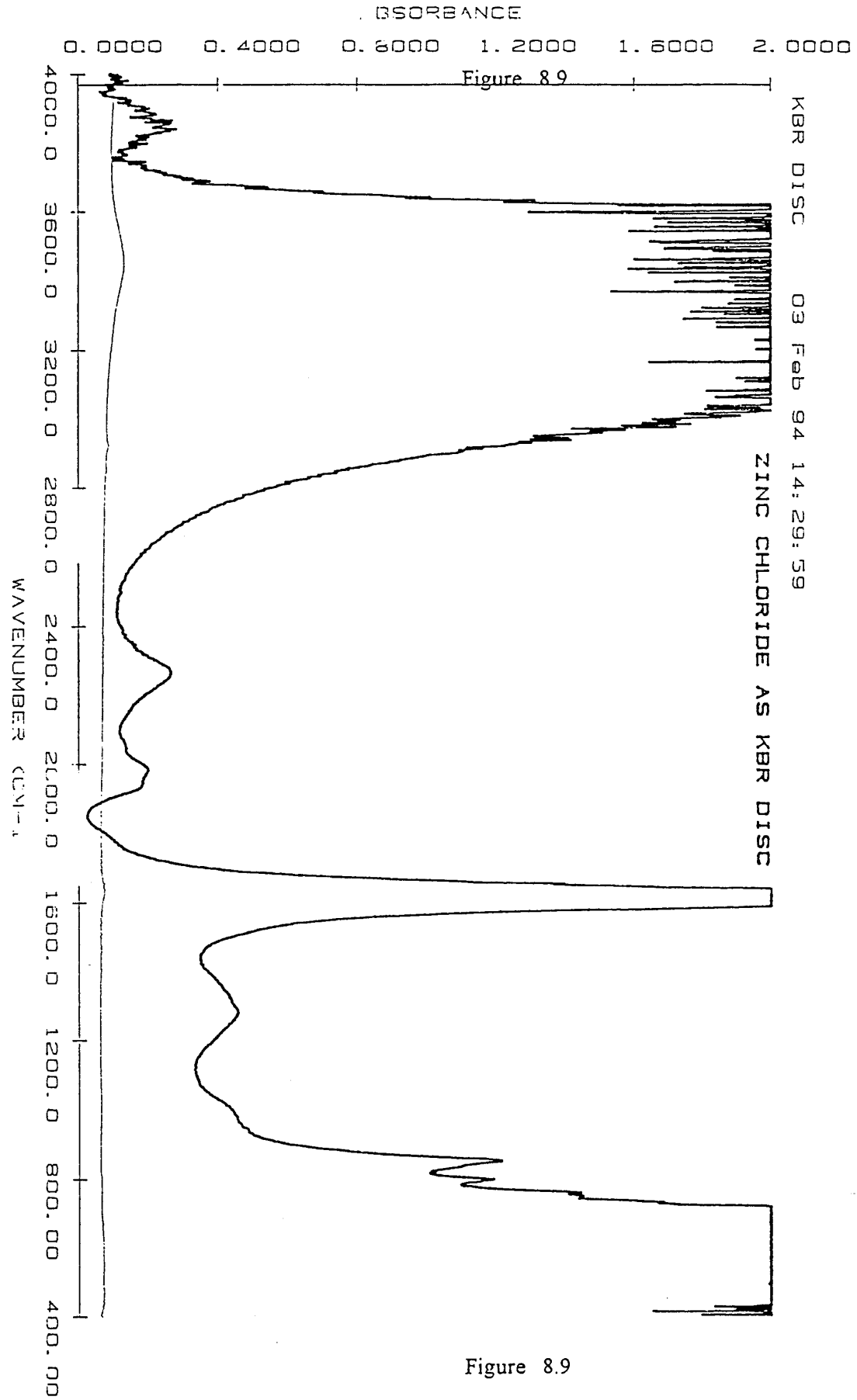

Figure 8.9

Figure 8.9

Figure 8.9

The infra red spectrum taken from a used batch of zinc chloride is reproduced in this figure. The sample was taken from a batch of zinc chloride which was in use within the laboratory.

its usage and storage. It is not possible, from these infrared data, to quantify the amounts of water present - only a comparative assessment is possible.

8.5.2. Thermographic Analysis

Graphs of the data taken from the TGA are shown in Figures 8.10 and 8.11. TGA involves heating up a sample to drive off any of its volatile components, in this study it is water which is being driven from the sample. The amount of water being removed is monitored by continuously weighing the sample throughout the period of the experiment. The monitoring is done by passing a current through the weighing mechanism in such a way as to keep the balance in its initial position. The current required to keep the equipment balanced is measured - being proportional to the weight change. Both samples were run over the temperature range 20^0C to 250 ^{o}C during a time period of 50 minutes.

Taking the results of the data gathered from the fresh sample of zinc chloride first see Figure 8.10. The graph shown clearly that between 50^{o}C and 100 ^{o}C water was being driven from the material at a fast rate, as shown by the steep gradient of the curve. This initial weight loss was followed by a slower rate of weight loss between 100 ^{o}C and 225 ^{o}C as indicated by the shallow gradient in this region of the graph. Finally there was then a further sharp loss of water between the temperatures of 225 ^{o}C and 250 ^{o}C - again indicated by the increased slope of the graph. Indicated on the graph are the percentage losses for the two steep regions, an average slope is taken for the intermediate region. The losses are:

1. An initial loss of 1.302 % which represents a loss of 1.037 mg.
2. A second loss of 1.166 % representing a weight reduction of 0.929 mg.

As can be seen from Figure 8.11 which is a graph of the thermographic data gathered from a run performed on the old sample of zinc chloride the weigh losses follow

a similar pattern to those of a fresh sample. Only this time the ratios of the

two losses are different being :

1 An initial loss of 1.188% representing a weight loss of 0.779 mg.

2. A second loss of 2.749% representing a weight loss of 1.801 mg.

These two sets of results are brought together in Table 2.

	Percentage Change		**Weight Loss / mg**	
Temp / ^{O}C	**New sample**	**Old sample**	**New sample**	**Old sample**
50 - 125	1.302%	1.188%	1.037	0.779
125 - 250	1.166%	2.749%	0.929	1.801

Table 8.2

Results from thermographic analysis of new and old samples of zinc chloride of sample sizes of 65.537 mg and 79.652 mg respectively.

The water expelled between 50 and 125^{O} C is water which resided on the surface of the zinc chloride (surface water). Whereas the water expelled between the temperatures 125 to 250^{O} C is water which was trapped within the crystal structure of the zinc chloride (crystal water). Using the mixing ratios shown above each milligram sample of the dopant solution will contain about 4% or 0.04 mg of zinc chloride.

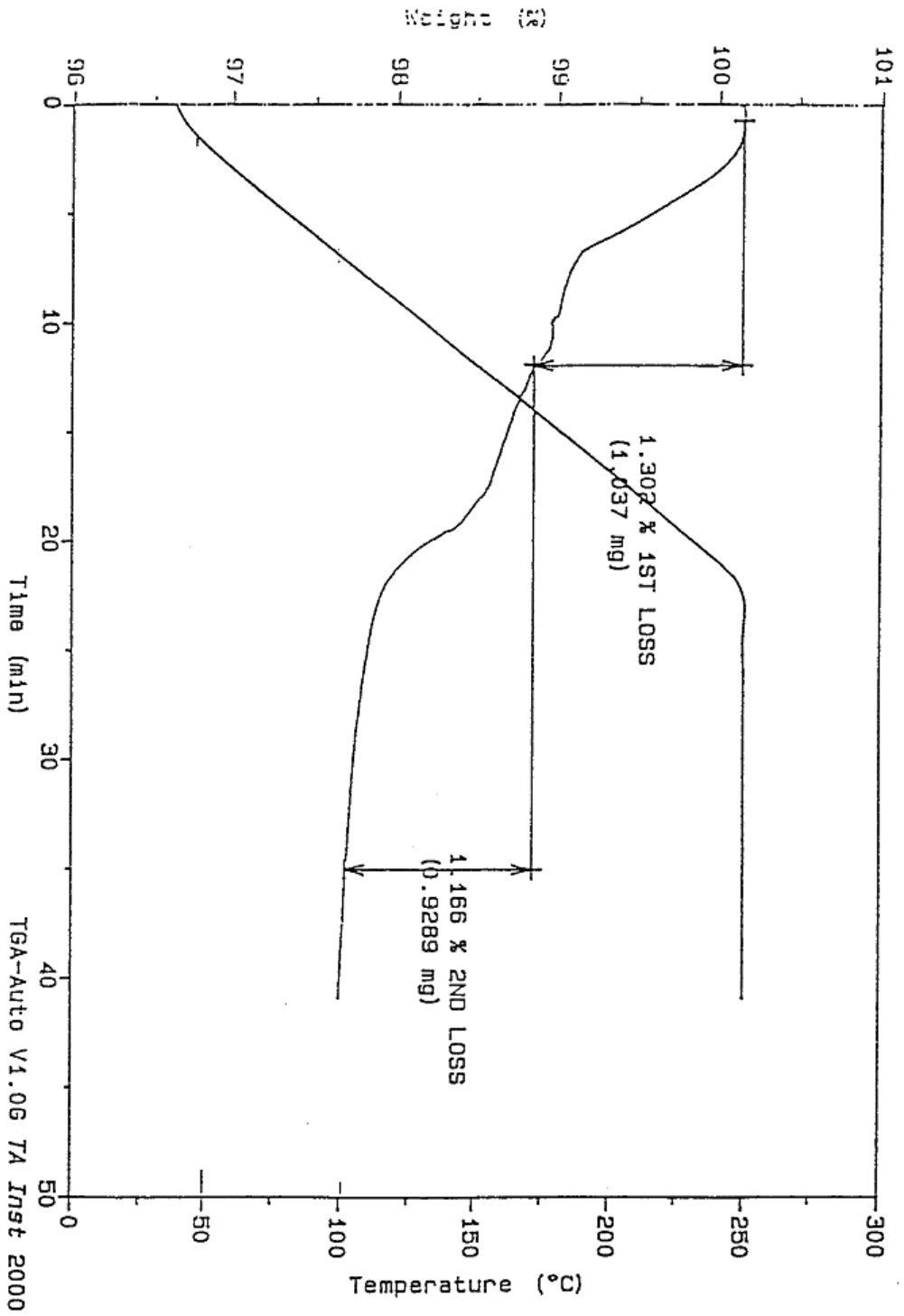
Sample: ZINC CHLORIDE - FRESH SAMPLE
Size: 79.6520 mg
Method: WATER CONTENT
Comment: 80 ML/MIN NITROGEN FAN OFF
TGA
File: C:ZNCL.003
Operator: NICKY SINGLETON
Run Date: 7-Feb-94 15:00
1.302 % 1ST LOSS
(1.037 mg)
1.166 % 2ND LOSS
(0.9289 mg)
Temperature (°C)
Time (min)
TGA-Auto V1.0G TA Inst 2000

Figure 8.10.

Figure 8.10

Illustrated here is the result of a thermographic analysis taken on a fresh sample of zinc chloride. The temperature range of the experiment was from room temperature up to 250 C^{o}.

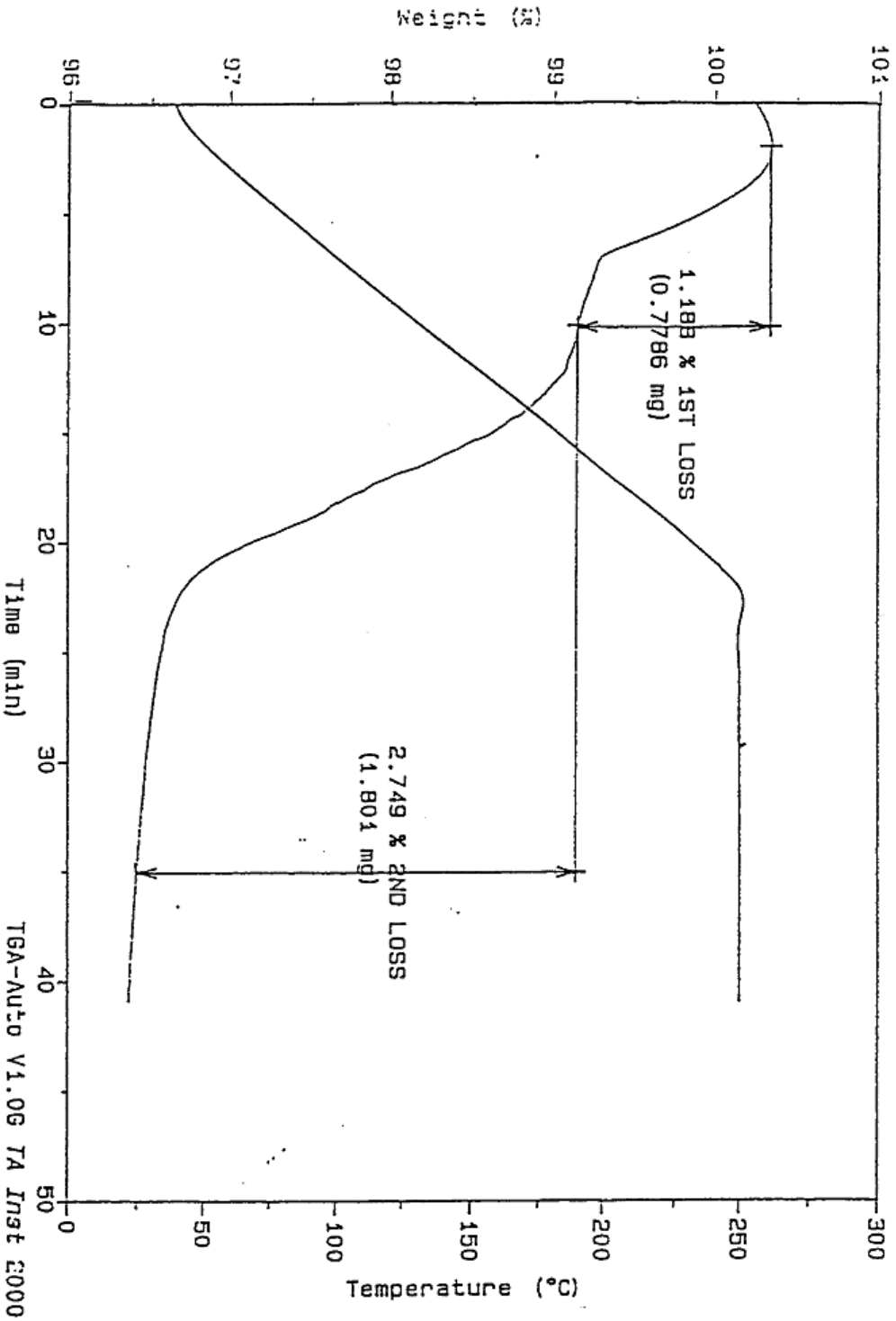
Sample: ZINC CHLORIDE - OLD SAMPLE
Size: 65.5370 mg
Method: WATER CONTENT
Comment: 80 ML/MIN NITROGEN FAN OFF
TGA
File: C:ZNCL.002
Operator: NICKY SINGLETON
Run Date: 4-Feb-94 12:09
1.188 % 1ST LOSS
(0.7786 mg)
2.749 % 2ND LOSS
(1.801 mg)
Weight (%)
Temperature (°C)
Time (min)
TGA-Auto V1.0G TA Inst 2000

Figure 8.11.

Figure 8.11

Shown in this figure is the data taken from a thermographic analysis of a used sample of zinc chloride - the sample was in regular use in the laboratory.

Therefore each milligram of the dopant solution if it is made from a new sample of zinc chloride will contain approximately 0.52×10^{-3} mg of surface water and 0.46×10^{-3} mg of crystal water giving a total of 0.98×10^{-3} mg.

Whereas if the dopant solution is made up using 'old' zinc chloride it will contain approximately 0.48×10^{-3} mg of surface water and 1.0×10^{-3} mg of crystal water giving a total of 1.48×10^{-3} mg**.** It is obvious therefore that when zinc chloride is incorporated into poly (ethylene glycol) into tunnel junctions it will introduce very large amounts of water - parts per thousand - into the junctions. This water would reveal itself as OH stretch modes in the IET spectra taken from junctions incorporating the polymer.

8.7 Discussion and Conclusions

Examination of the IET spectra of PEG_{400} solvent and PEG_{400} solution reveals that the major difference between them occurs at around 450 meV. At this position, peaks in the spectrum are assigned to the stretch vibrations of surface hydroxyl groups. Other minor differences can be observed at about 220 - 280 meV.

It is proposed that the difference at around 450 meV can be explained by the following models. In the first scenario when the PEG_{400} molecule is adsorbed onto the aluminium oxide surface the main mechanism is via coordinated oxygen -aluminium bonds with a smaller contribution from hydrogen bonding between the end OH groups and hydroxyls in the aluminium oxide surface due to the unrestricted rotation of the end groups. The available orientations of the end groups greatly favour positions which limit the formation of hydrogen bonds with the aluminium oxide surface.

In the other scenario where PEG_{400} / $ZnCl_2$ is incorporated in the IET junction it is proposed that the large amounts of water brought in by the zinc form hydrogen bonds with hydroxyl groups in the oxide surface. These bonds will give rise to the extra peak at approximately 450 meV in the spectrum of this material. There will exist a probability that a number of hydrogen bonds could be formed between the hydrogen in the end groups and the OH groups in the surface. This bonding would manifest itself as a very small increase in the intensity of the peak assigned to OH stretch modes in the spectrum of the zinc coordinated sample.

The height of the 450 meV peak in the spectrum is smaller than might be expected considering the amount of water present in the junction. But there will be competition for sites on the oxide surface from the chlorine ions released from the zinc chloride during its coordination with the poly (ethylene glycol). These ions will remain in the solution from which the junction is doped and therefore will compete with the polymer for bonding sites. The chlorine will want to form a bond with the lone pair electrons of the oxygen in the Al_2O_3 surface to form a covalent bond. This competition will restrict the number of the OH bonds which can be formed which will reduce the height of the 450 meV peak in the IET spectrum.

It is possible that there is a contribution to one or other regions of the spectrum from the interactions between the zinc-aluminium and chlorine-aluminium further studies utilizing other halides might elucidate these regions.

Recent EXAFS results for PEO / $ZnBr_2$ electrolytes have shown that halide ions are

located immediately adjacent to Zn^{2+} [19].

References

[1] Lamb J and Jacklevic R C 1968 *Phys. Rev.* **165** 821
[2] Jacklevic R C and Lamb J 1966 *Phys. Rev.* **17** 1139
[3] Salapino D J and Marcus S M 1967 *Phys. Rev.* **18** 495
[4] Comyn J, Horley C C, Oxley D P, Pritchard R G and Tegg J L 1981 *J. Adhesion* **12** 171
[5] Reynolds S, Oxley D P and Pritchard R G 1982 *Spectrochem. Acta.* **30 A** 103
[6] Brewis D M, Comyn J, Oxley D P Pritchard R G and Werrett C R 1984 *Surf. Int. A*nal **6** 1
[7] Mallik R R 1985 *PhD Thesis* Leicester Polytechnic[8] Mallik R R, Pritchard R G, Horley C C and Comyn J 1985 *Polymer* **26** 55
[9] Walmsley D G and Nelson 1982 *Tunnelling Spectroscopy, Capabilities, Applications and Techniques* ed. P K Hansma (New York: Plenum) p311
[10] Lal M and Stepto R F T 1977 *J. Polym. Symp.* **61** 401
[11] Line M J, Pritchard R G and Oxley D P 1989 *J. Phys C : Condensed Matter* **1** 6835
[12] Oxley D P, Bowles A J, Horley C C, Langley A J, Pritchard R G and Tunnicliffe D L 1980 *Surf. Interface Anal.* **2** 31
[13] Reynolds S 1983 *PhD Thesis* Leicester Polytechnic
[14] Reynolds S, Gregson L D, Horley C C, Oxley D P and Pritchard R G 1980 *Surf. Interface Anal.* **2** 31
[15] Reynolds S, Peasgood A, Oxley D P and Pritchard R G 1987 *J. Phys. C: Solid State Phys.* **20** 4297
[16] Kirtley J R and Hansma P K 1975 *Phys. Rev. B* **12** 531
[17] Koubek J, Volf J and Pasek J 1975 *Catal.* **38** 385
[18] Kazuo Nakamoto 1963 *Infrared Spectra of Inorganic and Coordinated Compounds* John Wiley & Sons (New York: London).
[19] Latham R J, Linford R G, Pynenburg A J and Schlindwein W S 1993 *J. Electrochem. Soc.* **140** 1056

Contents

CHAPTER 9

Conclusions

9.1 Top-metal and Bias reversal Effects on IET OH Mode Energy

It has been shown that the ration of width to thickness of the electrodes in IET tunnel junctions influences the apparent positions and breadth of spectral lines. The effect can be difficult to avoid experimentally and can be significant even when using a four-point-probe measuring techniques. The effect is a result of the finite resistance of the parts of the electrodes which form the junction area. Building upon some earlier work done by Giaever a simple treatment was developed involving a minimum thickness of electrode which allows such effects to be routinely corrected.

A programme of work on the peak shift of the 450 meV OH mode on reversing the applied bias revealed that the dependence on the nature of the top-metal electrode used was outside the resolution of the present experimental procedures, a result which substantiates the present theoretical thinking. It is also shown that the relatively large and non-uniform barrier and image contributions to the resultant field can be treated by super position with the applied field and that the effect of the barrier and image contributions upon bias reversal is negligible. This area of work has highlighted the subtle ways in which the tunnel junction environment remains benign in so far as the vibrating species are concerned.

9.1.2. IETS Using LB Films

In this series of experiments the important and technologically demanding technique of Langmuir Blodgett (LB) film manufacture and deposition was used to incorporate a monolayer of dopant within a tunnel junction. It was realised at the outset that using an LB film to dope an IET tunnel junction with a monolayer of material was going to be a very difficult assignment; this view was based upon the experiences of work done in the department by an earlier group. The results using an LB film of mixed stearic acid/barium stearate to dope an IET junction resulted in some of the very few IET spectra produced by this novel technique. The work also highlighted the very important part played in the tunnelling process by pin-holes, faults, and thin spots – an area in IETS to which very little attention seems to have been applied.

9.1.3. The Swelling and Adsorption on Alumina of p-HEMA

Hydrogels, of which poly 2-hydroxyethyl methacrylate (p-HEMA) is a very important member being the only non soluble in water, have many commercial and industrial applications. This study into the welling of a monolayer of p-HEMA is unique in that although the material has been extensively studies all of the other work has been done on what are effectively bulk samples. The data gathered by this present group shows that once water is incorporated into a hydrogel it takes on a limited structure with the first layer being thinner than the second and all subsequent layers.

The IETS results on the absorption of the hydrogel onto aluminium oxide suggest that the polymer has an ester group cleaved by a reaction with the surface to be adsorbed via a resonance stabilised bidentate bridging arrangement. The HEMA monomer however is hydrogen bonded to the alumina surface and appears not to

undergo cleavage by the ester group. It is proposed that the conformational restrictions within the monomer account for the different bonding mechanisms. It is also suggested that the spectrum from the polymer shows some evidence of co-ordinated water within the polymer.

9.1.4 An IETS Study of the Adsorption of a Polymeric Electrolyte onto Aluminium oxide

The IET spectra of polyethylene glycol and polyethylene glycol coordinated with zinc chloride are the first to be produced. The major difference between the major spectra of the two samples is the appearance of an extra peak at around 450 mV, a position which indicates the presence of OH vibrational modes. It is proposed that the extra peak in the spectrum taken from the coordinated sample provides some evidence that the coordination of the zinc within the PEG imposes conformational restrictions upon the coordinated system. These restrictions in the polymer result in it being presented to the oxide surface in a way which is conducive to hydrogen bonding of its end groups to surface hydroxyls which is revealed to the peak at 450 mV. The uncoordinated sample has less restrictions imposed upon it and it adheres to the aluminium oxide surface via coordinated oxygen/aluminium bonds with very little bonding to the OH. The previous suggestions do not lose sight of the fact that zinc is a very highly hydroscopic material and water bought into the sample by the zinc could also explain the differences between the two spectra.

Contents

APPENDICES

Appendix I

IETS Constant Curnent Bias and Modulation Circuitry

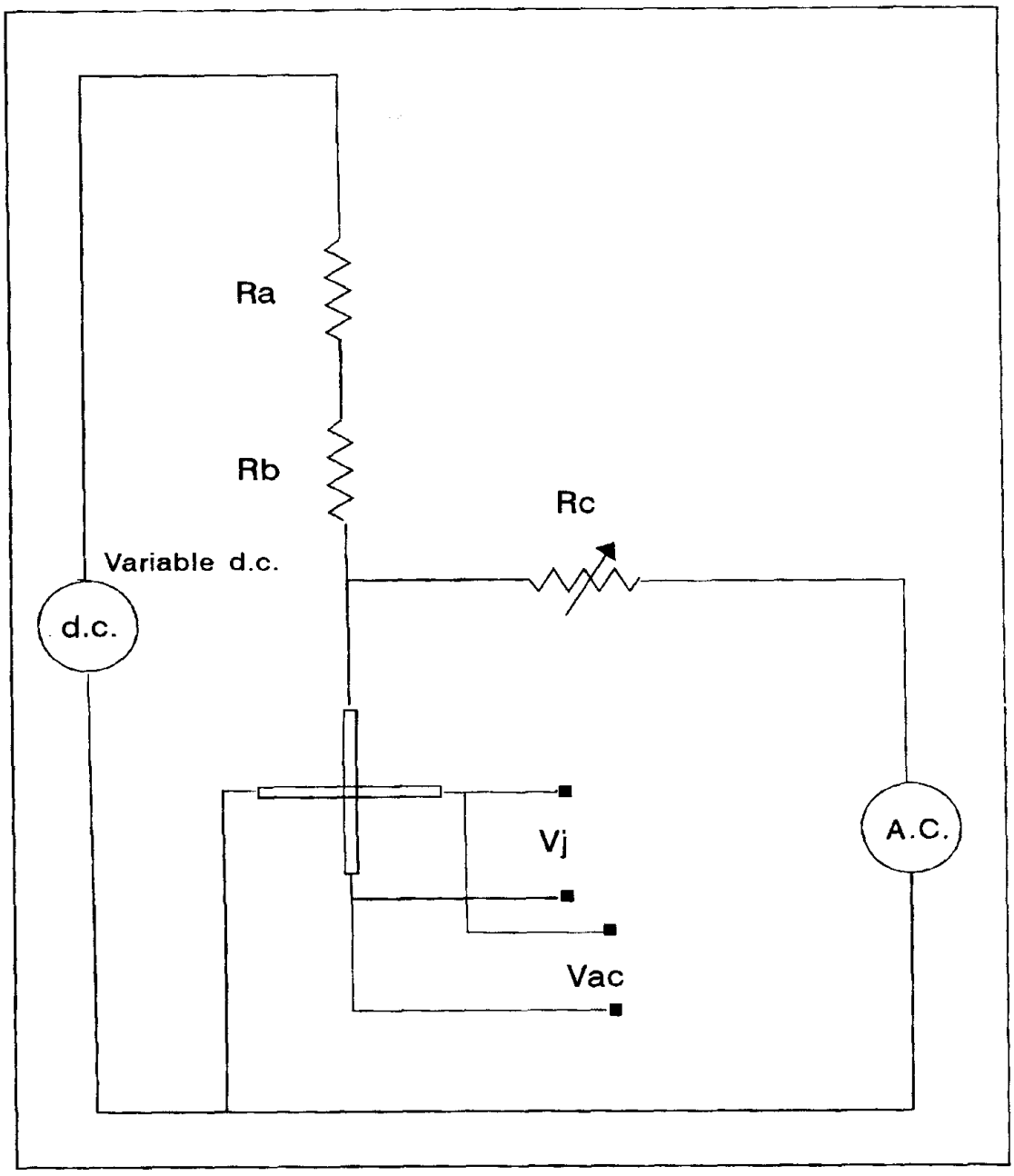

A simplified diagram of the constant current bias and modulation circuitry used in IETS.The do bias current is supplied through the series combination Ra, Rb. The ohmic drop across Ra serves to permit accurate measurement of the bias current. Rb is adjusted so that the appropriate bias voltage may be obtained, usually a maximum of 0.5V. Rc is usually chosen to be more than IOORj as the generator proviucs about IV rms which must be dropped to about I mV rms across the junction.

Appendix 2

The Lauda Film Balance Technical Details

Film Pressure System

Measuring Range	0-100 x 10^{-3}N
Sensitivity	0.1 x 10^{-3}N
Barrier Movement	25μm for 100 x 10^{-3}N
Barrier Length	11 x 10^{-2} m
Thickness Of Teflon Bands	10μm
Sensitivity (Y Axis)	50mV cm^{-1}

Area Measuring System

Maximum Measuring Area	0.1 m^2
Length Of Trough	0.7m
Width Of Trough	0.15m
Depth Of Trough	0.6 x 10^{-2}m
Volume Of Subphase	700mL
Sensitivity (X Axis)	5 mV cm^{-1}

Measuring Speeds	0.9 x 10^{-2} to 6.5 x 10^{-2} N min^{-1}

Film Pressure

Range Of Adjustment	0 – 100 x 10^{-3} N
Accuracy Of Optimum Settings	± 0.1 x 10^{-3}N
Temperature Range	0 to 50^{o} C

Listed above are a range of selected technical details transcribed from the service manual.

Appendix 2

Miketest Data Collection Software

```
10 REM MIKETST PROGRAM
20 REM ************************************************************
30 REM First set up IEEE devices
40 REM ************************************************************
50 OPEN "IEEECTRL" AS #1
60 OPEN "IEEEDATA" AS #2
70 REM IOCTL#1,"12"
80 REM IOCTL#2,"D0P1R8F1I+1.00E-3X"
90 IOCTL#1, "16"
100 IOCTL#2,"F2R0P0Q2X"
110 REM VALUE$=IOCTL$(#2) : PRINT VALUE$
120 REM ************************************************************
130 REM Now print instructions to user on the screen
140 CLS: PRINT"CONDUCTIVITY MEASURING ROUTINE"
150 PRINT:PRINT:PRINT
160 CLS
170 PRINT  "1 LOG NEW DATA"
180 PRINT  "2 PROCESS OLD FILE"
190 PRINT  "3 AVERAGE DATA"
200 PRINT  "4 END"
210 INPUT  "SELECT OPTION"; K
220 REM ************************************************************
230 REM Now choose which option to execute
240 ON K  GOTO 250, 840, 890, 880
250 CLS
260 PRINT "ENTER HEADER NAME"
270 LINE INPUT N$
280 TITLE$= N$+ ".HDR"
290 OPEN TITLE$ FOR OUTPUT AS #3: PRINT
300 CLS
310 C$=  "CONDUCTIVITY MEASURMENTS":PRINT #3,C$
320 U$ = "----------------------": PRINT #3, U$
330 PRINT C$
340 PRINT U$
350 PRINT,DATE$;TAB(30) TIME$
360 PRINT #3,DATE$;TAB(25)TIME$
370 INPUT "OPERATOR:", O$
380 PRINT #3," OPERATOR:"; O$
390 PRINT " ENTER FILE NAME"
400 F$= "ENTER FILE NAME:": LINE INPUT F$: PRINT #3,"file name ",F$
410 PRINT " ENTER DOPANT"
420 DOPE$=  "ENTER DOPANT:": LINE INPUT DOPE$: PRINT #3,"dopant", DOPE$
430 PRINT "ENTER DEVICE STRUCTURE. e.g.AL/ALOX/DOPANT/PB"
440 INPUT D$: PRINT #3,"device structure", D$
450 PRINT " Comments:"
460 LINE INPUT C$ :PRINT #3,"Comments",C$
470 CLOSE #3
480 REM ************************************************************
490 PRINT "ENTER DATA FILE NAME"
500 INPUT DF$: IF DF$ = "" THEN GOTO 490
510 NAM$=DF$+".DAT"
520 OPEN NAM$ FOR OUTPUT AS #3
530 INPUT "RUN TIME";RT$
540 TIME$= "0:0"
550 REM ************************************************************
560 REM **  Start of data logging PROPER                          **
570 REM ************************************************************
580 REM First read Keithley 195a digital multimeter
590 M$=IOCTL$(2)
600 IF LEFT$(M$,1)<>"N" THEN GOTO 1170 ELSE 610
610 M=VAL(MID$(M$,5))
620 Z=0
```